

Sheffield Hallam University

Fundamental studies of the analytical applications of an inductively coupled plasma source.

CAVE, Mark Richard.

Available from the Sheffield Hallam University Research Archive (SHURA) at:

<http://shura.shu.ac.uk/19433/>

A Sheffield Hallam University thesis

This thesis is protected by copyright which belongs to the author.

The content must not be changed in any way or sold commercially in any format or medium without the formal permission of the author.

When referring to this work, full bibliographic details including the author, title, awarding institution and date of the thesis must be given.

Please visit <http://shura.shu.ac.uk/19433/> and <http://shura.shu.ac.uk/information.html> for further details about copyright and re-use permissions.

POLYTECHNIC LIBRARY
POND STREET
SHEFFIELD S1 1WB

6840



**Sheffield City Polytechnic
Eric Mensforth Library**

REFERENCE ONLY

This book must not be taken from the Library

~~11/3~~
~~17.00~~

254.99

21.00

20/7/95

1603

28/3-20.59

ProQuest Number: 10694314

All rights reserved

INFORMATION TO ALL USERS

The quality of this reproduction is dependent upon the quality of the copy submitted.

In the unlikely event that the author did not send a complete manuscript and there are missing pages, these will be noted. Also, if material had to be removed, a note will indicate the deletion.



ProQuest 10694314

Published by ProQuest LLC (2017). Copyright of the Dissertation is held by the Author.

All rights reserved.

This work is protected against unauthorized copying under Title 17, United States Code
Microform Edition © ProQuest LLC.

ProQuest LLC.
789 East Eisenhower Parkway
P.O. Box 1346
Ann Arbor, MI 48106 – 1346

A thesis entitled

FUNDAMENTAL STUDIES OF THE ANALYTICAL APPLICATIONS
OF AN INDUCTIVELY COUPLED PLASMA SOURCE

presented by

MARK RICHARD CAVE, B.Sc., A.R.C.S.

in part fulfilment of the requirements for the degree of

DOCTOR OF PHILOSOPHY

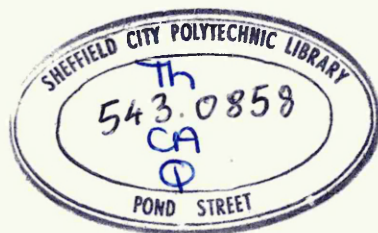
of the

COUNCIL FOR NATIONAL ACADEMIC AWARDS

London & Scandinavian Metallurgical Co. Ltd.,
Fullerton Road,
ROTHERHAM,
South Yorkshire.
S60 1DL

Department of Chemistry,
Sheffield City Polytechnic,
Pond Street,
SHEFFIELD.
S1 1WB

November 1980



7924511-01

Summary

The aim of this work has been to make a fundamental study of both nitrogen cooled and all argon inductively coupled plasmas (ICP), with particular regard to the parameters controlling the analytical usefulness of the plasma systems.

A versatile demountable plasma torch is described and comparisons between a number of different nebuliser systems have been made. The necessity for clearly defined power measurements is discussed and the measurement of power in the plasma using a dummy load and a direct calorimetric method described.

In order to make meaningful comparisons between different plasmas it has been found necessary to optimise the performance of the ICP. The variable step size simplex procedure is described and its successful application to the optimisation of SBR in different plasma systems.

Comparison of optimum operating conditions for the two plasma types has shown that the all argon plasma requires only one relatively low power setting (ca. 0.5 kW), whereas in the nitrogen cooled plasma the optimum power is apparently proportional to the difficulty of excitation of the spectral line to be used (optimal powers ranging from 0.26-1.16 kW). This result combined with simplex optimisation studies of the effect of matrix elements on optimal operating conditions has led to the conclusion that the nitrogen cooled plasma is probably closer to LTE than the all argon plasma.

A study of the effect of Na on Mn atom and ion lines is reported. A sodium interference effect was observed which could be closely correlated to the plasma tail flame viewing region used,

and was most critically dependent on the viewing height and injector flow rate. A method of minimising the sodium interference using the simplex procedure is described.

Using the knowledge gained from these plasma studies a number of refractory metallurgical alloys and standard steels have been successfully analysed using the ICP.

INDEX

	Page(s)
<u>Chapter 1</u> - <u>Introduction</u>	1
1.1 Theory of Emission Spectroscopy	1
1.2 Sources for Atomic Emission Spectroscopy	5
1.2.1 The Combustion Flame	5
1.2.2 Arcs and Sparks	6
1.2.3 The Grimm Glow Discharge Lamp	7
1.2.4 The Hollow Cathode Lamp	8
1.2.5 The Carbon Furnace	9
1.2.6 Plasmas	9
1.2.7 The d.c. Arc Plasma	10
1.2.8 The Capacitively Coupled High Frequency Plasma	10
1.2.9 The Microwave Induced Plasma	11
1.2.10 The Inductively Coupled Plasma	11
1.3.1 History and Development of the ICP	11
1.3.2 Analytical Advantages of the ICP as an Emission Source	19
1.4 Objectives of this Work	20
<u>Chapter 2</u> - <u>Instrumentation</u>	22
2.1 The Plasma Torch	25
2.1.1 Design Considerations for the Plasma Torch used in this Work	27
2.1.2 Torch Construction	29

2.1.3	Evaluation of the Torch	29
2.2	Sample Introduction	30
2.2.1	Evaluation of Nebuliser Systems for the Work	32
2.2.2	Experimental	35
2.2.3	Results and Discussion	38
<u>Chapter 3</u>	<u>- Power Measurements</u>	45
3.1	Experimental	45
3.1.1	Dummy Load Measurements	45
3.1.2	Direct Calorimetry Measurements	46
3.2	Results and Discussion	47
<u>Chapter 4</u>	<u>- Optimisation of Plasma Performance</u>	53
4.1	Simplex Optimisation	55
4.1.2	The Modified Simplex Method	58
4.2	Application of Modified Simplex to the Optimisation of the Performance of the ICP	62
4.2.1	Setting-up and Operation of the Simplex Optimisation	62
4.3	Experimental	65
4.4	Results and Discussion	66
4.4.1	Evaluation of the Simplex Procedure for Optimising the ICP	66
4.4.2	Evaluation of the Modified Torch	67
4.4.3	Comparison of Optimal Conditions Using 16mm and 4mm Slit Height	79

4.4.4	Comparison of Optimal Conditions in a Nitrogen Cooled Argon Plasma and an all Argon Plasma	88
4.4.5	Optimisation of the As 228.8 nm Atom line in the Presence of Cr Matrix	105
4.5	Conclusions	112
<u>Chapter 5 - Interference Effects in the ICP</u>		113
5.1.1	Sample Introduction	113
5.1.2	Vaporisation	114
5.1.3	Atomisation and Ionisation	115
5.1.4	Spectral Interference	118
5.2	Interference Studies on the Effects of Sodium Carried Out in this Work	119
5.2.1	Experimental	119
5.2.2	Results and Discussion	120
5.2.3	Conclusions	146
<u>Chapter 6 - Analysis of Metallurgical Samples</u>		151
6.1	Metallurgical Samples Analysed in this Study	151
6.2	Experimental Procedure for the Analysis of Metallurgical Samples	153
6.2.1	Sample Dissolution and Preparation of Standards	153
6.2.2	Plasma Operating Conditions	156
6.2.3	Selection of Spectral Lines	157
6.3	Results and Discussion	157
6.3.1	Ti Al Alloy	157
6.3.2	Al Ti B Alloy	161

6.3.3	BATS Alloy	161
6.3.4	Cr Metal	165
6.3.5	Tungsten Carbide	165
6.3.6	Cr Al	167
6.3.7	Si Al	169
6.3.8	BCS Steels	169

Chapter 7 - Conclusions and Suggestions for Further
Work 174

7.1	Comparisons of all Argon and Nitrogen Cooled Plasmas at Optimum Conditions	174
7.2	Simplex Optimisation as Applied to the ICP	184
7.3	Metallurgical Analysis Using the ICP	185

INDEX TO FIGURES

<u>Figure</u>	<u>Page(s)</u>
1. Schematic Diagram of Instrument	23
2. Double Pass Nebuliser Chamber	24
3. Demountable Plasma Torch	28
4. Nebuliser Designs	33
5. Vortex Nebuliser Chamber	34
6. Glass and Plastic High Solids Nebuliser	36
7. Teflon High Solids Nebuliser	37
8. Injector Tubes	40
9. Comparison of Noise Levels from Jet and Capillary Injector Tubes	40
10. Comparison of Meinhard and Glass High Solids Nebulisers	43
11. Comparison of Meinhard and Teflon High Solids Nebulisers	44
12. Power Output at Constant Grid Currents	48
13. Power Measurements at Simulated Plasma Conditions	50
14. Comparison of Dummy Load and Direct Calorimetric Power Measurements	51
15. Simplex Optimisation Examples	56
16. Variable Size Simplex Steps	60
17. Initial Simplex Matrix	63
18. Simplex Worksheet	64
19. Mn II 257.6 nm Univariate Search (Injector Ar Flow)	68
20. Mn II 257.6 nm Univariate Search (Plasma Ar Flow)	69
21. Mn II 257.6 nm Univariate Search (Coolant Ar Flow)	70

22.	Mn II 257.6 nm Univariate Search (Viewing Height)	71
23.	Mn II 257.6 nm Univariate Search (Power)	72
24.	Comparison of Torch Characteristics (Injector Ar Flow)	74
25.	Comparison of Torch Characteristics (Plasma Ar Flow)	75
26.	Comparison of Torch Characteristics (Coolant Gas Flow)	76
27.	Comparison of Torch Characteristics (Viewing Height)	77
28.	Comparison of Torch Characteristics (Power)	78
29.	Effect of Varying Plasma Gas Inlet Jet Sizes	80
30.	Effect of Varying Coolant Gas Inlet Jet Sizes	81
31.	As 228.8 nm Univariate Search (Injector Ar Flow)	82
32.	As 228.8 nm Univariate Search (Coolant Ar Flow)	82a
33.	As 228.8 nm Univariate Search (Plasma Ar Flow)	82b
34.	As 228.8 nm Univariate Search (Viewing Height)	82c
35.	As 228.8 nm Univariate Search (Power)	82d
36.	Comparison of Optimal Conditions for 4 and 16 mm Slit Heights	84
37.	Comparison of Optimal Conditions for 4 and 16 mm Slit Heights	85
38.	Comparison of Optimal Conditions for 4 and 16 mm Slit Heights	86
39.	Double Peaked Plasma Gas Univariate Search Graph for Ba (455.4 nm, Ar/N ₂ Plasma)	92
40.	Double Peaked Plasma Gas Univariate Search Graphs for Mn and Cu (Ar/N ₂ Plasma)	93
41.	Correlation between Optimal Injector Gas Flows and Viewing Heights	95

42.	Comparison of Optimal Power Data	97
43.	Normalised Optimum Power Graphs	101
44.	Effect of Cr Matrix on As 228.8 nm Optimal Conditions, Ar/N ₂ Plasma (Injector Ar Flow, Viewing Height and Plasma Ar Flow)	108
45.	Effect of Cr Matrix on As 228.8 nm Optimal Conditions, Ar/N ₂ Plasma (Coolant N ₂ Flow and Power)	109
46.	Effect of Cr Matrix on As 228.8 nm Optimal Conditions, Ar/Ar Plasma (Injector Ar Flow, Viewing Height and Plasma Ar Flow)	110
47.	Effect of Cr Matrix on As 228.8 nm Optimal Conditions, Ar/Ar Plasma (Coolant Ar Flow and Power)	111
48.	Effect of Li on Ca 393.4 nm Ion Line (154)	116
49.	Effect of Viewing Height on Na Interference	121
50.	Effect of Injector Ar Flow on Na Interference	122
51.	Effect of Increasing Na Concentration on Mn Optimum Conditions	124
52.	Comparison of Na Interference Effects on Mn Atom Lines	126
53.	Comparison of Na Interference in the ICP and an Air/C ₂ H ₂ Flame	128
54.	Effect of Reducing Injector Ar Flow on Na Interference (Mn Atom Lines)	129
55.	Effect of Increasing Injector Ar Flow on Na Interference (Mn Ion line)	130
56.	Effect of Increasing Injector Ar Flow on Na Interference (Mn 257.6 nm Ion Line, Greenfield Torch)	132
57.	Viewing Regions in the ICP Tail Flame Due to High Concentrations of Na	134
58.	Univariate Search for Minimisation of Na Interference (Viewing Height Ar/Ar Plasma)	136

59.	Univariate Search for Minimisation of Na Interference (Viewing Height, Ar/N ₂ Plasma)	137
60.	Univariate Search for Minimisation of Na Interference (Injector Ar Flow, Ar/Ar Plasma)	138
61.	Univariate Search for Minimisation of Na Interference (Injector Ar Flow, Ar/N ₂ Plasma)	139
62.	Univariate Search for Minimisation of Na Interference (Plasma Ar Flow, Ar/Ar Plasma)	140
63.	Univariate Search for Minimisation of Na Interference (Plasma Ar Flow, Ar/N ₂ Plasma)	142
64.	Univariate Search for Minimisation of Na Interference (Coolant Ar Flow, Ar/Ar Plasma)	143
65.	Univariate Search for Minimisation of Na Interference (Coolant N ₂ Flow, Ar/N ₂ Plasma)	144
66.	Univariate Search for Minimisation of Na Interference (Power, Ar/Ar Plasma)	145
67.	Univariate Search for Minimisation of Na Interference (Power, Ar/N ₂ Plasma)	147
68.	Ar/N ₂ Plasma H ₂ O Blank	178
69.	Ar/Ar Plasma H ₂ O Blank	179
70.	Effect of Na on the Mn 257.6 nm Ion Line Emission Profile (Ar/Ar Plasma)	183

INDEX TO TABLES

<u>Table</u>	<u>Page</u>
1. Comparison of Nebuliser Systems	41
2. Comparison of Optimised Torch Conditions	41
3. Comparison of 4 and 16 mm Slit Height Optimal Conditions	89
4. Spectral Lines Used for Optimisation Experiments in this Work	89
5. Optimal Operating Conditions for N ₂ Cooled and All Ar Plasmas	90
6. Spectral Lines Used for Optimisation Experiments in Greenfield's Work (157)	99
7. Linear Regression Data on Optimum Power Results	99
8. Spread of Optimal Conditions for N ₂ Cooled and All Argon Plasmas	103
9. Effect of Compromise Conditions on SBR	106
10. Effect of Minimisation of Na Interference on SBR	148
11. Ti Al Analysis	158
12. Al TiB Analysis	160
13. BATS 79 Analysis	162
14. Standard BATS Analysis	163
15. Cr Metal Analysis	164
16. Tungsten Carbide Analysis	166
17. Cr Al Analysis	168
18. Si Al Analysis	170
19. BCS Steels Analysis	172
20. Comparison of Signal and Noise Levels at Optimum Conditions for Mn Atom and Ion Lines in N ₂ Cooled and All Ar Plasmas	177

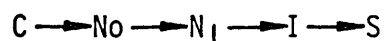
1. INTRODUCTION

1.1 THEORY OF EMISSION SPECTROSCOPY

The process of emission spectral analysis can be summarised as a number of steps -

- i) transition of atoms of the element under study in the example into the gaseous state in the excitation source ($C \rightarrow N_0$);
- ii) transition of a certain number of these atoms into the excited state ($N_0 \rightarrow N_1$);
- iii) spontaneous transition of the excited state atoms to the ground state with the emission of spectral line radiation ($N_1 \rightarrow I$);
- iv) selection of the radiation of the line of interest from the total radiation of the source by spectral instrument, and its transformation by the recording system into a measurable signal from the line under study ($I \rightarrow S$).

The whole procedure can hence be represented schematically:-



Consider first the transition $N_0 \rightarrow N_1$ where N_0 is the number of atoms in the ground state and N_1 is the number of atoms in the first excited state (i.e. a 'resonance' transition).

In the general case, where collisions with electrons are the dominant excitation process, statistical thermodynamics gives the following relation (1)

$$N_1 = \frac{1}{1 + R/N_e} g_1/g_0 N_0 \exp -(E/KT) \quad (i)$$

Where

- N_1 = number of atoms in state 1 per unit volume
- N_0 = number of atoms in state 0 per unit volume
- N_e = number of electrons per unit volume
- g_1 = statistical weight of level 1
- g_0 = statistical weight of level 0
- E = Energy difference between states 1 and 0
- K = Boltzmann constant
- T = thermodynamic temperature
- R = ratio of radiation and radiationless quenching transition rates

As the system approaches thermodynamic equilibrium such that N_e is very large as compared to R , the R/N_e approaches zero and hence

$$\frac{N_1}{N_0} = g_1/g_0 \exp -(E/KT) \quad (ii)$$

Which is known as the 'Boltzmann formula'.

To make this formula useful to the analytical spectroscopist it is necessary to relate the number of atoms in the excited state to the total number of atoms present i.e. the concentration of the analyte species. The total concentration of atoms N is given by the sum of the concentrations in each state, thus

$$N = \sum_{i=0}^{i=n} N_i$$

where n is the highest state that must be considered in the summation. It is convenient to define a quantity that expresses the population of states as a function of temperature known as the 'partition function', (2)

$$Z(t) = \sum_{i=0}^{i=n} g_i \exp(-E_i/kT) \quad (\text{iii})$$

and hence rewriting equation (ii) gives

$$\frac{N_1}{N} = \frac{g_1 \exp(-E_1/kT)}{Z(t)} \quad (\text{iv})$$

Consider now the next step in the process where spontaneous transition of atoms from the upper excited state to the ground state causes emission of radiation. ($N_1 \rightarrow I$). The probability per second that an atom in state 1 will spontaneously radiate its energy and return to the ground state is given by the Einstein Coefficient A_{10} . The energy given out by the emitted photon is equal to the energy difference between the two states E . Hence the power emitted from a small volume ΔV of the source is given by (2) :-

$$P = h\nu_0 A_{10} \Delta V N_1 \quad (\text{v})$$

where:- h = Planck's constant

ν_0 = frequency of the emitted photons

Since only a small amount of the total power emitted from the source can be detected by the spectrometer, it is more useful to

express equation (v) in terms of brightness (B).

B is defined as the power emitted per unit area per unit solid angle, so that equation (v) is divided by 4π to give the power per steradian, and by a unit area to give:-

$$B = \frac{h \cdot \nu_0 \cdot A_{10} \cdot L \cdot N_1}{4\pi} \quad (\text{vi})$$

Where L is the depth of the source along the viewing axis. The radiated photons are not monochromatic but are spread over a range of frequencies distributed about the central frequency ν_0 . The spectral profile of the line is usually expressed in the form of a normalised integral (2) such that $\beta(\nu) d\nu$ is the fraction of photons having frequencies in the range ν to $(\nu + d\nu)$ and

$$\int_0^{\infty} \beta(\nu) d\nu = 1 \quad (\text{vii})$$

So that B in equation (vi) is the integrated output, which is analytically more useful since spectrometers usually have a bandpass which is larger than the natural width of the analytical line.

Now, substituting for N_1 (from equation (iv)) into equation (vi), a relationship between the brightness of the source and the number of atoms of the analyte species can be obtained hence:-

$$B = \frac{1 \cdot h\nu_0 \cdot L \cdot N \cdot g_1 \cdot A_{10} \cdot \exp(-E/kT)}{4\pi \cdot Z(t)} \quad (\text{viii})$$

It must be noted that this equation is only an approximation for real atomic emission sources, since the assumptions made

in the derivation of equation (vii) are for that of an 'ideal source' and do not always apply in practice. For low concentrations of analyte, where self absorption is negligible, equation (vii) predicts a straight line calibration graph, as B is directly proportional to N. Another important consequence of equation (vii) is that B increases with increasing temperature and hence the best analytical sensitivity will be obtained with a high temperature source.

1.2 SOURCES FOR ATOMIC EMISSION SPECTROSCOPY

1.2.1 THE COMBUSTION FLAME

The flame was probably the earliest source to be used for atomic emission analysis, by Bunsen and Kirchoff (3) who pioneered the techniques observing the emission from easily ionised elements with a simple spectroscope. The flame has been mostly used in the analysis of solution samples, where the sample is introduced in the form of an aerosol.

There are a number of problems associated with flames. The degree of dissociation of molecules containing the analyte elements depends on the temperature and chemical composition of the flame. Formation of refractory compounds, particularly oxides in the flame can cause severe depressions of signals. This can be overcome to some extent by the use of flames enriched with a combustible gas, or reducing flames (e.g. $N_2O - C_2H_2$) (4,5,6)

The composition of the mixture of gases, also governs the temperature of the flame and hence the concentration of excited atoms of the analyte elements (see section 1.1). In traditional low-temperature flames (e.g. air-acetylene and air-propane with $T = 2100 - 2500K$) only easily ionised elements are excited. Flames with $T = 3000 - 3200K$ (hydrogen-oxygen, acetylene-oxygen,

propane-oxygen, acetylene-nitrous oxide) have been used for the analysis of both easily excited elements and elements traditionally more difficult to excite in flames (e.g. 6).

In the dicyanogen-oxygen and dicyanogen ozone flames temperatures reach 5000K or over, but these flames are hardly ever used in analytical practice due to the toxicity of cyanogen. In recent years the flame has been used more successfully (AAS), and its use for emission work is normally restricted to easily ionisable elements (e.g. Na, K, Li).

1.2.2 ARCS AND SPARKS

Arc and spark atomic emission sources are mainly used for the analysis of solid samples.

An arc is a continuous electrical discharge of high energy between two electrodes in which gas molecules and atoms in the discharge are ionised to form a thermal plasma from which radiation is emitted. The sample is usually packed into an anode electrode or, in the case of metallurgical analysis, the sample itself becomes the anode. An arc is struck between the two electrodes, and sample is vaporised and sputtered into the plasma region where excitation and emission occur. Relatively large amounts of sample are excited and hence detection limits are low, the discharge is however, relatively unstable due to random movement of the arc producing poor precision of 15% r.s.d. or worse.

By producing an intermittent discharge, as in the spark source, precision can be greatly improved with, however, a degradation in detection limit due to the relatively small amounts of sample volatilised (a few mg as compared to tens of mg in the arc).

Modern electrical discharge sources combine the characteristics of both the arc and spark to optimise both detectability and precision.

Further improvements have been made by sheathing the electrodes in inert gas helping to reduce background and stabilise the discharge.

There is an extensive bibliography on the theory, use and applications of arc and spark sources (e.g. 7,8,9).

The main disadvantages of this type of source for quantitative analysis, is its restriction to solid samples (although solutions can be analysed with some degree of success using the 'rotrode' (10)), because the sample is usually a solid, selective volatilisation can cause problems, and many interelement matrix effects are observed.

1.2.3 THE GRIMM GLOW DISCHARGE LAMP

The low pressure discharge lamp as described by Grimm (11) has been shown to be an interesting source for atomic emission analysis of solid samples. The sample is presented in the form of a conducting solid disc (non conducting samples must be mixed with a conducting material and pressed into a pellet). The sample is clamped onto the discharge chamber and is pumped down to 500 Pa and flush with inert gas. The discharge is initiated causing sputtering of small amounts of sample into the excitation region, which is viewed through a quartz window.

The calibration graphs are linear over a wide range of concentrations. Precision is good and interelement effects are found to be small. The method has been applied successfully to the analysis of metals (e.g. 12,13) and other materials (e.g.14).

1.2.4 THE HOLLOW CATHODE LAMP

The hollow cathode lamp is similar in many respects to the glow discharge source previously described. The sample again has to be in the form of a conducting solid. In the case of metal samples these are machined into cylindrical cavities which in themselves form the cathode. For non-conducting solids or solutions these are coated onto a metal or graphite hollow cathode (15). The cathode is mounted in a low pressure container, flushed with inert gas. A membrane separates the zones of excitation and evaporation which stabilises the discharge. When current is passed through the lamp sample is sputtered off the inside of the cathode, the resulting emission being observed through a quartz window.

The main use of the hollow cathode lamp (HCL) in recent years has been as a line source for atomic absorption spectrometry as first carried out by Walsh (16). The HCL, however, offers a number of features which make it attractive as a source for atomic emission (15):

- i) selective volatilisation
- ii) high stability;
- iii) high sensitivity for a wide range of elements;
- iv) refractory oxide formation is eliminated due to the inert gas atmosphere;
- v) low background;
- vi) sharp spectral lines due to the low pressure and temperature broadening effects.

Drawbacks to the HCL and Grimm's lamp are the preparation procedures for presenting non-conducting samples, and the necessity to

dismantle the source between successive samples can make analysis a lengthy procedure.

1.2.5 THE CARBON FURNACE

The carbon furnace, originally developed as an atom cell for AAS, has been used successfully as an atomic emission source (e.g. 17,18). The furnace usually consists of a graphite tube which is resistively heated. Sample in the form of solution is pipetted into the tube, or a few mg of solid sample can be placed in the tube. The tube flushed in an inert gas to prevent oxidation is heated in stages to evaporate the solution to dryness and to pyrolyse unwanted organic matrix. At the atomisation stage the tube is rapidly heated to temperatures of 2 - 3000°C producing a transient emission signal viewed along the axis of the tube.

Using this method very low detection limits can be obtained for a wide range of elements. The linear range is, however, small, and background is high and must be corrected for, the small sample size can cause low precision and inhomogeneous sampling and the relatively low temperature of the source prevents the excitation of some of the more refractory elements.

1.2.6 PLASMAS

The term 'plasma' is often used to describe any mass of 'hot' gas. In fact it has a much more exact physical definition concerning the degree of ionisation, temperature and size (19) of the system. For the purpose of this work the term 'plasma' will be used to describe one of four different types of atomic emission source:

- 1) the d.c. arc plasma (DCP);
- 2) the capacitively coupled plasma (CCP);
- 3) the microWave induced plasma (MIP);
- 4) the inductively coupled plasma (ICP)..

1.2.7 THE d.c. ARC PLASMA

The DCP is essentially a d.c. arc struck between two or more electrodes and stabilised by a flow of inert gas. The sample is introduced into the stabilising gas in the form of an aerosol produced by nebulisation which passes into the plasma where excitation occurs.

The development of the DCP has been reviewed by Kiers and Vickers (20) and Greenfield (21).

The most recent and perhaps successful DCP system is a commercial three electrode system which produces a stable 'Y' shaped discharge (22). Very low detection limits for a wide range elements are obtainable using the DCP with a wide dynamic range. The main disadvantages of the DCP are that, the discharge is in direct contact with the electrodes giving rise to contamination problems, the sample may pass around, rather than through, the plasma and hence the maximum excitation is not experienced by the analyte, and severe matrix effects are observed when the sample contains moderate amounts of easily ionisable elements.

1.2.8 THE CAPACITIVELY COUPLED HIGH FREQUENCY PLASMA

The CCP is formed between the plates of a capacitor in a high frequency circuit. One of the plates usually has a pointed electrode which concentrates the lines of force and at which the plasma is formed. Various methods for the introduction of sample have been used (21). As the plasma is in contact with the electrodes contamination problems occur, and easily ionisable elements can affect the plasma (21).

Of the four plasma sources considered the CCP is perhaps the least common.

1.2.9 THE MICROWAVE INDUCED PLASMA

The MIP derives its power from a high frequency (2450 MHz) magnetron at powers of 100W to 1KW. The magnetron is coupled via a waveguide and resonance cavity producing either a capacitively coupled, or, more commonly, inductively coupled plasma. The inductively coupled plasma is usually sustained in a small bore (2mm i.d.) quartz tube, with flow of Ar or He. The source is characterised by high electron temperatures and low excitation temperatures, (2) consequently elements which cannot be excited in the other plasma types can be excited in the MIP (e.g. halogens). The main problem with this source is that it is easily extinguished by large quantities of water or other solvents (23). Consequently the source has found popularity as a detector in gas chromatography (24,25) where only small amounts of sample in the form of gas are passed into the plasma, and the wide range of elements detectable can be utilised.

1.2.10 THE INDUCTIVELY COUPLED PLASMA

THE ICP originally developed in the early 1960s, has gained much popularity over recent years. The source utilises high frequency (7 - 50 MHz) applied to a coil at powers of (0.5 - 15KW) to induce a discharge in an argon or nitrogen/argon gas flow.

Since this work utilises the ICP, a more detailed discussion of the development of this source and its spectroscopic analytical properties will follow.

1.3 HISTORY AND DEVELOPMENT OF THE ICP

1.3.1 It is generally agreed that Babat's work first published in 1942 in Russian (26), and later in English (27), was the forerunner of the ICP used today. Babat found that a ring discharge, once established could be maintained while the pressure was raised to

atmospheric pressure. Electrodeless discharges up to this time were well known but were formed at low pressures. Using a HF (2 to 77 MHz) push-pull vacuum tube oscillator, of his own construction, Babat was able to reach power outputs of 100kW. With a quartz cylinder 15 cm in diameter and 150 cm long containing air at pressures from 0.1 to 760 torr he produced powerful, and what must have been quite spectacular electrodeless discharges. The induction coil used was of about five turns and made from square section copper tube (1 x 1 cm). The discharge or plasma was initiated successfully at atmospheric pressure with a NaCl seeded flame and also a dc arc.

Babat's work was concerned only with static non-flowing plasmas, and it was not until 1961, with the work of Reed (28), that flowing plasmas were reported. The plasma was formed in a single quartz tube mounted in a brass base, with a tangential gas inlet at the base giving a vortex gas flow, which helped to stabilise the discharge, and prevent it 'blowing' out of the tube. The plasma was initiated by an inductively heated carbon rod downstream from the main plasma. Different mixtures of gases were used, but argon was found to be the simplest gas in which to start and generate the plasma. In a paper published later on in 1961 (29), Reed described a torch with three concentric silica tubes with a centre powder feed which he used for crystal growing. This torch formed the basic design for ICP torches used today, which have changed very little from the Reed design.

In 1963 the ICP was first put to use as a spectroscopic source by Greenfield and co-workers who made a patent application for a plasma torch (30,31). It was Greenfield who made the next important modification of the plasma by forming an annular shaped discharge. The torch is described in Greenfield's review (32). "This (the torch) consisted of three concentric tubes. The two outer quartz tubes were used to contain the plasma, and the inner tube, of borosilicate glass, was used to inject an aerosol through the plasma

once it was formed. The torch was concentric with the work coil of the generator, which in this case was a 2.5 KW 36 MHz generator. Argon was fed tangentially into the inner quartz tube, the HF field applied by the work coil and a pilot plasma produced by a Tesla coil or graphite rod. Once the plasma formed, argon was introduced tangentially into the outer tube to stabilise the plasma and keep it off the walls of the cell. A hole was then punched through the flattened base of the plasma by the introduction through the injector of an aerosol in argon. The aerosol entered the torch, passed through a tunnel of plasma, and a long narrow tail flame resulted, it was the tail flame which was used as a spectroscopic source." The torch described above was reported by Greenfield in 1964 (33) and this is the first paper to actually describe the use of an ICP as a potential source for atomic emission analysis.

At first there was some disagreement about the desirability of an axial channel through the centre of the plasma. In 1965 Wendt and Fassel (34) used a laminar flow torch arrangement, which produced a 'solid' ellipsoidal plasma similar to that produced by Reed (28,29), claiming an advantage of less turbulence over the vortex flow arrangement. Veillon and Margoshes (35) used a similar arrangement, but failed to include the injector tube at all. They reported serious solute vaporisation interferences resulting, presumably, from the inefficient heating of analyte as it passed around instead of through the discharge.

One of the earliest features of the ICP to be discovered is its relative freedom from interference effects. Greenfield in his early ICP paper (33) found that the well known interference of phosphorus and aluminium with the emission from calcium was completely eliminated.

Further papers were published by Greenfield on the uses of different gases in forming the plasma (36), and the use of a high power low frequency (6 MHz 25 kW) generator (37) and its application to the determination of phosphorus and phosphate in rock. Other workers

were now also beginning to publish papers giving examples of analytical applications and properties of the inductively coupled plasma discharge (38,39).

It was not until 1969 when Dickinson and Fassel (40) achieved powers of detection superior to any ICP values previously published, that the technique seemed to offer a powerful analytical tool to rival atomic absorption spectrometry. Dickinson and Fassel used a three tube torch similar to the original Greenfield (30,31) design but smaller, with an ultra-sonic nebuliser for sample introduction. they attributed their greatly reduced detection limits to:

- (a) the desolvation of the nebulised solution before introduction of the sample into the plasma;
- (b) the development of the plasma shape from "tear-drop" to toroidal, to allow more efficient introduction of aerosol into the plasma (Fassel had obviously found that the central channel advocated by Greenfield (9) was an improvement over the ellipsoidal plasma);
- (c) the addition of a remote tuning facility for optimal coupling of the generator to the plasma.

Detection limits for all the elements investigated (Ce, Ta, Th, U, Zr, Hf) all fell in the ng.cm^{-3} range, and for many metals linear concentration ranges of 2 - 4 orders of magnitude were obtained. Other papers also showed the sensitivity and versatility of the ICP. Greenfield (41) showed that determinations at the ppm ($\mu\text{g.cm}^{-3}$) level could be carried out on mm^3 quantities of sample of solutions of inorganic and organic materials (e.g. blood and oil). Limits of detection for barium 1.7×10^{-10} g, and aluminium 1.1×10^{-9} g were obtained with relative standard deviations between 3 and 5%.

Kirkbright (42), using a nitrogen flushed spectrometer, was able to obtain detection limits of 1.7 ppm for sulphur and 0.15 ppm for phosphorus. The linear range extended over 5 orders of magnitude for these two elements, to above 1000 ppm. In an extension of this work Kirkbright (42) determined iodine, mercury, arsenic and selenium.

Some workers (44,45,) were interested in the introduction of solids, in the form of powders, qualitative results were quite easily established, quantitative analysis was found to be more difficult.

The ICP was also compared to other analytical methods. In 1972 Boumans and de Boer (46) compared an ICP with an argon separated nitrous oxide/acetylene flame. They found the stability of the plasma to be comparable with the flame.

Fassel (24) reviewed "Electrical Flames" and concluded that the detection limits which could be obtained with the ICP were, with few exceptions, comparable with or greatly superior to, the best which could be obtained with flame atomic absorption, emission or fluorescence. He also confirmed that a plasma similar in configuration to his own and that of Greenfield (33) was free from matrix effects experienced by Veillon and Margoshes(35).

Kirkbright and Ward (42) predicted, using a theoretical model, the characteristics of an ICP for optical emission analysis compared to an inert gas shielded nitrous oxide/acetylene flame. A longer linear calibration range was predicted for the plasma source owing to the greater freedom from self-absorption under optimum operating conditions, and the long residence time of the analyte species was expected to produce freedom from solute vaporisation effects. The predictions were verified experimentally and the advantages of the use of the plasma source were demonstrated in the analysis of aluminium alloys for a number of metals.

Fassel and Kniseley(49) published an assessment of the ICP compared with other techniques and again confirmed its overall superiority, and that it was a promising excitation source for multielement analysis. Greenfield in his review (32) pointed out that it was not just 'promising' but had been in everyday use for practical analysis for four years in his laboratory. In a paper published in 1975 (50) Greenfield gives details of an ICP coupled to a 30 channel direct reading spectrometer with fully automatic sequential sampling and read-out. The read-out was processed by an off-line computer. With this equipment he was able to perform simultaneous multielement analysis at both trace and major levels.

In recent years (1976 - 1980), the ICP has been reviewed by a number of authors. Greenfield (51,21,32) has reviewed plasma jets, microwave, capacitatively coupled sources, and the ICP in a three part article. Barnes (52) has produced an extensive review of the literature up to 1978 with 331 references. Sharp's review (2) contains some theoretical considerations of emission spectrometry. These reviews include that of Fassel (53,54) de Galan (55,56) Barnes (57,58) and Robin (59).

The wide range of applications papers that have appeared in the literature shows that ICP atomic emission has been widely accepted as an instrumental method for multi-element analysis. These applications include determinations of trace elements in soft, hard and saline waters (60,61,62,63) major and trace elements in geological materials (64,65,66,67) analysis of steels and many other alloys in the metallurgical field (69,70,71,72,73,74a,74b,75,76 77,78,79), trace elements in foods and beverages (80,81,82,83,84,85) and the analysis of trace elements in biological samples. (76,86.87, 88,89,90,91). The use of the ICP has not only been restricted to atomic emission spectroscopy; atomic absorption spectroscopy (AAS) and atomic fluorescence spectroscopy (AFS) has also been studied. Wendt and Fassel (92) Greenfield (93), Barnett (94,95), Bordonali

(96,97) and Veillon and Margosnes (98) made exploratory measurements with ICP - AAS. Bordonali and Biancifiori (97) also received a patent in 1972 covering the analysis of trace elements by ICP - AAS. Magyar (99) has coupled an AA spectrometer by a periscope type arrangement to an ICP source for AA measurements of elements not easily excited by flames. Application of the ICP in emission rather than absorption has, however, proved to be more widely accepted, even in the light of the recent evaluation by Abdallah (100) who suggested reasons for the limited success in early measurements.

The use of the ICP as an atom reservoir for AFS has been studied by Montaser (101) using electrodeless discharge lamps as the excitation source, and Epstein (102) who used pulsed dye laser excitation. The plasma itself, whilst aspirating a solution of the relevant element, has been used as the excitation source for flame AFS by Epstein (103) and Omenetto (104).

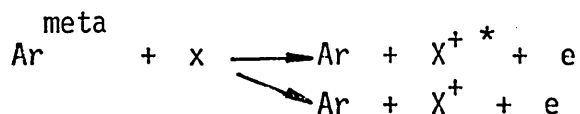
A more novel application of the ICP has been its use as a detector in gas (105,106) and liquid (107) chromatography.

Much work has gone into understanding the processes that form the plasma and the mechanisms that occur within it. Greenfield (31) has reviewed the earlier papers on plasma measurements, and diagnostics, but as Barnes points out (5i) these earlier papers have used widely different systems at dissimilar conditions.

More recently Mermet (108,109,110,111,112,113), Kalnicky (114,115) and Kornblum (116,117,118) have reported and reviewed work designed to elucidate mechanisms in the plasma, using more nearly comparable conditions. Major spectroscopic investigations of interferences were performed by Fassel (119,120,115) Kornblum and de Galan (118), Mermet (110,111) and Boumans and de Boer (121,122,123,124).

Spatial distributions of the spectroscopic measurements have been made, using the mathematical technique of Abel inversion transformations, by Kornblum and de Galan (116,117,118) and Kalnicky (114,115).

Recently Jarosz (125) reported results of a new study of smoothing experimental curves for Abel transformation. From this and other work (108,109,110,114,115,116,126) an appraisal of the existence of local thermodynamic equilibrium (LTE) in all argon plasmas has been made. The results of these studies show that LTE does not exist in the all argon plasma. This has led to the suggestion of a non-thermal excitation mechanism (127) involving collisions of the second kind with argon metastables, known as "Penning" ionisation:



This is particularly attractive since the excitation energies of the metastable argon levels of 11.55 and 11.71 e V (127) correspond well with the excitation energies of singly ionised species found in the plasma.

In a recent study Alder et al (126) have shown that, although the central channel of the plasma system under consideration was not in LTE, the presence of water in the analyte aerosol passing through the plasma increases the electron density and hence the ionisation and excitation temperatures. They conclude that a high electron temperature would considerably reduce the importance of analyte ionisation via Penning ionisation and hence that analyte excitation and ionisation in the ICP are primarily dominated by electrons.

1.3.2 ANALYTICAL ADVANTAGES OF THE ICP AS AN EMISSION SOURCE

In summarising the properties of the ICP there are four main advantages of the source attractive to analytical spectroscopists:

- 1) multi-element capability;
- 2) low detection limits, due to the high temperatures experienced by the analyte passing through the plasma (6 - 7000K) and the inherent low background of the source;
- 3) the source is optically 'thin' and linear calibration ranges of 4 - 5 orders of magnitude are widely reported;
- 4) relative freedom from interference effects compared with other techniques (particularly arc/spark sources and possibly AAS).

As Greenfield has commented (128): "In all probability the ideal source for all OES (optical emission spectrometry) will never be found." He then goes on to list some properties that an ideal source would have:

- i) applicability to all states of matter;
- ii) capability of exciting lines of a large number of elements;
- iii) a wide dynamic concentration range free from matrix effects;
- iv) freedom from interference;
- v) convenience of operation;

vi) low purchase, operation and maintenance costs;

vii) high precision and detectability.

He then continues: "of all sources currently available, the inductively coupled plasma torch most nearly satisfies these criteria."

1.4 OBJECTIVES OF THIS WORK

The purpose of this study is to apply the ICP to the detection of trace and major elements in alloys whose major constituents (e.g. B, Ti, Si, W,) are highly refractory. Presently such alloys are analysed by a number of different analytical techniques in the sponsoring Company's laboratory (London Scandinavian Metallurgical Company), these include AAS, x-ray fluorescence, d.c. arc direct reader emission spectrometry, neutron capture, and wet-chemical methods. The ICP, because of its low limits of detection, multi-element capability and long linear calibration ranges, offers a potential method for analysing such alloys for both major and trace constituents with one technique.

Since there are relatively few ICP systems being used for routine analysis of metallurgical samples as compared, for example, to the well documented arc and spark emission sources, there is very little data on the methods and problems that might be encountered when using an ICP for this particular type of analysis. Evaluation of the ICP for this task, therefore, presents a number of questions. Firstly sample preparation; samples for this work will be presented in the form of solutions. Methods of dissolution which have worked well when only one or two elements are to be determined may not produce quantitative solutions of all the elements when multi-element analysis is to be carried out, and this must be examined.

Having prepared the sample in a suitable manner for analysis one finds that the spectral emission lines in an ICP are different from those found in arc and spark tables and hence the best lines for different concentrations of elements with minimum spectral interference have to be chosen.

Finally, since ICP systems in present use are far from standardised, using different torch designs, plasma gases and, in particular, different applied powers, it is necessary to find out which system will be analytically most useful. This can only be sensibly achieved by making comparisons between systems operated at optimum conditions.

The utilisation of the 'Simplex' optimisation technique in this study, as applied to the many variables which are thought to effect excitation of particular lines has given some insight into which parameters are most important, and how each parameter relates to the others. Using this optimisation procedure with a variety of plasma torch configurations, plasma gases, and matrices useful evidence should be obtained not only for the optimisation of analytical parameters, but also on excitation processes.

The fundamental insights gained as outlined above will be used to develop a flexible analytical system for the analysis of a range of metallurgical samples not favourable to analysis by other techniques.

2. INSTRUMENTATION

A schematic diagram of the instrumentation used in this work is shown in Figure 1.

The ICP torch, which will be discussed in more detail later, is mounted concentrically in a 3 turn water cooled, copper induction coil. The RF power is supplied to the coil by a 5kW, 27MHz free running generator (Radyne R50P, Radyne, Wokingham, England).

The gas is supplied to the torch by a purpose-built 'gas-box', which contains five rotameters, allowing direct switching of the plasma from start up, to running conditions. The flow of coolant gas (which can be switched from argon to nitrogen or vice versa), plasma gas, and injector gas can be finely controlled from the gas box allowing optimum operating conditions to be obtained.

The analyte is introduced into the plasma in the form of an aerosol which is produced by an all glass pneumatic nebuliser, constructed in the manner of Scott (129). Solution is either drawn up at the natural up-take rate of the nebuliser, or is fed by a peristaltic pump (60 rpm 'Mini Pump', Schuco International, London, England) and the venturi effect produces a fine mist of analyte solution droplets. The larger droplets are removed using a double pass nebuliser chamber (Figure 2) and the resulting aerosol of analyte passes through the central injector tube of the torch into the plasma.

For the majority of the work carried out here the nebuliser has been pumped, in order to minimise interference effects due to changes in solution viscosity or sample 'head' which cause changes in uptake rate and hence apparent interference (149) in the plasma.

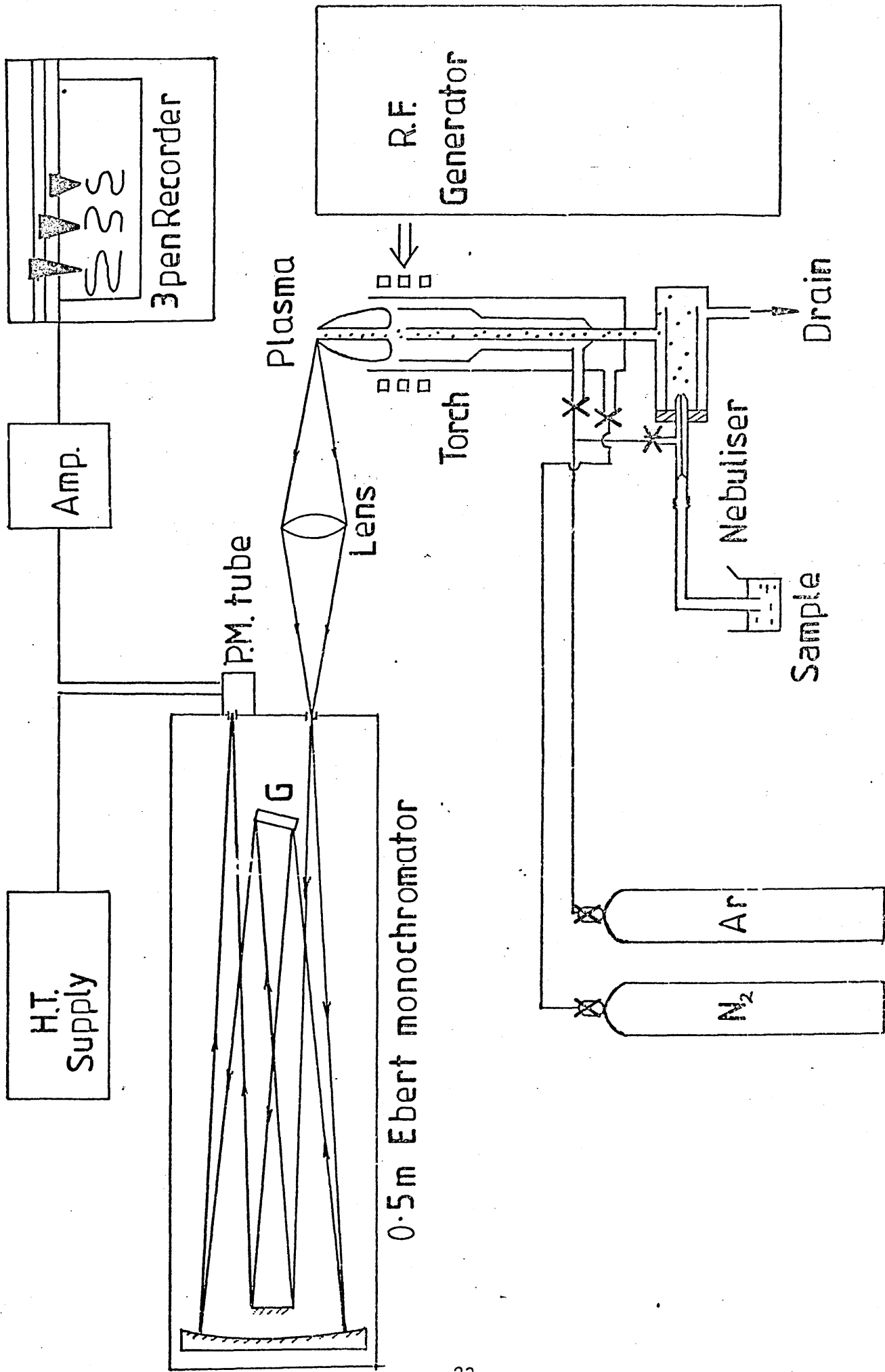
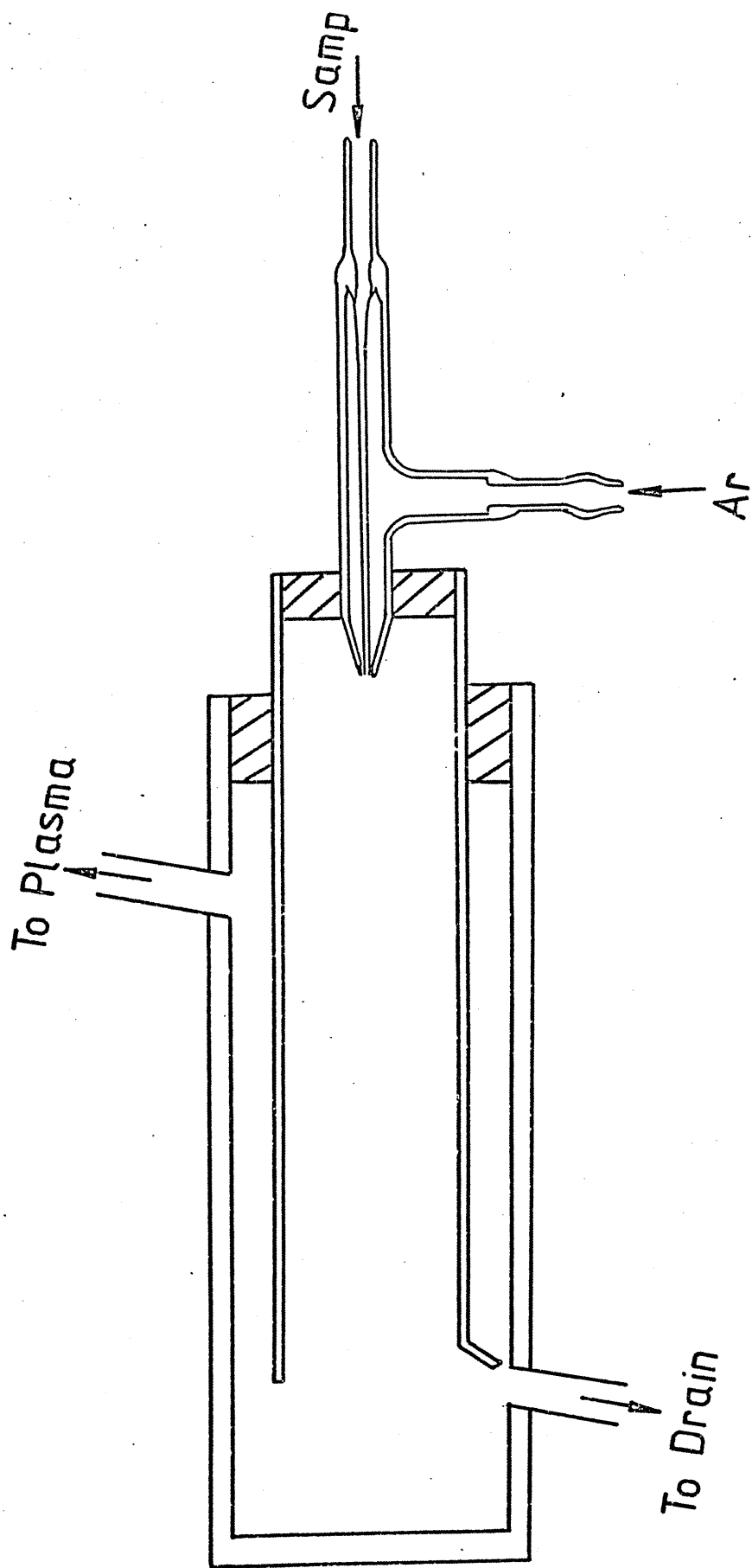


Fig 1



Double Pass Nebuliser Chamber

Fig 2

An image of the plasma is projected 1 : 1 onto the 25 μm entrance slit of the monochromator using a 2.5 cm focal length quartz lens. The spectroscopic lines of interest from the analyte species can then be selected by the 0.5 m Ebert scanning monochromator (Jarrel Ash (Europe), Le Locle, Switzerland). The radiation is then focussed via a 25 μm exit slit onto a Hamamatsu R106 photomultiplier tube which is operated at 600 - 1000V. The signal from the photomultiplier tube is amplified by a linear picoammeter (LM10; Chelsea Instruments Limited, London) and is fed into a three pen potentiometric chart recorder (Type MC641-32, Watnabe Instrument Corporation, Tokyo, Japan).

2.1 THE PLASMA TORCH

The ICP discharge tube arrangement provides a container through which the discharge gas flows and in which the discharge is created and maintained.

The three concentric tube design with tangential gas introduction first used by Reed (29) in his pioneering work, has not yet been superceded although the shapes of the tubes and the nature of the gas flows have been modified by several workers.

The basic construction is a three concentric tube arrangement with a narrow annulus between the outer and intermediate tube, through which a vortex flow of coolant gas is introduced (usually either argon or nitrogen), this helps to stabilise the plasma and to hold the discharge away from the torch walls to prevent melting of the outer silica tube. Plasma gas (usually argon) can be introduced between the inner tube and intermediate tube although in smaller torch designs this gas flow is often not required as the coolant gas is sufficient to provide cooling and also to sustain the plasma. Finally an inner tube or 'injector' which is normally 1 - 2 mm internal diameter, introduces the analyte aerosol in a flow of

argon with sufficient velocity to penetrate the base of the discharge.

The two torch designs which have been most widely used in analytical work are those of Greenfield et al. (50) and Fassel and Kniseley (49). Both designs are of fixed geometry but have different diameters (25 mm and 18 mm i.d. respectively) in keeping with the different diameters of the induction coils used by these two groups of workers. The torch of Fassel and Kniseley also incorporates a flared inner plasma tube, often referred to as the 'tulip configuration'. Modifications to these earlier designs have been carried out by a number of workers. By modifying computer models of the ICPs devised by Miller and Ayen (130) and Barnes and Schleicher (131), Allemand and Barnes (132) were able to design a streamline torch configuration. Their torch was machined from boron nitride with a flared inner tube which markedly reduced the consumption of coolant argon. Both Savage and Hieftje (133) and Allemand and Barnes (134) have constructed miniaturised torch designs. Kornblum et al. (135) have used a more novel arrangement in which the torch is water cooled, and in doing so have reduced their gas consumption by ten-fold.

Demountable configurations have also been used, in which a holder is employed into which the plasma torch tubing can be inserted or removed at will. These include torches used by Dickinson and Fassel (40), Boumans and De Boer (46), Alder and Mermet (112), Mermet (100,136), Ohls and Krefta (137), Lichte and Koirtychan (138), and Windsor (139).

Reed (29) recognised that plasma stability is achieved when the gases, particularly the coolant gas are introduced tangentially into the torch, producing a vortex flow.

Although plasmas can be operated with laminar flows, tangential flow is still the preferred method of gas introduction. Genna et al. (140) described a modification of the gas flow introduction which both promoted easy ignition and reduced coolant gas consumption. This was achieved by increasing the tangential velocity of the coolant gas by constructing a jet at the coolant gas entry orifice.

2.1.1 DESIGN CONSIDERATION FOR THE PLASMA TORCH USED IN THIS WORK

In designing a torch for this work advantageous features of different torch designs described in the literature were combined to produce the configuration shown in the scale diagram (Figure 3).

The following design criterion were used:

- 1) Demountable design to obtain maximum versatility and ease of exchange of tubes, as well as enabling the effects of injector and inner tube shapes to be investigated.
- 2) The use of a flared or 'tulip' shaped intermediate or plasma gas tube - a design favoured mainly in Fassel type torches but also predicted to be favourable for lower gas consumption and ease of ignition by Allemant (132) in his computer study.
- 3) The incorporation of removable tangential jets in the plasma gas and coolant gas entries - this follows directly the work of Genna (140) who showed that jet gas inlets could reduce the amount of gas needed to sustain the plasma.
- 4) The torch size, particularly the size of the outer tube was governed by the induction coil size, as

Demountable Plasma Torch

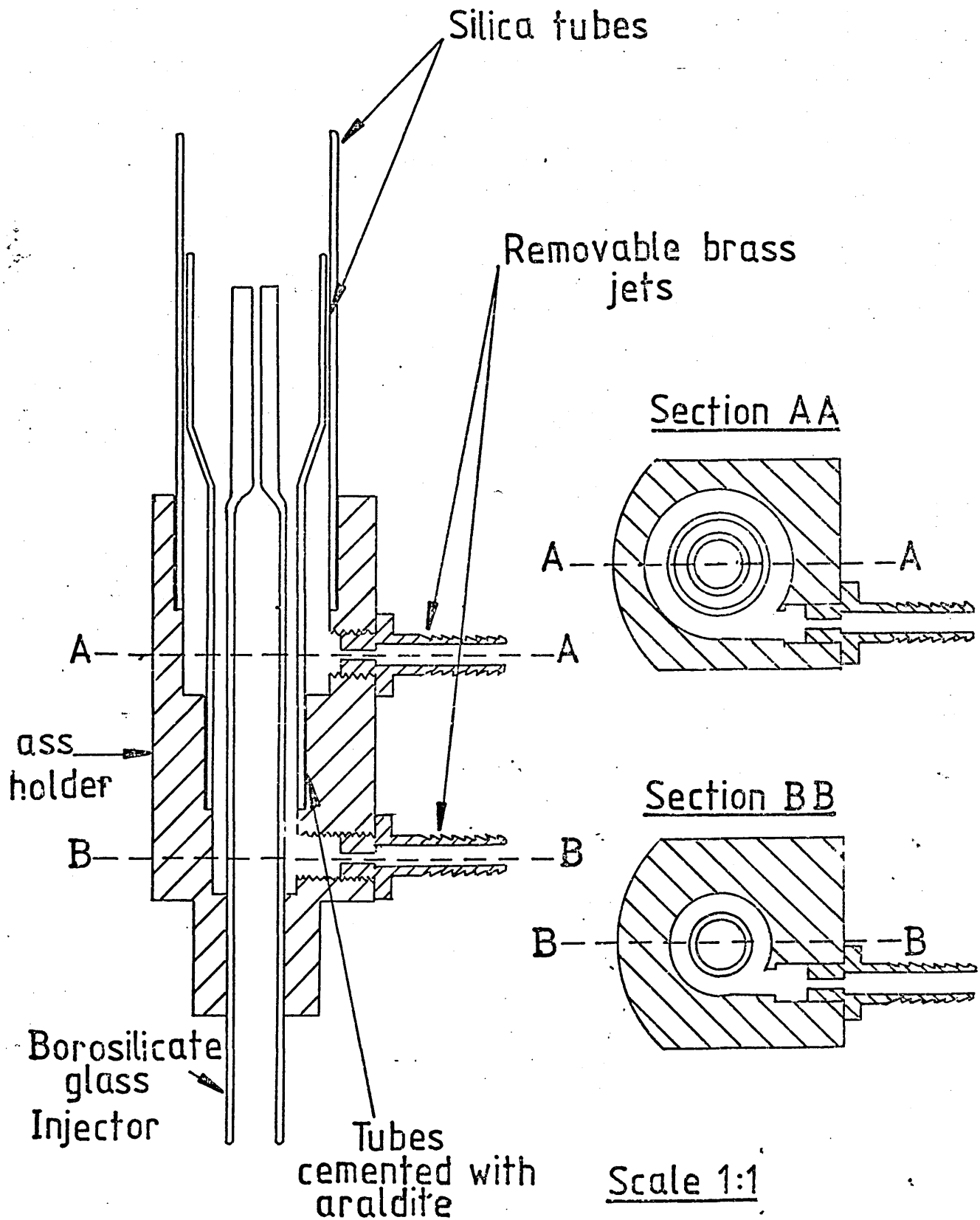


Fig 3

this was designed to take the larger Greenfield style torch.

- 5) The ability to operate on both argon and nitrogen coolant, in order to make comparisons between the two types of plasma.

2.1.2 TORCH CONSTRUCTION

Two silica tubes (1.5 mm thick) were mounted into a support machined from brass. Given the need to align the tubes precisely with a 0.5 mm annulus between outer and intermediate tube, the tubes were cemented into the support with an epoxy resin and held in position with a former while the glue hardened. It was not found practicable to maintain the close tolerance between the tubes using 'O' - ring seals.

The injector tube was made from borosilicate glass and was centered in the torch and held at a position 6 mm below the intermediate tube, with a former, whilst being cemented into the brass base. The tubes could then be removed from the base by pyrolysing the resin in a furnace at 3 - 400°C.

The gas inlets (removable threaded brass jets) were fitted tangentially as shown in Figure 3. A series of jets of differing sizes (1,2,3 and 4 mm i.d.) were prepared, enabling different gas velocities to be achieved.

The torch assembly was mounted on a nylon base plate which bolted onto the movable staging supplied with the generator to align the torch within the induction coil.

2.1.3 EVALUATION OF THE TORCH

The torch was evaluated by comparing the signal to background

ratio obtained with this new torch design operated under optimised conditions with the signal to background obtained when a two-piece Greenfield torch (50) was operated under optimal conditions. The method of optimisation and the results of the evaluation will be discussed later.

In general, the new torch was found to operate well over a wide range of gas flows with both nitrogen and argon coolant. Coolant gas flows as low as 1.5 l min^{-1} can be used without difficulty with an all argon plasma, and thus the total gas consumption can be as low as 3 l min^{-1} of argon, although these flows do not, as it will be shown, produce the best analytical performance.

2.2 SAMPLE INTRODUCTION

Sample introduction into the ICP of solids, liquids and gases has been extensively reviewed by Barnes (52). This work has been concerned with the continuous nebulisation of sample solutions into the plasma, and consequently only sample introduction systems of this type will be discussed here.

The production of aerosols by means of ultrasonic breakdown of liquids has been used with the ICP (e.g. 33,39,121,122). The ultrasonic nebuliser has been shown to produce superior limits of detection (due mainly to the increased amount of analyte supplied to the plasma) to pneumatic nebulisers. They have, however, not gained wide acceptance due to cost, problems with memory effects, and the requirement for desolvation apparatus to prevent the plasma from being extinguished.

The conventional concentric pneumatic nebulisers, made generally from metal, as used in flame spectrometry, are of limited use in ICP work because the high flow of gas required to operate them is too high for the optimum operating conditions of the plasma.

The two most commonly employed pneumatic nebulisers for ICP work are the all glass concentric nebuliser (141) (Figure 4a) and the cross flow nebuliser (142) (Figure 4b). The former consists of a narrow annulus, surrounding a narrow sample capillary. The high velocity flow of nebuliser gas produces reduced pressure at the capillary tip, drawing sample solution through the capillary, where it is shattered into a fine aerosol by the high velocity gas flow. The cross flow nebuliser operates in a similar manner; the nebuliser gas flow in this case is at 90° to the sample uptake capillary. Recently the cross flow design has been modified by Meddings et al. (143) (Figure 4c) and Novak et al. (144). These two sets of workers have realised that the original design required careful adjustment of the capillaries for optimum performance, and that these adjustments are required frequently to keep the nebuliser operating well over long periods of time. In the modified design the fine capillaries are replaced by more substantial glass tubes drawn down to fine jets at the ends, the jets are then positioned so that a given solution uptake rate is obtained at the required gas flow and pressure. The tubes are then fused together by a glass bar so that, once constructed, the nebuliser required no further adjustment. Meddings et al. using this modified design, with careful control of gas flows, have been able to obtain 0.5% r.s.d. in routine analysis in their laboratory.

The main disadvantage with the above mentioned nebulisers is that the sample solution has to pass through a narrow capillary (~ 0.5 mm i.d), so that care has to be taken that sample solutions contain no small particles which can block the nebuliser. It has been found that solutions containing high salt content (5 - 10%) can cause a build up of material at the capillary tip impairing nebuliser performance and eventually causing a blockage. Suddendorf and Boyer (145), and Woolcott and Sobel (146) have constructed nebulisers in which a narrow gas exit hole drilled in

the apex of a 'V' groove is mounted such that sample solution can be pumped along the groove (Figure 4d). When the solution encounters the high velocity flow of gas from the exit hole it is shattered into a fine aerosol which is suitable for introduction into the ICP. In this design the solution is not confined to a narrow capillary and hence clogging is not a problem. Solutions containing high salt content as well as high suspended solids (146) (e.g. tomato soup, milk of magnesia and evaporated milk) can be nebulised without problems.

Apel et al. (147) have developed a nebuliser in which the sample is pumped onto a fritted glass disc through which the nebuliser gas is passed producing an aerosol of sample solution (Figure 4e). The nebuliser is highly efficient but can handle only small sample solution flow rates, and some memory effects are observed.

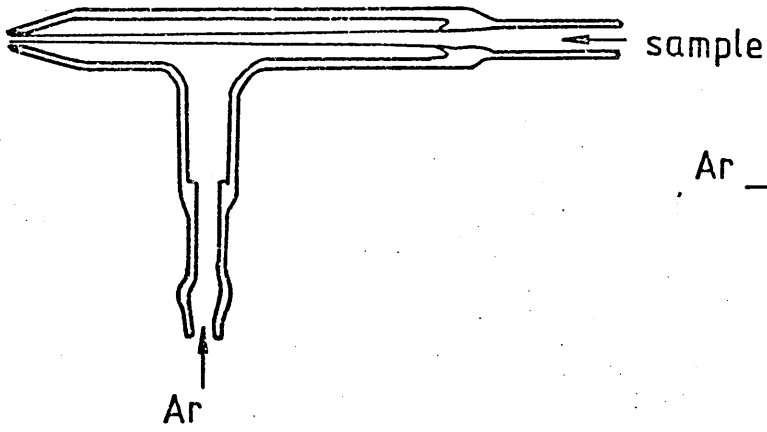
2.2.1 EVALUATION OF NEBULISER SYSTEMS FOR THIS WORK

Evaluation of nebuliser systems has been carried out in two stages. Firstly a commercial Meinhard nebuliser (T - 230 - A2) and a similar nebuliser constructed in the manner described by Scott (129) connected either to a cyclone type nebuliser chamber (Figure 5) (from an SP 900 flame spectrophotometer, Pye Unicam, Cambridge, England) or a 'double-pass' cloud chamber constructed in a manner similar to that described by Scott (148) (Figure 2) were used to determine the efficiencies (i.e. ratio of aerosol produced per unit time to ratio of solution uptake per unit time) of the four combinations of nebuliser systems.

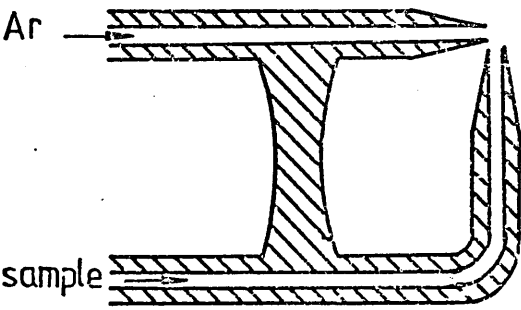
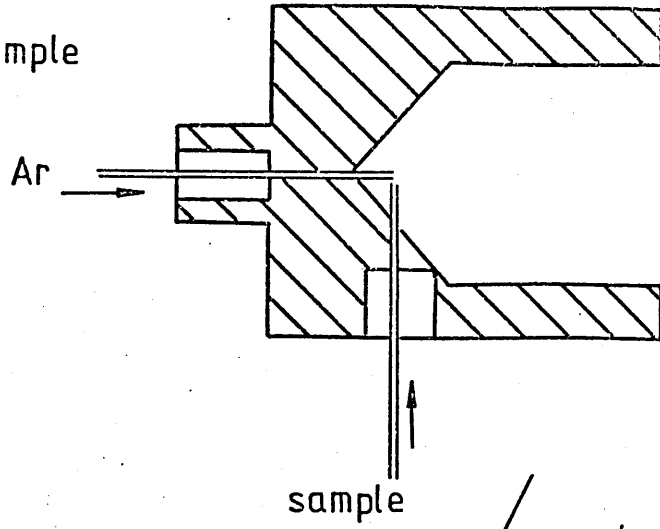
Secondly the nebuliser systems were then connected to the plasma, and the signal to noise ratios of each system, operated under identical conditions, were measured and compared.

Two 'high solids' nebuliser designs (as described in section 2.2) were also constructed, one from glass and plastic (Figure 6) and

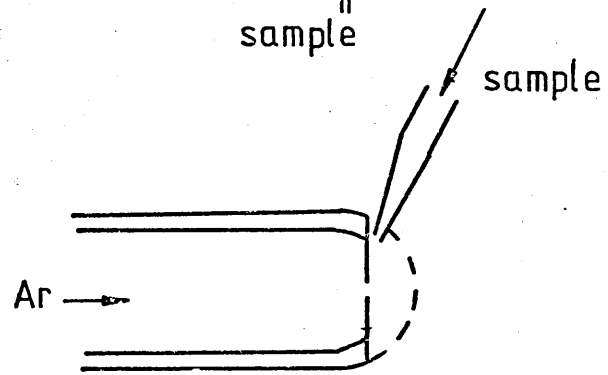
(a) glass concentric



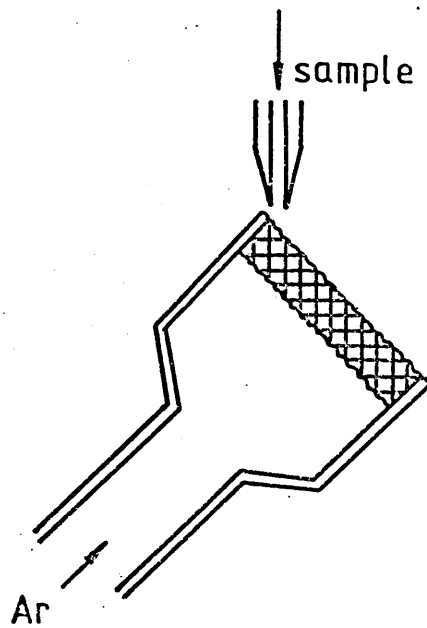
(b) cross-flow



(c) modified cross-flow

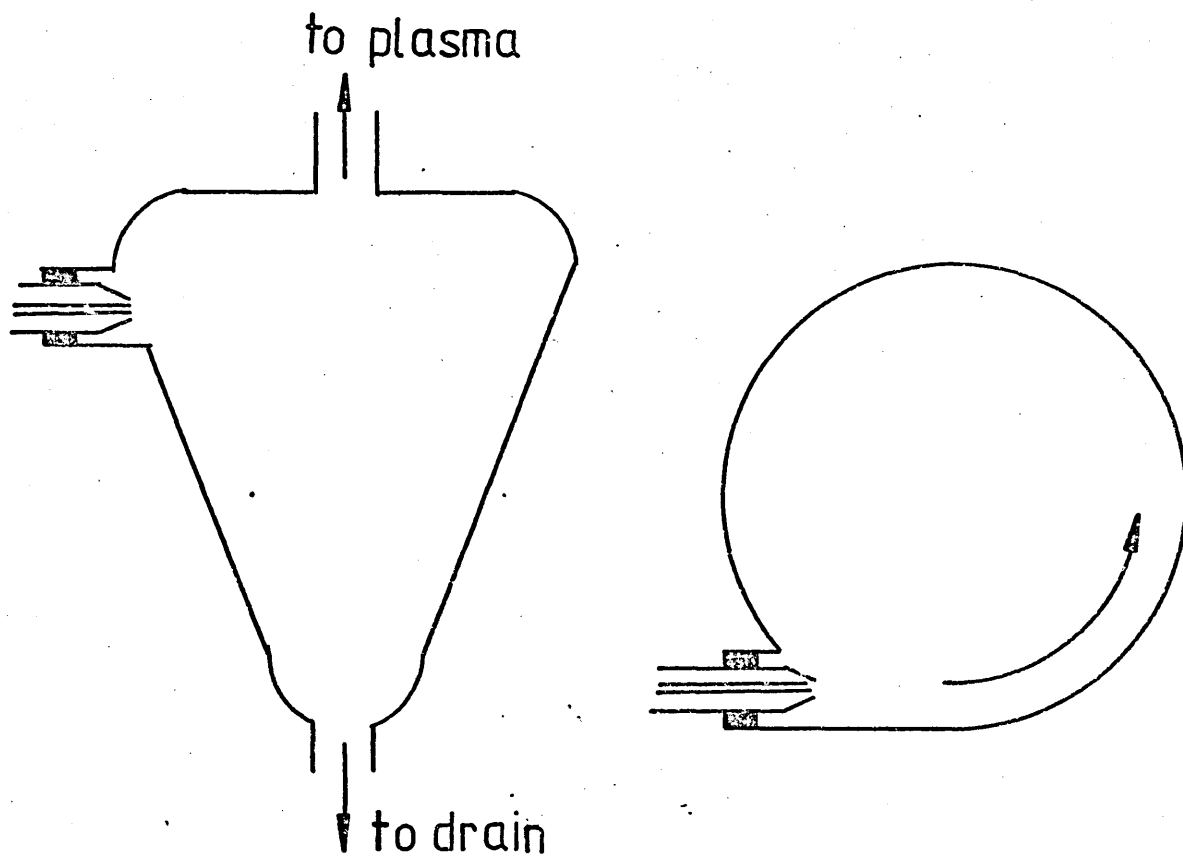


(d) high-solids



(e) fritted glass disc

Fig4



Vortex Nebuliser Chamber

Fig 5

one from teflon (Figure 7). Preliminary comparisons of the signal to noise ratios of these nebulisers were compared to those obtained with the constructed all glass concentric design using identical operating conditions of the ICP.

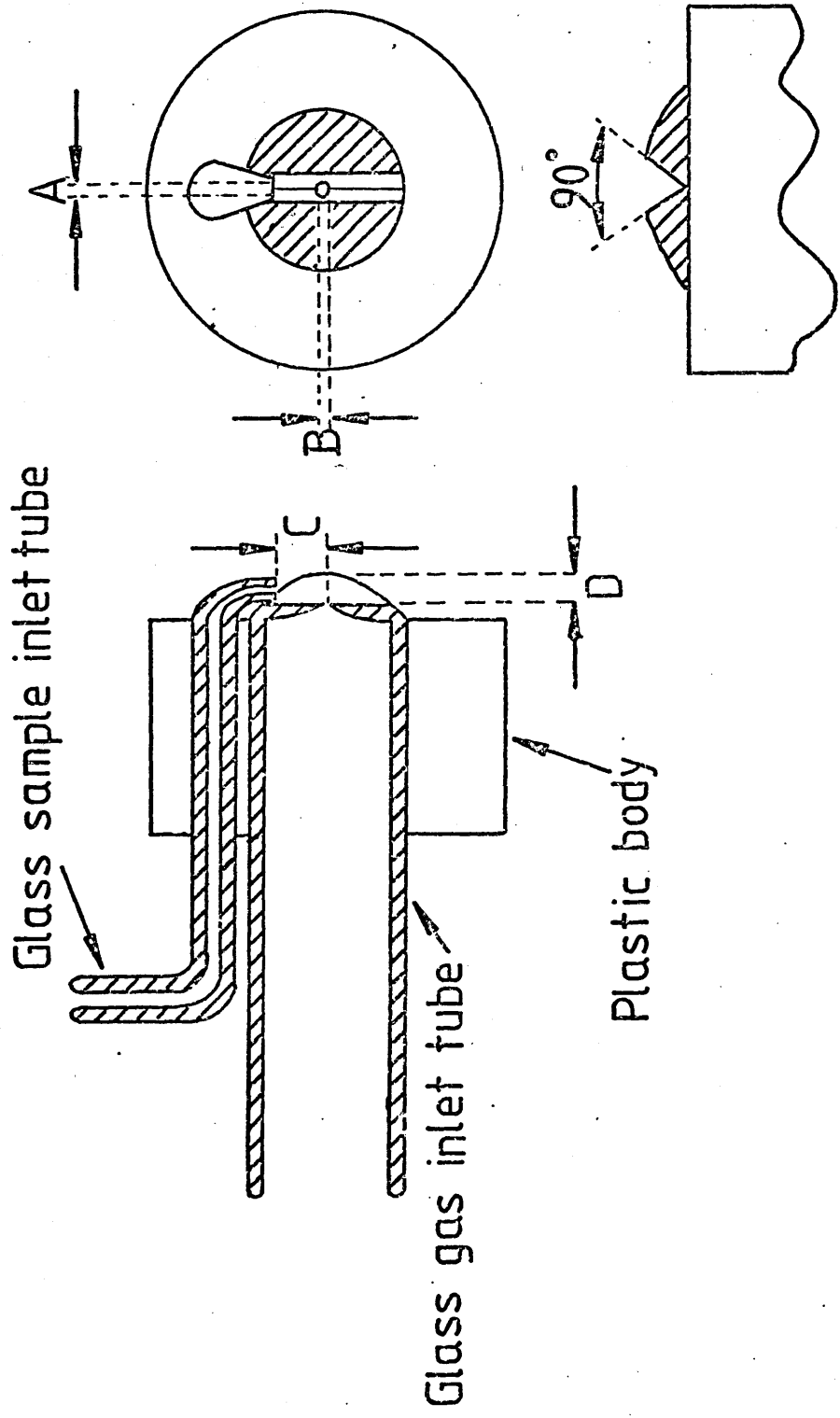
2.2.2 EXPERIMENTAL

The efficiency experiment was carried out by measuring the uptake of the nebuliser over a given time and by collecting the aerosol produced by the given nebuliser/chamber combination, from the outlet of the cloud chamber on dry silica in two 'U' tubes connected in series, over that same period of time. The 'U' tubes were weighed before and afterwards to determine the amount of water, in the form of an aerosol, produced (no significant increase in weight of the second 'U' tube was found). The performances of the nebulisers were then compared by measuring the signal to noise ratios (SNRs) at the same plasma conditions for a 10ppm aluminium solution.

Plasma operating conditions:-

Injector Argon flow:-	0.6 l min ⁻¹
Plasma Argon flow:-	1.7 l min ⁻¹
Nitrogen Coolant flow:-	12.4 l min ⁻¹
Viewing Height:-	32 mm
Power:-	0.4 kW
Spectral line:-	Al I 396.1 nm

The glass and plastic high solids nebuliser was compared to the constructed all glass concentric nebuliser using the double pass spray chamber, measuring the SNR for a solution of 6 ppm Mn. The high solids nebuliser was pumped at 1.65 ml min⁻¹ uptake, the glass concentric nebuliser was operated at its natural uptake

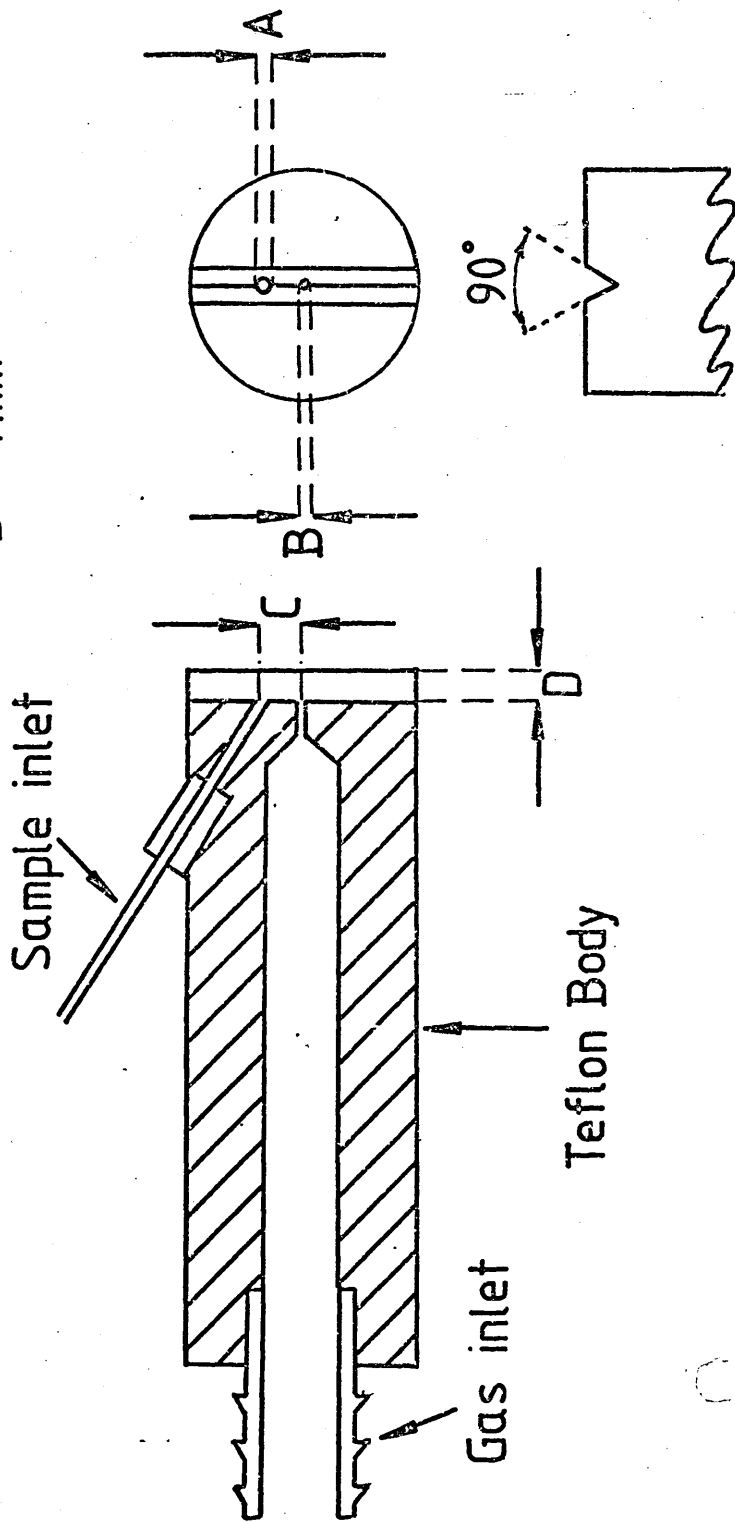


- A = 1mm
- B = ~0.4 mm
- C = 3mm
- D = 2mm

Glass & Plastic High Solids
Nebuliser

Fig 6

A = 1mm
B = 0.4mm
C = 1mm
D = 1mm



Teflon High Solids Nebuliser

Fig 7

rate of 0.9 mls min⁻¹.

Plasma operating conditions:-

Injector Argon flow:-	0.5 l min ⁻¹
Plasma Argon flow:-	1.7 l min ⁻¹
Nitrogen Coolant flow:-	5.4 l min ⁻¹
Viewing Height:-	18 mm
Power	0.42 kW
Spectral line:-	Mn II -57.6 nm

Finally the teflon high solids nebuliser was compared to the all glass concentric nebuliser, using the double pass spray chamber, by measuring the SNR for a solution of 1 ppm Mn, and a solution of 1 ppm Mn containing 20% w/v sodium chloride. Both nebulisers in this case were pumped at 1.65 mls min⁻¹.

Injector Argon flow:-	0.58 l min ⁻¹
Plasma Argon flow:-	11.3 l min ⁻¹
Argon Coolant flow:-	6.2 l min ⁻¹
Viewing Height:-	27 mm
Power	0.42 kW
Spectral line:-	Mn I 403.1 nm

2.2.3 RESULTS AND DISCUSSION

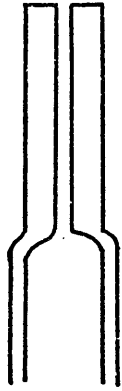
The results of the nebulisation efficiency experiments are summarised in Table 1. It can be seen that the vortex flow cloud chamber is more efficient than the double pass construction for both nebulisers used. Under prolonged operation, however, with the cyclone chamber water droplets condense in the capillary tip of the injector tube causing a spitting effect. This build up of droplets can be relieved by using a jet type injector

tube (Figure 8), this, however, produces a less well defined aerosol stream (as compared to the capillary injector which produces a narrow filament of aerosol) leading to reduced amounts of analyte passing through the central channel of the plasma, hence producing a lower signal and also increased noise on the base line and signal (Figure 9). These results show that the cyclone chamber allows a larger proportion of the aerosol produced through to the plasma than the double pass arrangement, thus larger signals are obtained. The extra proportion of aerosol produced, however, contains larger water droplets than those produced from the double pass chamber, which condense on the inside of the injector tip causing the observed effects. From the SNRs obtained for the different combinations of chamber and nebuliser it appears that the cyclone chamber produces better performance at the plasma. In the long term the double pass chamber is, however, superior, due to the smaller droplet size produced. The double pass chamber and capillary injector were therefore adopted for the rest of the work described here.

The differences in the efficiencies of the two nebuliser are mainly attributed to the differing uptake rates (the commercial nebuliser has an uptake of 2.5 mls min^{-1} and the constructed nebuliser 0.9 mls min^{-1}), whereas the amount of aerosol appearing at the plasma is very similar for each nebuliser, as confirmed by the comparable SNRs obtained (Table 1).

Figure 10 compares the traces obtained from the glass and plastic high solids nebuliser with the constructed concentric nebuliser. The high solids nebuliser produces a 60% larger signal, with, however, greater noise on the background and signal, this is mainly due to pulsation from the pump supplying the solution. This shows that the simply constructed high solids nebuliser has potential use as an ICP nebuliser.

Injector Tubes



Capillary Injector



Jet Injector

Fig 8

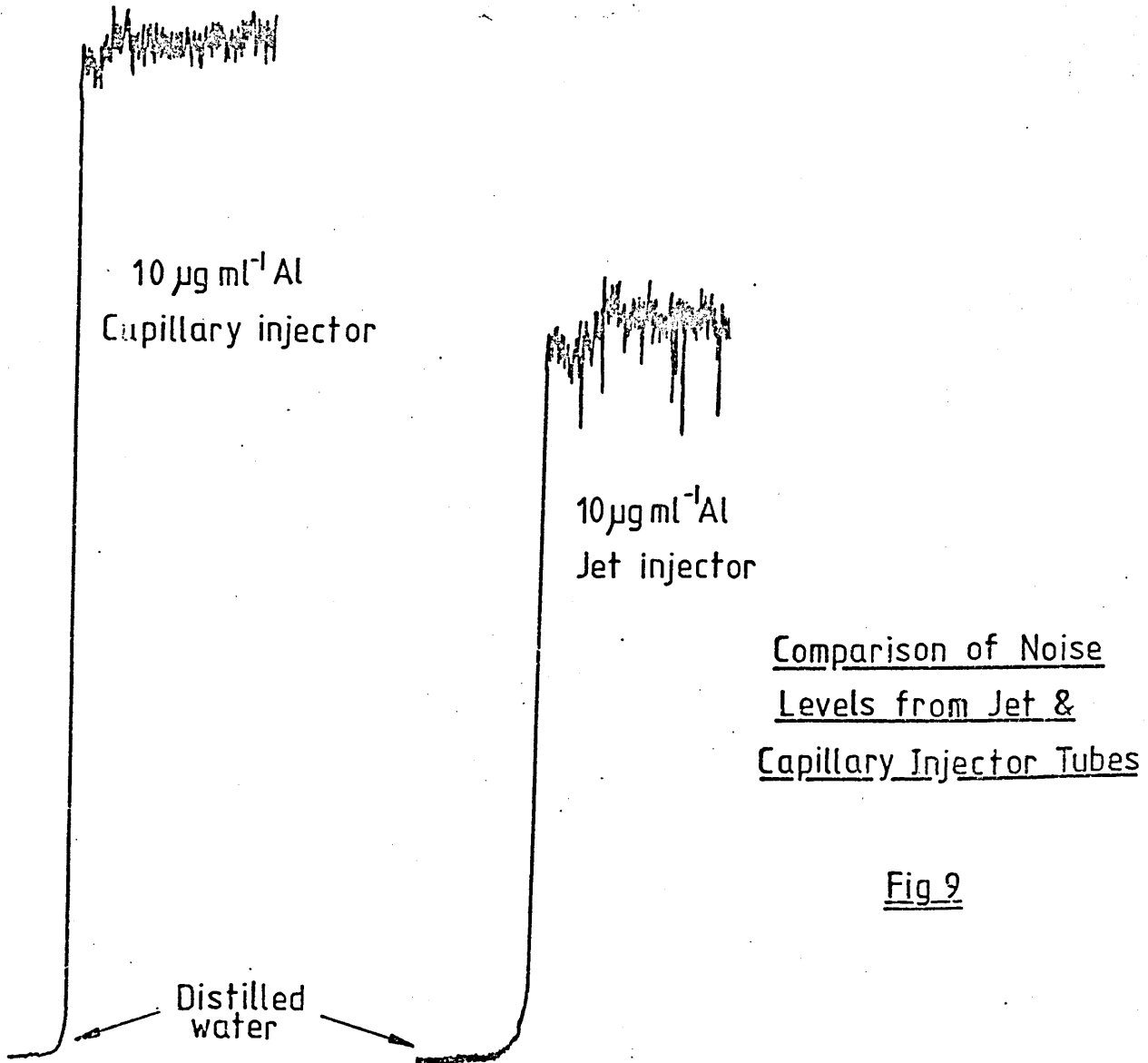


Fig 9

Comparison of Nebuliser Systems

Nebuliser System	Efficiency (%)	SNR
S.P.+Double Pass	4.0	6.1
S.P.+Cyclone	5.5	7.6
Com.+Double Pass	0.97	6.4
Com.+Cyclone	2.9	9.7

S.P.=Constructed 'Meinhard'
Com.=Commercial "

Table 1

Comparison of Optimised Torch Conditions

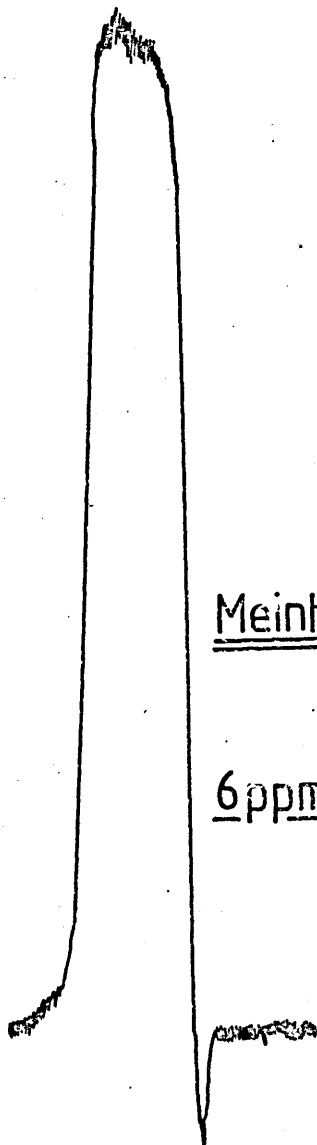
Torch	Coolant Gas	Gas flow rates [l min ⁻¹]			Height (mm)	Power (kW)	SBR
		Coolant	Plasma	Injector			
Greenfield design	N ₂	4.0	2.5	0.6	19	1.3	0.4
New design	N ₂	4.6	10.0	0.4	21	12	1.2
New design	Ar	4.6	13.0	0.38	20	0.6	1.5

Table 2

In constructing the teflon high solids nebuliser the sample entry was placed nearer the gas exit orifice to reduce the pulsation effect. Figure 11a shows the traces obtained comparing the two nebulisers for a 1 ppm solution of manganese, showing comparable results and the removal of the pulsation effect. Figure 11b illustrates how the teflon nebuliser can handle high salt content solution, compared to the concentric nebuliser.

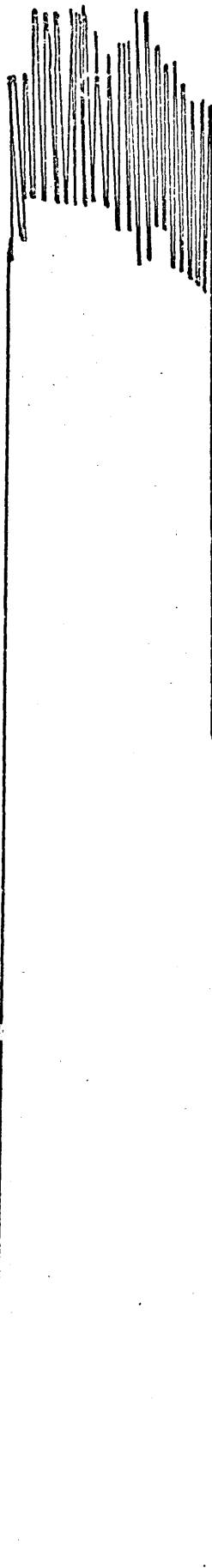
This simple and rugged nebuliser shows promise for ICP analysis of samples containing high salt content (e.g samples that have to undergo alkaline fusion before dissolution) and, because it is constructed from teflon, for the analyses of more intractable samples which can only be dissolved in hydrofluoric acid, which cannot be handled by nebulisers made from glass.

Comparison of Meinhard
& Glass High Solids Nebulisers



Meinhard

6 ppm Mn



Glass
High Solids

6 ppm Mn

Fig 10

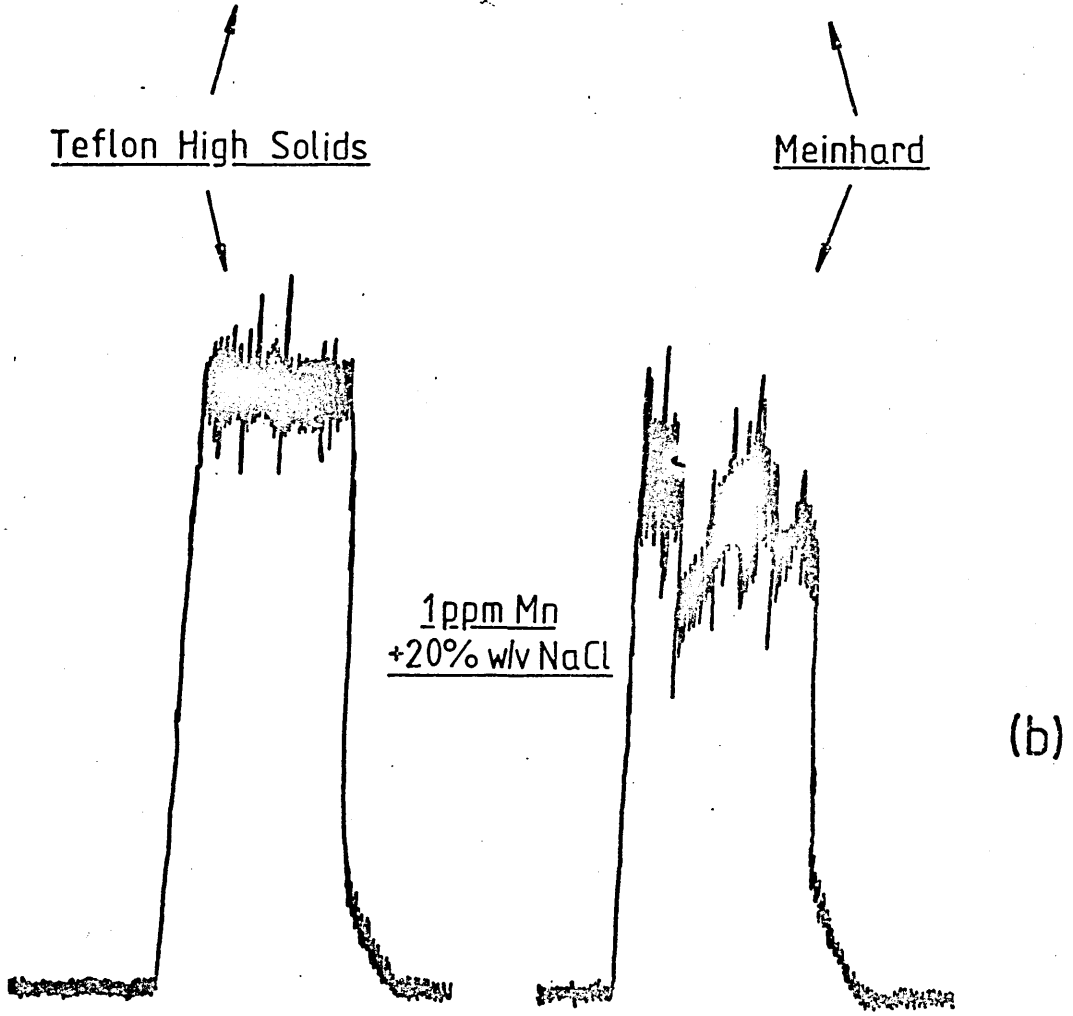
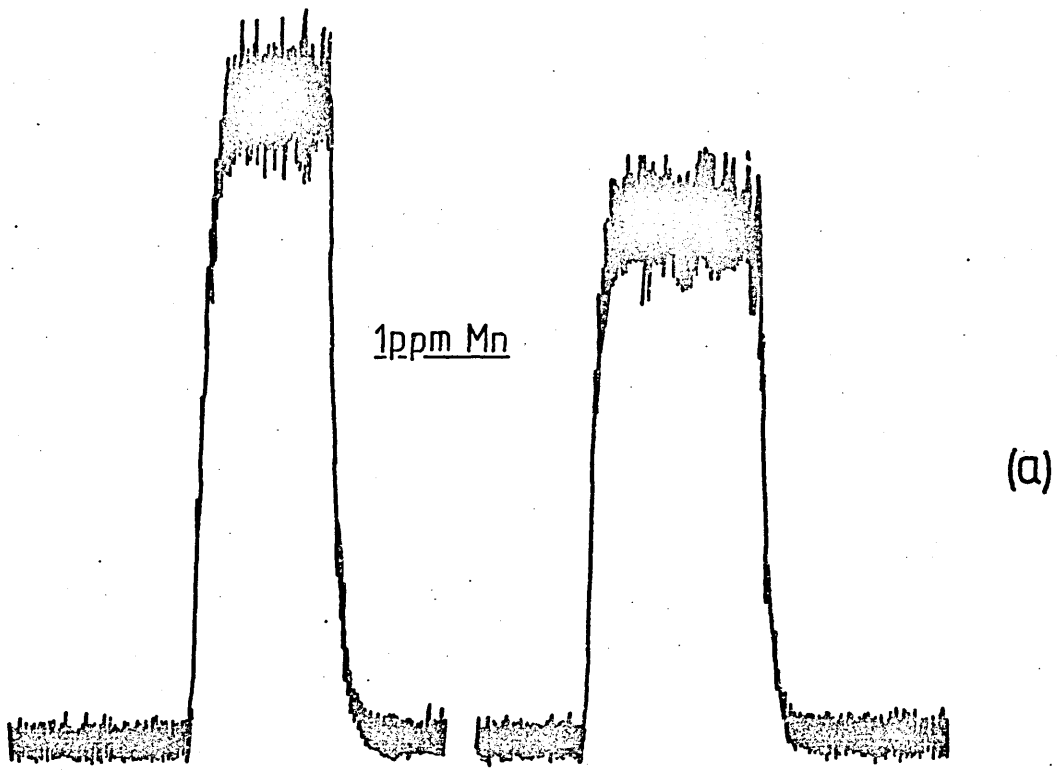


Fig11

3. POWER MEASUREMENTS

Of all the parameters quoted in publications describing the operating conditions of different ICP systems, the 'power' of the plasma is perhaps the most ambiguous. The term power usually refers to the forward power supplied to the load coil. Since, however, there are many differing ICP systems in use, the efficiency of the coupling of the forward power will be different from system to system depending on the torch design, coil size and geometry, frequency of the RF generator, and type of gas used for the discharge. Thus for meaningful comparisons between different systems it is the 'power in the plasma' which must be measured.

The standard method for measuring power in the plasma is based upon a British Standard method (150a) intended for use with induction heating metallic loads. Since the coupling conditions of a metallic load are not obviously the same as those of a plasma, work has been carried out (150b) to test the validity of this method. It has been shown that as long as the metallic load is operated under the same coupling conditions produced by a plasma the power coupled into the metallic load can be used as a measure of power in the plasma. This method has been used to measure the power in the plasma, as well as direct calorimetric power measurement, for the system used in this work.

3.1 EXPERIMENTAL

3.1.1 DUMMY LOAD MEASUREMENTS

The dummy load used consisted of a bundle of copper and iron rods

encased in a glass jacket, constructed to fit into the three turn induction coil. Inlet and outlet tubes on the glass jacket allowed water to be continuously passed around the metal load. The rapidly oscillating current in the RF coil induced currents in the load and hence heating. The amount of heat applied to the load per unit time (i.e. power) was then measured calorimetrically using the temperature difference between the water flowing in and the water flowing out, and the flow rate of the water.

The coupling efficiency of the plasma is characterised by the grid current, anode current, and anode voltage values of the oscillator valve in the generator. To match these values with the dummy load the ratio of iron to copper rods in the coil was adjusted by moving the load up or down to produce the correct coupling conditions.

Two sets of measurements were performed. The power dissipated in the load was measured at fixed grid current values for varying plate powers (i.e. anode voltage x anode current) to establish the relationship between grid current, plate power and power coupled into the plasma.

Secondly the power was measured in the load at simulated plasma conditions (for a nitrogen cooled plasma). Simulated plasma power measurements were also carried out with the brass base of the demountable torch (described in section 2.1.2) placed underneath the dummy load in the normal operating position, to determine if there were any power losses due to RF coupling into the brass.

3.1.2 DIRECT CALORIMETRY MEASUREMENTS

Direct calorimetry experiments were carried out to confirm the results obtained with the dummy load.

A one metre long silica condenser was placed on top of the torch

in the manner of Greenfield and McGeachin (150b). The flow of water through the condenser was measured, together with the inlet and outlet temperatures whilst the plasma was operating. The gas flows through the torch were measured using the rotameters controlling the gases to the plasma. The temperature of the gases emerging from the top of the condenser were measured using a thermocouple. The combination of power found in the water and exhaust gases was then used as a measure of the power in the plasma. In an attempt to measure any energy loss by radiation a 'T' piece was fitted onto the inlet water pipe of the condenser and a solution of nigrosine dye (c a. 7g l^{-1}) was pumped into the condenser coolant water at a rate of 3 ml min^{-1} producing a radiation absorbing coolant.

Power measurements were made for both an all argon plasma and a nitrogen cooled plasma. The gas flows used for the two types of plasma are as follows:

1) all argon:-

Injector argon flow	-	0.49 l min^{-1}
Plasma argon flow	-	11.35 l min^{-1}
Coolant argon flow	-	4.6 l min^{-1}

2) nitrogen cooled:-

Injector argon flow	-	0.49 l min^{-1}
Plasma argon flow	-	10.4 l min^{-1}
Coolant nitrogen flow	-	4.6 l min^{-1}

3.2 RESULTS AND DISCUSSION

Figure 12 shows how the plate power is related to the power

Power Output at constant
Grid Currents

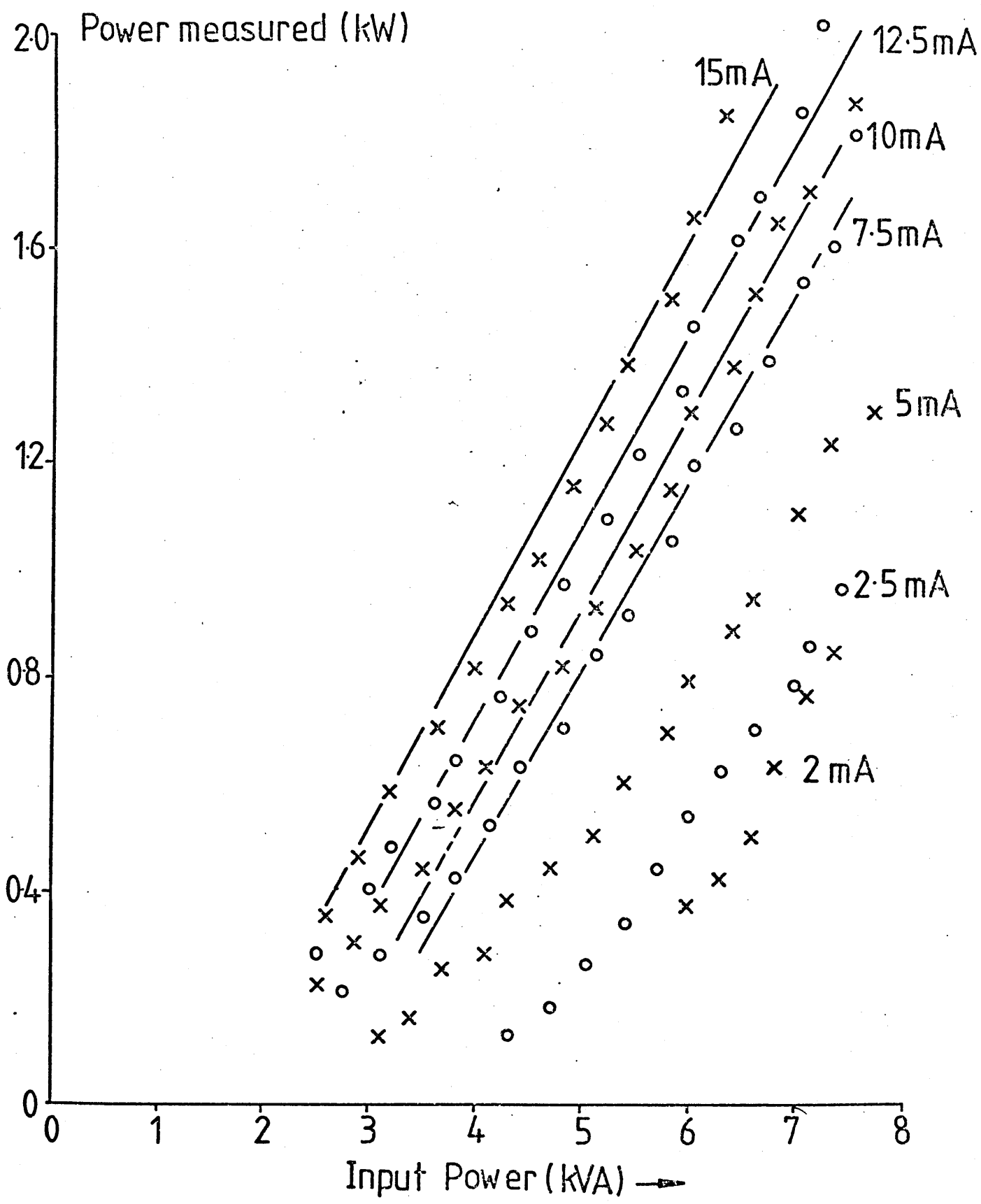


Fig 12

measured in the dummy load (and hence in the plasma) at different grid current values. For grid current values above 7.5mA the 'plate KVA' vs 'power measured' graphs are approximately straight parallel lines equally spaced for equal steps in grid current. For these values a least squares equation can be calculated:-

$$\begin{array}{rcc} \text{power in the plasma} & = & 0.351 \text{ plate power} + 0.047 \text{ grid current} - 1.29 \\ \text{(kW)} & & \text{(KVA)} \qquad \qquad \qquad \text{(mA)} \end{array}$$

Below values of 7.5 mA the above relation does not hold, and hence plasmas with coupling characteristics which produce low grid currents must have their power measured by estimation from the graph in Figure 12.

Figure 13 compares the measured power at simulated plasma conditions with and without the brass torch holder present, and shows that within experimental error there are no power losses to the holder. A curve is also plotted of the power in the plasma, as calculated from the above empirical equation, which shows good agreement with that obtained by the plasma simulation experiment.

The results of the direct calorimetric power measurements are summarised in Figure 14.

The power in the coolant water and gases is compared to the power as obtained from the dummy load equation. For both types of plasma the direct calorimetric method gives a lower power than for the dummy load estimation. This is to be expected, for, as has been pointed out (150b), direct calorimetry will always produce a lower limit of the actual power, because losses due to radiation of energy from the plasma fireball have not been included. The use of a dye in the condenser coolant was an attempt to minimise these losses, but as shown in Figure 14 there is no significant difference between the power in the condenser water when dye was added and when tap water on its own was used. Estimation of these radiation

Conditions

+ — Power from empirical equation

o — " without brass base

x — " with " "

⌈ — experimental error in power measurement

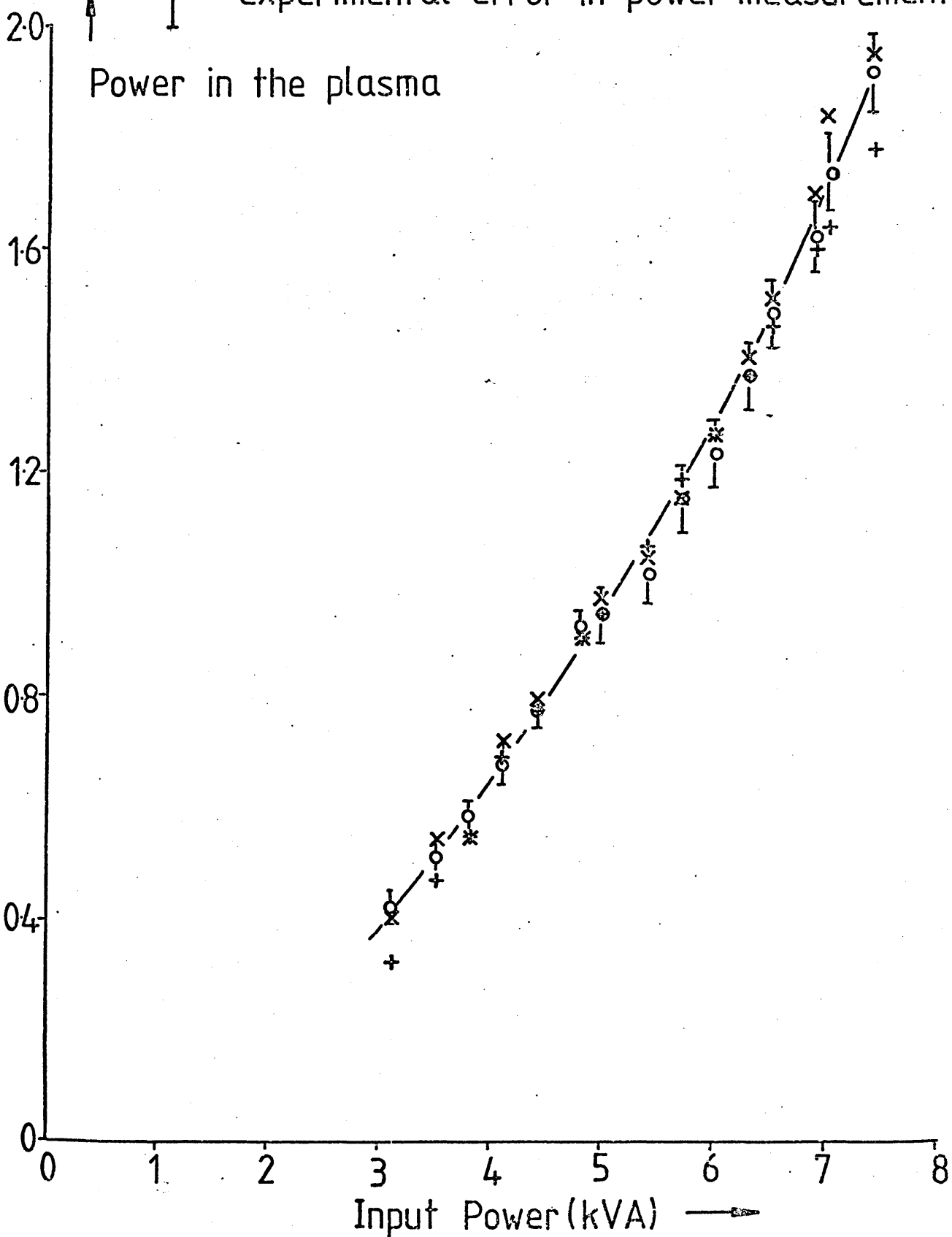


Fig13

Comparison of Dummy Load & Direct Calorimetric
Power Measurements

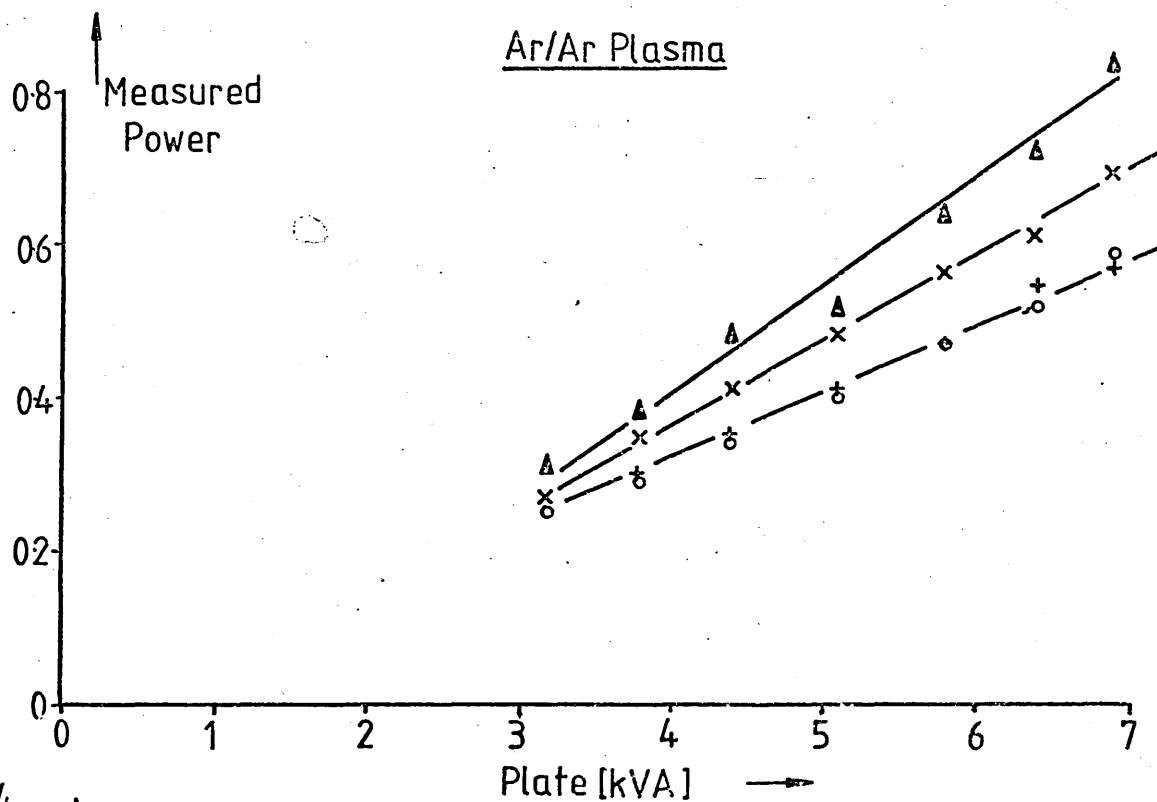
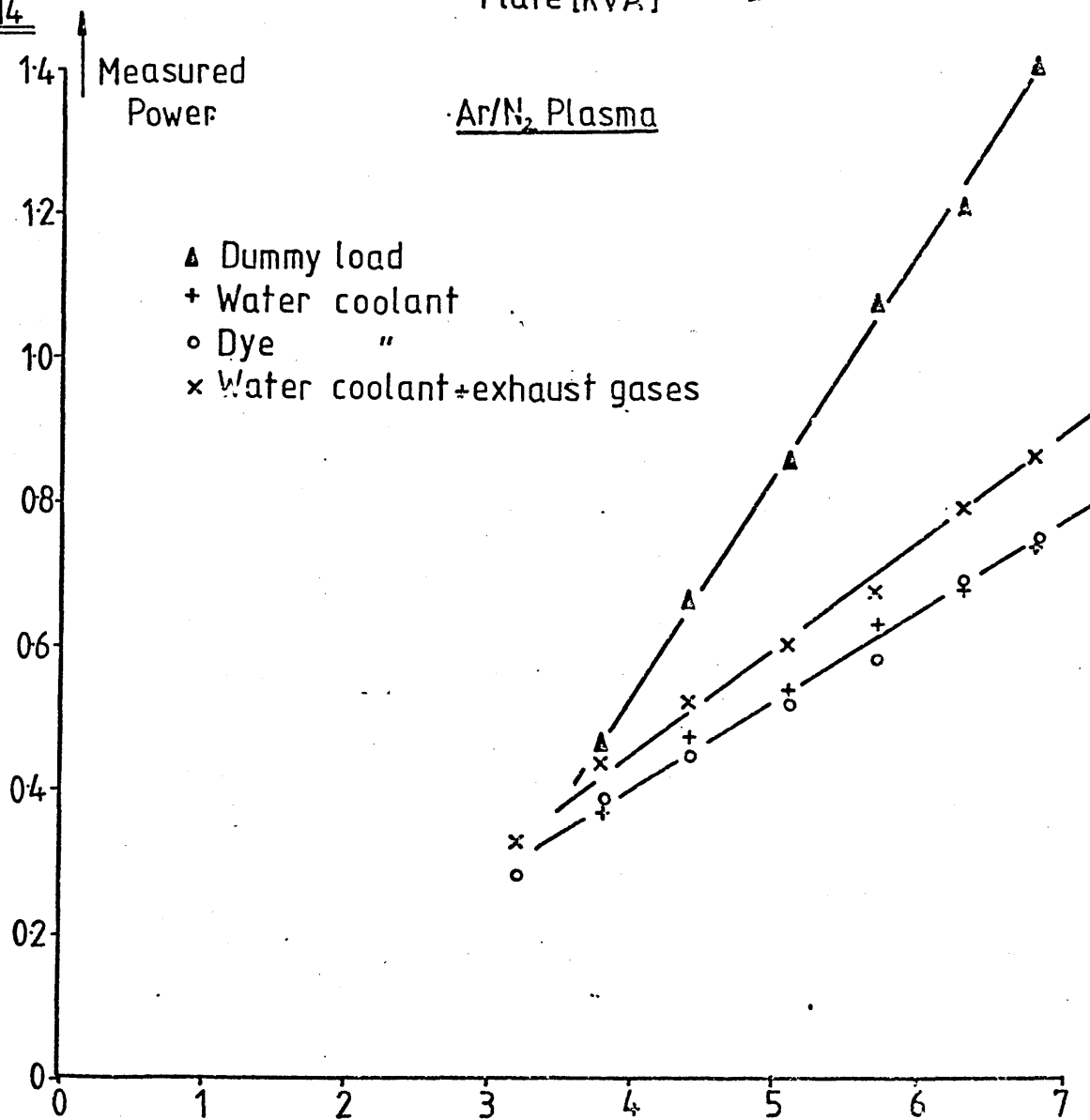


Fig 14



losses are not feasible, as an accurate value of the temperature of the plasma is required and this is not known. Greenfield and McGeachin (150b) have shown that by choosing an appropriate temperature of the plasma a radiation loss which will account for the difference between the power measured by the two methods, can be found. Since the temperatures chosen for the plasma to make these calculations (10,400 K for the high power generator and 9,900 K for the low power generator) are reasonable Greenfield claims that the results of calorimetry with plasmas supports the equation derived from the dummy load experiments. The power lost due to radiation in Greenfield's experiment was ~10% with the high power generator and ~20% in the low power generator, as shown in Figure 14 the power lost in the all argon plasma due to radiation is 13 - 18% is as the power increases, and 0 - 36% in the nitrogen cooled plasma, for the system used here. As the generator and torch are different from those used by Greenfield the calorimetric results for this study can be said to tentatively agree with the dummy load measurements since radiation losses are of similar magnitude.

It is evident that measurement of power in the plasma cannot be made without uncertainty, nevertheless the dummy load experiment provides a systematic measurement of power the value of which is confirmed by the calorimetry experiments. The dummy load equation has thus been adopted for measurement of power in this work.

It must be noted that the power in the plasma will always be lower than the more commonly quoted forward power, as there will never be 100% coupling of the power to the coil into the plasma. Greenfield and McGeachin (150b) suggest that approximately 50% of the forward power is coupled into the plasma for their system. This may not be the case for the system used here, but this figure can be used as a rule of thumb for comparing the powers quoted here with the forward powers quoted in other ICP publications.

4.1 OPTIMISATION OF PLASMA PERFORMANCE

Early development of the ICP (see section 1.3.1) was carried out by two set groups of workers. These groups, one led by Greenfield (33) and the other by Fassel (34), at an early stage took divergent routes: the former used higher power with nitrogen as coolant, and the latter used lower power with argon coolant. More recently, there has been considerable discussion in the literature (e.g. 50,123,151) of the effect of power on analytical sensitivity, and the advocates high power and low power have tended to polarise. Similarly the use of argon or nitrogen as coolant gas has been the subject of controversy.

Experiments designed to discover which system is the better have not always been conclusive. For example, the results of Boumans and de Boer (123) showing the effect of power on the signal to background ratio (SBR) cannot be taken as conclusive as a fixed observation height was used and the optimum viewing height has been shown to vary with the power in the plasma (152,153,154,155).

Clearly, a rigorous optimisation technique is required which will enable the establishment of a true optimum involving all the plasma variables and, hence, an acceptable comparison of intrinsic merit independent of the associated spectrometric system to be achieved.

In order to optimise the ICP it is necessary to decide upon an optimising criterion which will be a fair measure of the analytical usefulness of the plasma. The criterion of detection limit as often used in the literature as a measure of the performance of a particular spectroscopic method, would seem an obvious choice for

this purpose. It has been shown (156), however, that because detection limit is a function of the noise on the background which is in turn a function of background and photomultiplier dark current, that optimising detection limit would also involve optimising the measuring system and hence would not be a true measure of the ICP alone.

Greenfield and Thorburn Burns (156) suggest that signal to background ratio (SBR) would be a fairer measure of intrinsic merit, although SBR is not independent of the measuring system, the total signal and background emitted from the plasma will be directly proportional to the signal and background as measured at the photomultiplier. Thus the SBR from a particular plasma will be different when measured on different readout systems, but when two different plasmas are being compared the magnitude of the SBR for the two plasmas will always be in the same order, regardless of readout system. In this work, therefore, SBR has been adopted as the optimisation criterion, so that the optimum intrinsic merit results from the plasma systems studied here will be able to give some general conclusions about similar systems used by other workers with differing readout equipment.

Having decided upon the property of plasma to be optimised it was then necessary to choose those parameters which controlled the property. Since SBR is a measure of the intrinsic merit of the plasma alone those parameters directly influencing the plasma were chosen for the optimisation these being the power, the height of observation, and the flow rates of the coolant, plasma and injector gases.

Since the plasma variables have been shown to be interdependent (152,153,154,155) optimisation of one parameter at a time will not produce a true optimum. Traditionally, a factorial optimisation experiment is used to solve such a problem, but these experiments may be very time consuming and tedious, unless some factors are given

priority, with attendant risks of not obtaining a true optimum. Greenfield and Thorburn Burns (157) have successfully used an alternating variable search method for optimising the plasma. An alternative approach is a modification by Nelder and Mead (158) of the original simplex method described by Spendley et al. (159) which offers an elegant and speedy solution to the problem.

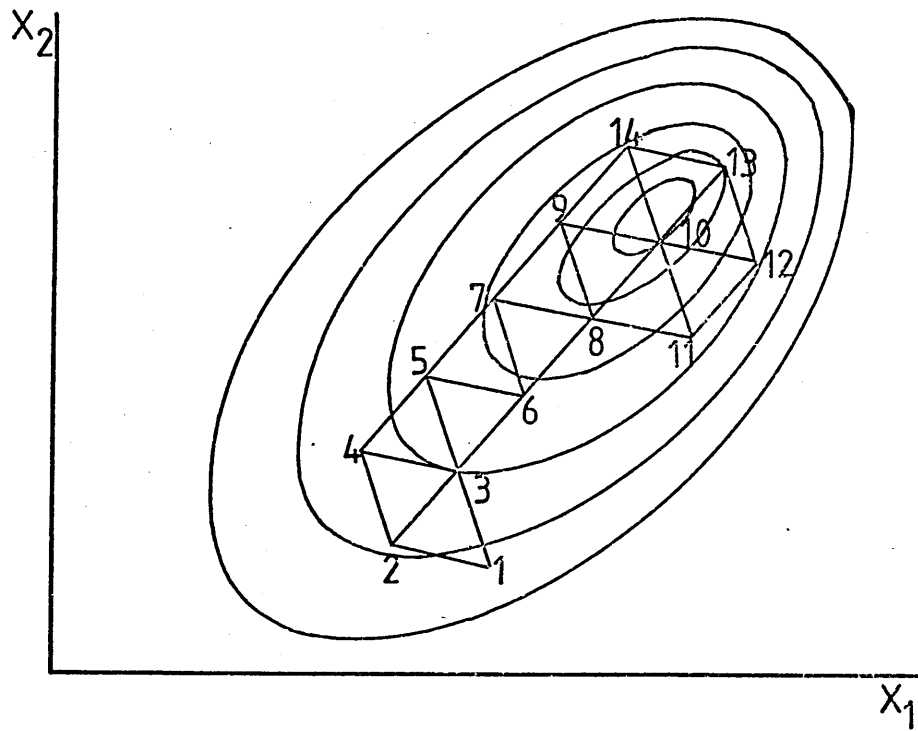
4.1 SIMPLEX OPTIMISATION

A simplex is a geometric figure defined by a number of points equal to the number of parameters considered in the optimisation plus one (i.e. one more than the number of dimensions of the factor space). For the simplest multi-factor problem namely an optimisation of two parameters, the simplex is therefore a triangle. In the following discussion a two parameter optimisation will be considered since this is most easily visualised, however, the theory applies equally well to any number of variables.

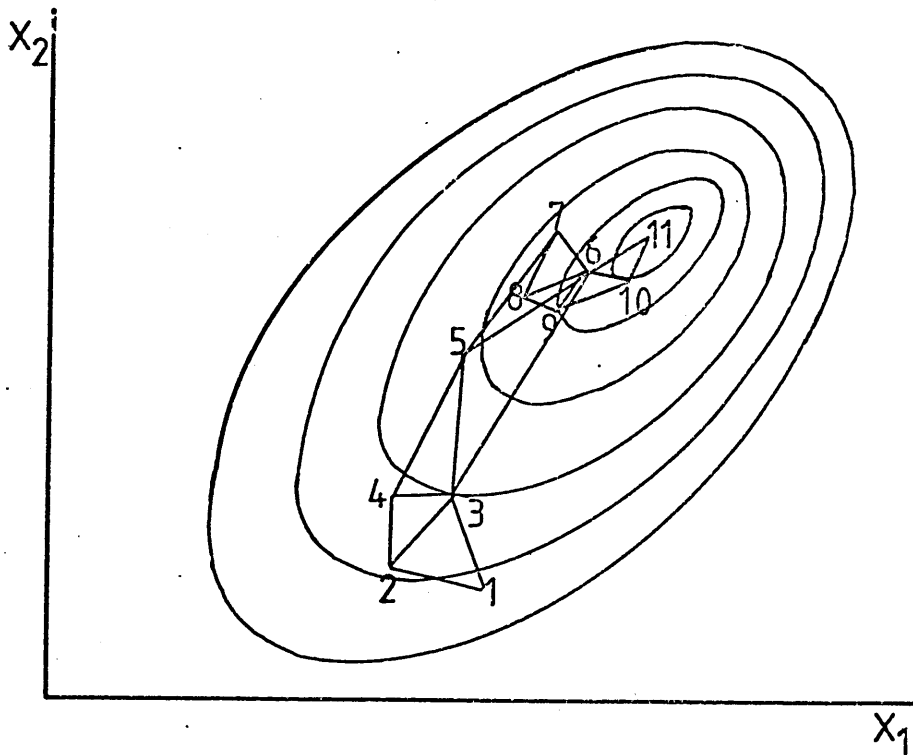
Consider the response surface in Figure 15a with parameters X_1 and X_2 , the contours are lines of iso-response, optimisation for highest response is required. The optimisation starts with points 1, 2 and 3. These points form an equilateral triangle with point 1 showing the worst response of the three. It is logical to conclude that the response will probably be higher in the direction opposite to this point. Therefore the triangle is reflected about the side joining points 2 and 3 to produce point 4. The response is re-evaluated at the new point 4 and the triangle is reflected away from the new worst point, which in this case is point 2. In this way, using successive simplexes, one moves along the response surface towards the optimum. This gives rise to the first rule of the simplex method:-

Rule 1: *The new simplex is formed by rejecting the point with the worst result in the preceding simplex and replacing it with its mirror image across the line defined by the remaining two points.*

Simplex Optimisation Examples



(a) Single step size simplex



(b) Variable step size simplex

Fig 15

In the initial stages of an optimisation the new point in a simplex will usually yield a better result than at least one of the two remaining points, because the simplexes will tend to move towards an optimum. When the new point has the worst response of the simplex, this usually occurs as the optimum is approached, application of Rule 1 would lead to a reflection back to the point which was itself the worst in the preceding simplex. The repetition of rule 1 would then lead to an oscillation between the two simplexes thus halting the progress of the procedure. For example consider simplex 8,10,11 in Figure 15a the worst response is at point 11, applying Rule 1 would lead back to point 9, and then again to point 11 etc. Thus Rule 2 must be used.

Rule 2: *If the newly obtained point in a simplex has the worst response, do not apply rule 1 but instead eliminate the point with the second lowest response and obtain its mirror image to form the new simplex.*

This effect usually occurs as the optimum is neared and the simplex 'overshoots'. Applying Rule 2 allows the simplex to continue, changing direction and again to approach the optimum. In the region of the optimum, the simplexes circle around the provisional optimal point. In Figure 15a the provisional optimal point is vertex number 10, if, however, the response at any point was measured erroneously high the simplexes would hold onto a false maximum. To counter this Rule 3 is used.

Rule 3: *If one point is retained in three successive simplexes (in the case of n variables in $n + 1$ successive simplexes), determine again the response at this point. If it is the highest in the last three simplexes it is considered as the optimum which can be attained with simplexes of the chosen size.*

If not the simplex has become fastened to a false maximum and the optimisation is restarted.

Finally, because the factor space chosen will not be infinite due

to the physical constraints of the system, the possibility that the new vertex will fall outside the factor space and hence have an unknown response, may occur. Thus Rule 4 is formulated.

Rule 4: If a point falls outside one of the boundaries, assign an artificially low response to it and proceed with rules 1 - 3.

The effect of applying Rule 4 is that the outlying point is automatically rejected without bringing the succession of simplexes to an end.

These four basic rules form the 'Simplex Method' first devised by Spendley et al. (159).

4.1.2 THE MODIFIED SIMPLEX METHOD

In the original simplex method the step size is fixed. If the initial step size is too small compared to the factor space the optimum will be approached slowly; if it is too large, the optimum is determined with insufficient precision. In the latter instance a new simplex with smaller step size can be started at the provisional optimum. This was the method used by Long (160). However, a modified simplex method in which the step size is variable throughout the whole procedure offers a more elegant, and efficient, solution. The principal disadvantage is that the simplicity of the calculations in the original simplex method no longer exist, this can, however, be outweighed by the reduction in the number of steps required to reach the optimum.

Nelder and Mead (158) formulated a method for introducing variable step size in the simplex procedure. This can be visualised by considering the initial triangle (i.e. simplex) BAW in Figure 16(i), in this case it is not necessarily an equilateral triangle. Instead of the single reflection of the basic simplex method,

Nelder and Mead's modification allows the simplex to move in one of four alternate ways. Let each point on the triangle BAW have a position vector \bar{B} , \bar{A} , \bar{W} respectively, then the basic step can be defined by:-

$$\bar{R} = \bar{P} + (\bar{P} - \bar{W}) \dots\dots\dots i)$$

Where:

P = the centroid of the line joining B and A

W = the point with the worst response

R = the new simplex vertex.

This is equivalent to the basic reflection in the original simplex method. The effect of this is shown in Figure 16(i). This can be modified by expanding the new simplex to produce E (Figure 16(ii)) defined by:-

$$\bar{E} = \bar{P} + a(\bar{P} - \bar{W})$$

Where:

$a (>1)$ = the expansion factor (usually 2)

A contraction of the simplex can be made to produce Cr (Figure 16(iii)) defined by:-

$$\bar{Cr} = \bar{P} + \beta (\bar{P} - \bar{W})$$

Where:

$\beta (<1 \text{ but } >0)$ = contraction factor (usually $\frac{1}{2}$)

Finally a contraction back into the preceding simplex (Figure 16(iv)) defined by:-

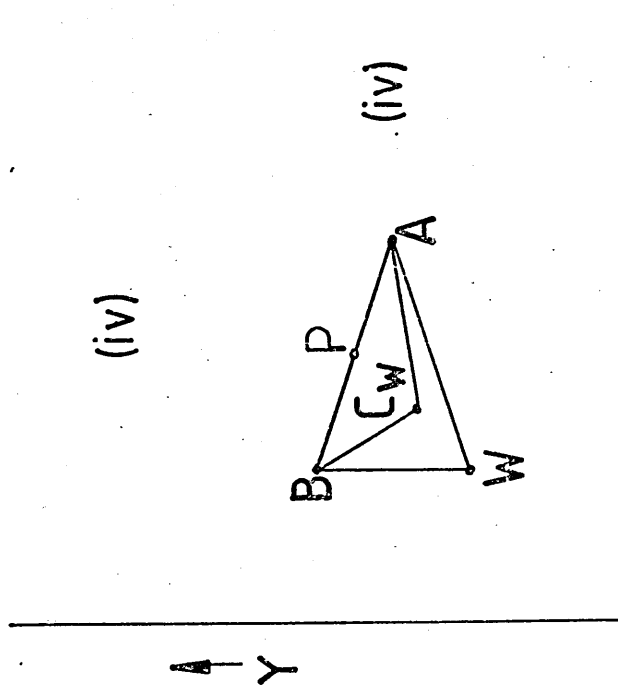
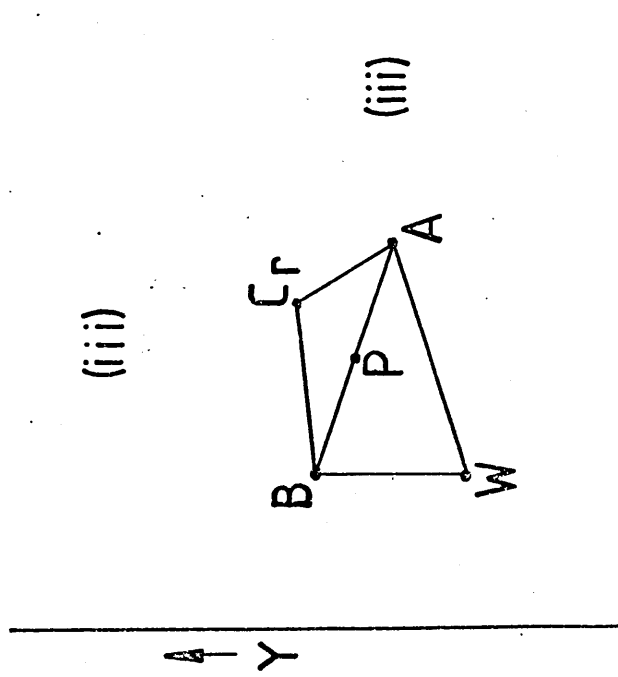
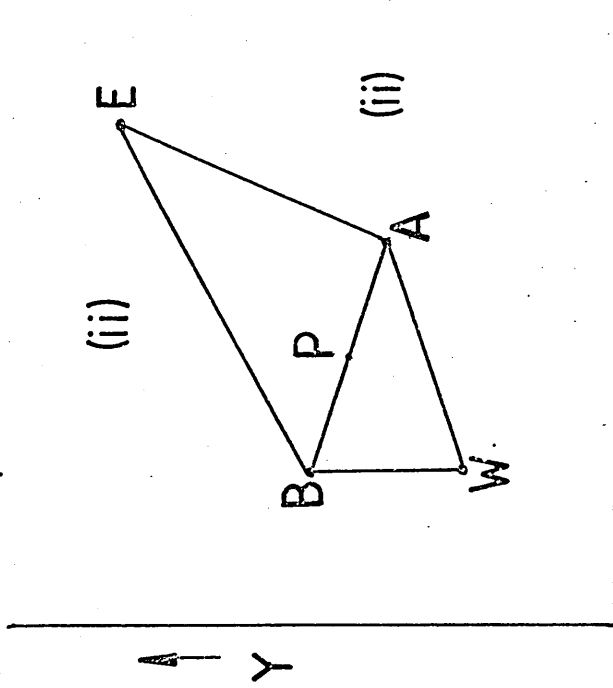
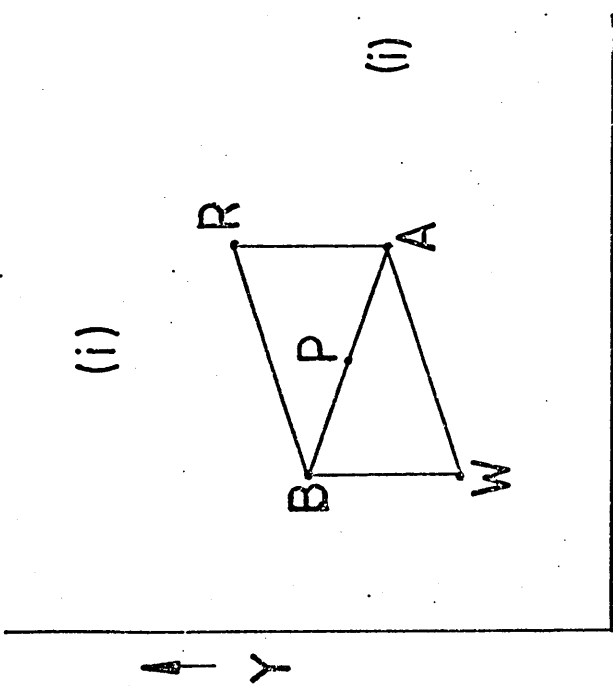


Fig16

$$C_w = P - \beta (P - W)$$

To ascertain which of the four points to use to construct the next simplex the following procedure is used.

Observe the response at R and Cr, if the response at R is greater than at Cr then calculate E. If the response at E is greater than at R use E, if not use R. If the response at Cr is greater than at R calculate Cw. If the response at Cw is greater than at Cr use Cw, if not use Cr.

Thus the method of Nelder and Mead modifies Rule 1 of the basic simplex procedure allowing the expansion and contraction of each new simplex speeding the progress to the optimum. Rules 2 - 4 remain unaltered and are applied in the same manner as for the basic simplex.

Figure 15b shows a comparison of the modified simplex method with the basic simplex on the same response surface.

Note how the variable step simplex contracts down to identify the optimum without the need for cycling around a provisional optimum value.

More recently there have been further modifications to the variable step size simplex to improve its efficiency (161,162,163).

The gain in efficiency (i.e. reduced number of steps) is, however, outweighed by the extra calculations and hence time required to evaluate each new vertex, particularly in the system used here as the calculations are carried out by 'hand' rather than computer program.

4.2 APPLICATION OF MODIFIED SIMPLEX TO THE OPTIMISATION OF THE PERFORMANCE OF THE ICP

The use of simplex optimisation in analytical chemistry has recently been reviewed by Deming and Parker (164). It was evident, however, that no one had published work on the optimisation of the ICP using the above method. In the following section a detailed account of the application of the modified simplex method of Nelder and Mead (as described in section 4.1.2) to the optimisation of SBR in the ICP for the five major variables of injector gas, plasma gas, and coolant gas flow, viewing height and power will be given.

4.2.1 SETTING-UP AND OPERATION OF THE SIMPLEX OPTIMISATION

The choice of initial step size is a critical feature of this optimisation procedure. Yarbrow and Deming (165) have demonstrated that it is desirable to begin with a large step size to ensure that most of the factor space is explored before the simplex collapses on to the optimum. These authors described a matrix and accompanying equations (Figure 17), which were used, in this work, to design the initial simplex. The five dimensional initial simplex was set up as shown in Figure 17. The value S_n is called the 'step size' for the n th variable, this is calculated by subtracting the lowest feasible value for that variable (denoted by X_n in the matrix) from the highest feasible value. For the ICP these lowest and highest values depend on the physical constraints of the instrument and whether or not a stable plasma can be formed. The values p_n and q_n can then be calculated for each variable and by adding these values to the appropriate X_n value, as shown in the matrix, the initial simplex can be formed.

The initial simplex, once calculated, was transferred to the initial simplex worksheet (an example of which is shown in Figure 18). The columns headed F1, F2 and F3 are the injector, plasma,

Initial Simplex Matrix

Vertex	Dimensions					
	1	2	3	4	n-1	n
1	x_1	x_2	x_3	x_4	x_{n-1}	x_n
2	$p_1 + x_1$	$q_2 + x_2$	$q_3 + x_3$	$q_4 + x_4$	$q_{n-1} + x_{n-1}$	$q_n + x_n$
3	$q_1 + x_1$	$p_2 + x_2$	$q_3 + x_3$	$q_4 + x_4$	$q_{n-1} + x_{n-1}$	$q_n + x_n$
4	$q_1 + x_1$	$q_2 + x_2$	$p_3 + x_3$	$q_4 + x_4$	$q_{n-1} + x_{n-1}$	$q_n + x_n$
-	-	-	-	-	-	-
n	$q_1 + x_1$	$q_2 + x_2$	$q_3 + x_3$	$q_4 + x_4$	$p_{n-1} + x_{n-1}$	$q_n + x_n$
n+1	$q_1 + x_1$	$q_2 + x_2$	$q_3 + x_3$	$q_4 + x_4$	$q_{n-1} + x_{n-1}$	$p_n + x_n$

where :-

$$p_n = \frac{S_n}{n\sqrt{2}} [\sqrt{n+1} + (n-1)]$$

$$q_n = \frac{S_n}{n\sqrt{2}} [\sqrt{n+1} - 1]$$

Fig 17

and coolant gas flows respectively (these are expressed as mm on the sheet as directly measured from the rotameter). P is power column and H is the viewing height. The SBR, for the six sets of variables, was then measured using the ICP for the particular element under study. Rule 1 was then applied and the vertex producing the worst SBR was discarded. Calculation of the four possible sets of new variables was then carried out using the equations shown in the bottom left of the worksheet. Each column was summed (excluding the value of the worst vertex) and divided by five to produce P (for an n dimensional simplex divide by n). The value of the worst vertex was denoted by W. Hence giving the new vertexes R, Cr, Cw and E (using an expansion factor of 2 and a contraction factor of $\frac{1}{2}$). The SBR for the latter was then determined on the ICP (as described in section 4.1.2) and hence the new vertex was found. The initial simplex was then copied onto the second worksheet, replacing the worst vertex with the new vertex. Rule 1 was reapplied and the process was then repeated.

The simplex procedure was terminated when no significant difference was observed in the SBR of successive vertices. A univariate search (166), in which four of the five parameters were held constant at their optimum values, as obtained using the simplex procedure, and the fifth varied as the SBR was measured, was used to confirm the success of the simplex optimisation. This search also yielded valuable information on the influence of each parameter on the performance of the plasma.

4.3 EXPERIMENTAL

The instrumentation for the optimisation experiments has been described in chapter 2. An all glass concentric nebuliser constructed in the manner of Scott (129) was used in all experiments, the sample being supplied at 1.65 ml min^{-1} by a peristaltic pump.

Initial experiments were carried out using a 16 mm slit height, this was changed to 4 mm for later experiments. The signal was measured by spraying a solution of the sample under study and measuring the difference between the signal obtained and the signal due to distilled water being sprayed into the plasma under the same conditions. The background was measured by taking the difference between the signal when distilled water was sprayed and the signal when a shutter was placed in front of the spectrometer slit (i.e. the signal from the photomultiplier dark current). Hence SBR could be calculated.

4.4 RESULTS AND DISCUSSION

4.4.1 EVALUATION OF THE SIMPLEX PROCEDURE FOR OPTIMISING THE ICP

Initial optimisations of the plasma were performed with signal to noise ratio as the optimisation criterion. These results are not presented since noise was found to be difficult to measure and thus optimum regions defined by the simplex were inconclusive. Further to this SBR was adopted for all further optimisation experiments. For the initial SBR optimisation the Mn 257.6 nm ion line was chosen as a sensitive and easily excited emission line. Optimisation was carried out in an all argon plasma using the demountable modified torch with a slit height of 16 mm and a $1 \mu\text{g ml}^{-1}$ Mn solution. The progress of the simplex to the optimum was fairly rapid and achieved in nineteen steps. Figures 19 - 23 summarise the results of the optimisation and univariant search, and demonstrate the successful confirmation of the simplex optimisation for the five essential parameters. The shaded area on each graph corresponds to the region identified as optimal by the simplex procedure. Figure 19 shows the flow rate of injector gas to be a critical parameter and confirms the success of the optimisation experiment. The plasma gas flow rate was not very critical (Figure 20); above about 10 l min^{-1} little change was observed in the SBR despite large variations in the plasma

gas flow rate. Figure 21 illustrates the success of the simplex procedure in identifying the optimum coolant argon flow rate. Similarly, the optimum observation height was clearly identified by the simplex and shown also to be a critical parameter which was optimal at approximately 20 mm above the top turn of the three-turn load coil. (Figure 22).

It is perhaps the identification of the optimum power to be used in plasma spectrometry which has generated the greatest controversy. Figure 23 illustrates how well the simplex procedure enables optimum power to be defined; in this case, with an argon cooled plasma a relatively low optimum power (0.6 kW coupled into the plasma) was indicated.

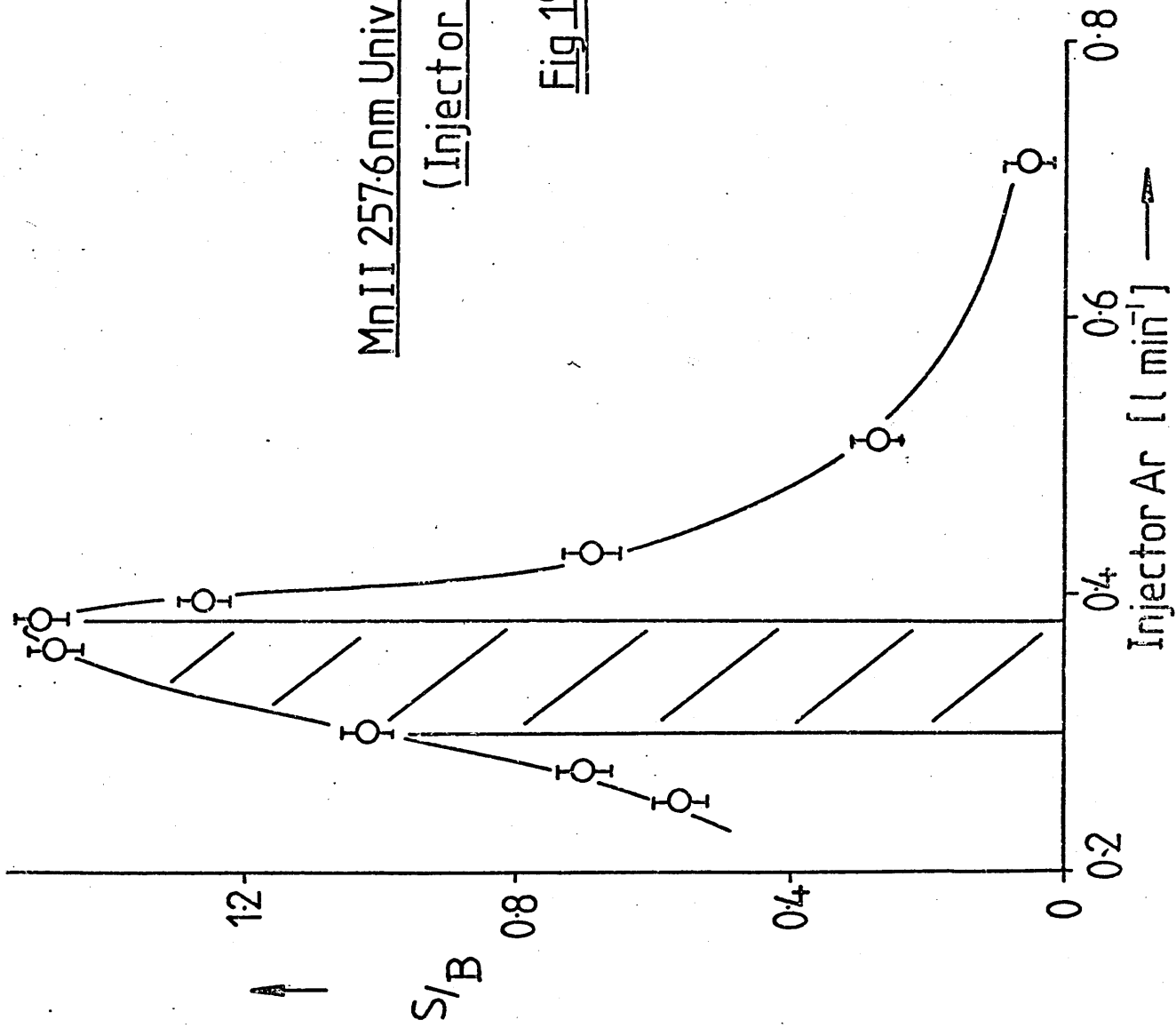
The relative ease and speed of optimisation of the plasma as found in this experiment, combined with good agreement between the univariate search and simplex optima proved the success of the simplex optimisation procedure and led to further studies of the ICP using this method of optimisation.

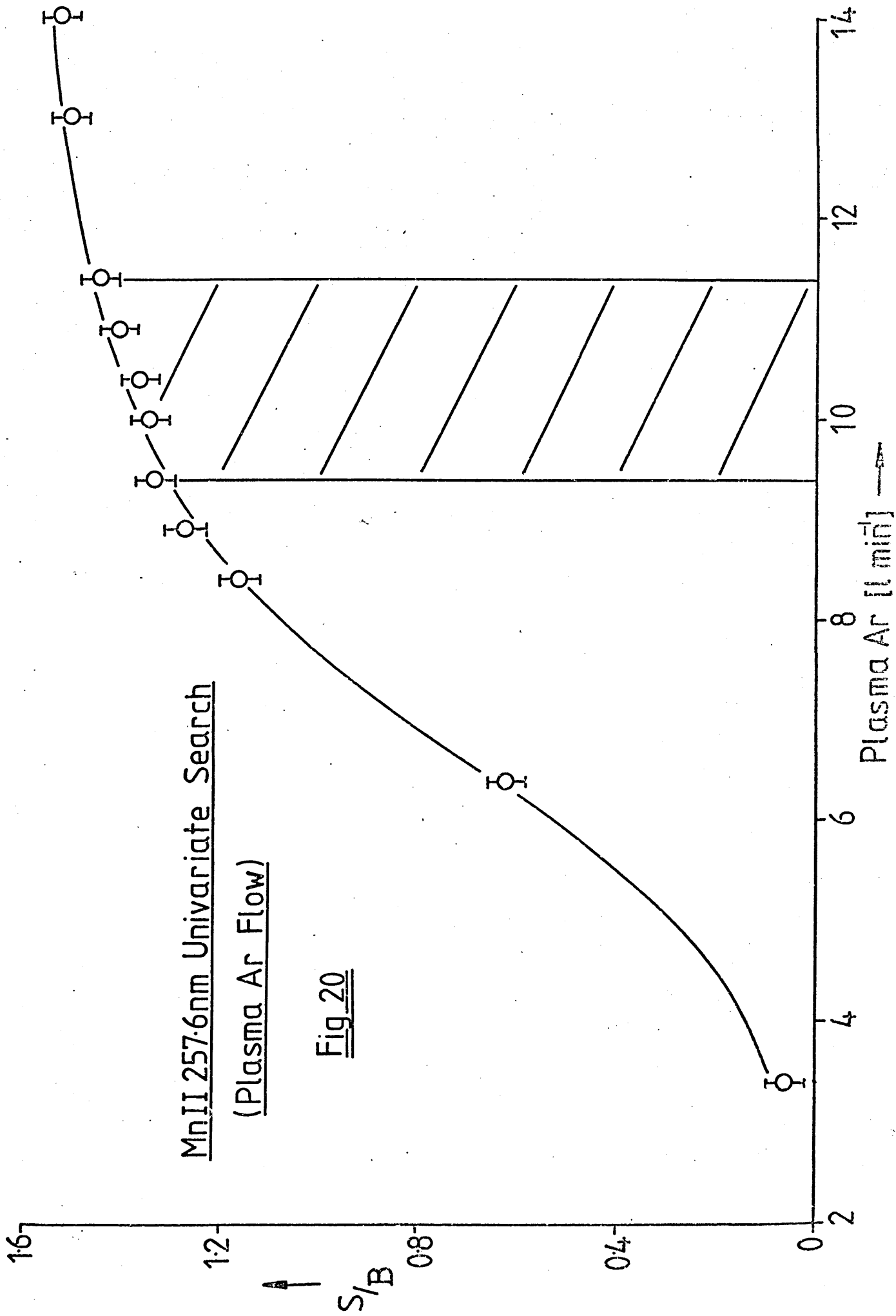
4.4.2 EVALUATION OF THE MODIFIED TORCH

Having developed a method for optimising the ICP, it was thus possible to compare the SBR obtained with the new torch design (described in section 2.1.2), operated under optimised conditions, with the SBR obtained when a two piece Greenfield torch (50) was operated also under optimal conditions, and thus evaluate their respective performances. The systems were optimised using the simplex procedure, using the Mn 257.6 nm ion line with a 16 mm entrance slit at the monochromator, and a $1 \mu\text{g ml}^{-1}$ Mn solution. The Greenfield torch was optimised for the nitrogen cooled argon plasma for which it was designed; problems were encountered with softening of the silica tubes of this torch when argon was used as coolant. The operation of the new design torch was optimised with both argon and nitrogen as coolant gas.

MnII 257.6nm Univariate Search
(Injector Ar Flow)

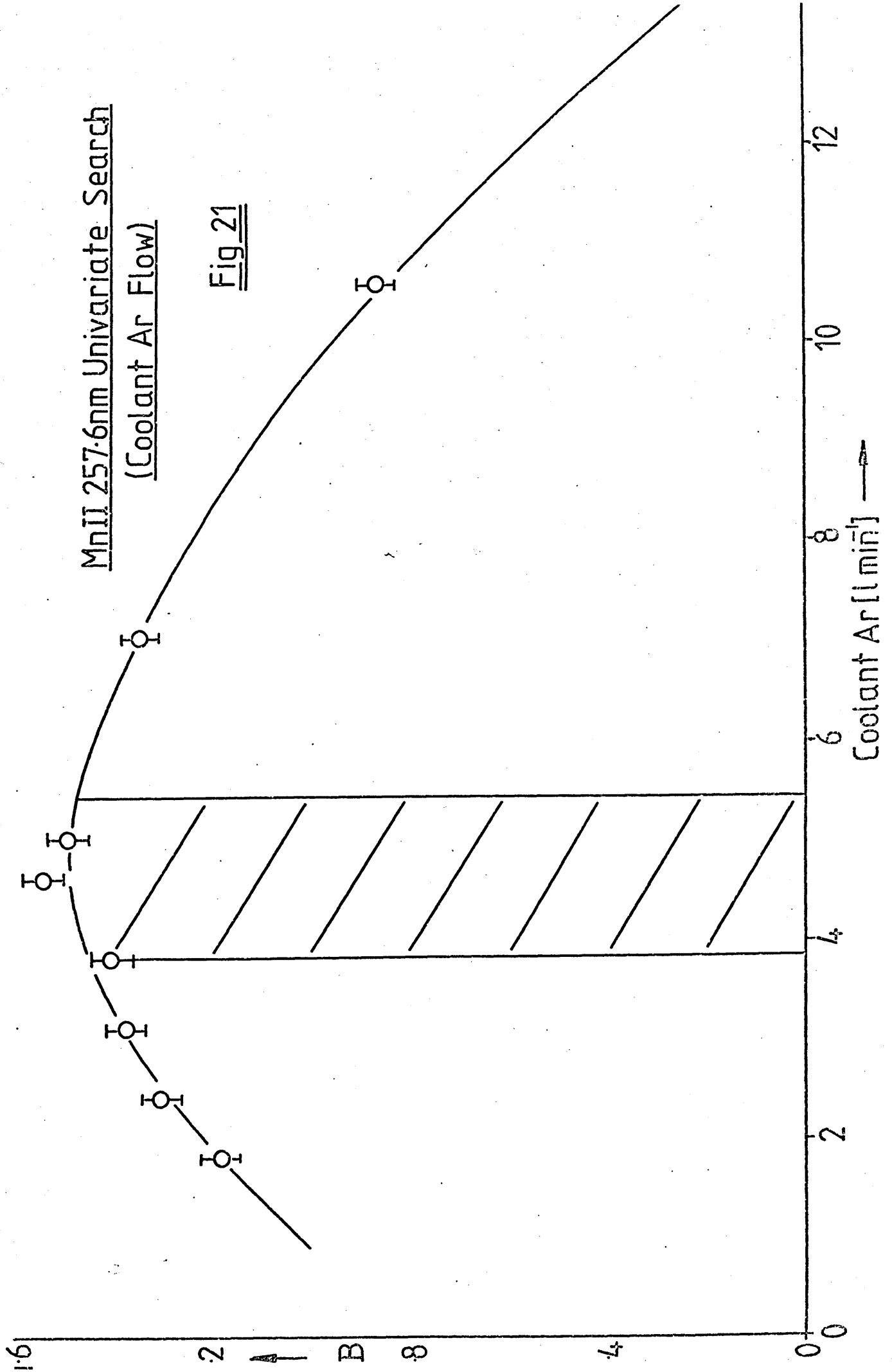
Fig 19





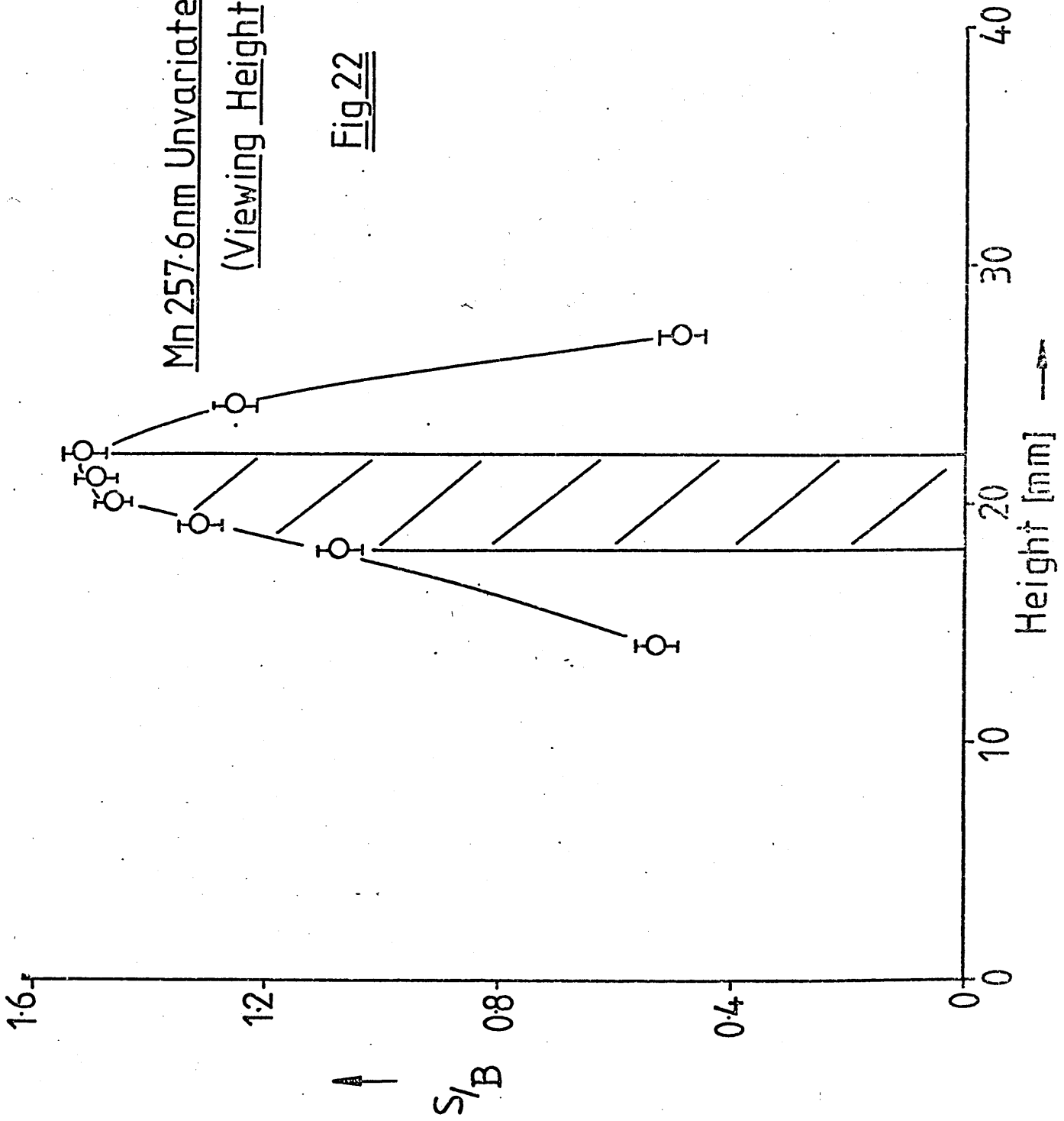
MnII 257.6nm Univariate Search
(Coolant Ar Flow)

Fig 21



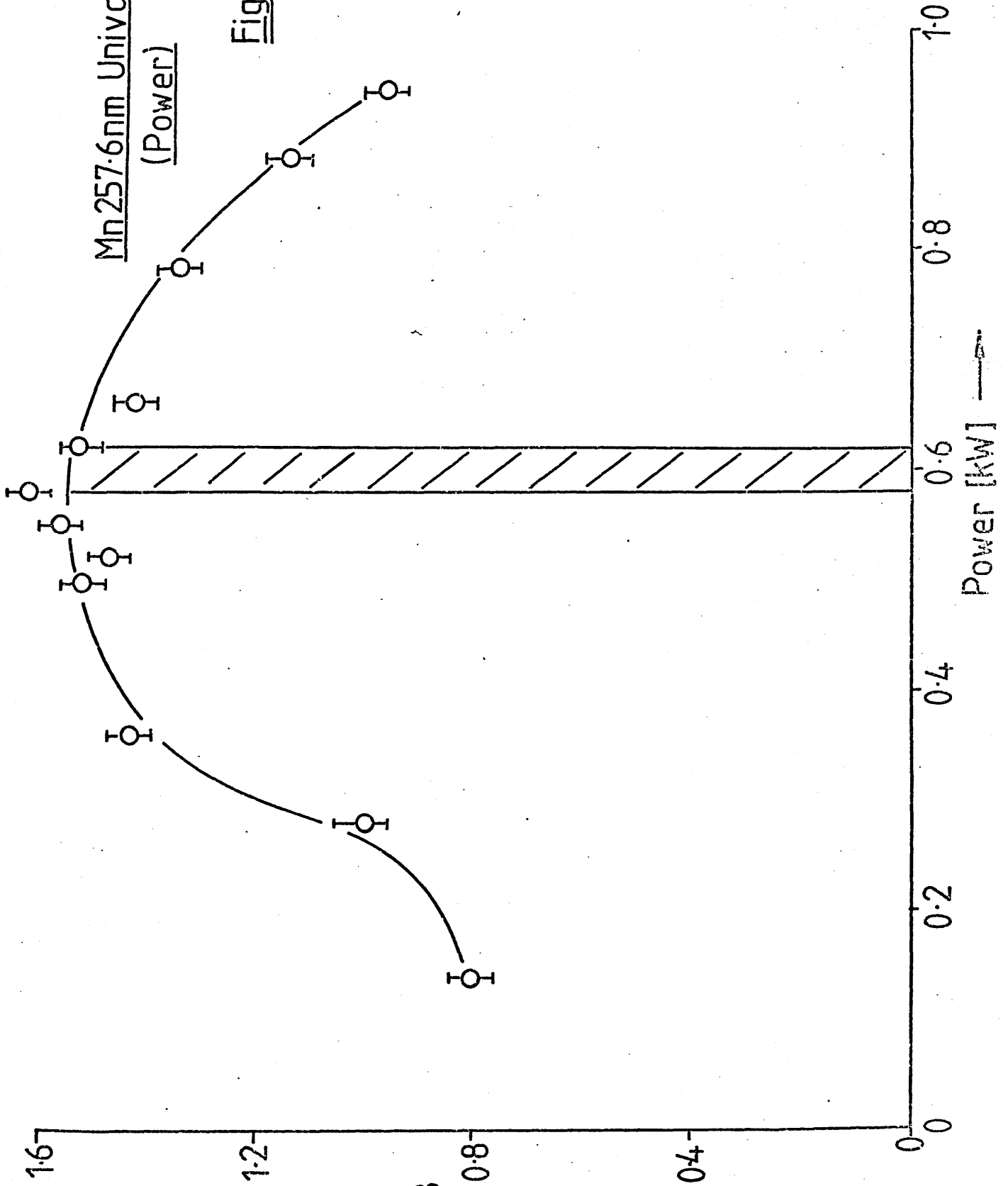
Mn 257.6nm Univariate Search
(Viewing Height)

Fig 22



Mn 257.6nm Univariate Search

Fig 23



Having optimised the two torches the univariate searches confirmed that the simplex had, where possible identified true optima; the exceptions occurred when instrumental constraints precluded achievement of the indicated value. The univariate searches (Figures 24 - 28) were also instructive in indicating the different characteristics of the torches.

Figure 26 shows that similar nitrogen coolant gas flows were optimal for either torch. Only when argon was used did the coolant gas flow rate appear to be critical. Figure 25 shows clearly that lower flows of argon as plasma gas were optimal in the operation of the Greenfield torch. The flared nature of the intermediate tube in the modified torch probably explains this phenomenon. In contrast, the lower optimal injector gas consumption for the modified torch compared to the Greenfield torch (Figure 24) was probably the result of a more complex inter-relationship between gas flows and plasma characteristics. Figure 27 shows the optimal viewing height to be essentially similar for each combination; however, it should be recalled that a slit height of 16 mm and a 1 : 1 image were used and this may have disguised more subtle differences. As discussed later in this chapter, lower power is optimal in the all argon plasma compared to the nitrogen cooled plasma (Figure 28). Unfortunately, under the optimal gas flows it was not possible to couple more than c.a. 1.2 kW power into the plasma when the present torch design was used with nitrogen coolant.

Table 2 summarises the optimised plasma conditions for both the torches investigated and also shows the SBR obtained on aspiration of a $1 \mu\text{g ml}^{-1}$ Mn solution at optimum conditions. Clearly there is an improvement of a factor of three in SBR with the new torch design for this particular element. Similar noise levels are found for both torches and therefore a gain in detectability was also observed.

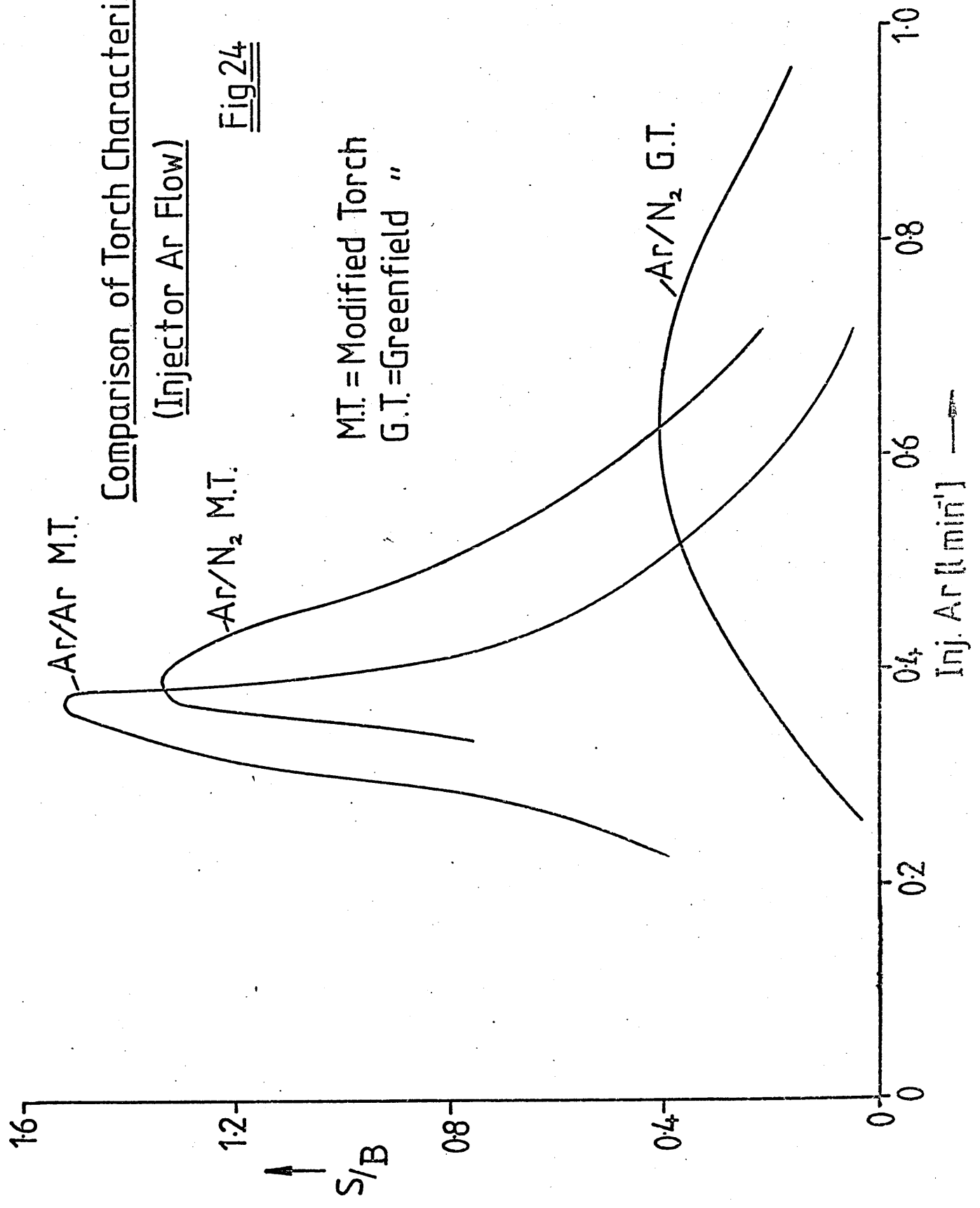
Comparison of Torch Characteristic
(Injector Ar Flow)

Fig 24

Ar/Ar M.T.
Ar/N₂ M.T.

M.T. = Modified Torch
G.T. = Greenfield "

Ar/N₂ G.T.

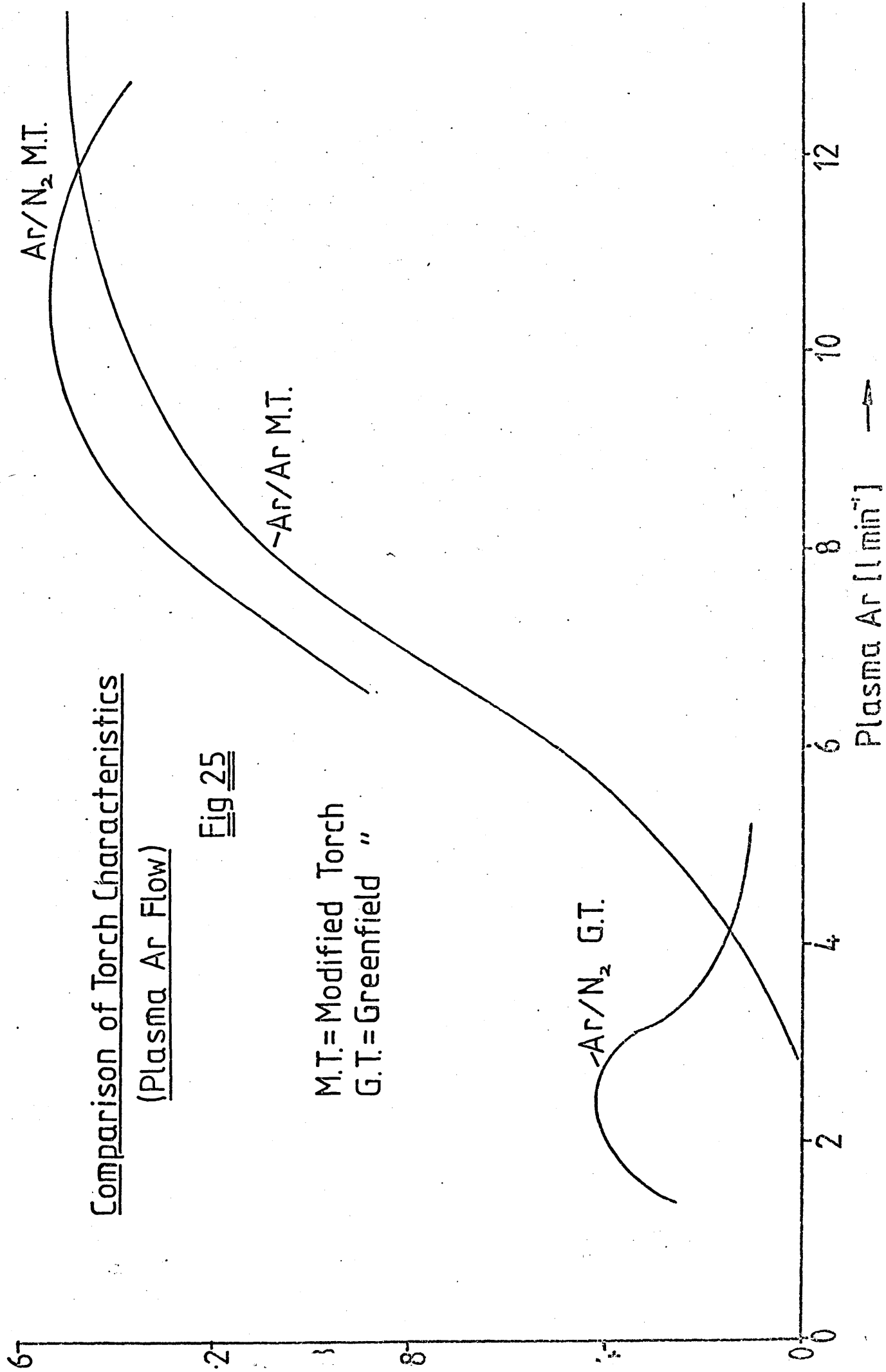


Comparison of Torch Characteristics

(Plasma Ar Flow)

Fig 25

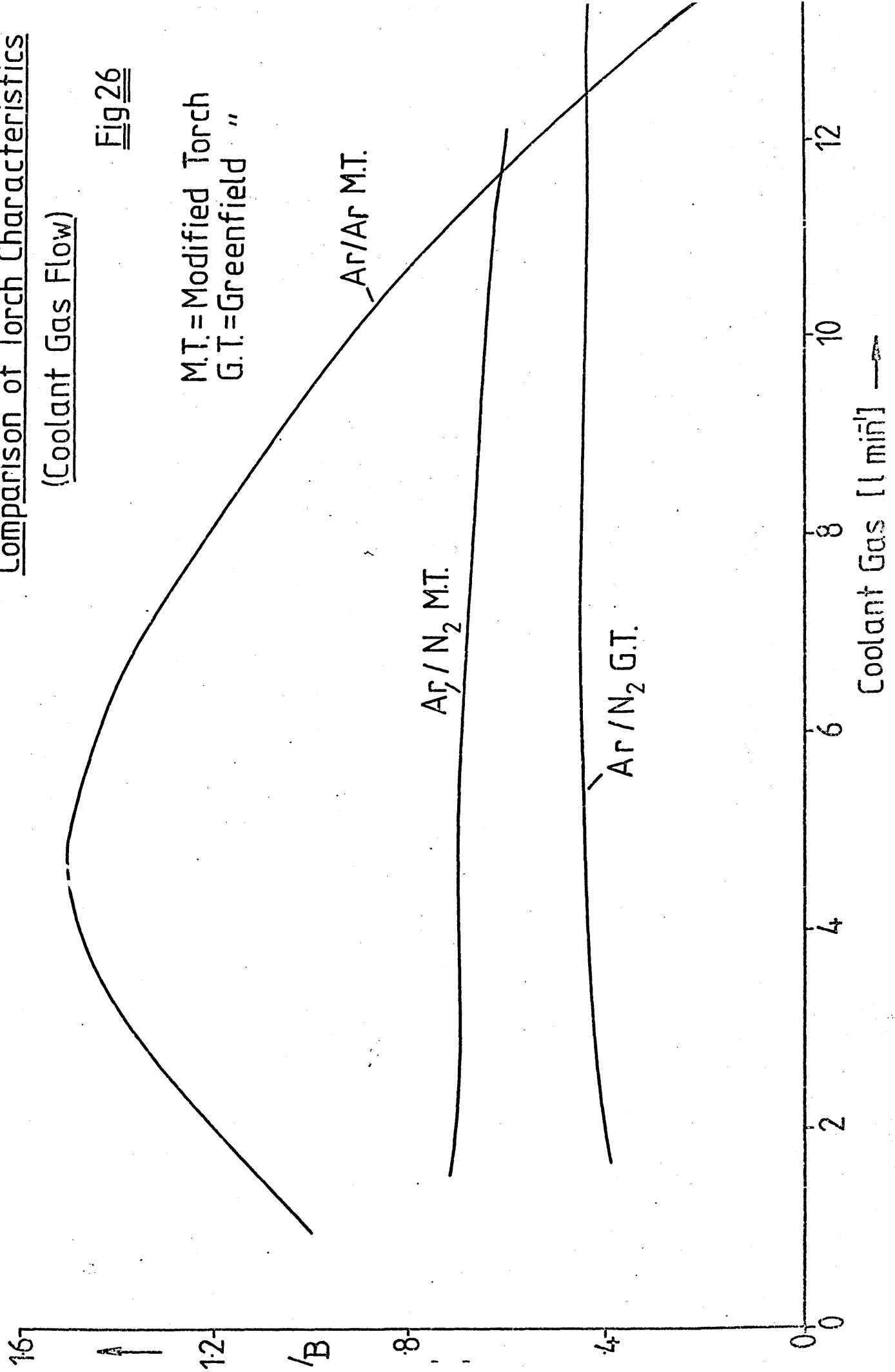
M.T.= Modified Torch
G.T.= Greenfield "



Comparison of Torch Characteristics
(Coolant Gas Flow)

Fig 26

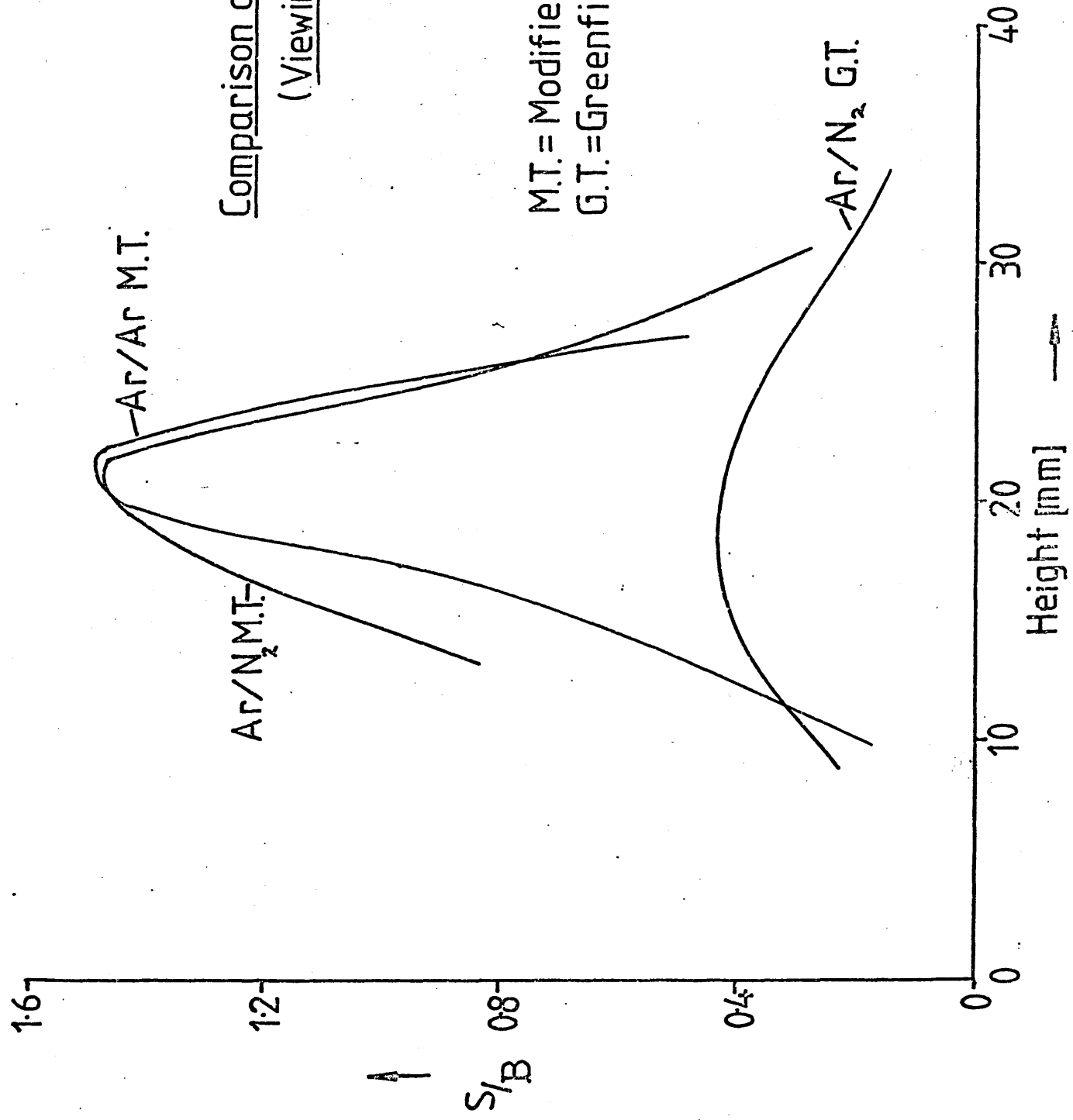
M.T. = Modified Torch
G.T. = Greenfield "



Comparison of Torch Characterist
(Viewing Height)

Fig 27

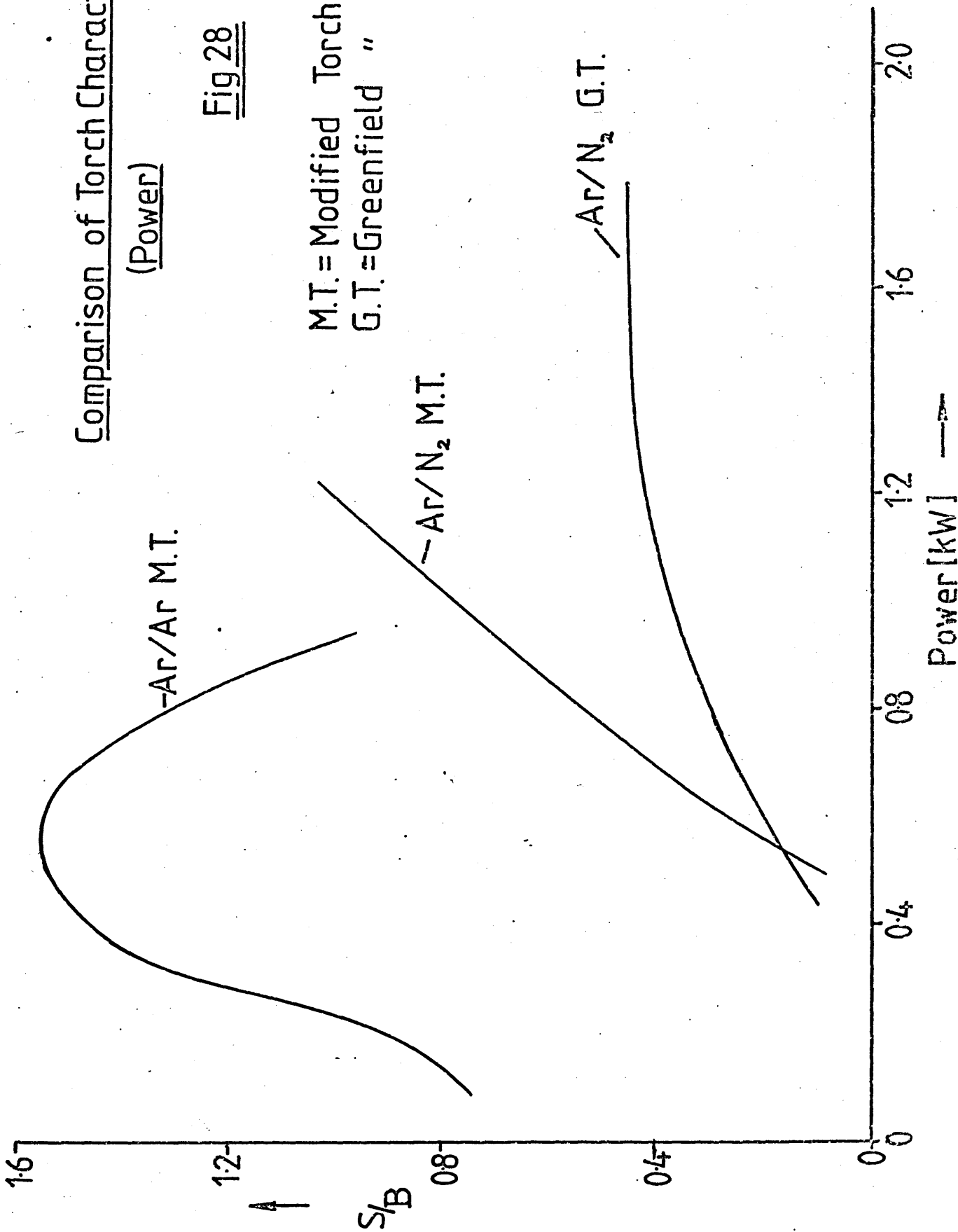
M.T. = Modified Torch
G.T. = Greenfield "



Comparison of Torch Characteristics

(Power)

Fig 28



Once the performance of an argon-cooled plasma on the new torch with the 3 mm plasma inlet jet and the 2 mm coolant gas jet had been optimised, the effect of varying the jet sizes on the univariate searches was investigated. Although not a rigorous optimisation, and therefore not a true comparison, such experiments can produce useful information. Figure 29 shows the effect of altering the plasma gas inlet jet on the SBR as the plasma gas flow is varied. Larger jet sizes whilst increasing gas consumption also increase sensitivity. The effect of changing jet sizes for the coolant gas inlet is more interesting (Figure 30). A high tangential velocity seems required here, and above a certain jet size analytical performance deteriorates.

The modified torch described in section 2.1.2 and subsequently here offers considerable promise in optical emission spectrometry with an ICP. It would appear to offer considerable advantages when either argon or nitrogen cooled plasmas are used in situations requiring either operation over a wide range of gas flows or in other non-routine situations where versatility is required.

4.4.3 COMPARISON OF OPTIMAL CONDITIONS USING 16 mm AND 4 mm SLIT HEIGHT

Following the evaluation of the new torch using simplex optimisation, further experiments were carried out to make comparisons between optimal conditions for different elements using the new torch. Arsenic was chosen as a traditionally more difficult element than manganese for determination by atomic emission spectroscopy. An optimisation experiment was thus carried out on the As 228.8 nm atom line in an all argon plasma using $100 \mu\text{g ml}^{-1}$ solution of As, and a slit height of 16 mm.

The results are summarised in Figures 31 - 35, again good agreement between the regions defined as optimal by the simplex and the maxima of the univariate search graphs was found.

Effect of Varying Plasma Gas Inlet Jet Sizes

Δ = 1 mm i.d.
 \times = 2 mm i.d.
 \circ = 3 mm i.d.
 $+$ = 4 mm i.d.

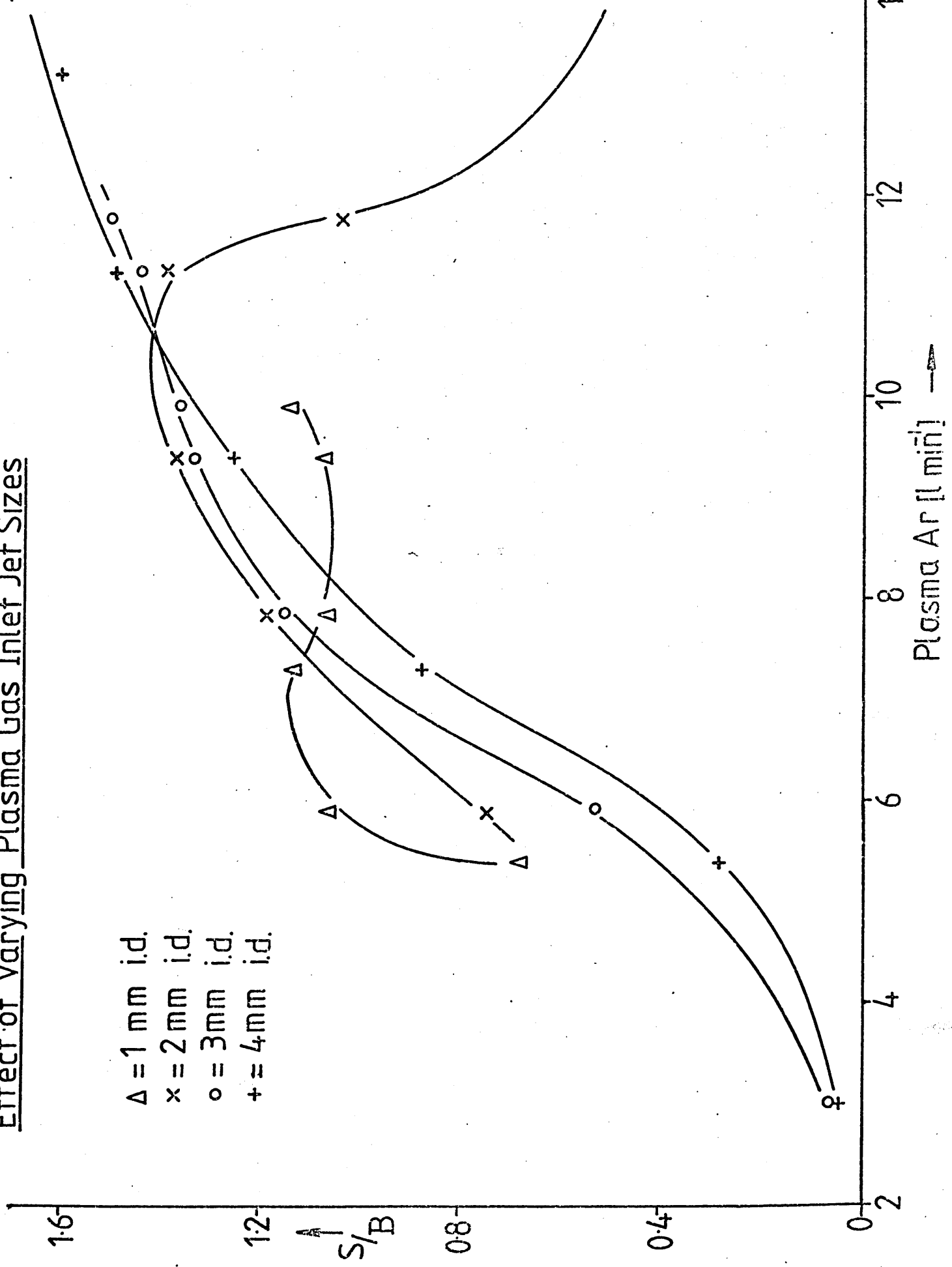


Fig 29

Effect of Varying Coolant Gas Inlet Jet Sizes

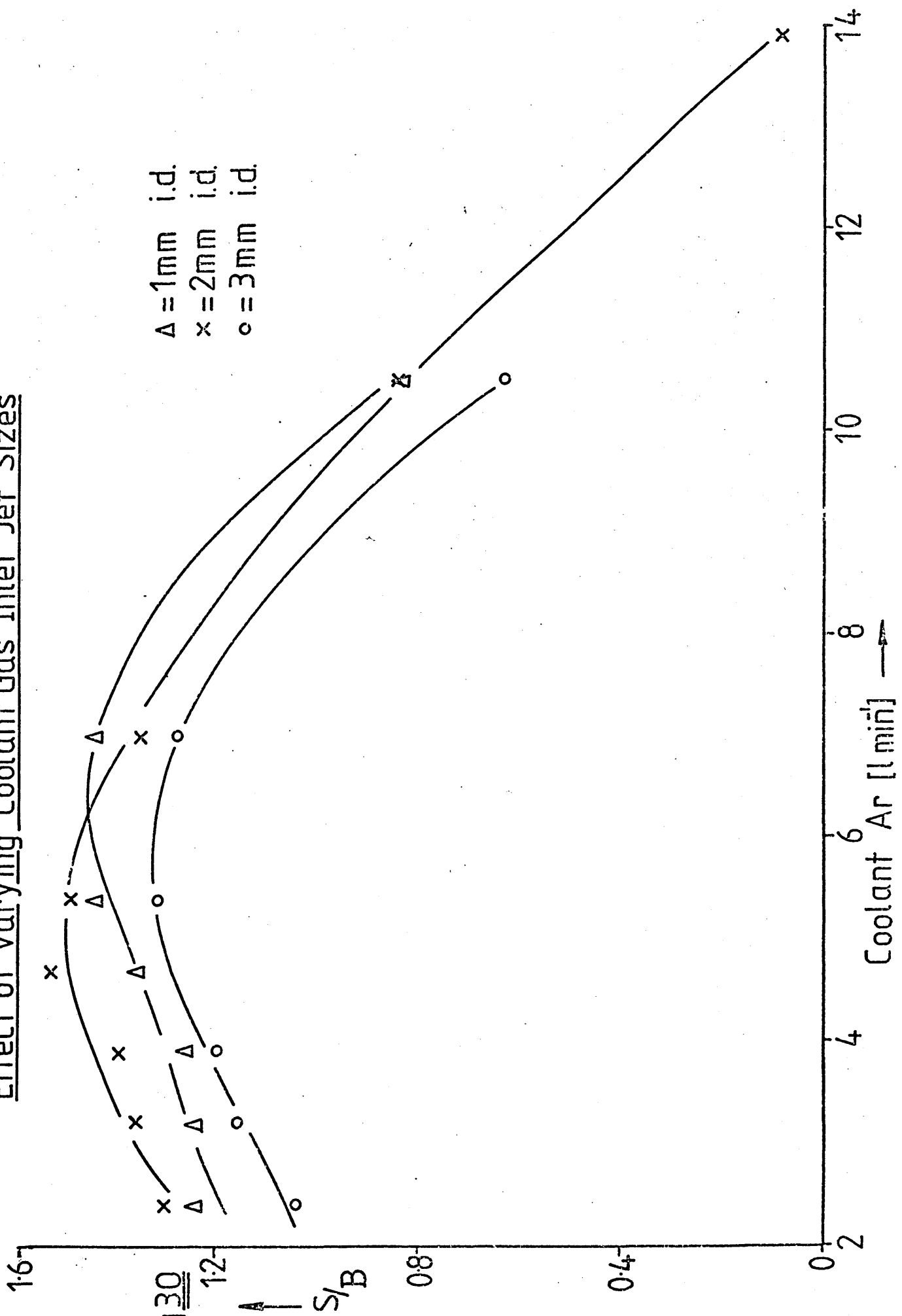


Fig 30

As 228.8nm Univariate Search (Injector Ar
Flow)

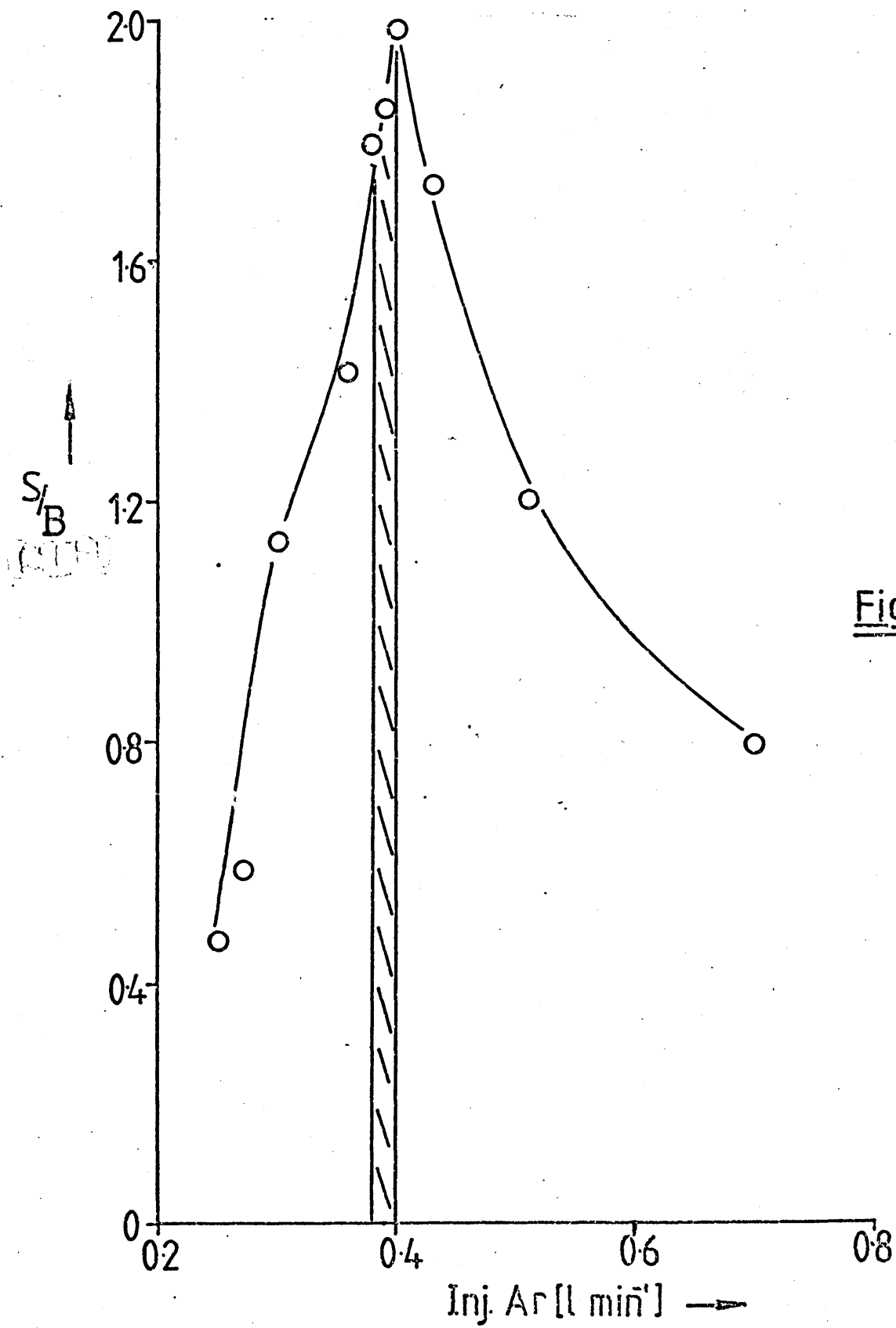


Fig.31

As228-8nm Univariate Search (Coolant Ar Flow)

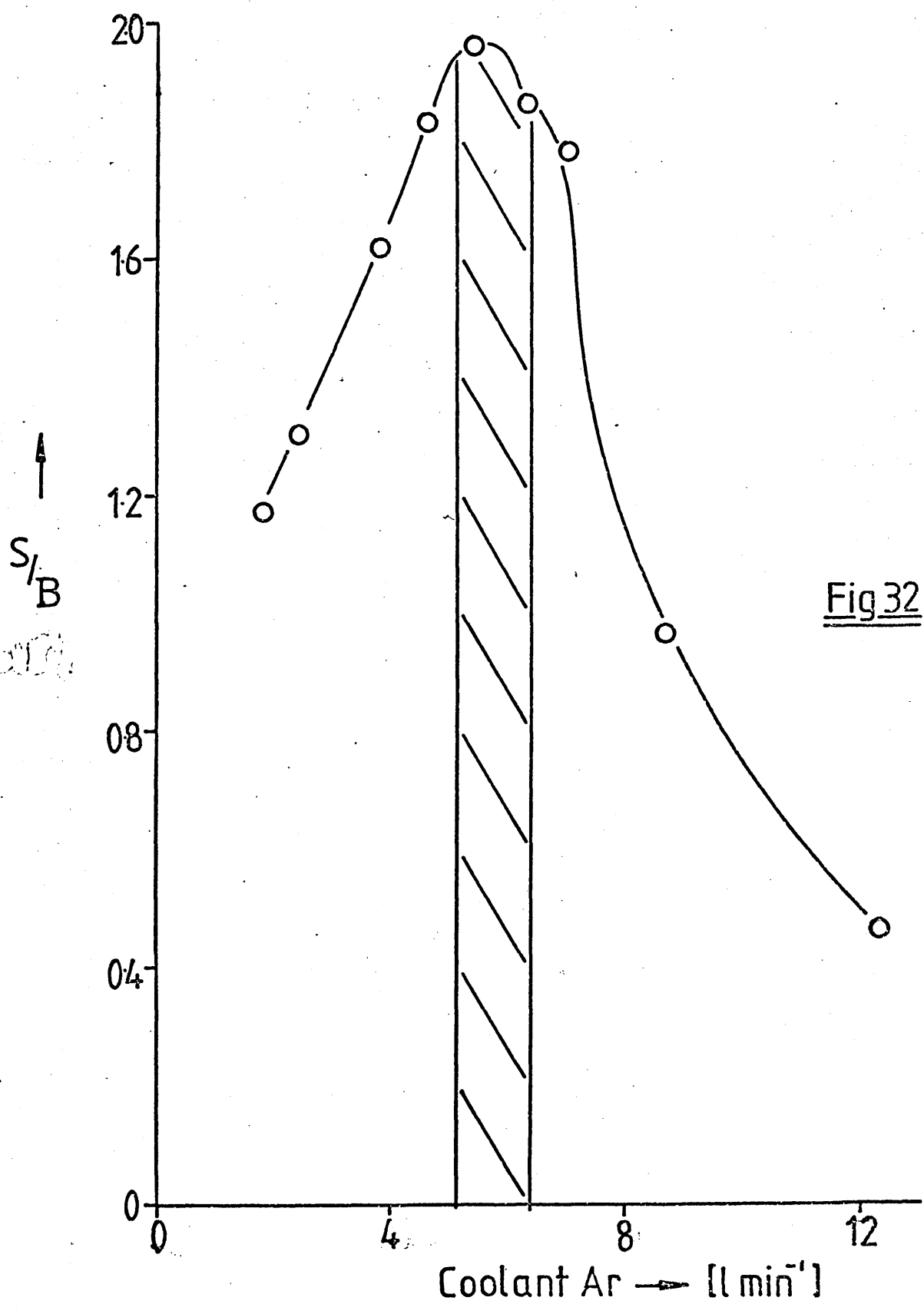


Fig 32

As 228.8nm Univariate Search (Plasma Ar Flow)

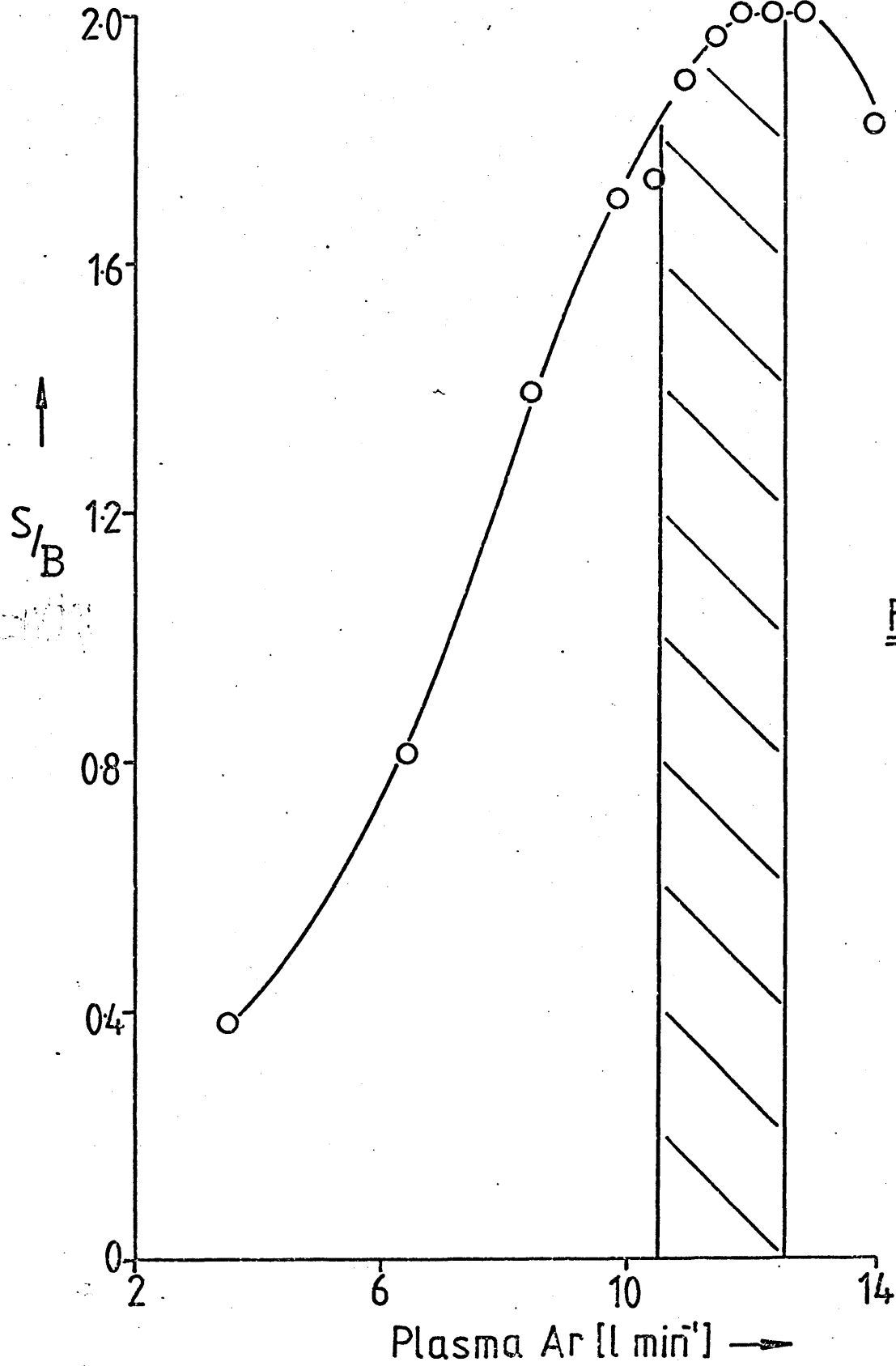
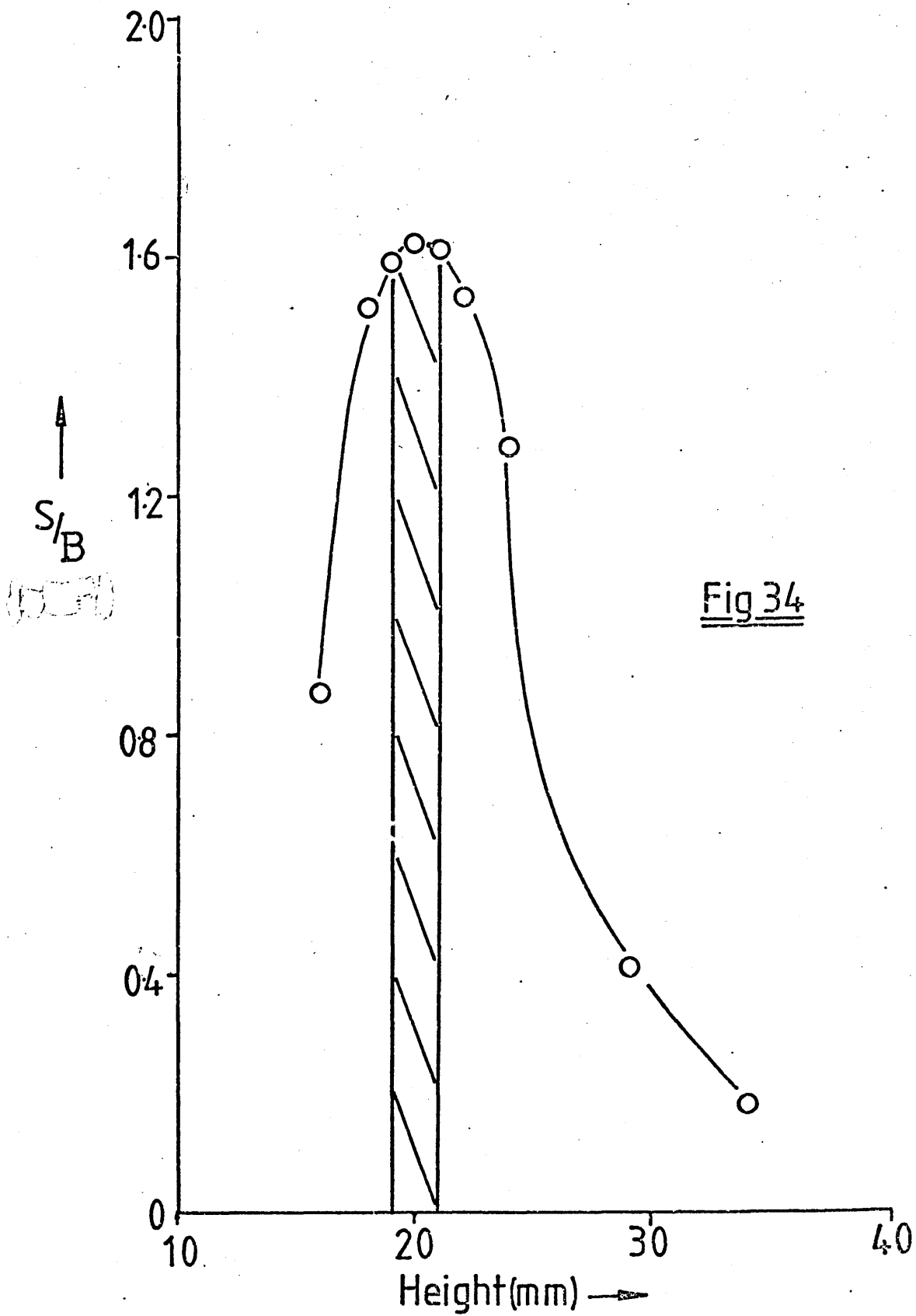
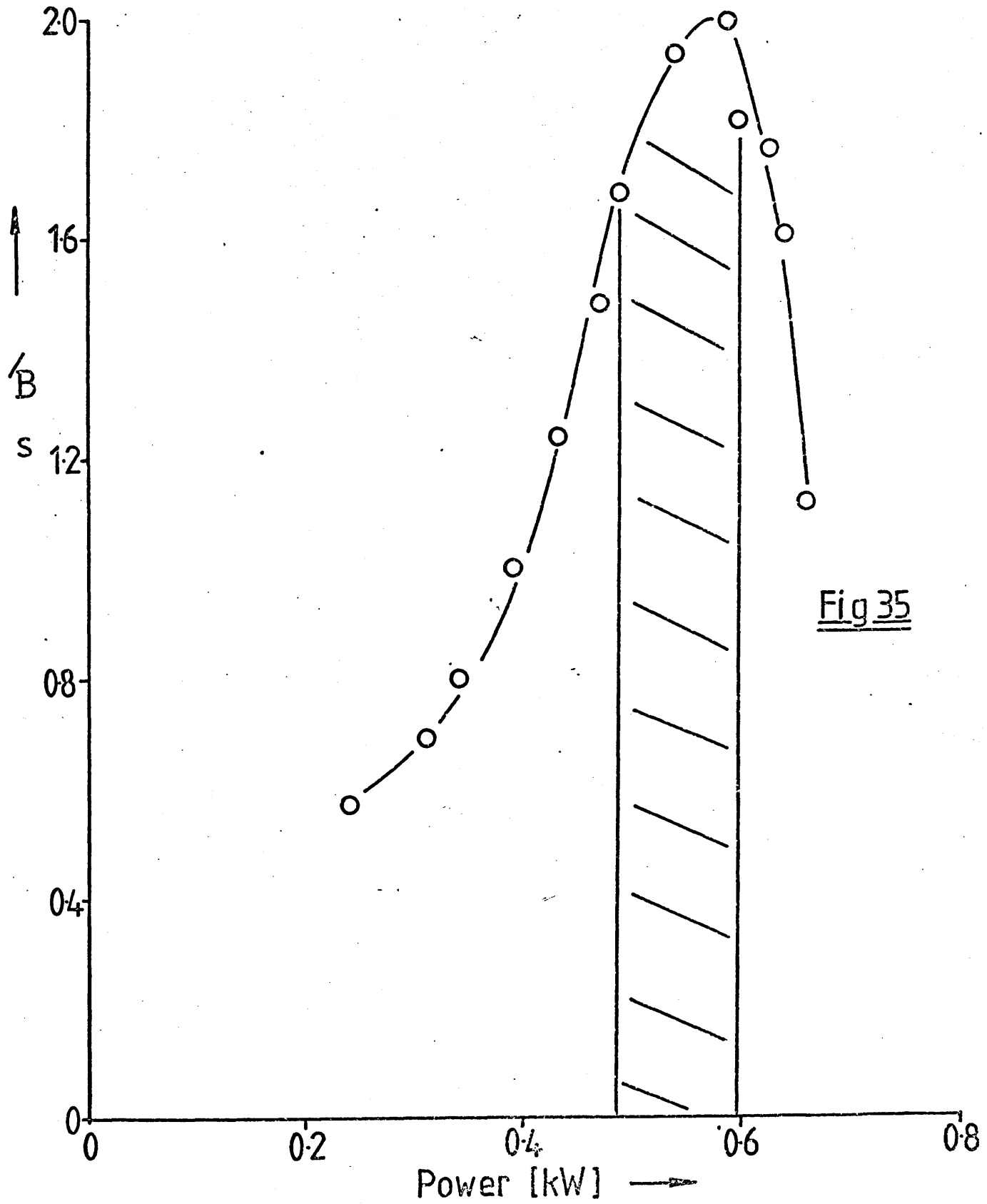


Fig 33

As 228.8nm Univariate Search (Viewing Height)



As 228.8nm Univariate Search (Power)



The injector gas flow rate and viewing height (Figures 31 and 34) were again found to be the most sensitive parameters when using the modified torch (see also Figures 19 and 22 for Mn results with the modified torch). The power (Figure 34) was optimised successfully and was found to be similar to that obtained for the Mn ion line (257.6 nm) (i.e. approximately 0.6 kW).

The three optimal values for the viewing height for the As and the two Mn optimisations were all found to be approximately 20 mm above the load coil. This was a somewhat unexpected conclusion, as other workers have suggested that different lines might have varying optimum viewing heights in the tail flame (152-155) and it was thought that this could be due to the relatively large section of the plasma tail flame viewed (16 mm). It was decided that a reduction in the spectrometer slit height would help to resolve the optimal viewing regions if they occurred in differing sections of the tail flame. Hence a slit height of 4 mm was chosen and the Mn 257.6 nm ion line was re-optimised using the smaller slit height. The results of this optimisation are summarised in Figures 36-38 along with the original optimal conditions obtained using a 16 mm slit height. The decreased slit height produces an increase in SBR which would be the case if the majority of Mn emission emanated from a relatively small section of tail flame (<4 mm high) so that a reduction of the slit height would not reduce the signal significantly, but since contributions to the nett background signal come from all parts of the tail flame, reducing slit height would cut out a certain amount of background. Thus reduction of the height of tail flame viewed would produce increased SBR. The univariate search graphs show that there is essentially no difference in the optimal gas flows for the two slit heights, although the shapes of the curves differ due to the changed relationship between signal and background, this is most marked in Figure 37(a) where the coolant nitrogen univariate search curve is almost flat for the large slit height, whereas for the smaller slit height the SBR shows a more sharply defined optimum.

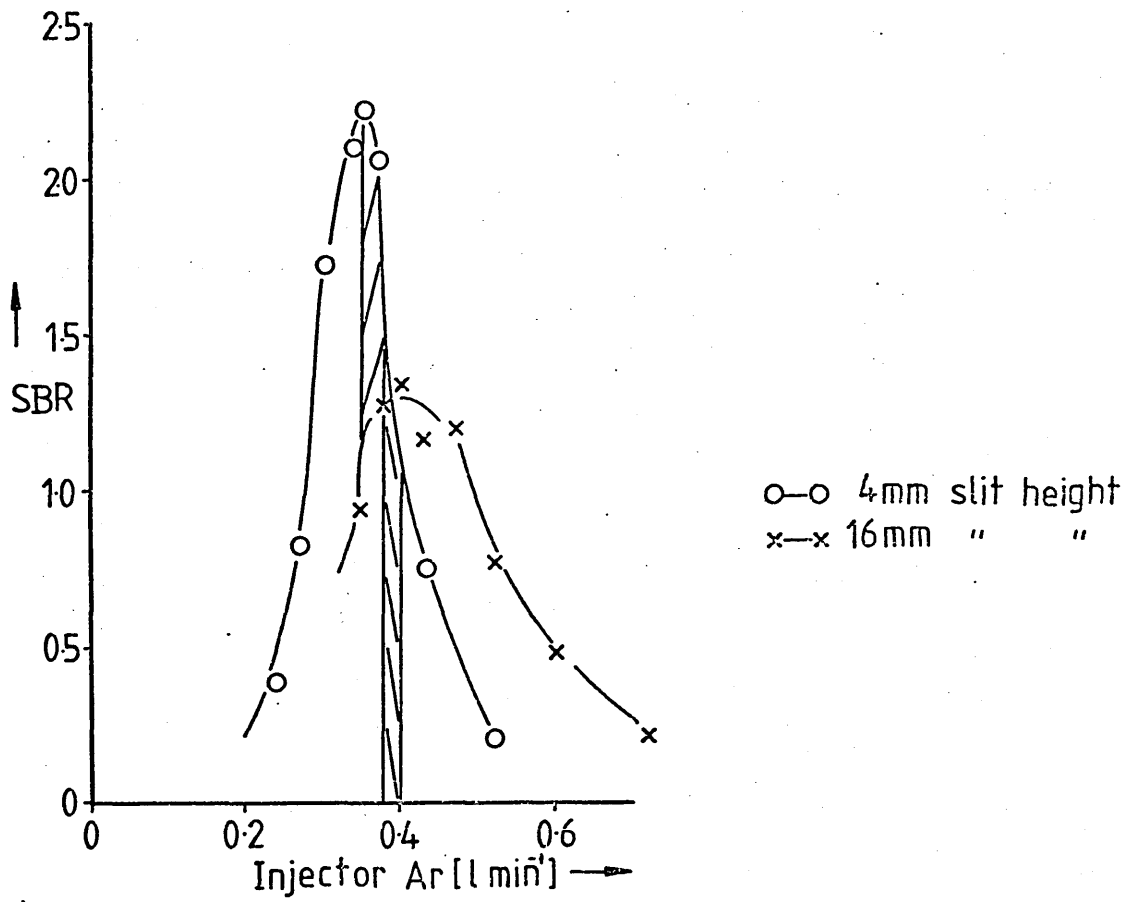


Fig 36(a)

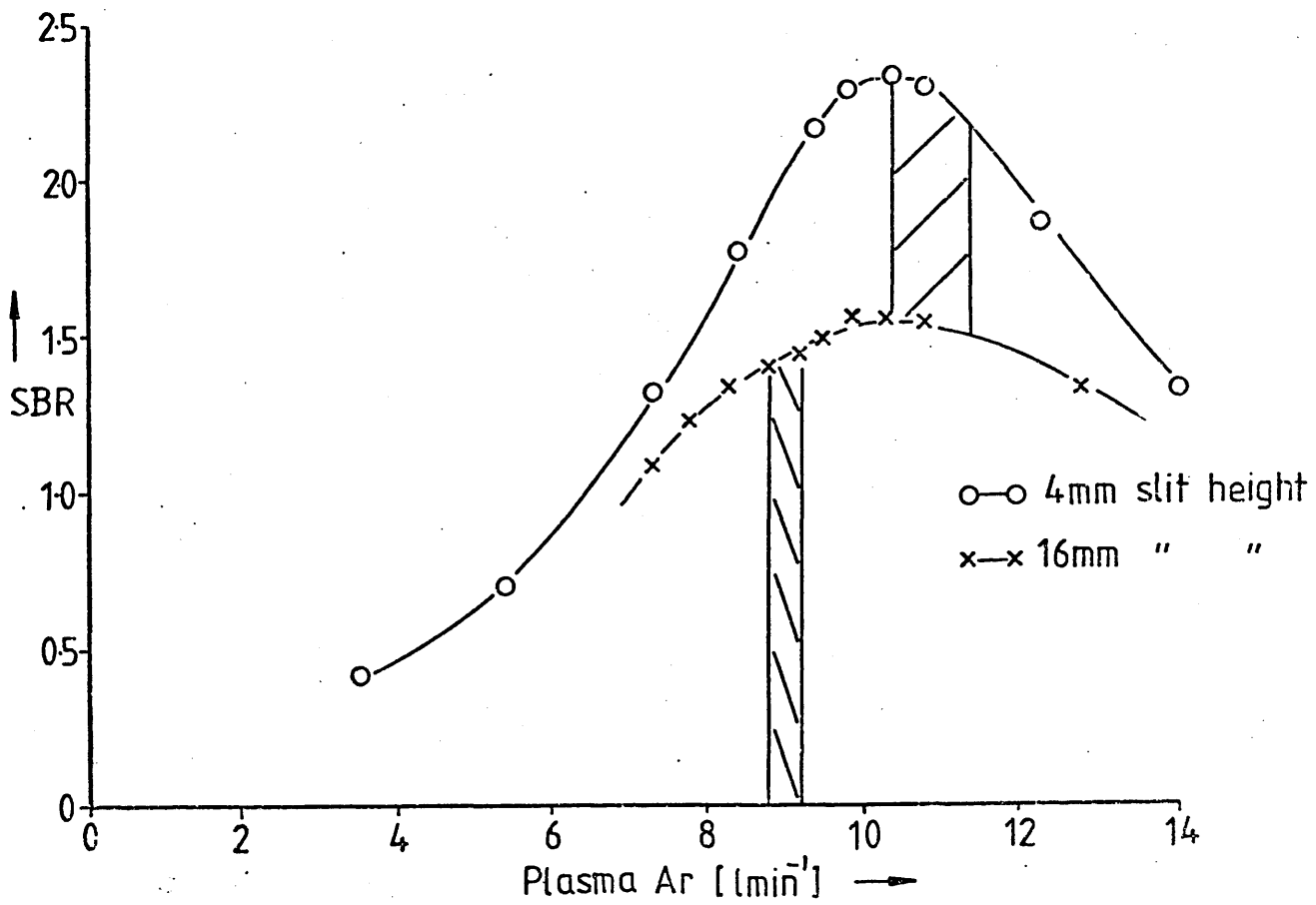


Fig 36(b)

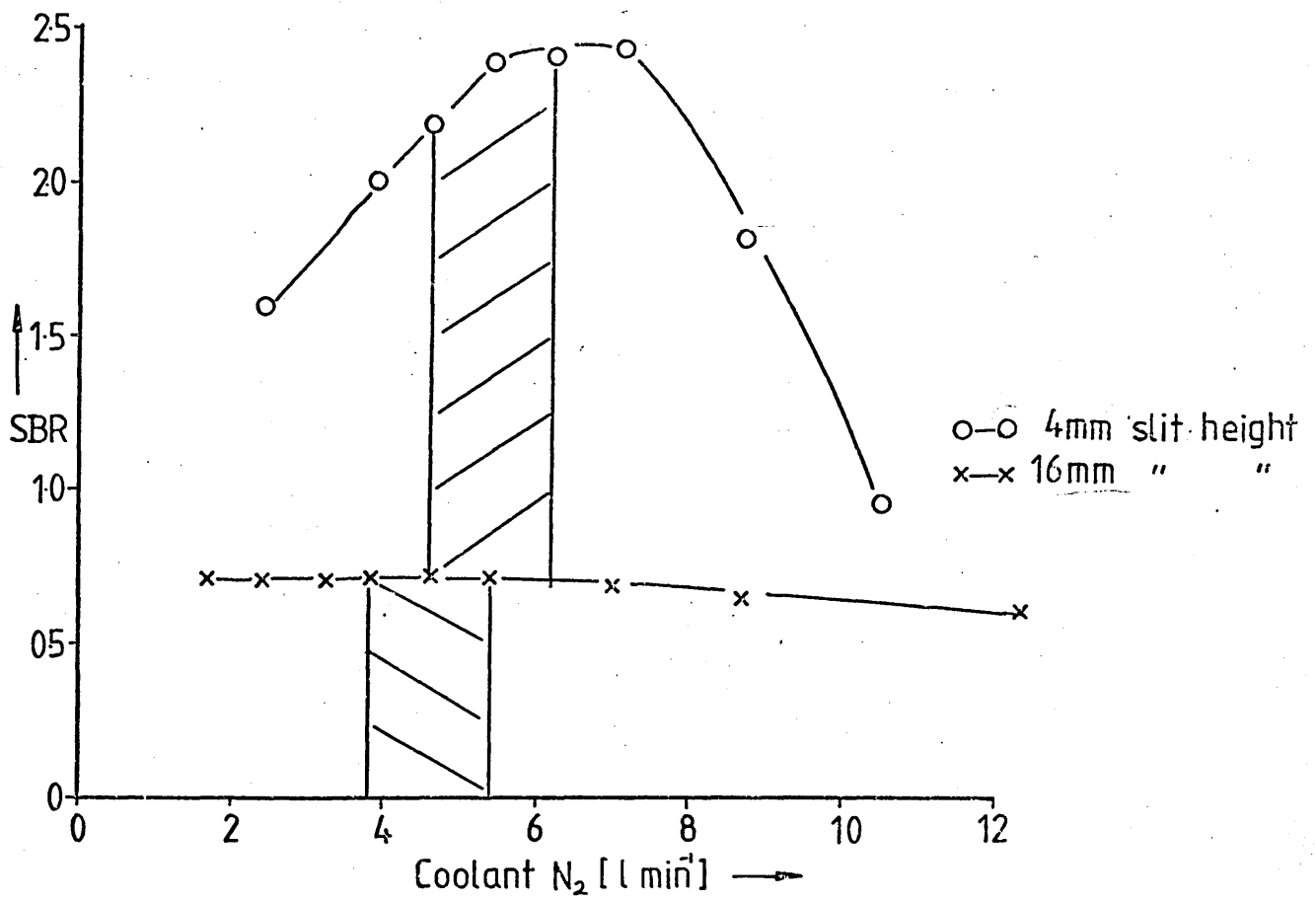


Fig. 37(a)

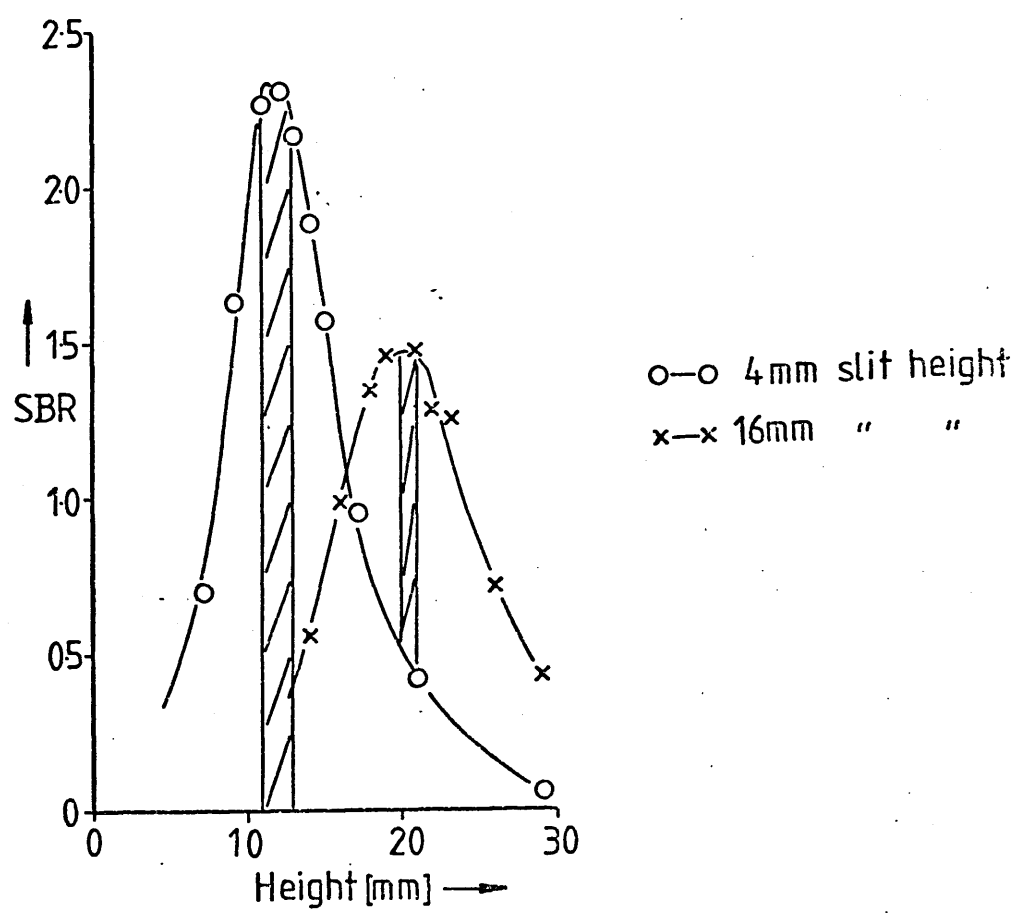


Fig. 37(b)

Slit Heights

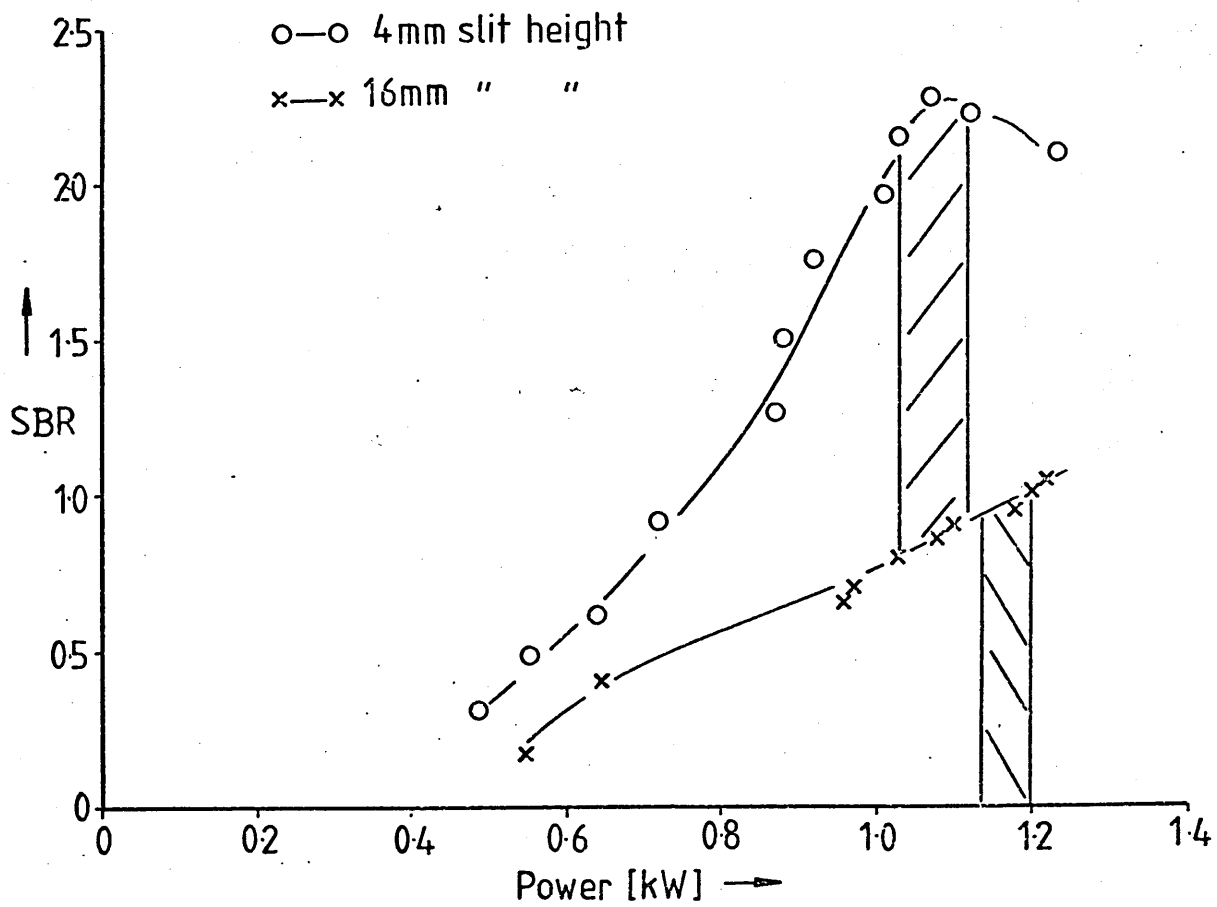


Fig 38

As perhaps might be expected the viewing heights for the two optimisations (Figure 37b) show the largest discrepancy moving from the original 20 mm to 12 mm above the load coil showing that the larger slit was concealing underlying trends. The power optimum also shows a shift from 1.2 to 1.06kW (Figure 38) when the slit height is reduced, and it appears that a defined optimum was obtained for the smaller slit height whereas the physical constraints of the instrument did not allow a true optimum to be obtained for the larger slit height.

Having established that variation of the slit height did not markedly effect the optimal gas flows for the Mn 257.6 nm ion line in a nitrogen cooled plasma, an assumption was made that this would also be true for the optimal gas flows for the Mn 257.6 nm ion line in an all argon plasma, and the As 228.8 nm ion line in an all argon plasma. Hence a rigorous re-optimisation for these two lines was not carried out for the smaller slit, but the univariant searches for power and viewing height were repeated using the 4 mm slit height. The results of those experiments as well as for the rigorously optimised Mn line are summarised in table 3.

The optimal power and viewing heights for Mn and As in an argon cooled plasma were only changed marginally with the 4 mm slit height. The SBR for the Mn line in the argon cooled plasma was increased, as for the nitrogen cooled plasma, presumably for the reasons discussed earlier. The SBR for As was however, fractionally reduced, this could be due to the reduced signal from the argon background continuum at lower wavelengths and hence reducing the slit height does not significantly decrease the background signal, thus keeping the SBR virtually constant.

This short investigation has shown that SBR is a function of the length of tail flame viewed, it is debatable, however, as to whether 'slit height' or 'height of plasma viewed' is an essential variable in the optimisation of the plasma and hence should be included in

the simplex procedure, or it is in fact part of the readout system which is not being optimised. For the purposes of this work, a fixed slit height of 4 mm has been adopted, enabling different sections of the tail flame to be resolved sufficiently to allow the determination of the part of the tail flame in which optimal SBR, for different elements, is to be found.

4.4.4 COMPARISON OF OPTIMAL CONDITIONS IN A NITROGEN COOLED ARGON PLASMA AND AN ALL ARGON PLASMA

Having developed a successful technique for optimising the plasma, and constructed a torch that could be used with argon or nitrogen as coolant it was now possible to obtain the optimal operating conditions for a number of different elements and spectral lines in the two different kinds of plasmas. This information can then be used, not only to find out how to obtain best analytical performance from this system, but also to help settle wider issues, discussed earlier in this chapter, i.e. should low or high power be used, or is an all argon plasma superior to a nitrogen cooled argon plasma?

As it was not practicable to optimise every line of every element a set of atom and ion lines were chosen with varying 'difficulties of excitation' (defined as the excitation potential plus the ionisation potential for that line and expressed in e V) which would be representative of the large number of spectral lines available for emission spectroscopy, these are listed in table 4.

Optimisation of these lines was carried out using the previously described simplex optimisation technique, with both argon cooled and nitrogen cooled plasmas using the modified demountable torch design and a 4 mm slit height.

The optimised conditions and optimal SBR for each line in each type of plasma are shown in table 5. Except for the optimisation of

Comparison of 4&16mm Slit Height Optimal
Conditions

Element	Wave-length /nm	Coolant Gas	Optimum Conditions, 16mm slit			Optimum Conditions, 4mm slit		
			Power, kW	Height, mm	SBR	Power, kW	Height, mm	SBR
Mn II	257.6	N ₂	>1.2	21	1.2	1.06	12	2.3
Mn II	257.6	Ar	0.58	21	1.5	0.54	18	4.2
As I	228.8	Ar	0.59	20	2.0×10^{-2}	0.59	18	1.5×10^{-2}

Table 3

Spectral Lines Used for Optimisation Experiments in this Work

Element	Wave-length /nm	A / eV	B / eV	A+B
As I	228.8	6.7	—	6.7
B I	249.8	4.9	—	4.9
Mn II	257.6	4.8	7.4	12.2
Mo II	281.6	4.52	7.38	11.9
V II	309.3	4.38	6.74	11.1
Cu I	324.8	3.8	—	3.8
Ca II	393.4	3.15	6.05	9.2
Mn I	403.1	3.1	—	3.1
Ba II	455.4	2.7	5.2	7.9

A=Excitation Potential

B=Ionisation Potential

Table 4

Element	Wave-length /nm	Energy of Excitation/eV	Coolant Gas	Gas Flows [l min ⁻¹]			Viewing Height m	Power W	SBR
				Coolant	Plasma	Injector			
As I	228.8	6.7	Ar	5.4	12.3	0.40	18	0.59	1.5×10^{-2}
B I	249.8	4.9	Ar	5.4	9.4	0.36	21	0.46	1.25
Mn II	257.6	12.2	Ar	5.0	14.0	0.37	18	0.54	4.2
Mn I	403.1	3.1	Ar	8.7	14.0	0.58	26	0.50	11.9
Ba II	455.4	7.9	Ar	4.6	12.0	0.40	22	0.50	37.5
As I	228.8	6.7	N ₂	4.0	10.0	0.38	14	1.16	9.6×10^{-3}
B I	249.8	4.9	N ₂	4.6	8.9	0.45	14	0.82	0.49
Mn II	257.6	12.2	N ₂	6.2	10.4	0.35	12	1.06	2.3
Mo II	281.6	11.9	N ₂	6.6	10.4	0.35	12	0.96	0.34
V II	309.3	11.2	N ₂	6.2	10.5	0.43	13	0.81	8.2
Mn I	403.1	3.1	N ₂	7.0	3.1	0.49	26	0.26	16.7
Ba II	455.4	7.9	N ₂	5.4	1.7	0.72	29	0.49	37.0
Ca II	393.4	9.2	N ₂	6.0	9.4	0.46	17	0.69	54.0
Cu I	324.8	3.8	N ₂	5.0	12.0	0.68	29	0.49	4.8

Optimal Operating Conditions for N₂ Cooled & All Ar Plasmas

Table 5

the Ba 455.4 nm ion line in an nitrogen cooled plasma, all of the regions found to be optimal by the simplex procedure agreed closely with the maxima of the univariant search graphs hence confirming the success of the simplex optimisation. For the Ba line it was found that when carrying out the univariate search for the plasma gas flow rate the SBR peaked at a much lower flow rate than was indicated by the simplex method. It was concluded that the simplex had become stranded at a false optimum, and hence a new set of starting parameters were calculated and the simplex was restarted. The new optimal regions obtained by the second simplex search were found to agree with the univariate search graphs. Figure 39 shows the univariate search graph for the plasma argon flow. The cross-hatched region between 10 and 12 lmin^{-1} argon was the region originally identified as optimal by the simplex. This particular experiment showed that the simplex search was not infallible in finding the optimum, the univariate search was, however, able to show this and allowed a new simplex to be carried out and hence the correct optimum to be found.

In the following discussion of optimal conditions in the two types of plasma not all of the univariate search graphs will be presented, as many of these are similar and can be visualised by comparison with the fairly representative univariate searches discussed previously (see Figures 19-23 and 31-35). Only those univariate search graphs necessary either to illustrate interesting features or an important point will be shown.

Consider first the optimal coolant gas flow rates. Of all the five parameters the coolant flow seems to exert the least influence on the optimal SBR. All of the univariate search graphs are similar (see Figures 21, 26 and 32) for both types of plasma. The gas flows for both argon and nitrogen gas are similar (approximately 4 to 6 lmin^{-1}), except for the Mn 403.1 nm atom line where a slightly higher gas flow is optimal in both plasmas. The reason for this is not clear, although by visual inspection of the plasma

Double Peaked Plasma Gas Univariate Search Graph
for Ba(455.4 nm, Ar/N₂ plasma)

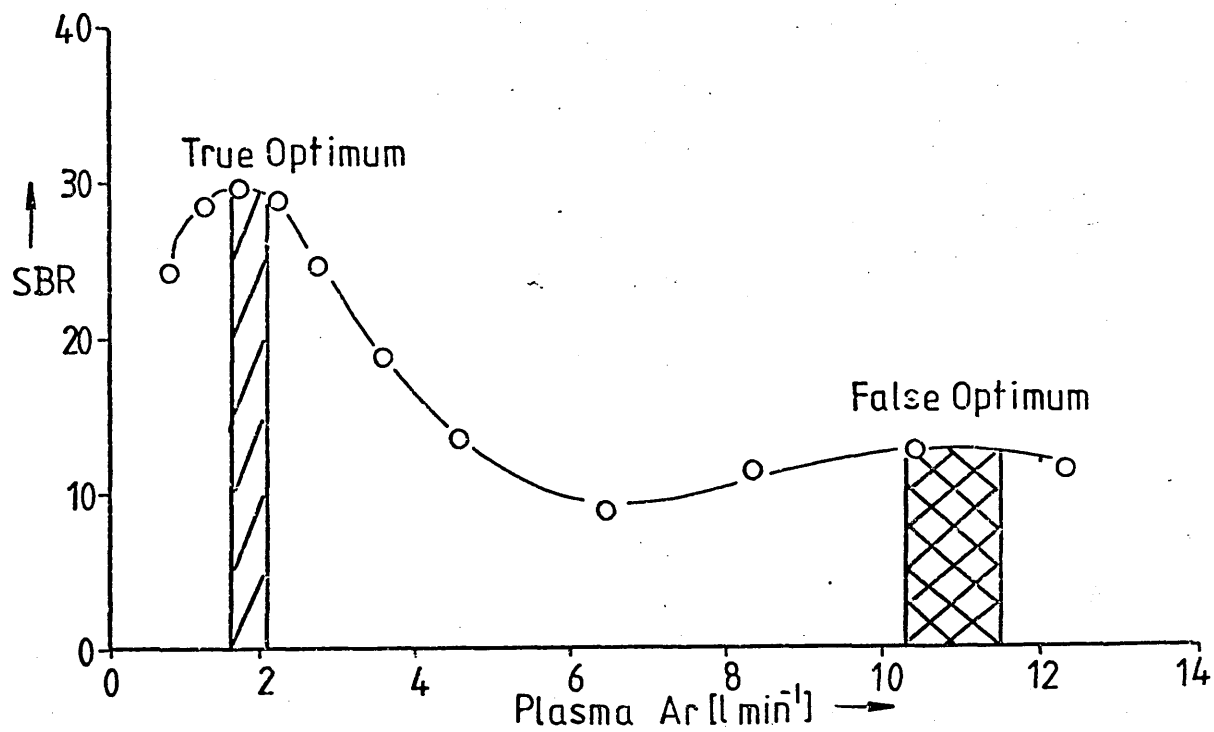


Fig 39

Fig 40(a)

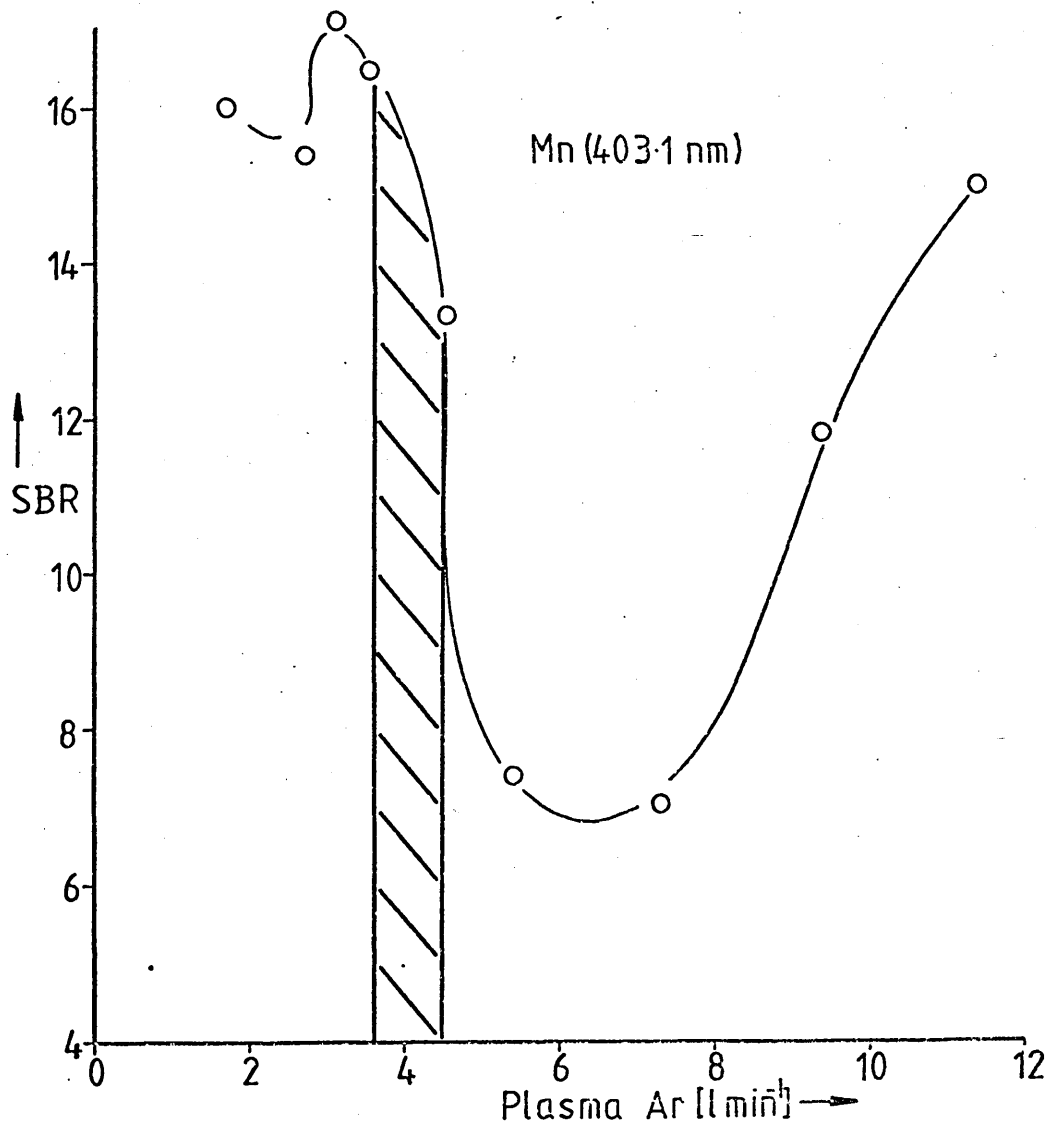
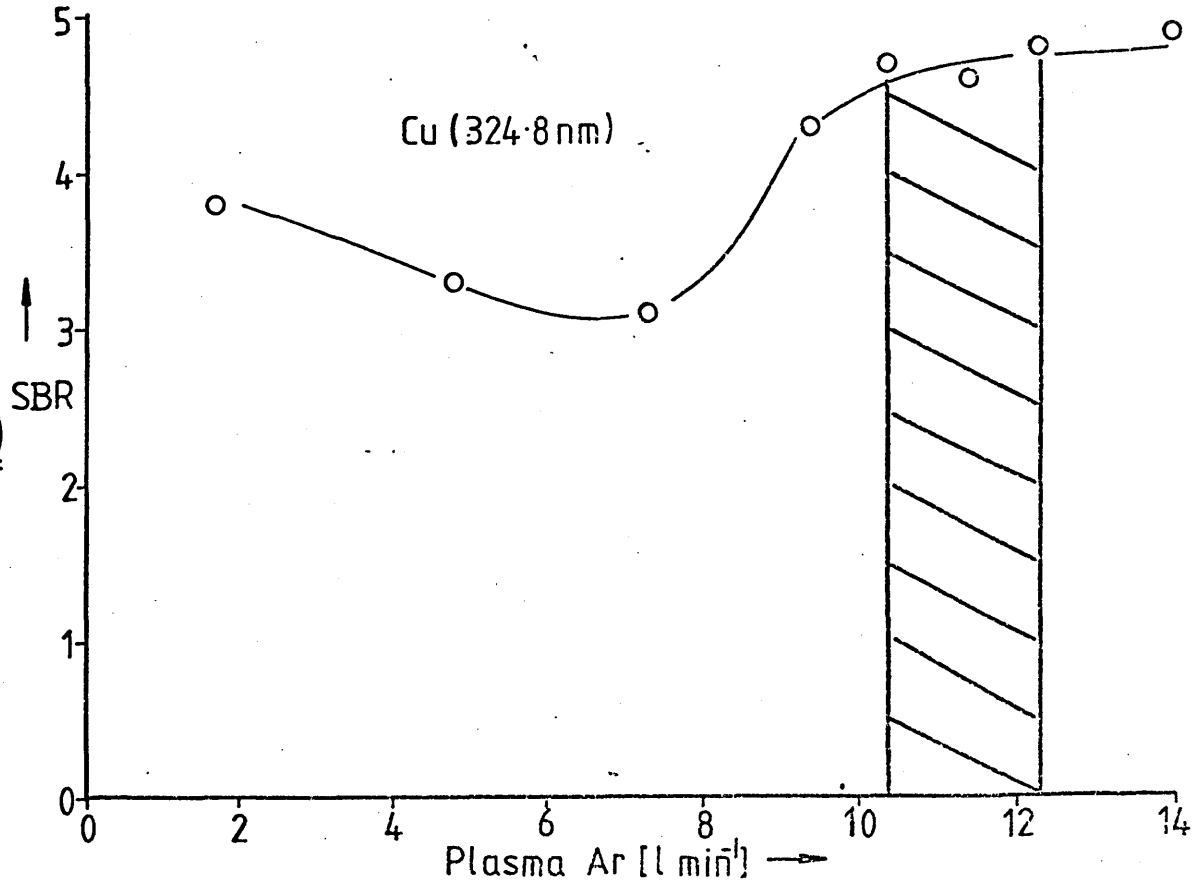
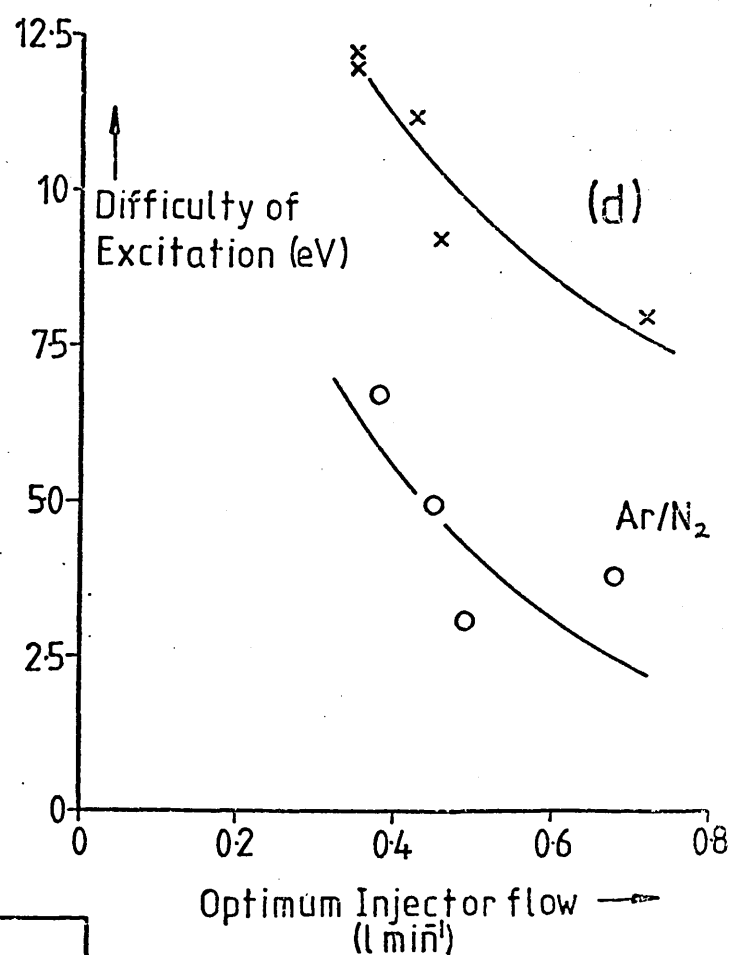
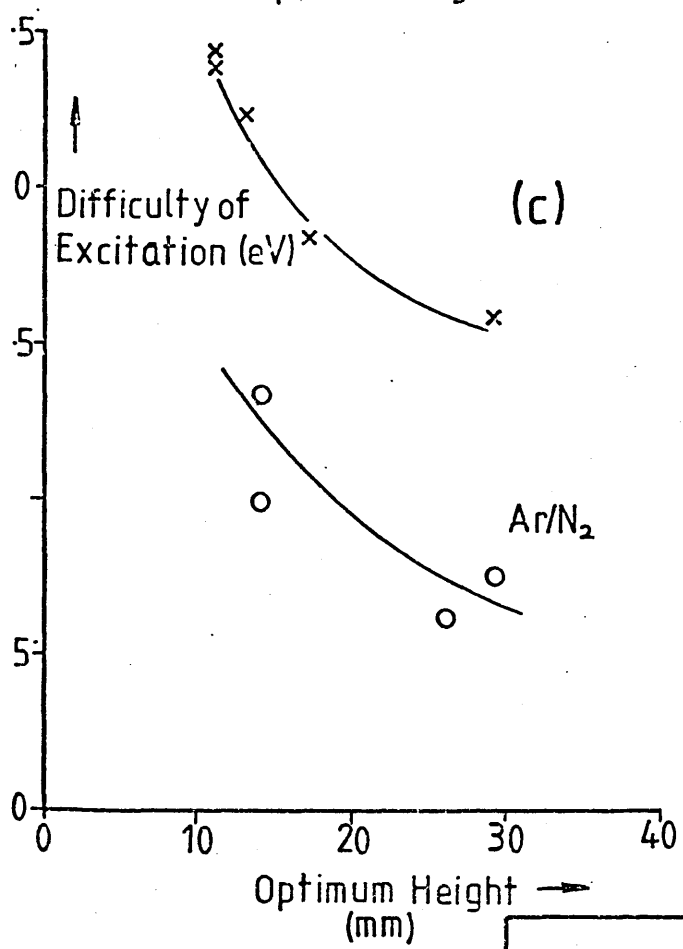
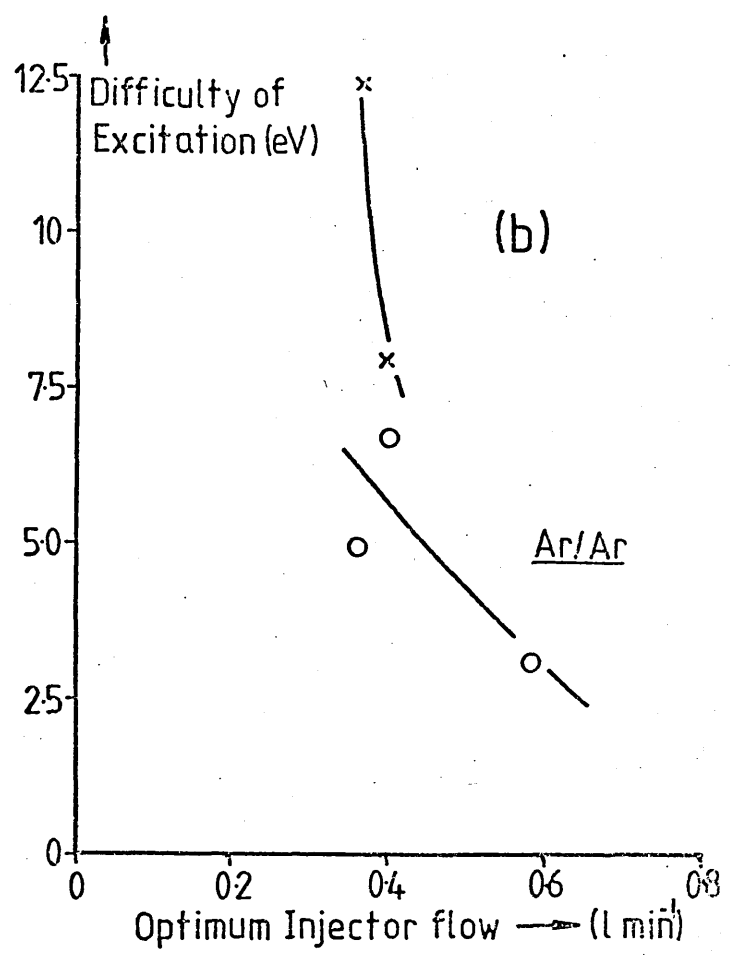
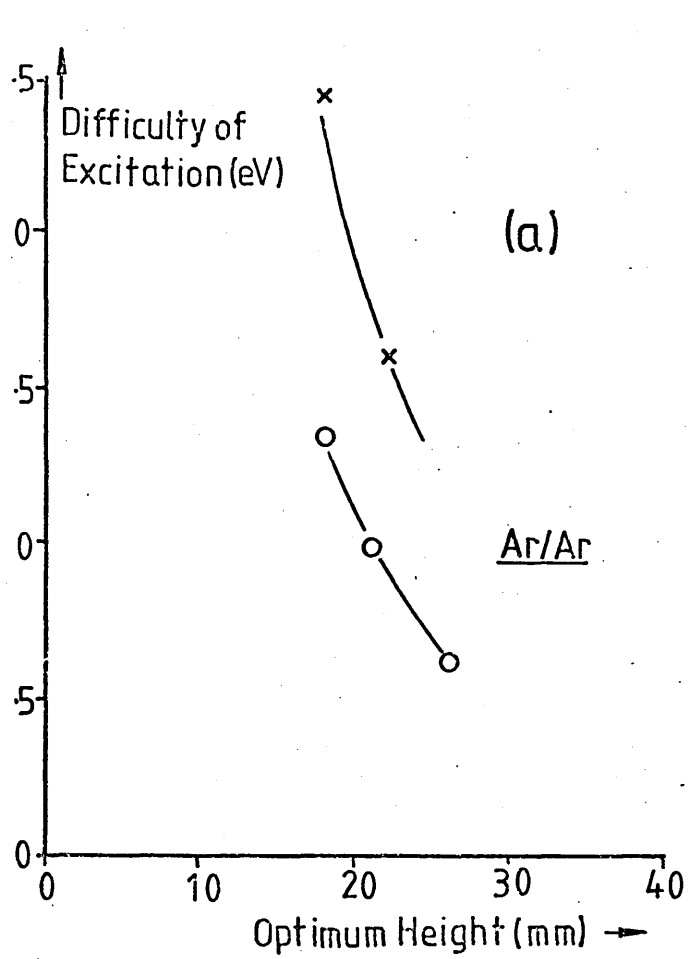


Fig 40(b)



high coolant gas flows produce flat 'doughnut' shaped plasmas with a larger diameter central channel than for low coolant gas flow rates, for this particular torch system. This may help to increase the SBR for the low excitation potential (3.1 eV) Mn 403.1 atom line .

The optimal plasma gas flows for the all argon plasma fall in the range of 9 to 14 lmin^{-1} and all show a characteristic shape in their univariate search graphs similar to that shown in Figure 33, with a steady increase in SBR from low to high gas flows, 'peaking' in the range mentioned above. For the nitrogen cooled plasma, however, there appears to be two types of optimal settings for the plasma argon flow; one at low flow rates (approximately 2 - 3 lmin^{-1}) and one at higher flow rates (approximately 9 - 12 lmin^{-1}). In fact the univariate search graphs for Ba II, Mn I, and Cu I all exhibit double 'optima' (Figures 39 and 40) showing one peak at low and one at high plasma gas flows. The lower gas flow is optimal for Ba II and Mn I, but the higher flow is optimal for Cu I. As discussed earlier the simplex originally became stranded at the wrong optimum for Ba II until a new simplex was carried out. All three of these lines have low excitation potentials, less than 4e V (see table 4), and the other lines studied, which have higher excitation potentials (>4 eV), do not exhibit these double optima but behave in a similar manner to those lines studied in the all argon plasma. The reason for this behaviour is perhaps related to how much coolant nitrogen diffuses into the central plasma argon flow. For low plasma argon flows it would be expected that the coolant nitrogen would diffuse into the argon to a greater extent than for high argon flow rates. Hence, as the argon flow rate increases, the characteristics of the plasma would change from a predominantly nitrogen cooled plasma to a predominantly all argon plasma thus producing the two peaks in the univariate search graphs (Figures 39 and 40).



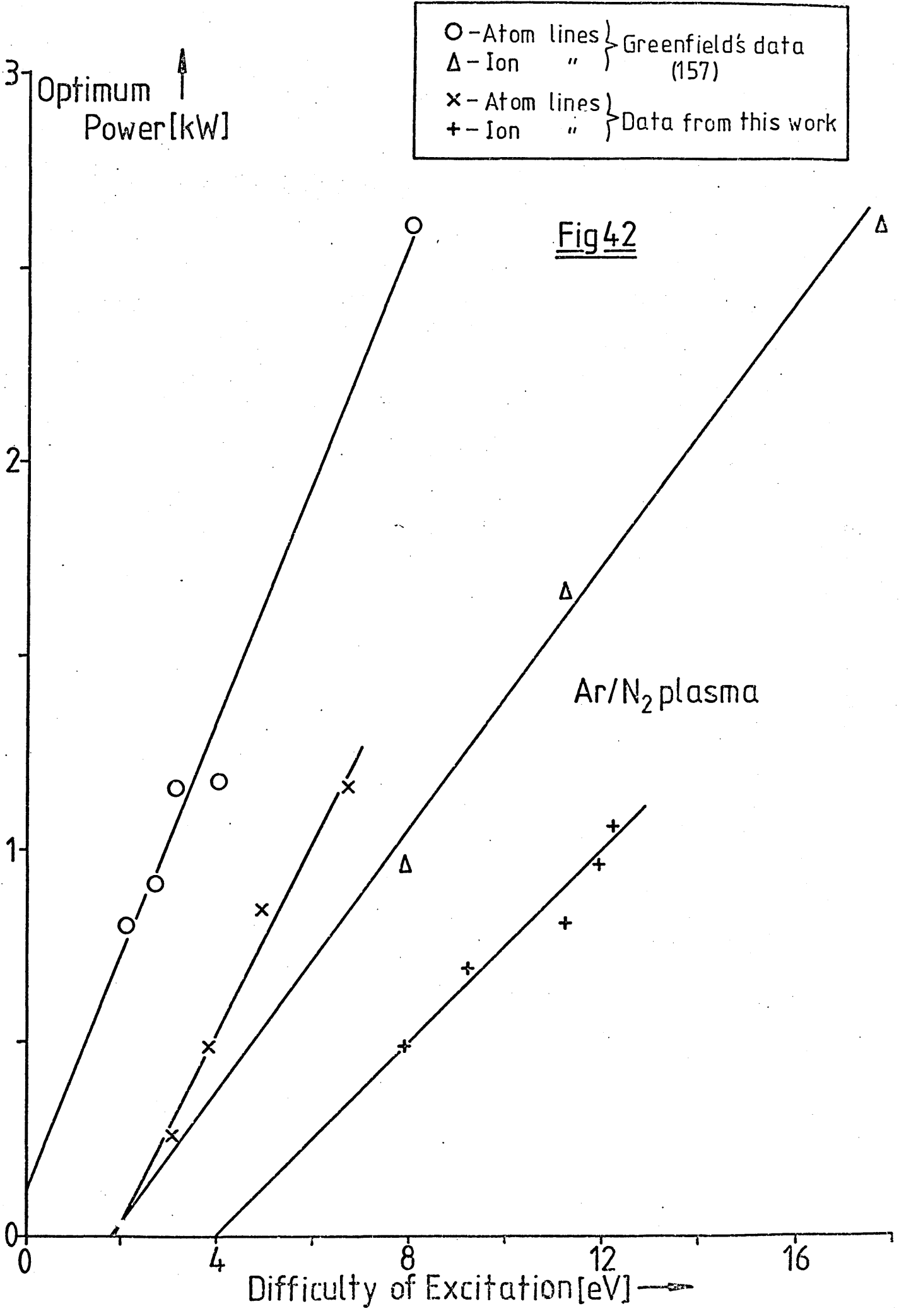
x ion lines
o atom lines

Fig 41

There are other factors involved, as the plasma gas flow rate also imparts subtle changes in position and shape to the plasma, which must also have some influence in the shape of the univariate search graphs.

The next two parameters, viewing height and injector flow rate, will be discussed together, as the results show that the two are closely inter-related. SBR is found to be highly dependent on these two parameters. The univariate search graphs shown in Figures 31 and 34 are typical for all optimisation carried out. A small movement away from the optimum value (1 or 2 mm in the case of viewing height or 0.02 to 0.04 lmin^{-1} in the case of injector argon flow) produced a sharp decrease in SBR.

An interesting correlation can be found between the difficulty of excitation for each line and for both injector flow rate and viewing height. Figure 41 shows graphs of injector flow rate and viewing height plotted against difficulty of excitation for each type of plasma. It can be clearly seen that the graphs for viewing height and injector gas flow for a particular plasma are very similar, such that for increasing difficulty of excitation lower viewing heights and lower injector gas flows are optimal. The explanation for this appears to be concerned with how long the analyte species takes to pass through the plasma fireball and how far away from the fireball the analyte species is when viewed. Clearly, if the injector gas flow is increased the velocity of the injector gas plus analyte aerosol exiting from the injector tube tip will increase, and hence the analyte species will spend less time in the excitation region of the plasma (i.e. the tunnel through the centre of the plasma) and thus experience less excitation. Analyte species with a high difficulty of excitation will therefore require a low injector gas flow so that they can spend enough time in the plasma for sufficient excitation to take place, whereas a species with low difficulty of excitation requires only a short time in the plasma and hence higher injector gas flows are optimal.



Similarly for viewing height, the nearer the plasma fireball the species is viewed the more excited it will be, having just passed through the excitation region, so that low viewing heights would be optimal for species with high difficulty of excitation and vice versa.

It must be remembered that SBR is the optimising criterion being used, and hence background also effects the above discussion. Background will always be higher nearer the plasma fireball but for those analyte species with high difficulty of excitation the signal will be proportionally higher than those species with low difficulty of excitation near the fireball and thus the above conclusions still hold true.

Finally the comparison between optimal powers in the two different types of plasma produces the most interesting and perhaps most important results of this set of optimisation experiments.

In all of the simplex optimisations using the 4 mm slit height it was possible to find an optimal power which was confirmed using univariate searches, producing graphs similar to that shown in Figure 34. The most striking feature of the comparison of optimal powers, as shown in table 5, is that for the argon plasma the optimal powers cover a range of 0.46 to 0.59 kW for elements with 'difficulties of excitation' ranging from 3.1 to 12.2 eV. Whereas in the nitrogen cooled plasma the optimum power increases as the difficulty of excitation increases so that the optimum powers range from 0.26 to 1.16 kW for the same range of difficulty of excitation. If a graph is plotted of difficulty of excitation against optimal power two lines can be produced, one for neutral lines and one for ion lines. This is similar to the data obtained by Greenfield and Thorburn Burns in their optimisation experiments (157). Figure 42 shows the optimal power data for the nitrogen cooled plasma as obtained in this work along with Greenfield and Thorburn Burns' data, plotted against difficulty of excitation.

Spectral Lines Used for Optimisation Experiments in Greenfield's Work(157)

Element	Wave-length /nm	Difficulty of Excitation /eV	Power /kW
Na I	589.6	2.1	0.8
Cs I	455.5	2.7	0.91
Al I	396.1	3.1	1.15
Zn I	307.6	4.01	1.19
Zn I	307.2	8.01	2.6
Ba II	455.4	7.91	0.95
V II	309.3	11.12	1.66
Al II	281.6	17.7	2.6

Table 6

Linear Regression Data for Optimum Power Results

Data	Slope / (kW/eV)	Intercept / kW	Correlation Coefficient	Standard Error of Estimate / %
Greenfield Atom lines	0.31	0.11	0.992	10.7
This Work Atom lines	0.25	-0.49	0.991	6.4
Greenfield Ion lines	0.17	-0.31	0.993	13.5
This Work Ion lines	0.12	-0.50	0.973	6.0
Normalised Atom lines	0.30	-0.73	0.998	10.4
Normalised Ion lines	0.16	-0.82	0.985	9.2

Table 7

The lines drawn through each set of points are those obtained by a linear regression analysis, the intercept, slope, correlation coefficient and standard error of estimate, from this analysis of these four sets of data are summarised in table 7. The lines produced from the data found in this work have high correlation coefficients (>0.99) and standard error of estimates $<7\%$ (showing that there is a 95% chance that the data points will be $<7\%$ in error from the regression line), and hence giving statistical justification to a linear relationship between optimal power and difficulty of excitation. Both of the regression lines for this work cut the power axis at c.a. -0.5 kW, thus leading to negative powers being optimal for lines with low difficulties of excitation, which is of course nonsensical. If this postulated linear relationship were true it would be expected that the lines would pass through the origin.

This could be the case if the methods used (as described in chapter 3) were measuring the power in the plasma 0.5 kW too low; this is not easily checked as there are no completely reliable methods for measuring power in the plasma.

The regression lines produced from Greenfield and Thorburn Burns' data are shifted to higher powers than the lines from this work, but the two pairs of lines for neutral and ion lines have similar slopes (table 7). In their study power was measured in a similar way and was subject to similar uncertainties.

Table 6 summarises the data produced by Greenfield and Thorburn Burns. It can be seen that they have optimised two ion lines (V 309.3 nm and Ba 455.4 nm) that have been optimised in this study and they have optimised one atom line (Al 396.1 nm) which has approximately the same excitation potential as the Mn 403.1 atom line used here. By subtracting the average difference in optimal power between the two sets of data for these points away from all the Greenfield data points one set of 'normalised' data can be obtained.

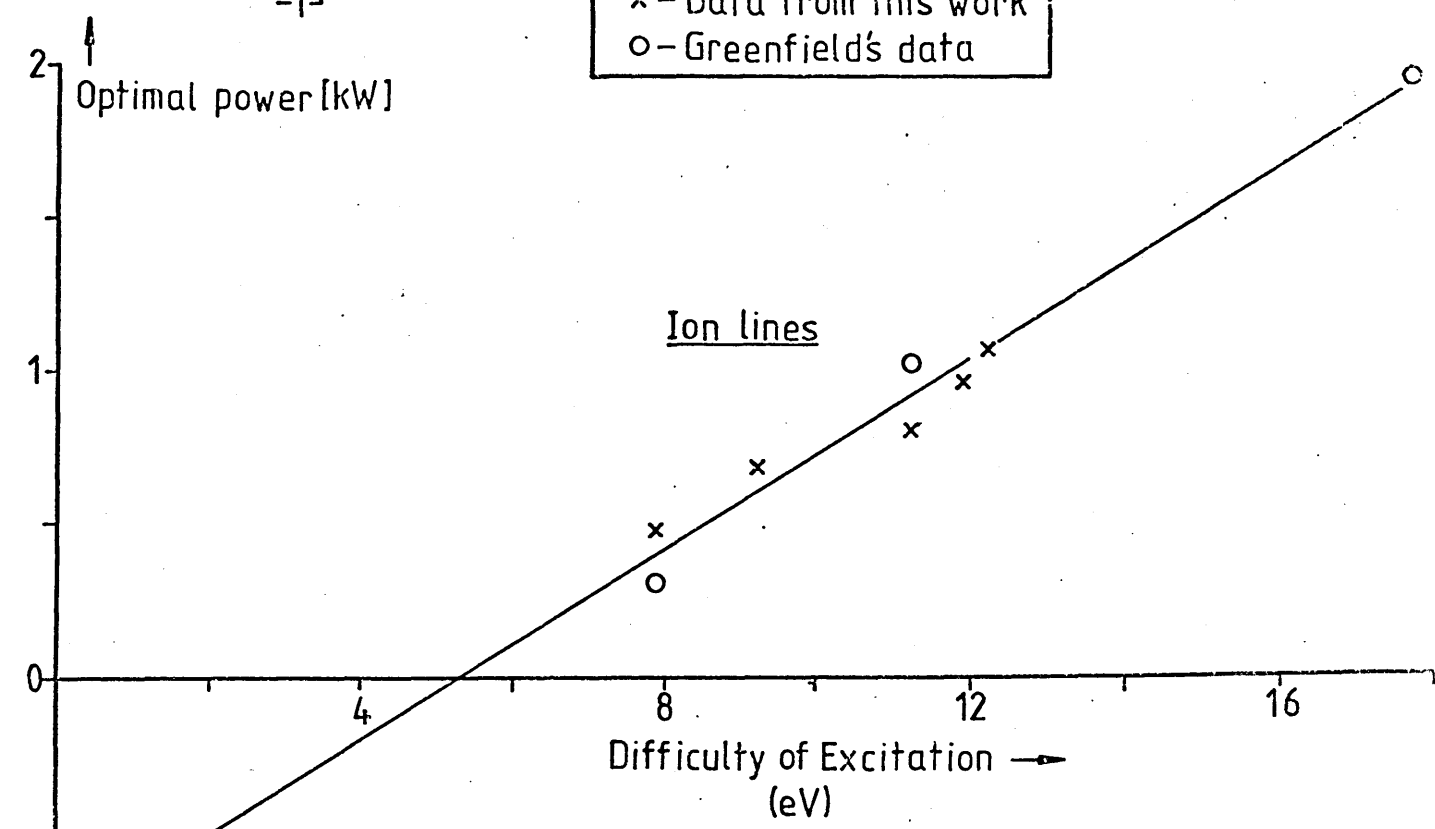
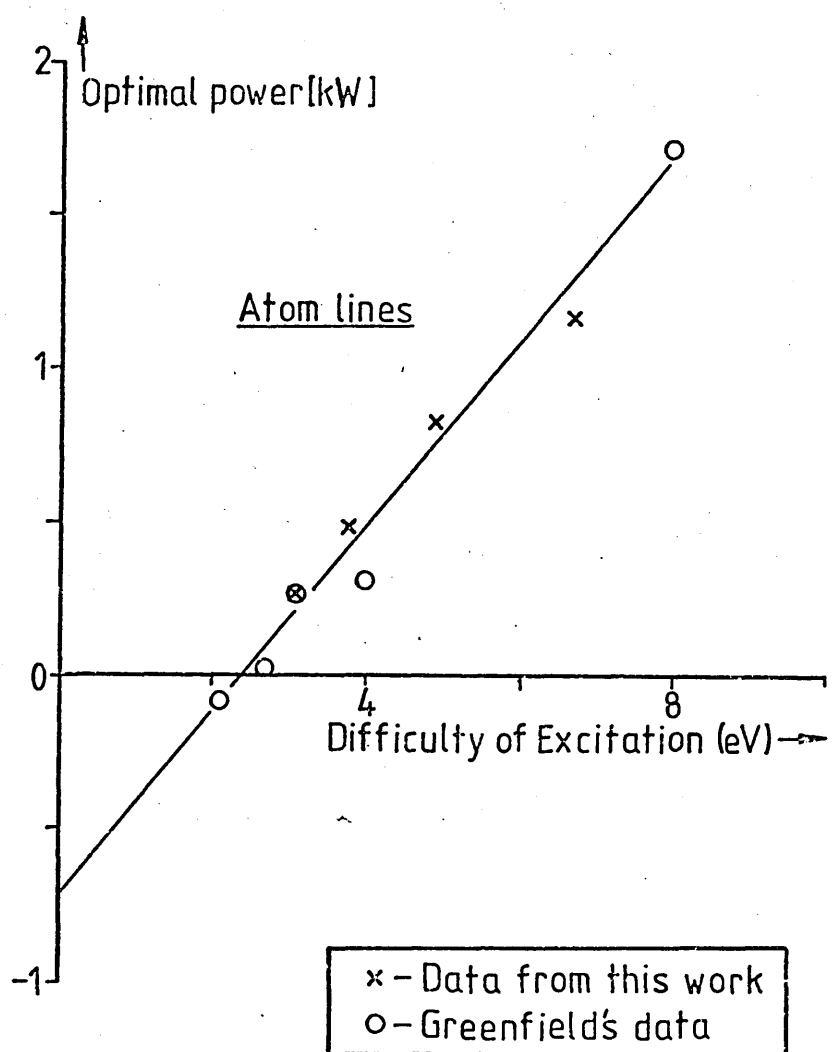


Fig 4.3

The normalised data is plotted in Figure 43 for both ion and atom lines along with regression lines for each set of points. The statistical data from the regression analysis is also shown in table 6. The correlation coefficients for the two lines are >0.98 and the standard errors of estimate $<11\%$. Thus, allowing for probable errors in the absolute measurement of power in the plasma, between the two sets of data, it is evident that the same phenomena is being shown by both sets of optimisation experiments.

This difference in behaviour between the two types of plasma studied seems to suggest a fundamental difference in excitation mechanism between each type. It has been pointed out (157) that the behaviour of the nitrogen cooled plasma is in agreement with a spectroscopic source that is in local thermodynamic equilibrium (LTE). It would be expected that when LTE does exist that the greater the difficulty of excitation of a particular line the greater would be the temperature required in the source to produce maximum sensitivity for that line; since it is reasonable to assume higher power will produce higher temperature, the results obtained for optimum performance of the nitrogen cooled plasma qualitatively agree with the existence of LTE. Since no such relationship has been shown for the all argon plasma it can be tentatively suggested that a non-LTE excitation mechanism is dominant (e.g. Penning ionisation (127) as discussed in chapter 1 section 1.2.8).

With regard to the question of high or low power it is obvious that the magnitude of the power used will be dependent on the type of plasma being operated. For the all argon plasma it appears that one power setting at 0.5 kW in the plasma can be used for all analyses. Although the results of these optimisation experiments cast some doubt on the validity of the power measurements used, the value of 0.5 kW, even if in error by 100%, would correspond to forward powers of approximately 1 - 2 kW which is generally regarded as 'low power'.

Spread of Optimal Conditions for N₂Cooled & All Ar Plasmas

Coolant Gas	Gas Flows [l min ⁻¹]			Height /mm	Power /kW
	Coolant	Plasma	Injector		
Ar	4.6 - 8.7	9.4 - 14.0	0.36 - 0.58	18 - 26	0.46 - 0.59
N ₂	4.0 - 7.0	1.7 - 10.4	0.35 - 0.72	12 - 29	0.26 - 1.16

Table 8

When nitrogen coolant is used it has been shown that it is necessary to 'tune' the power to the particular spectroscopic line being used for best performance. Thus, for a nitrogen cooled plasma to be used at its full potential, the ability to couple both low and high powers (4 - 5 kW forward power) into the plasma is required.

In making an overall comparison between the two plasmas table 5 shows that for those lines optimised in both types of plasma the all argon plasma gives superior performance for all but the Mn 403.1 atom line. The increases in SBR for the argon plasma are not large (a factor of 2 at best), from this data, however, it can be concluded that the argon plasma gives, in general, marginally better SBRs than its nitrogen cooled counterpart.

This result is in disagreement with the conclusions of Greenfield and Thorburn Burns (157); since, however, six out of the eight lines used in the comparison of plasma types could not be truly optimised in their study when an all argon plasma was used, due to low enough powers not being available on the RF generator, the conclusions made can only be regarded as specific to their system, whereas the comparisons made in this work were at true optima, (although avoiding lines with very high difficulties of excitation (>12.2 e V) and very low difficulties of excitation (<3.1 e V) due to the physical constraints of the spectrometer and RF generator used). Thus, for the range of lines covered in this work the results obtained perhaps have more general significance.

A further point of interest that arises from the comparison of optimal conditions is that the spread of optimal parameter settings for the argon plasma cover a smaller range than those of the nitrogen cooled plasma. This is illustrated in table 8 which lists the spread of optimal conditions for each parameter. It is not known if this is a peculiar trait of the torch design used for this work or whether it has more general applicability. It would, however, be a factor to consider if simultaneous multi-element analysis was to

be carried out where one set of compromise conditions would be required for all the spectral lines used in the analysis. Thus it would appear, at least on the system used here, that an all argon plasma would be more amenable to this task since its optimal range of parameter settings cover a relatively small region compared to those of a nitrogen cooled plasma.

A short experiment was carried out to test this hypothesis. The optimal conditions for the Mn 257.6 nm ion line were chosen as compromise conditions for each type of plasma, and the ratio of the SBR as obtained in the all argon plasma to the SBR as obtained in the nitrogen cooled plasma for optimal conditions and for compromise conditions were compared.

The results are shown in table 9. Three of the four lines show an increase in the ratios of SBR when compromise conditions were used, this is particularly noticeable for the Mn atom line for which the ratio is increased by an order of magnitude. This gives a tentative indication that an all argon plasma would produce better results when used at compromise conditions than would the nitrogen cooled plasma.

4.4.5 OPTIMISATION OF THE As 228.8 nm ATOM LINE IN THE PRESENCE OF Cr MATRIX

The optimisation results discussed in the previous section, although giving useful information about the performance and mechanism of the two types of plasma studied, are not necessarily of great practical use, since very little 'real' analysis is carried out in solutions containing distilled water and one element at low concentrations. Frequently the sample contains a number of matrix elements at high concentrations as well as the analyte species.

The sponsoring company for this project were interested in the analysis of low levels of As (~1 ppm in the solid) in chromium metal.

Effect of Compromise Conditions on SBR

Element	Wave-length /nm	A	B
As I	228.8	1.98	2.0
B I	249.8	2.5	1.95
Mn I	403.1	0.71	9.57
Ba II	455.4	1.01	1.64

A-Ratio of SBR in an all Ar plasma to SBR in a N₂ cooled plasma (optimum conditions)
 B- " " " " " " " " " " " " " " " " " (compromise conditions)

Coolant Gas	Gas Flows [lmin ⁻¹]			Height /mm	Power /kW
	Coolant	Plasma	Injector		
Ar	5.0	14.0	0.37	18	0.54
N ₂	6.2	10.4	0.35	12	1.06

Compromise Conditions Used

Table 9

It was thus decided to use the experience gained in optimising the plasma to discover the best operating conditions for the detection of As in chrome metal, and also to make comparisons between the optimum conditions with and without the matrix element present.

The simplex optimisation procedure was applied to the optimisation of the As 228.8 nm atom line.

Two solutions were used to measure the SBR of the As in Cr matrix, one containing 10g l^{-1} Cr and one containing 100 ppm As + 10g l^{-1} Cr. The signal due to As was measured by subtracting the signal due to Cr matrix from the signal due to As + Cr matrix, and the background was measured as the difference between the signal when Cr matrix solution was sprayed and when a shutter was placed across the monochromator entrance slit.

The univariate searches and the optimal regions as defined by the simplex optimisation for As in Cr matrix in both types of plasma are shown in Figures 44 & 45, along with the univariate search graphs for the optimisation of As in distilled water.

The most obvious effect of having Cr matrix present is that the optimal SBR for the As line are reduced with respect to the optimal SBR without the matrix and the univariate search graphs are 'flattened out' showing that the presence of Cr has reduced the overall sensitivity and also the dependence of SBR on each parameter.

The main difference between the two plasma systems being that the optimal conditions, when Cr is present in the nitrogen cooled plasma (Figures 42 and 43), remain essentially unchanged from those where distilled water is the matrix, whereas a number of shifts in optimal settings can be seen in the all argon plasma (Figures 46 and 47). The reasons for these shifts are not clear, although it is interesting to note that the optimum power in the all argon plasma (Figure 47) is

Effect of Cr Matrix on As 228.8nm Optimal Conditions, Ar/N₂ Plasma
(Injector Ar Flow, Viewing Height, & Plasma Ar Flow)

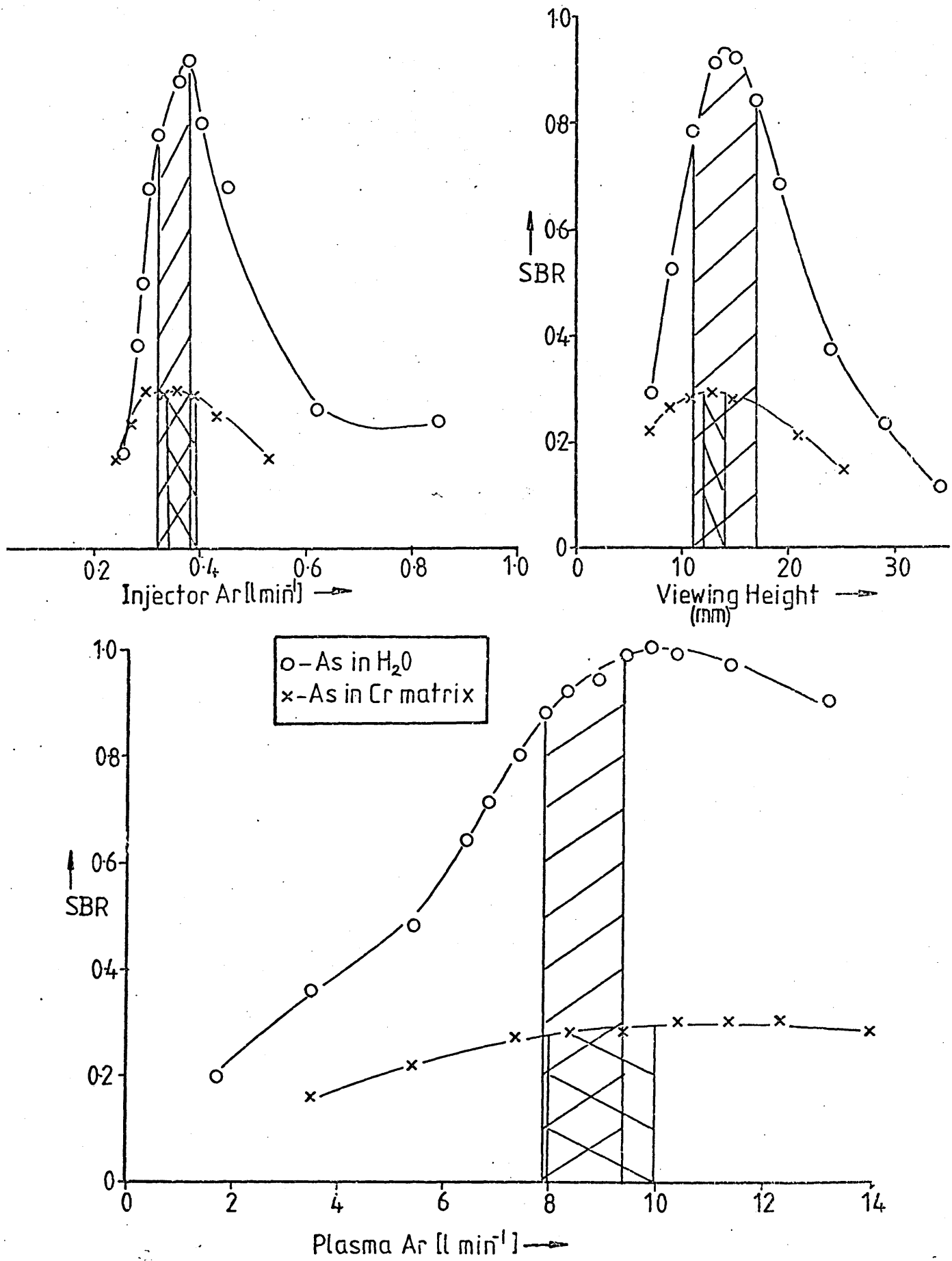


Fig 44

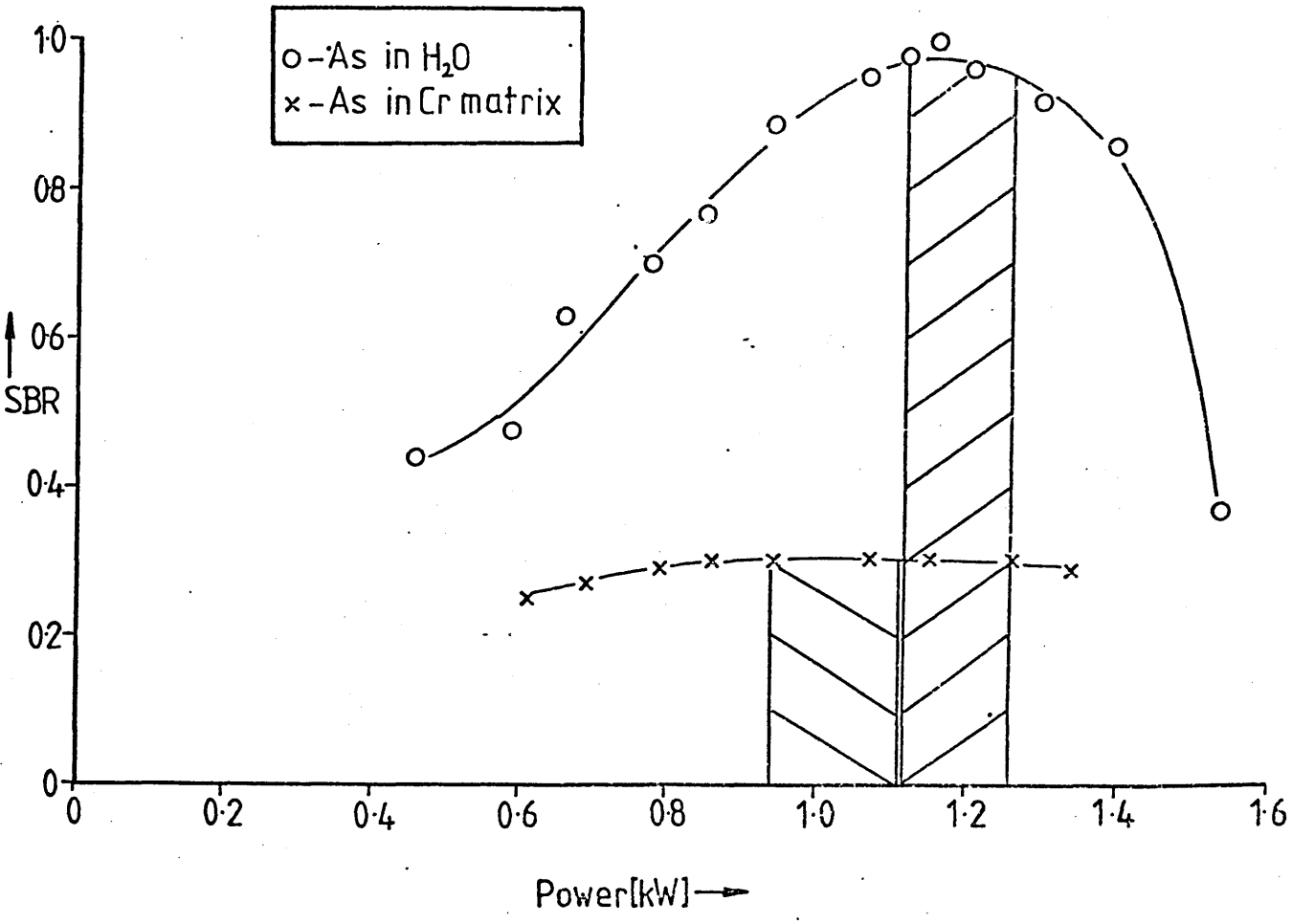
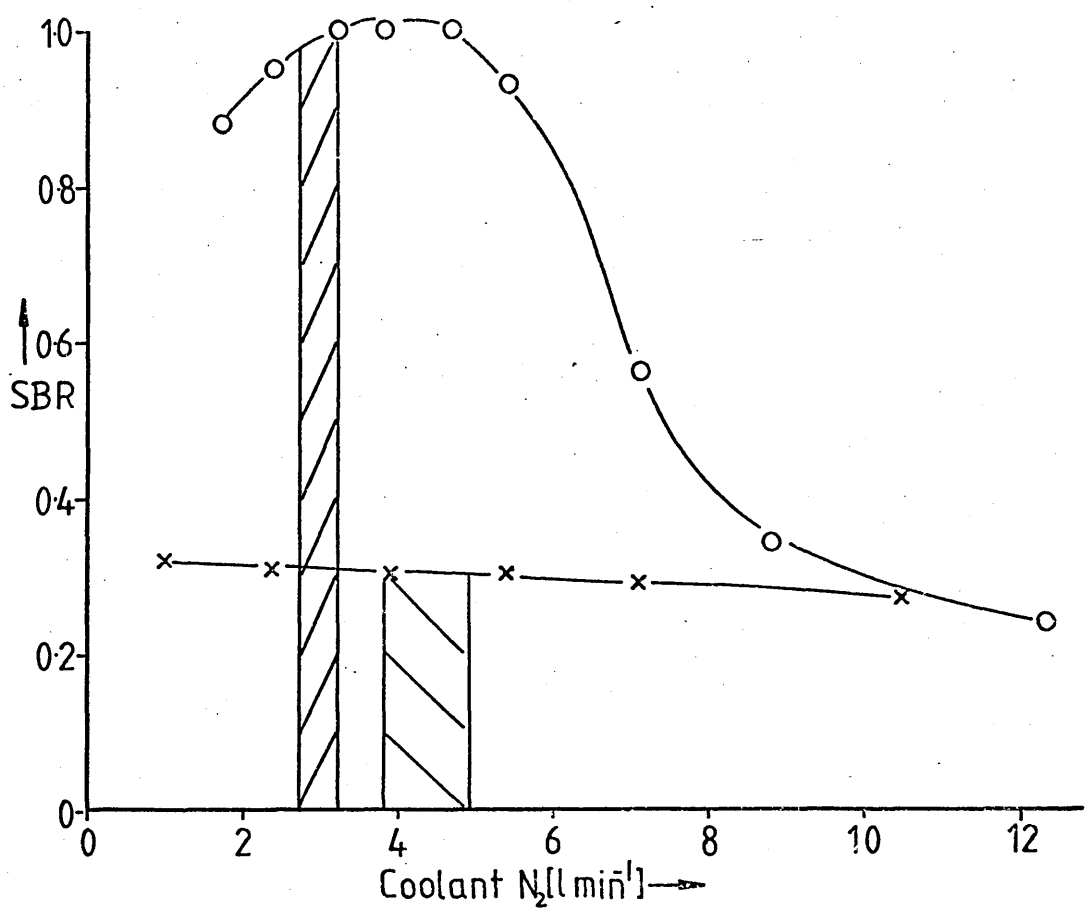


Fig 45

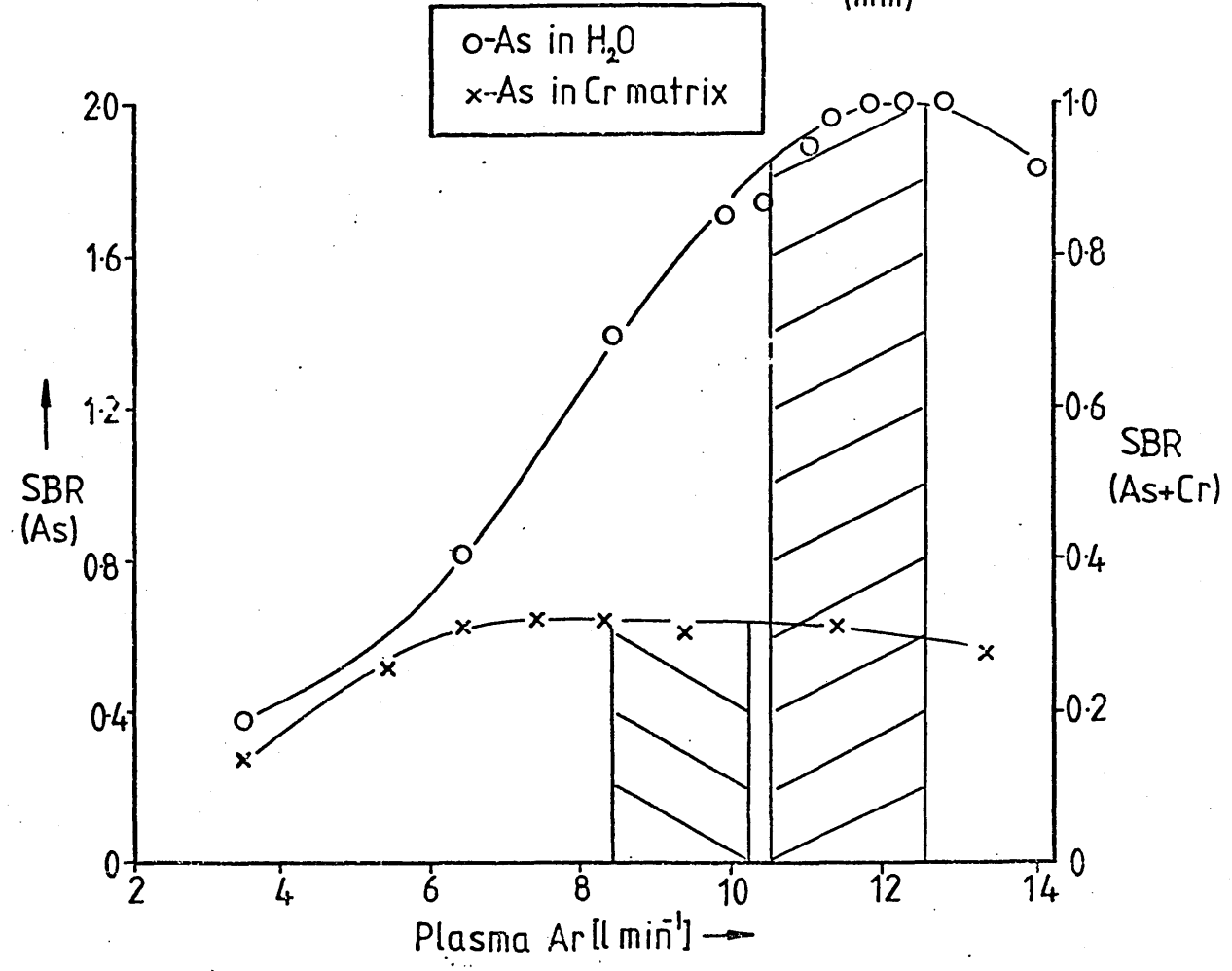
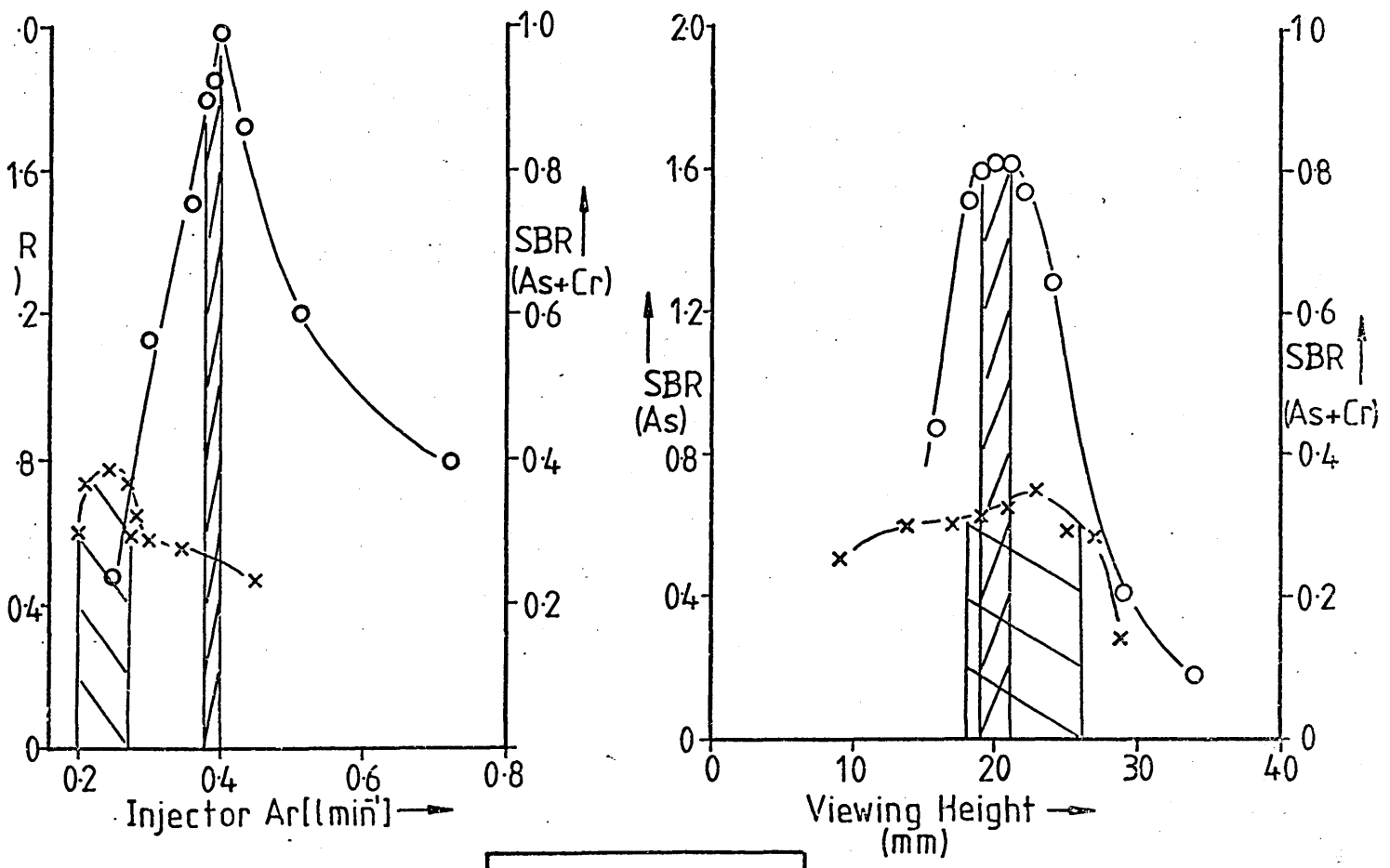
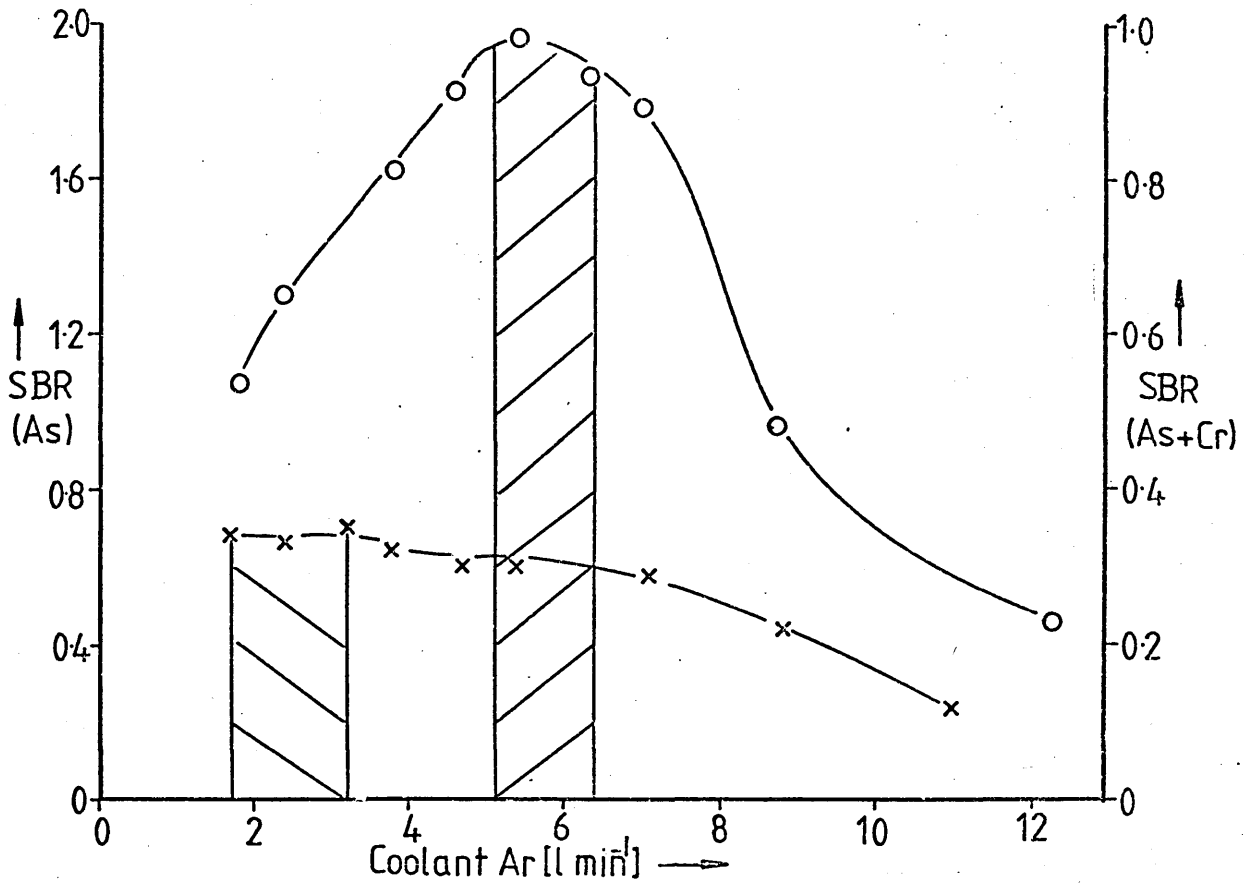


Fig 4.6



○ - As in H₂O
 x - As in Cr matrix

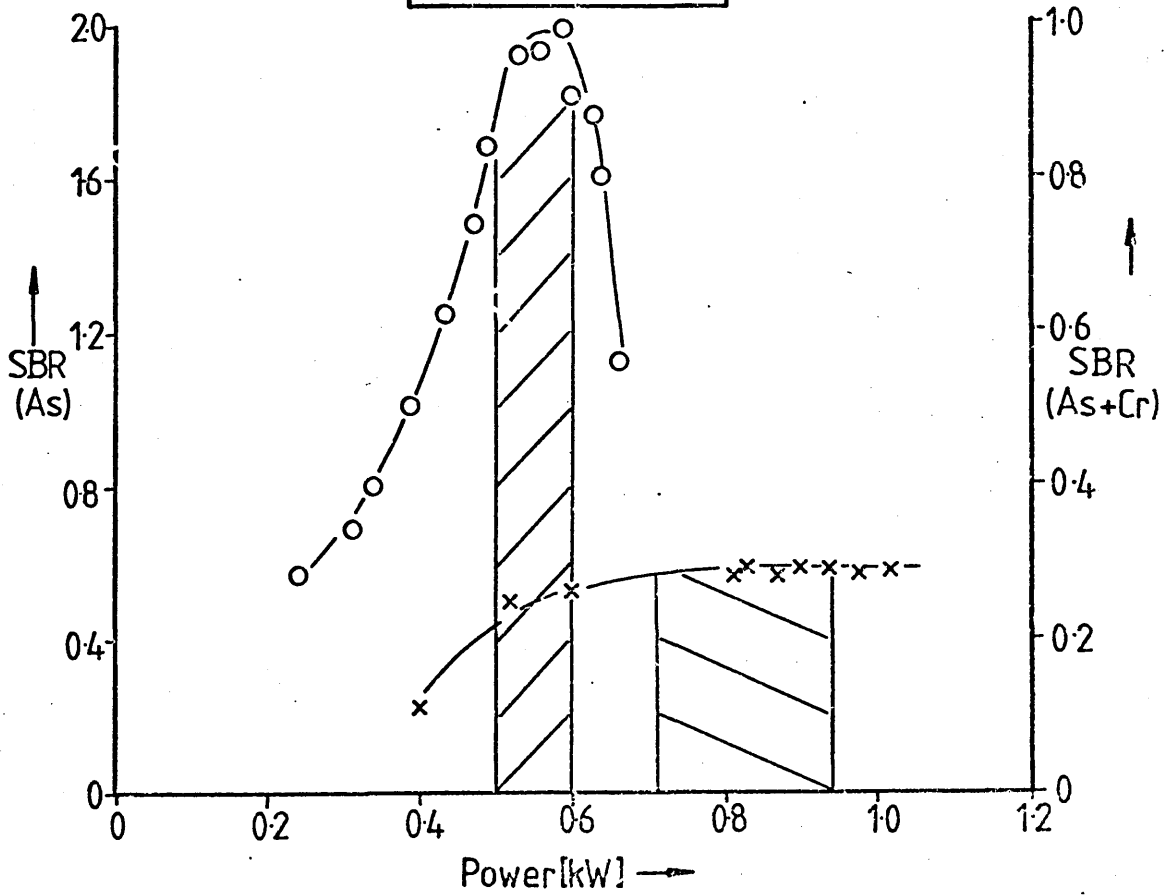


Fig 4.7

moved to higher powers in the presence of Cr.

Alder et al. (126) have shown that the presence of water in an all argon plasma substantially increases the electron density in the central channel of the ICP and hence excitation due to electron collisions will be favoured as compared to Penning ionisation excitation (127). It may be speculated that the addition of large amounts of Cr to the matrix may similarly further increase the electron density essentially 'thermalising' the plasma so that electron collisions become entirely dominant as the excitation process, and hence the optimum power is shifted closer to the optimum power of the nitrogen cooled plasma which is thought to be closer to LTE (i.e. excitation from electron collisions).

These results are interesting in that the nitrogen cooled plasma optimal conditions appear to be more tolerant to large amounts of matrix than the argon plasma, which may need re-optimising for different matrixes even though the same spectral line is being used.

4.5 CONCLUSIONS

The results in this chapter have shown the simplex method to be a fast and effective method for optimising the ICP, the results of which can give fundamental insight into the different properties and mechanisms of the two types of plasma studied.

A more detailed discussion of the conclusions from these optimisation experiments will be presented later in chapter 7.

5. INTERFERENCE EFFECTS IN THE ICP

The early literature on interferences in the ICP extrapolated experience gained in flame emission spectroscopy to suggest that the higher temperatures obtained in the plasma would produce an 'ideal' interference-free spectroscopic source (e.g. 33,47).

As the use of the ICP became more wide spread, however, many varied and often conflicting reports on different types of interference were published. The literature on interferences has been reviewed most extensively by Kornblum and de Galan (118), and Barnes (52). Robin (127), in his review, gives an interesting and rationalised discussion on ICP interferences.

The majority of ICP interferences can be categorised into one or more of the following headings:

- i) sample introduction;
- ii) vaporisation;
- iii) atomisation and ionisation;
- iv) spectral interference.

In the following discussion the above headings will be used to describe the different types of interferences that have been reported to occur in ICP systems similar to that used in this work. (i.e. those systems using continuous nebulisation of solution samples).

5.1.1 SAMPLE INTRODUCTION

The variation of the uptake rate of the sample solution by the

nebuliser has been found to be a source of 'apparent' interferences in the plasma. There are a number of factors which can effect the uptake rate, and hence amount of analyte reaching the plasma. Of these perhaps the two most important are the 'head' of sample solution being drawn up and the viscosity of the sample solution.

Greenfield et al. (149) have made a detailed study of the latter effect, and it has been shown that the increased viscosity of some common solvents (e.g. phosphoric acid) can markedly decrease the nebuliser uptake rate hence causing an apparent depression of the signal at the plasma. In order to counteract these effects it is necessary to either match the viscosity of sample and standard solutions making sure that the head of solution does not significantly change during nebulisation or, more simply, to pump the solution into the nebuliser at a constant rate so that viscosity and sample head effects do not control the uptake rate. The latter has been the approach used in this work and is described in more detail in chapter 2.

5.1.2 VAPORISATION

The classic solute vaporisation interference effects as observed in flame spectrometry (e.g. phosphate on calcium) are greatly reduced in the ICP due to the much higher temperatures experienced by analyte species. They have, however, been shown to exist (e.g. 118, 119,167) Larson et al. (118) showed that by careful choice of viewing height and other operating parameters the vaporisation interference effect of Al and Ca would be virtually removed.

It appears that viewing height and injector flow rate (parameters that are closely inter-related, as shown in chapter 4, section 4.4.4), greatly influence the magnitude of vaporisation interferences (118).

Recently Reeves et al. (168) have studied molecular emission spectra of compounds, that form stable oxides, in the ICP (Y, Sc, Gd, Sm,

Lu, and Zr). They have identified regions low down (c.a. 10 - 15 mm above the load coil) and high in the tail flame (>35 mm) where monoxide emission occurs, and hence solute vaporisation interferences might be expected to be found. This evidence suggests that compound formation and reduced volatility effects occur only in certain parts of the tail flame, and can therefore be minimised by careful choice of the section of tail flame to be viewed, which is controlled mainly by the viewing height and injector flow rate.

5.1.3 ATOMISATION AND IONISATION

The effect of concomitant elements, particularly easily ionised group I or group II metals has produced a number of conflicting reports. For example Scott (167) observed that lithium produced an enhancement effect on atom lines and depressed ion lines. Merryfield and Loyd (169), however, observed potassium to depress atom lines emission and to have virtually no effect on ion lines. From such reports and other work (e.g. 114,170) it became clear that the interferences observed in the ICP were not analogous to the more straight forward ionisation interferences observed in flame or arc and spark sources.

Recently studies of the effects of easily ionisable elements in the ICP have been carried out using photodiode array detectors (153,154,155) which allow spatial profiles of the plasma tail flame to be examined. The results of these studies give some indication as to why the observed effects of easily ionisable elements vary from publication to publication. The graph shown in Figure 48 represents the spatial profile obtained by Kawaguchi *et al.* (154) when their photodiode array/ICP system was used to examine the emission intensity of the Ca 393.4 nm ion line at different viewing heights with and without lithium concomitant. It can be seen that the presence of lithium shifts the calcium

Effect of Li on Ca 393.4nm Ion Line (154)

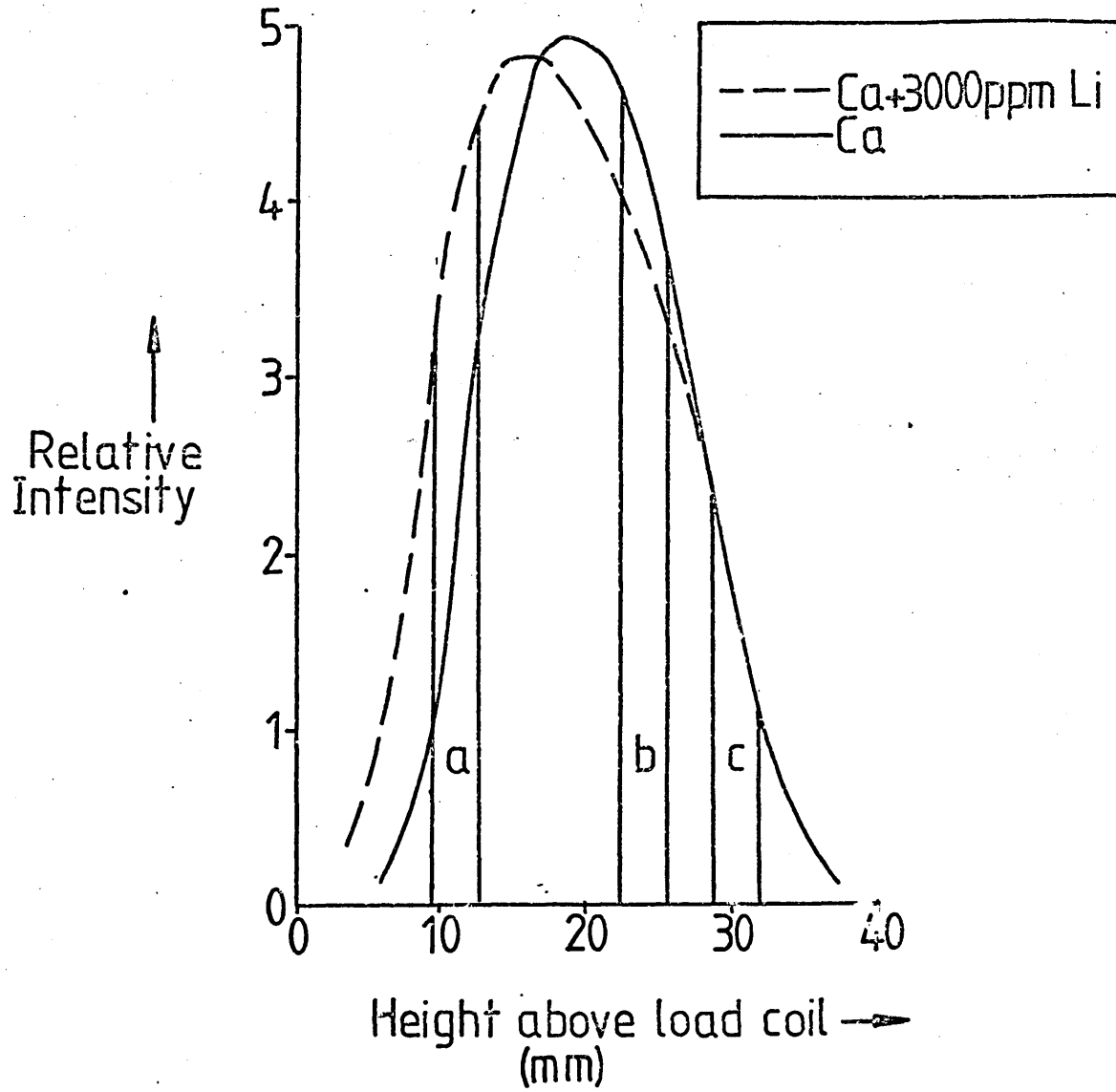


Fig. 48

profile to lower heights in the tail flame. Thus, by viewing the tail flame at different heights the presence of lithium could be said to enhance the signal (viewing region a), depress the signal (viewing region b) and to have no effect (viewing region c). It would appear, therefore, that these so called 'ionisation' effects, like the volatilisation effects, are closely related to the section of tail flame being used for analysis, and the conflicting reports are probably due to the different conditions and systems that are being used by workers in this field.

The mechanisms of these interference effects are not clear; Kornblum and de Galan conclude from their study (118) that they are the combined action of three processes:

- i) volatilisation interference;
- ii) enhancement of the excitation temperature;
- iii) shift of the ionisation equilibrium.

Robin (127) suggested that, since similar interference effects are observed on both atom and ion lines of one element, the easily ionisable element enables the analyte species to be more easily volatilised. So that the interference effect is due mainly to vaporisation rather than ionisation effects.

In a study where the effect of large amounts of sodium tetraborate on rare earth element emission from ICP was being considered, Broekaert et al. (171) suggested that the large quantities of concomitant were quenching the Ar metastables on the plasma thus causing interference effects. This is perhaps not quite the same effect as observed with more simple sodium salts (e.g. Na Cl) since the borate anion appeared to be the active interferent. It is, nevertheless, a mechanism that may play a part in some of the more complex interferences in the ICP.

In conclusion, reports in the literature show that ionisation type interferences do occur in the plasma. These interferences, because of the unique nature of the plasma, cannot be compared to the ionisation interferences observed in flames and arc/spark sources.

The interference effects of easily ionisable elements in the ICP can usually be tuned out, or at least reduced to a minimum by appropriate choice of operating parameters, particularly viewing height and injector flow rate.

5.1.4 SPECTRAL INTERFERENCE

Spectral interferences can be caused by a number of effects. Atomic spectral line emission and molecular band emission produced by concomitants or decomposition products occurring within the spectral band pass, used to view the spectral line of interest, can cause apparent spectral overlap. In order to reduce this effect it is necessary to use a high resolution spectrometer, although, even with the best spectrometer true spectral line coincidence will be observed. This can only be overcome by choosing a different analytical line that does not suffer from this problem. When the line of interest is partially resolved within spectrometer band pass correction procedures can be carried out (e.g. 122 and 172) which can subtract the contribution due to the interfering line.

Changes in the background signal due to stray light from grating ghosts and scattered light from the inside of spectrometers (173) can also cause interferences. This can be reduced by the use of holographic gratings and improved spectrometer design, as well as selective filters (174) to remove particularly intense unwanted emission from reaching the detector (e.g. when large amounts of Ca are present in the sample matrix).

Finally, there are line broadening and radiative recombination

background interferences as described by Larson and Fassel (175) and Ediger and Fernandez (176) in which collisionally broadened lines have been shown to produce significant background changes at wavelengths 10 nm from the parent line centre. If the background is well behaved (i.e. a flat base line on either side of the line) a simple background correction procedure can be used to measure the background signal at a given distance either side of the line and hence to subtract the contribution of the background. If, however, the background near to the analytical line slopes steeply or is structured (i.e. contains small atomic lines or molecular bands) care has to be taken as to where background is measured (172) so that erroneous readings are not produced. In some cases the background will be too complicated to apply any meaningful correction, and hence a different line must be chosen where the background change is minimal or at least amenable to a background correction procedure.

5.2 INTERFERENCE STUDIES ON THE EFFECTS OF SODIUM CARRIED OUT IN THIS WORK

The use of sodium carbonate/sodium peroxide fusion to effect dissolution of certain alloys has led to the investigation of the effect of sodium (which would be present at 15 mg cm^{-3} in a typical final solution) on the signal from Mn atom and in lines at optimum and other conditions.

5.2.1 EXPERIMENTAL

The instrumental set up used was as described in chapter 2. The nebuliser was pumped at 1.65 ml min^{-1} to avoid any spurious effects from uptake variation and a 4 mm slit height was used. The simplex minimisation of interference experiments were carried out in a similar manner to the simplex optimisations described in chapter 4.

5.2.2 RESULTS AND DISCUSSION

The literature had shown that both viewing height and injector gas flow rate could greatly influence the magnitude of the interference observed from easily ionisable concomitants. Initial experiments were therefore carried out to compare the signal obtained from a $1 \mu\text{g ml}^{-1}$ Mn solution and a $1 \mu\text{g ml}^{-1}$ Mn + $1000 \mu\text{g ml}^{-1}$ Na solution at varying viewing heights and injector gas flow rates for both the 403.1 nm atom line and the 257.6 nm ion line using both nitrogen cooled and all argon plasmas. The optimum operating conditions for each line and plasma type, as summarised in table 5, chapter 4, were used. The term % interference used here is defined below.

$$\% \text{ interference} = \frac{S_2 - S_1}{S_1} \times 100$$

where:

S_1 = signal from Mn solution

S_2 = signal from Mn + Na solution

The results of these experiments are shown in Figures 49 and 50. At the optimum conditions used for both the atom and ion line in the all argon plasma very large positive interferences were observed at low viewing heights (15 - 20 mm above the load coil) the interference from the atom line being particularly high over the whole viewing range covered. At higher viewing heights (25-30 mm) the positive interference is reduced in both lines, the ion line experiencing a slight negative interference. For a simple ionisation interference an enhancement of the atom line and a depression of the ion line would be expected. Although this does occur at one particular viewing region (25 - 30 mm), this does not explain the positive interference on both lines at lower viewing heights.

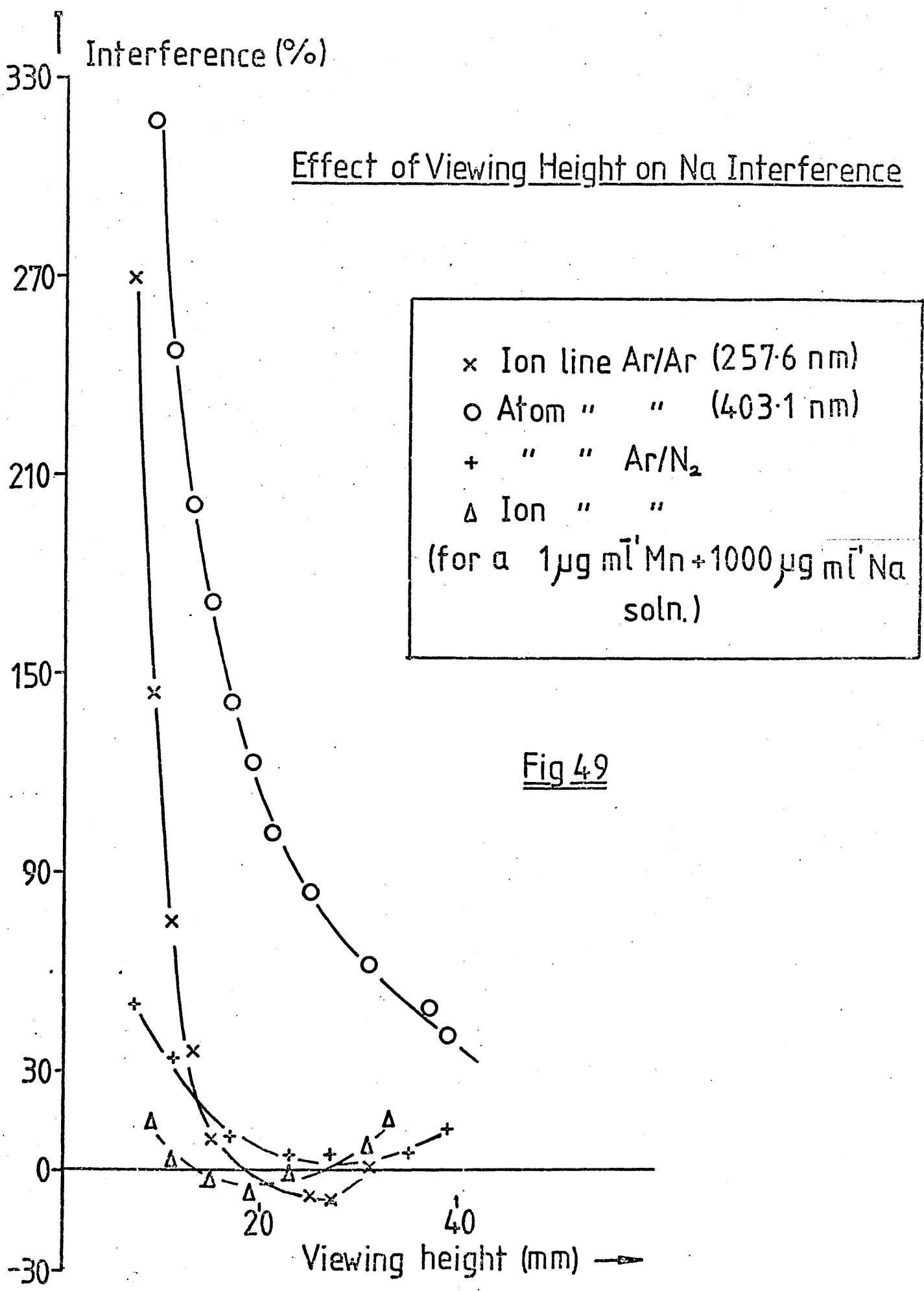
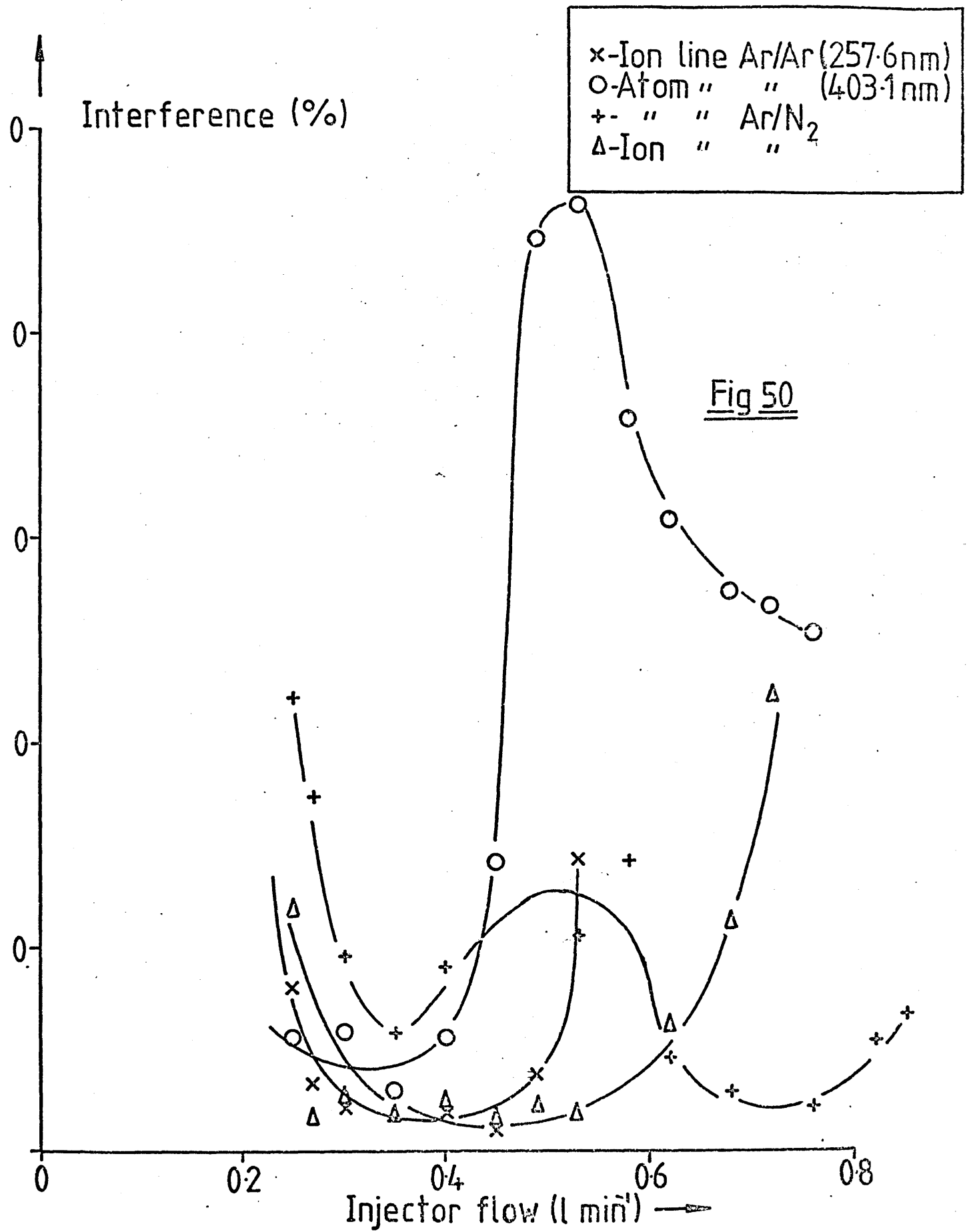


Fig 49

Effect of Injector Ar Flow on Na Interference



The atom and ion line in the nitrogen cooled plasma show similar trends to their argon cooled counterparts, but with very much decreased interference effect. The reason for the particularly high interference on the atom line in the all argon plasma is perhaps apparent from Figure 50. The optimum flow rate for the Mn I line in an all argon plasma (0.58 lmin^{-1}) almost exactly coincides with the flow rate for maximum interference. A similar but smaller interference maximum can be seen for Mn I in the nitrogen cooled plasma close to its optimal injector gas flow (0.49 lmin^{-1}). The optimal injector gas flows for the ion line in the two types of plasma (0.37 lmin^{-1} all argon, 0.35 lmin^{-1} nitrogen cooled plasma), however, coincide with interference minima. The explanation of these effects will be discussed later in this chapter.

Having established that both injector gas flow and viewing height were indeed critical to the control of interference caused by the Na concomitant, further work was then performed to investigate the effect of changing the Na concentration on the Mn optimum conditions in both types of plasma. Figure 51 summarises the results for increasing sodium concentration on a $1 \mu\text{g ml}^{-1}$ Mn solution for both the atom and ion line operated at their optimum conditions in both types of plasma. Again it is evident that the atom line suffers the greatest interference in both types of plasma, particularly in the all argon plasma where significant enhancement of the Mn signal is observed even at low Na concentration (i.e. $10 \mu\text{g ml}^{-1}$). For the ion lines the interference is much less (<10%) up to concentrations of c.a. $10,000 \mu\text{g ml}^{-1}$ Na, above this level, however, a negative interference occurs. This may be due, to some extent, to the reduced efficiency of the concentric nebuliser for high dissolved solids solutions. Little significance should therefore be attached to the results above $5000 \mu\text{g ml}^{-1}$ Na concentration.

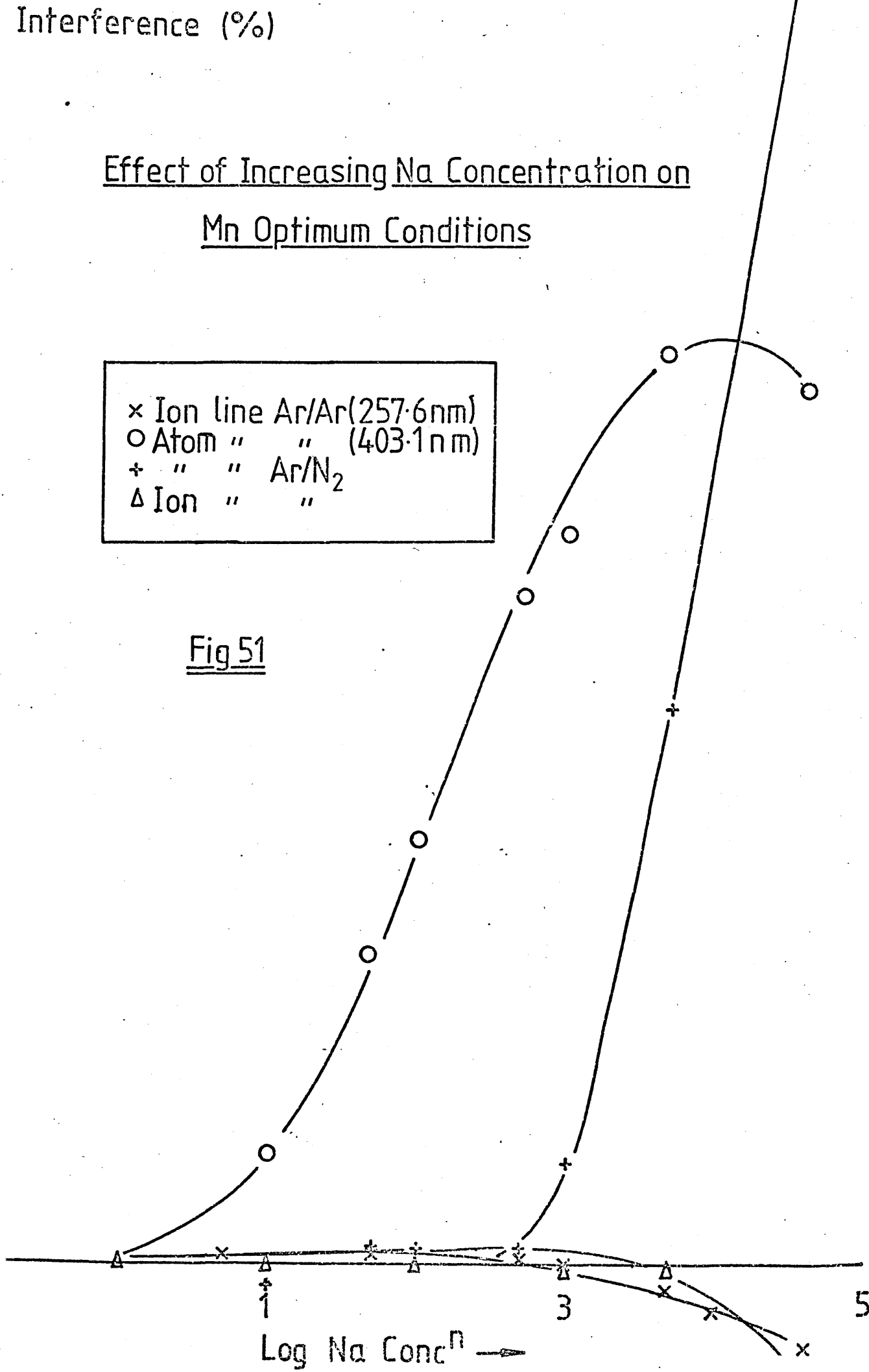
At this point in the study it was necessary to define the origin of the effects of Na concomitant. Considering the total ICP system

Interference (%)

Effect of Increasing Na Concentration on
Mn Optimum Conditions

× Ion line Ar/Ar(257.6nm)
○ Atom " " (403.1nm)
+ " " Ar/N₂
Δ Ion " "

Fig 51



being used, there were three areas which might have been responsible or have made some contribution to the observed effects. These being, the nebuliser and sample introduction system, the plasma itself, and the spectrometer.

Stray light effects in the spectrometer had been accounted for in all the preceding experiments by spraying blank solutions containing the appropriate amount of sodium and subtracting any change in background from the Mn + Na signal (the levels of stray light were found to be negligible for all but the highest concentrations of Na, i.e. $>5000 \mu\text{g ml}^{-1}\text{Na}$).

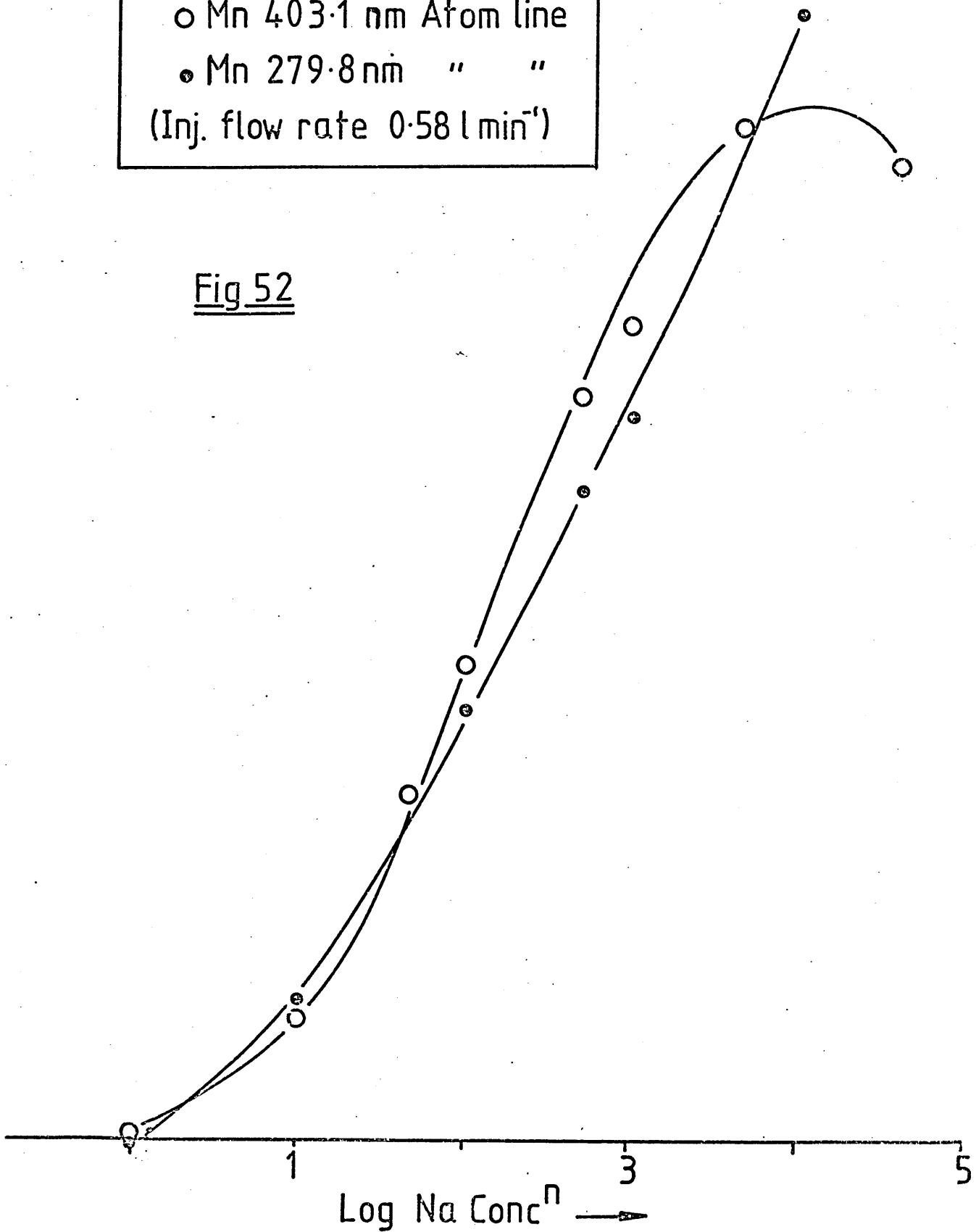
Since, however, the atom and ion line were being measured in two parts of the spectrum, approximately 150 nm apart, there might have been some other artefact of the spectrometer that was causing the large differences in behaviour between atom and ion lines. To check this, the effect of increasing sodium ion concentration on a Mn atom line (279.8 nm) closer to the ion line was studied. The results are shown in Figure 52, the plasma was operated at the same conditions that were optimal for the Mn 403.1 nm line, the increasing amounts of Na being added to a $1 \mu\text{g ml}^{-1}$ Mn solution. As can be seen the results are very similar to those found for the 403.1 nm atom line, and hence interferences from the spectrometer system were discounted.

To check that the sample introduction system was not causing Na interference effects, the nebuliser and double pass spray chamber were connected up to an emission (Air/C₂H₂) burner so that the sample aerosol that was previously passing into the plasma, passed into the flame. Since Mn is not appreciably ionised in the Air/C₂H₂ flame the addition of increasing concentrations of Na into the flame, whilst observing the emission from the Mn 403.1 nm atom line with the same spectrometer system, should not significantly effect the Mn signal. If large enhancements of the atom line were to be observed in the flame, as seen in the plasma, due to increasing

Comparison of Na Interference Effects on Mn Atom Lines

○ Mn 403.1 nm Atom line
● Mn 279.8 nm " "
(Inj. flow rate 0.58 l min⁻¹)

Fig 52



concentration of Na, then it would be concluded that the Na was causing a preferential distribution of the Mn into the smaller droplets that are passed through the spray chamber (i.e. ionic redistribution) and hence an increase in signal at the plasma (177).

Since the amount of aerosol produced by the ICP nebuliser is far less than that required for optimum performance of the emission burner, the Mn solution concentration was increased to $20 \mu\text{g ml}^{-1}$, even then the signal to noise ratio was poor, this is shown by the large error bars on the graph (Figure 53). The results in Figure 53 compare the effect of increasing Na concentration on the 403.1 nm atom line emission signal from a $20 \mu\text{g ml}^{-1}$ Mn solution when the nebuliser system was operated at both the optimum flow rate for the Mn atom line in an all argon plasma (0.58 l min^{-1} Ar) and the Mn ion line in an all argon plasma (0.37 l min^{-1}) with an all argon ICP and the air/C₂H₂ emission burner. Within experimental error the results from the emission burner do not show any large enhancements of the Mn 403.1 nm atom line signal at either of the nebuliser flow rates used. Using the all argon plasma, however, large interference effects with the higher nebuliser flow rate were observed as seen in previous experiments (Figures 51 and 52) with the $1 \mu\text{g ml}^{-1}$ Mn solution. Thus showing that the interference effect of Na was not occurring in the nebuliser system, and must, therefore, be a mechanism occurring within the plasma itself.

Another interesting feature of Figure 53 is the decreased interference on the 403.1 nm atom line in the all argon plasma when the injector flow rate was reduced. This would follow directly from the study of the effect of injector flow rate on Na interference (Figure 50); reducing the injector flow rate from its optimal value (0.58 l min^{-1}) moves the emission signal away from the injector gas flow of maximum interference. Similarly in Figure 54, using a $1 \mu\text{g ml}^{-1}$ Mn solution in an all argon plasma, the interference on both the 279.8 nm and the 403.1 nm atom lines are decreased when the injector flow rate is

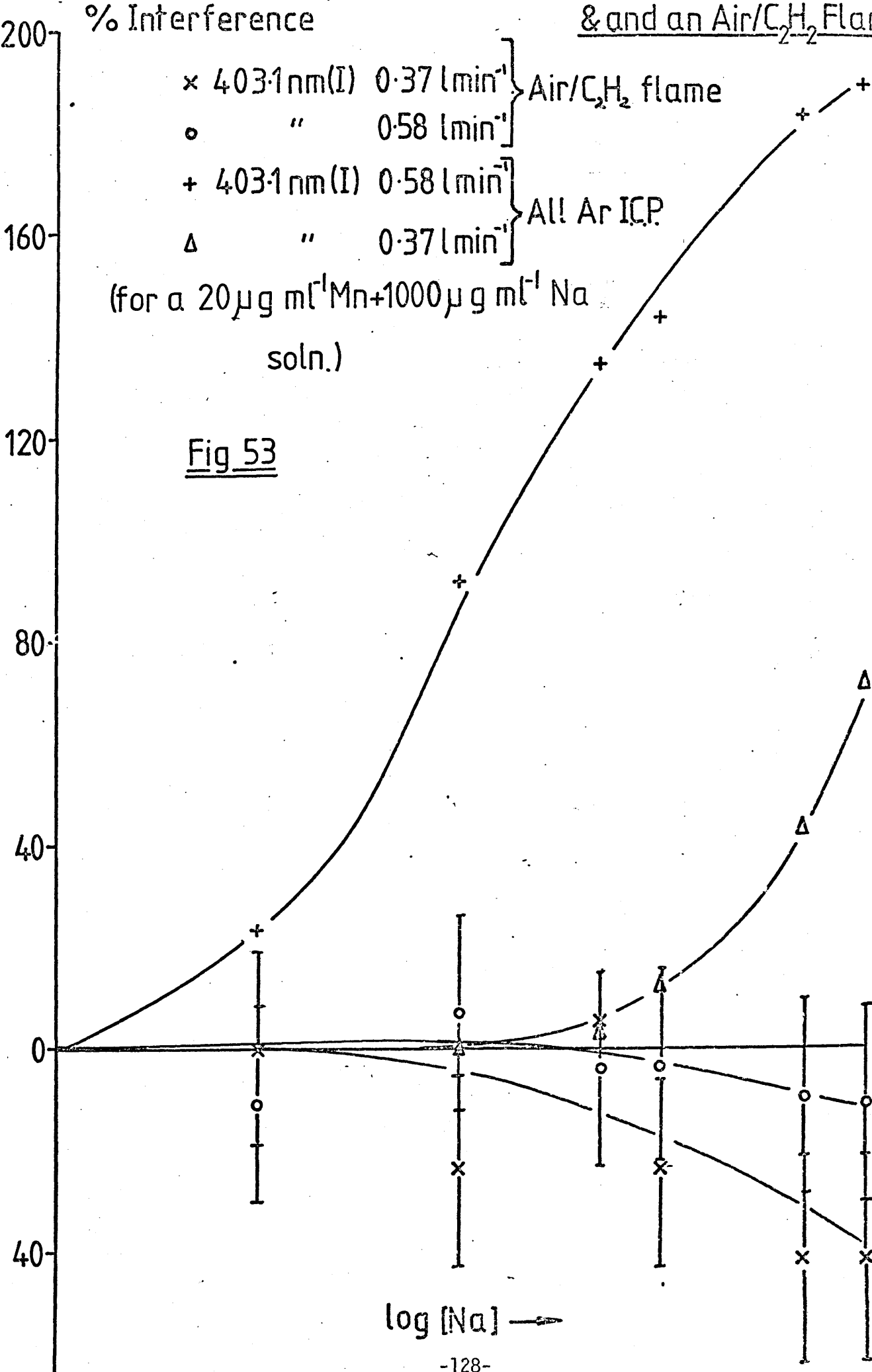
& and an Air/C₂H₂ Flame

% Interference

- × 403.1nm(I) 0.37 lmin⁻¹ } Air/C₂H₂ flame
- " 0.58 lmin⁻¹ }
- + 403.1nm(I) 0.58 lmin⁻¹ } All Ar ICP
- Δ " 0.37 lmin⁻¹ }

(for a 20 μg ml⁻¹ Mn + 1000 μg ml⁻¹ Na soln.)

Fig 53

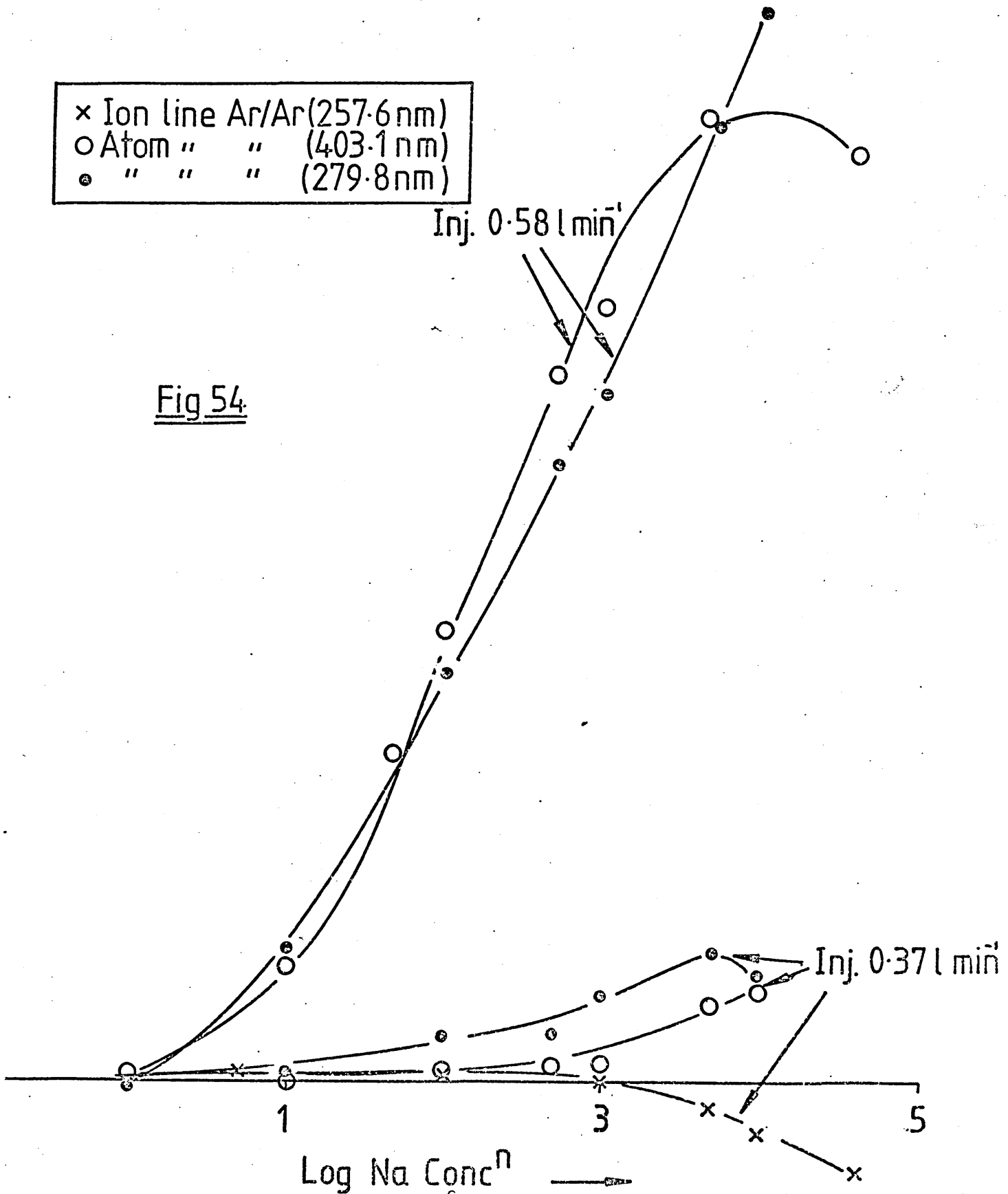


log [Na] →

Effect of Reducing Injector Ar Flow on Na Interference
(Mn Atom Lines)

× Ion line Ar/Ar(257.6nm)
○ Atom " " (403.1nm)
● " " " (279.8nm)

Fig 54

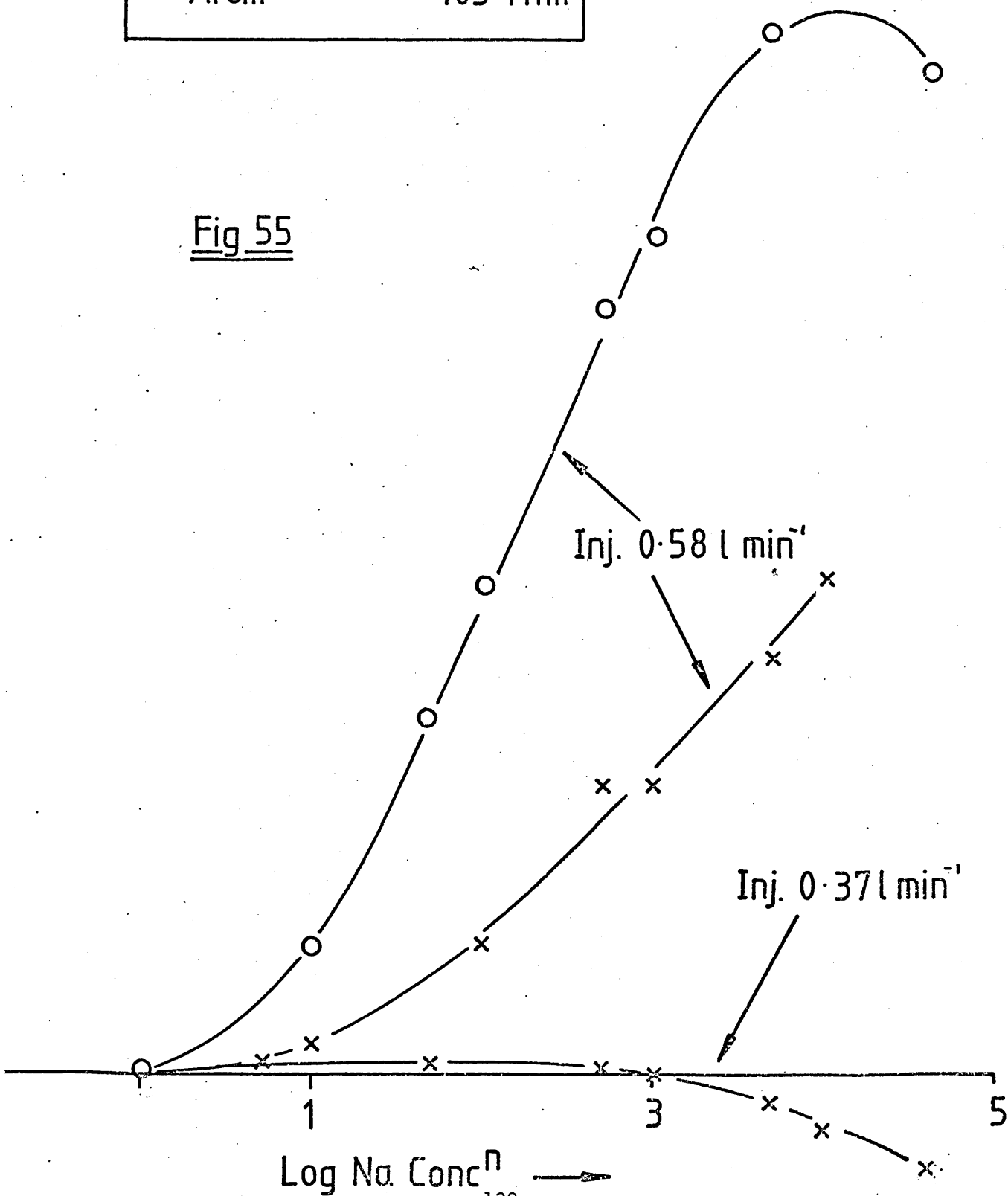


Effect of Increasing Injector Ar Flow on Na Interference

(Mn Ion Line)

x- Ion line Ar/Ar 257.6nm
o- Atom " " 403.1nm

Fig 55



decreased to the ion line optimum value (0.37 l min^{-1}). Conversely an increase on the interference of the 257.6 nm ion line in an all argon plasma is observed (Figure 55) when the injector flow rate is increased to that optimal for the atom line (0.58 l min^{-1}). Clearly these effects do not differentiate between an atom and ion line, again showing the mechanism occurring in the plasma is not as seen in flame and arc/spark sources.

This effect is not peculiar to the demountable torch design alone; Figure 56 shows that in a Greenfield torch, operating with nitrogen coolant, increasing injector gas flow rates move the sodium interference from negative to positive when studying the emission from the Mn 257.6 nm ion line at optimal conditions.

In carrying out the preceding Na interference experiments a number of qualitative effects were observed in the physical appearance of the plasma that showed strong correlation with the interferences found. Figure 57 shows a diagram of the plasma (either nitrogen cooled or all argon as the effects are similar in both) and the observed regions or zones when a high concentration of Na solution is aspirated. Region 1 is colourless, above this, region 2, is a bright well defined yellow 'tongue'. Region 3 is again colourless and merges into region 4, which is yellow, but less well defined and more diffuse than region 2. The existence of these regions in the plasma and their relative positions with respect to the viewing region appear to be very important in explaining the interference effects observed. Consider a small viewing region moving upwards from the tip of the plasma fireball. When the Mn emission is observed in regions 1 and 2 large positive interferences on both the atom and ion line in both types of plasma occur. Moving up into region 3 the positive interferences disappear and in some cases particularly the nitrogen cooled plasma, a small negative interference is observed. Moving the viewing region still higher into the tail flame (region 4) positive interference on both lines in both types of plasma re-occurs although not to such a large

Effect of Increasing Injector Ar Flow on Na Interference

(Mn 257.6 nm Ion Line, Greenfield Torch)

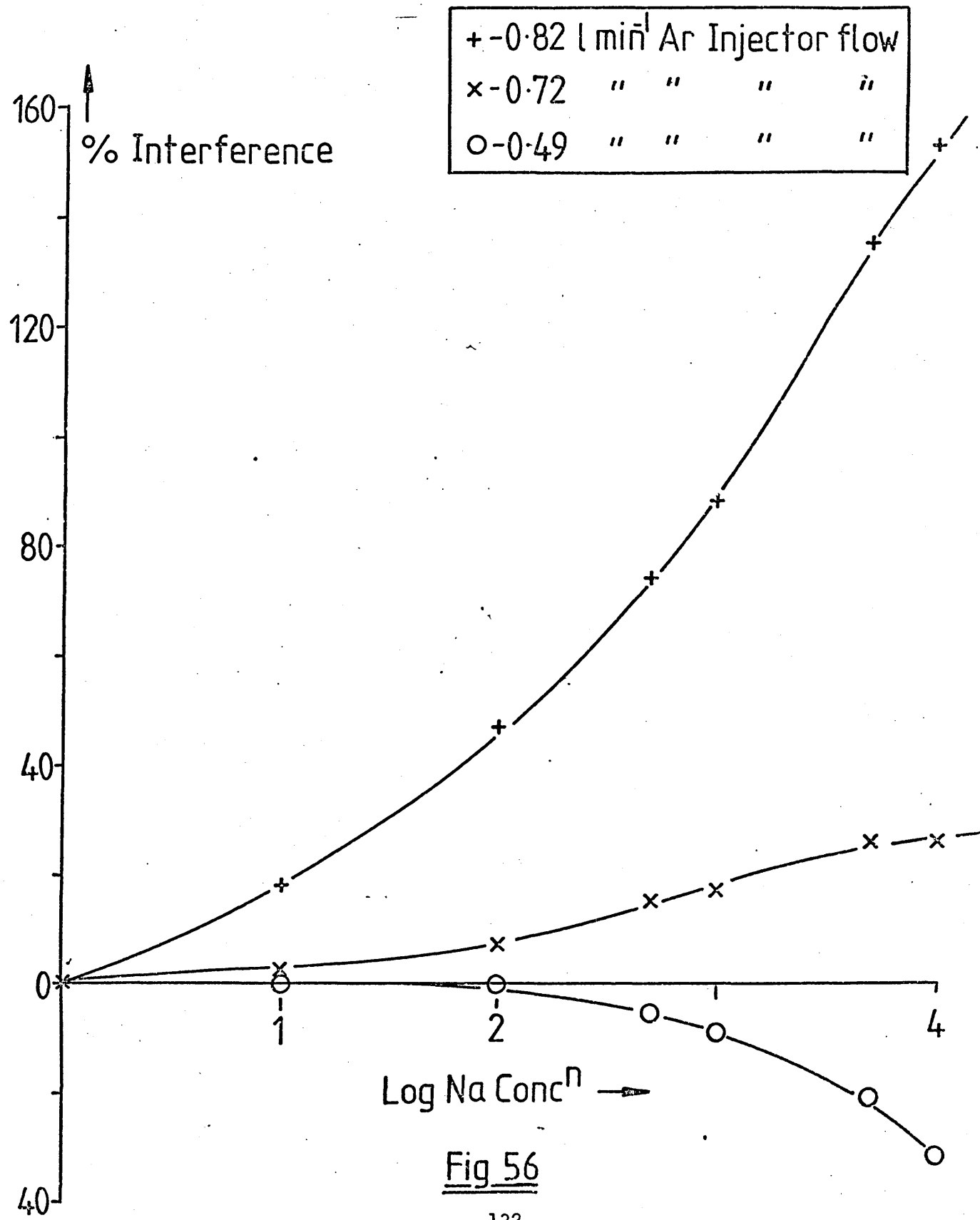


Fig 56

extent as in regions 1 and 2.

Using this information it is now possible to interpret the results in Figure 49 where the effect of viewing height on Na interference was studied. As viewing height is increased from low to high values the viewing region moves up through the tail flame and thus high positive interference moving to a minimum and then back to positive interference is observed as each of the regions (1,2,3 and 4) are entered.

The injector flow rate controls the position of regions 1 and 2 relative to the plasma fireball. At low injector flow rates the yellow 'tongue' is located inside the central channel of the plasma. As the injector flow is increased region 2 extends further above the fireball, until at very high injector flow rates region 2 merges into region 4 and region 3 disappears.

Thus for high injector gas flows region 2 extends higher into the tail flame and hence into the viewing region causing large positive interference. This explains the effects observed in Figures 53 -56. It appears to be an unfortunate coincidence that the optimum conditions for the 403.1 nm atom emission in both plasmas (particularly the all argon plasma) are also conditions which produce large interferences.

Since the Na interference observed is closely linked with viewing region it is understandable that both viewing height and injector gas flow rate are found to influence the magnitude of the interference, as both these parameters are closely linked with viewing region. All the ICP controlling parameters are, however, interdependent to some extent and must also effect the Na interference.

It was therefore decided to use the simplex optimisation technique, described in chapter 4, to find a set of operating conditions that would minimise the Na interference effects, and the univariate

Viewing Regions in the
ICP Tail Flame Due to
High Concentrations of

Na

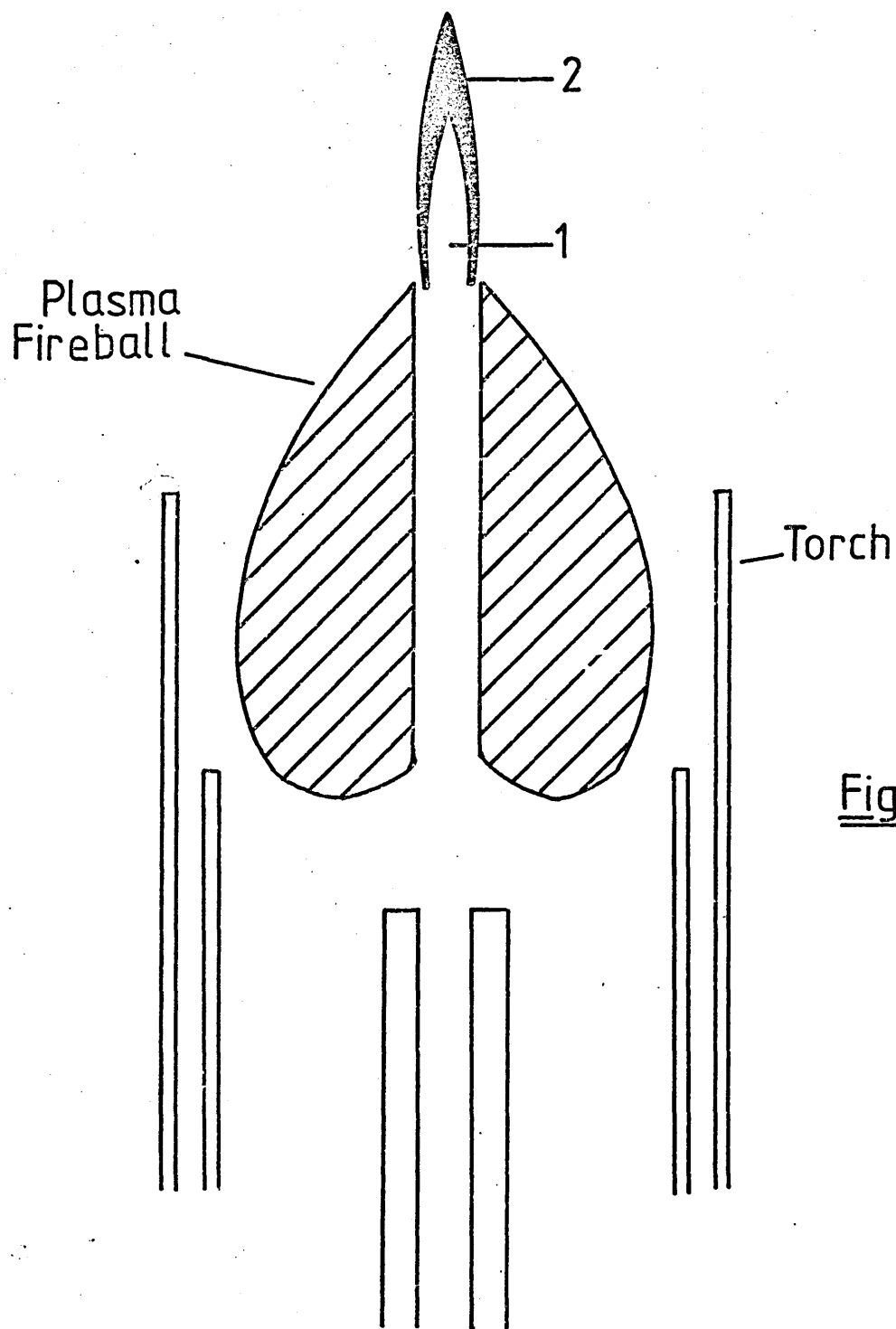


Fig 57

search graphs, used to check the simplex results, it was thought would also yield information as to how each parameter is related to the Na interference.

Using signal to background divided by percentage interference (SBIR) as the optimising criterion, to obtain maximum SBR with minimal interference, two simplex optimisation experiments were carried out on the Mn 403.1 nm atom line (since its optimum operating conditions were most effected by Na interference), one using an all argon plasma and one using a nitrogen cooled plasma. The SBIR was always considered positive, even if the interference became negative, for ease of operation and to simplify the interpretation of the results. The SBR percentage interference were measured by aspirating solutions of $1 \mu\text{g ml}^{-1}$ Mn and $1 \mu\text{g ml}^{-1}$ Mn + $1000 \mu\text{g ml}^{-1}$ Na respectively for the nitrogen cooled plasma, and for the all argon plasma $5 \mu\text{g ml}^{-1}$ Mn and $5 \mu\text{g ml}^{-1}$ Mn + $1000 \mu\text{g ml}^{-1}$ Na respectively.

The optimum conditions, as identified by the simplex procedure, for maximum SBIR are shown in Figures 58 -67 along with the univariate search graphs which show the variation of SBR, percentage interference, and SBIR, with each operating parameter in the two types of plasma. As optimum SBIR was approached by the simplex and low levels of interference were found (0-5 %), the size of the experimental error on the SBIR increased rapidly, and hence the point of termination of the simplex was not easily defined. Nevertheless, the optimal regions as shown in figures 58 -67 were found to be in good agreement with the univariate search graphs.

Figures 58 - 59 show the results for the viewing heights in the two plasmas. The interference curves for both plasmas have the characteristic shape as shown already in Figure 49 and may be explained in terms of the regions shown in Figure 57. Viewing heights of c.a. 10 - 20 mm above the load coil correspond to regions 1 and 2, heights of 20 - 24 mm correspond to region 3 and viewing

- × % Interference
- Signal to Background ratio S/B
- △ Ratio of S/B to % Interference

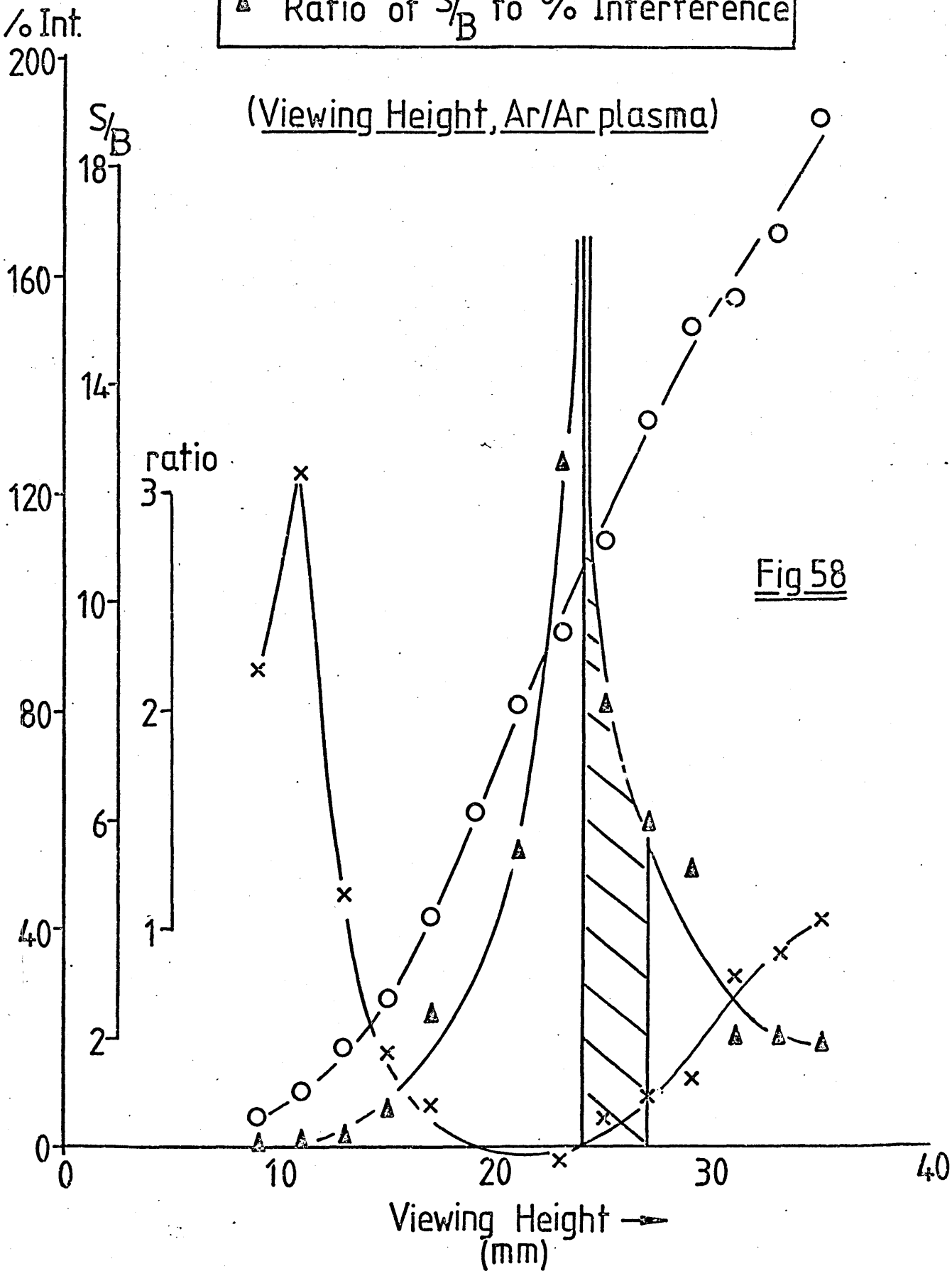


Fig 58

Univariate Search for Minimisation of Na Interference
 (Viewing Height, Ar/N₂ plasma)

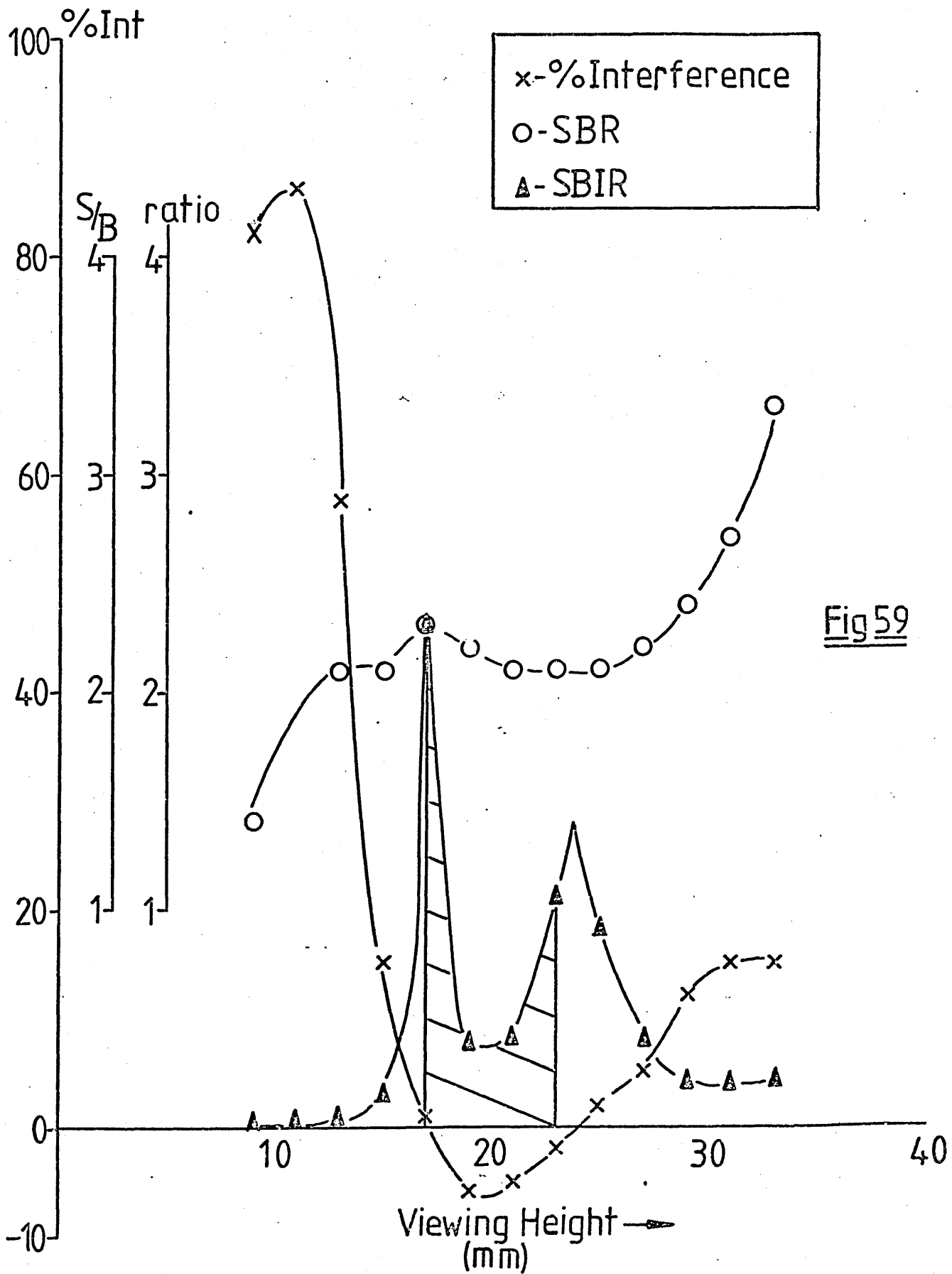


Fig 59

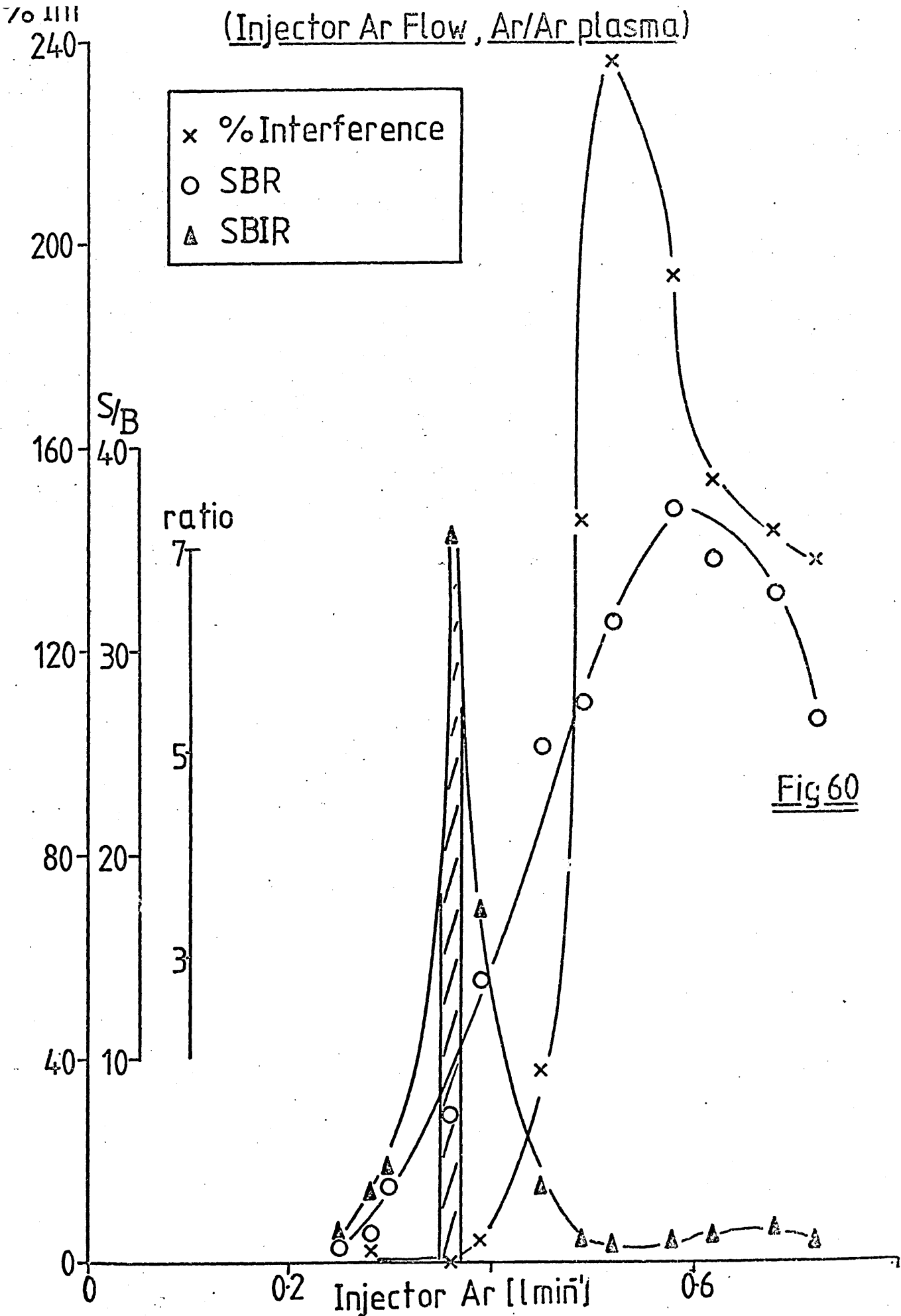


Fig 60

(Injector Ar Flow, Ar/N₂ plasma)

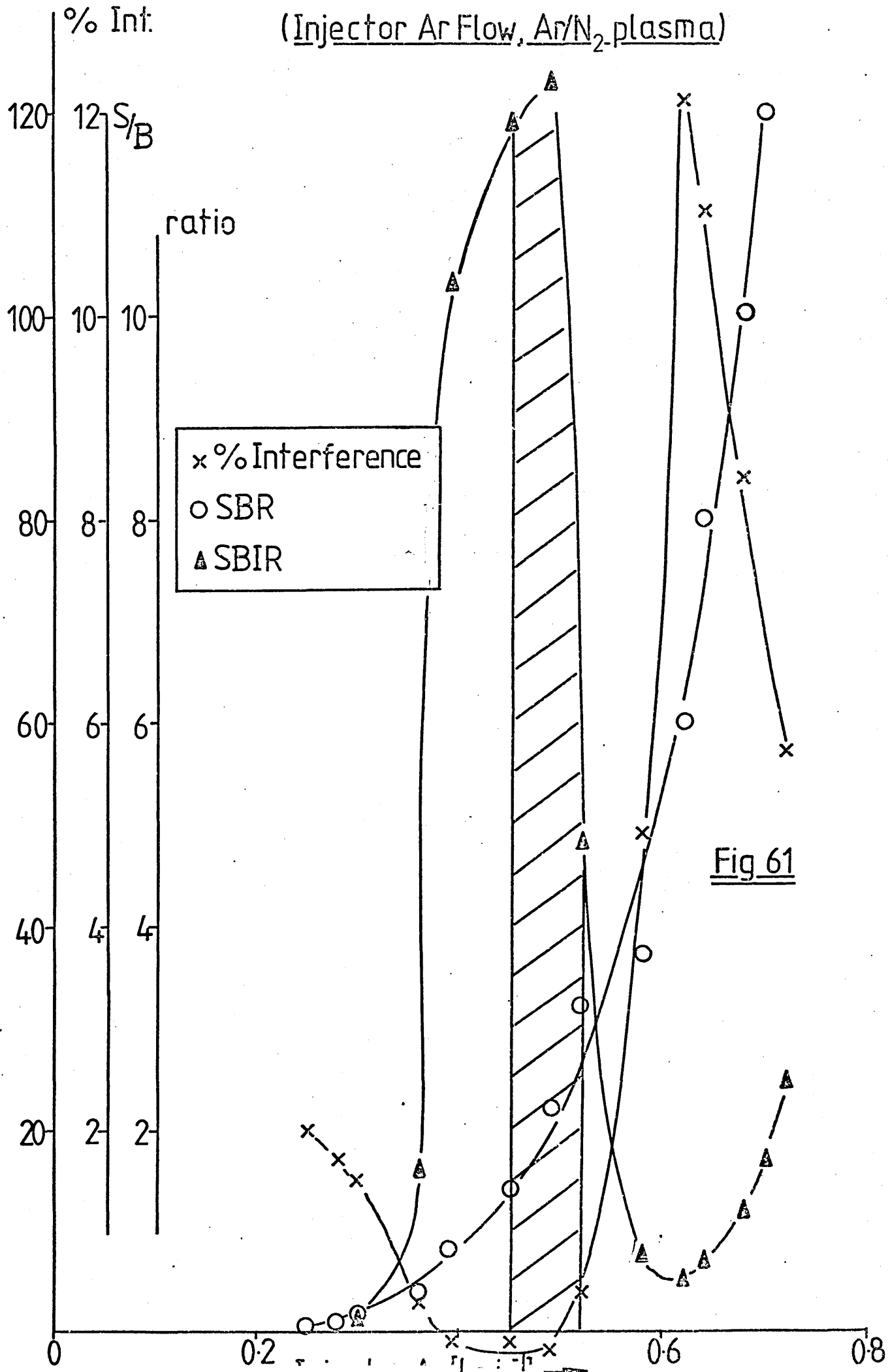


Fig 61

(Plasma ArFlow, Ar/Ar plasma)

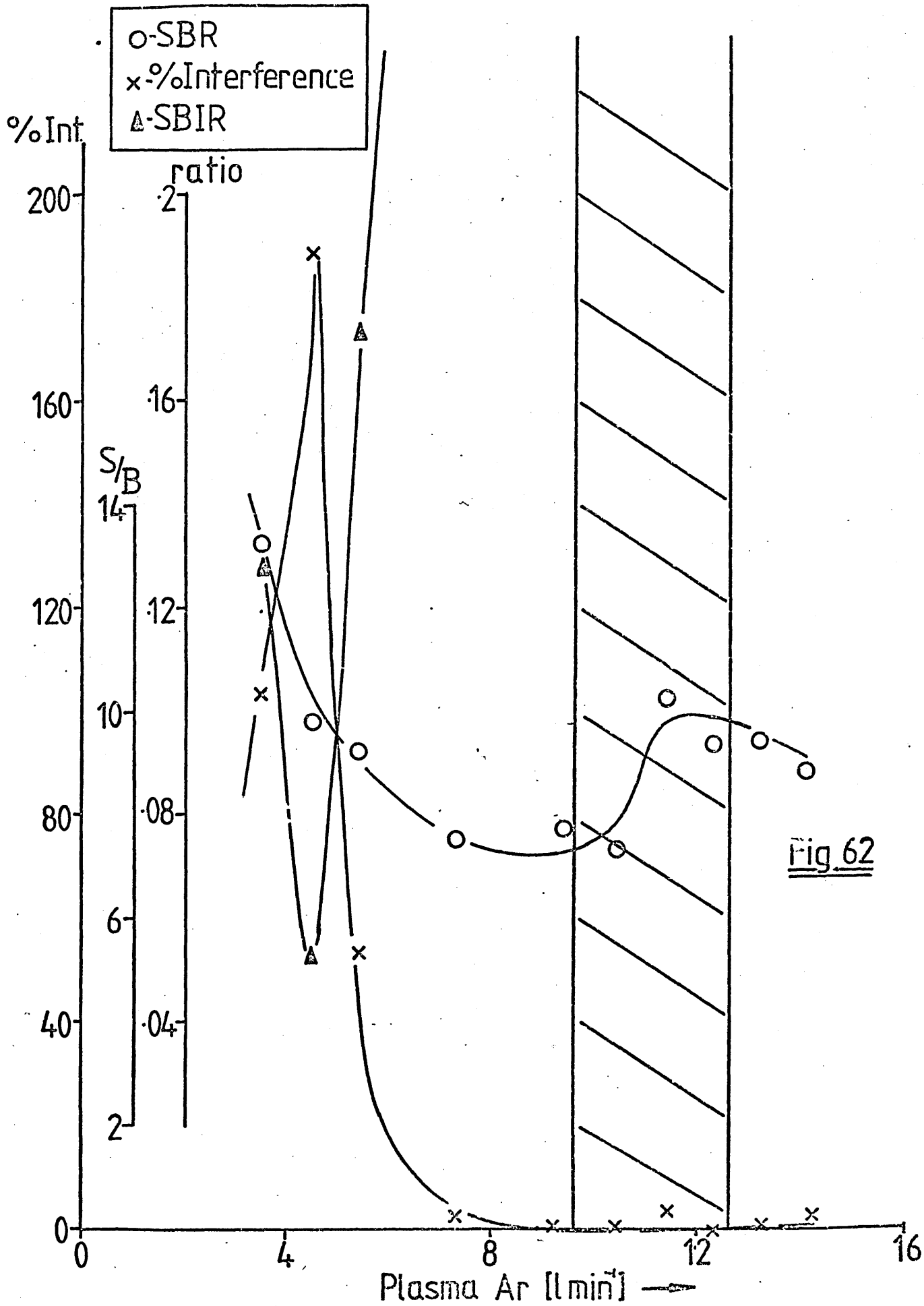


Fig. 62

heights 25 mm correspond to region 4. In the nitrogen cooled plasma where the interference is negative over a short section of tail flame (Figure 59), two peaks are observed in the SBIR curve. As these two peaks are indistinguishable within experimental error the simplex defines an optimal region covering both of the SBIR peaks.

Figures 60 and 61 illustrate the effect of injector argon flow rate on the two plasmas. The interference curves are again very similar and have the same characteristic slope as shown in Figure 50. As the injector flow rate increased region 2 (Figure 57) extends further out from the central channel until at c.a. 0.5 l min^{-1} the yellow 'tongue' starts to enter the viewing region causing positive interference. At c.a. 0.6 l min^{-1} region 2 extends into region 4 and maximum interference is observed. For both types of plasma there is a large 'trade off' in SBR in order to minimise interference for this particular parameter.

Figures 62 and 63 show that over a wide range of gas flows the plasma gas flow rate has a minimal effect on the Na interference. For lower flow rates, (6 l min^{-1} Ar on the all argon plasma and 4 l min^{-1} Ar in the nitrogen cooled plasma) both types of plasma become physically shorter and the yellow tongue (region 2) appears to extend higher into the tail flame thus causing positive interferences.

The coolant flows for the two types of plasma (Figures 64 and 65) over given ranges ($0 - 6 \text{ l min}^{-1}$ Ar in the all argon plasma and $5 - 8 \text{ l min}^{-1}$ N_2 in the nitrogen cooled plasma) again show little influence on the Na interference. In the all argon plasma increasing the argon coolant flow has a similar effect to decreasing to plasma argon flow. The plasma becomes short and flat and the diameter of the central channel increases allowing region 2 to extend higher into the tail flame producing positive interference.

(Plasma Ar Flow Ar/N₂ plasma)

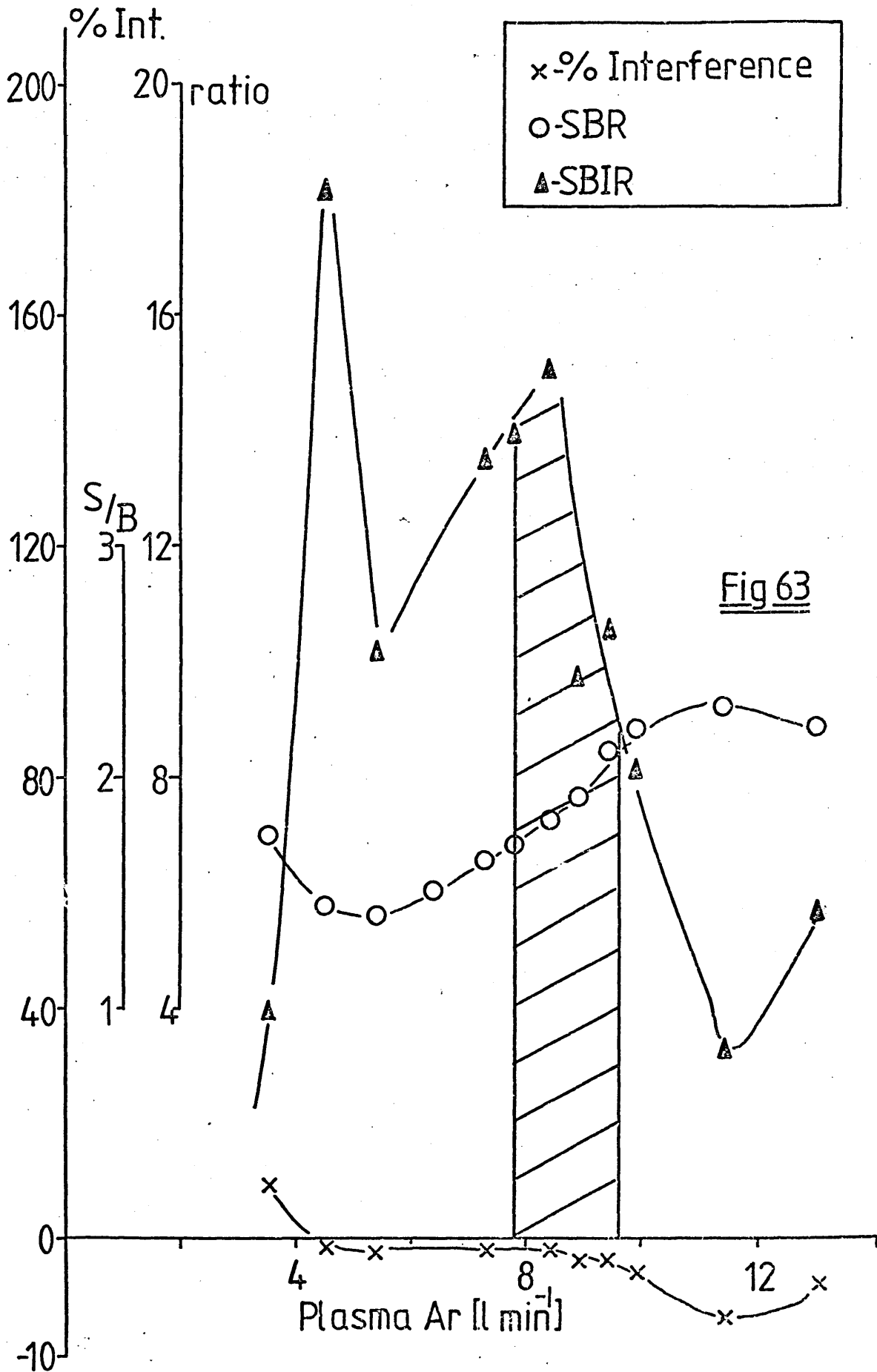


Fig 63

(Coolant Ar Flow, Ar/Ar plasma)

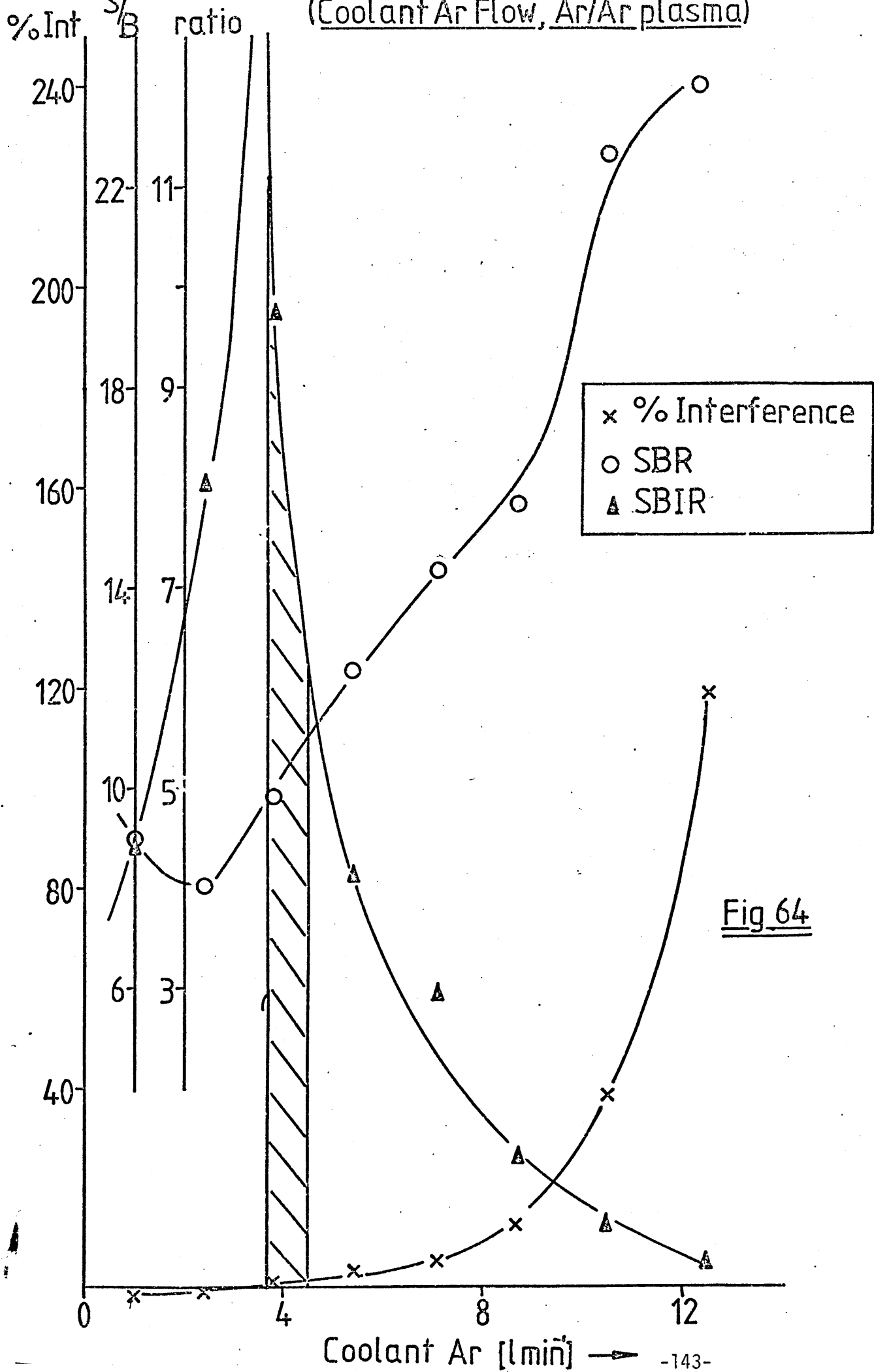
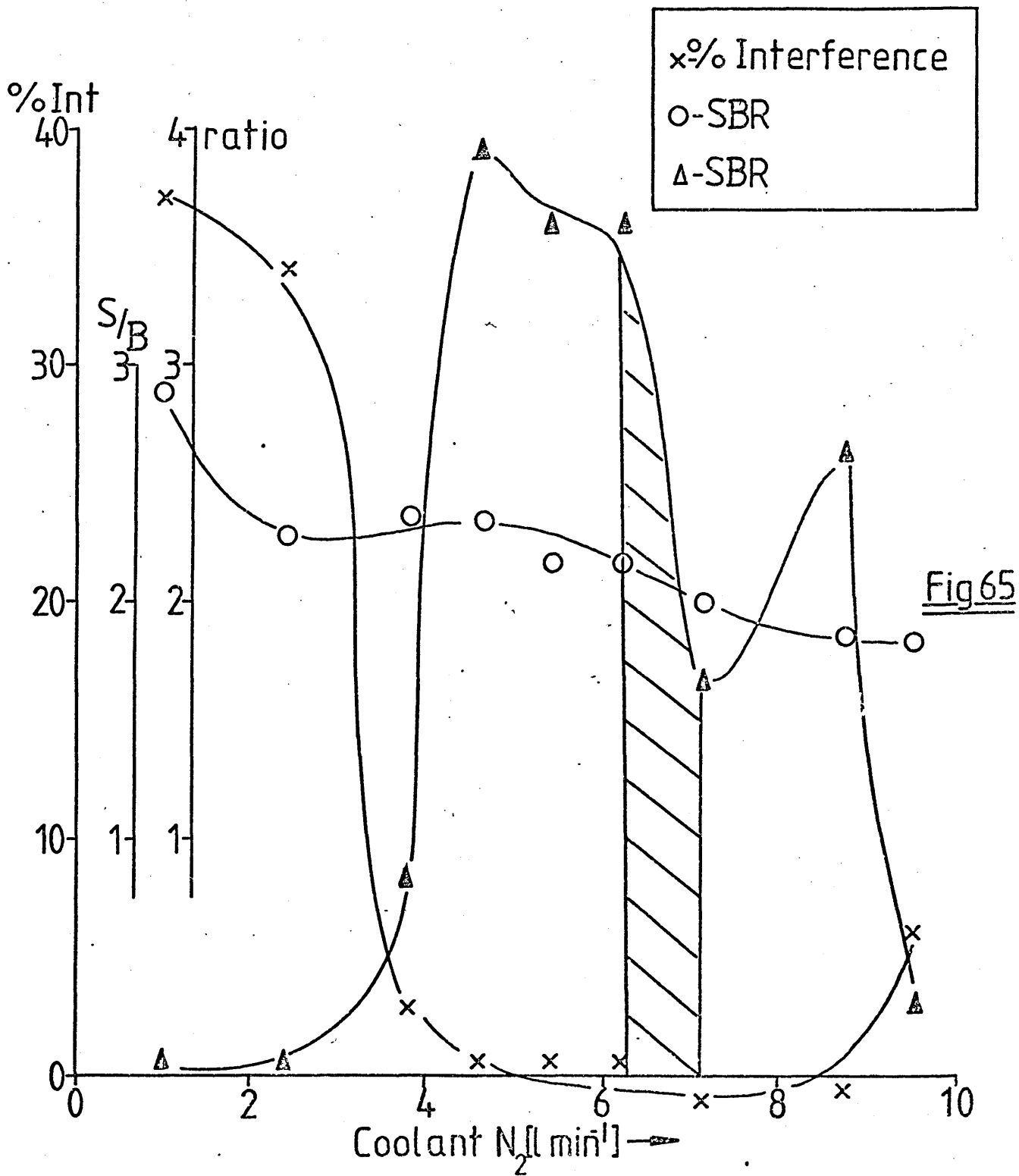


Fig 64

Univariate Search for Minimisation of Na Interference (Coolant N₂ Flow Ar/N₂ plasma)



Univariate Search for Minimisation of Na Interference
 (Power, Ar/Ar plasma)

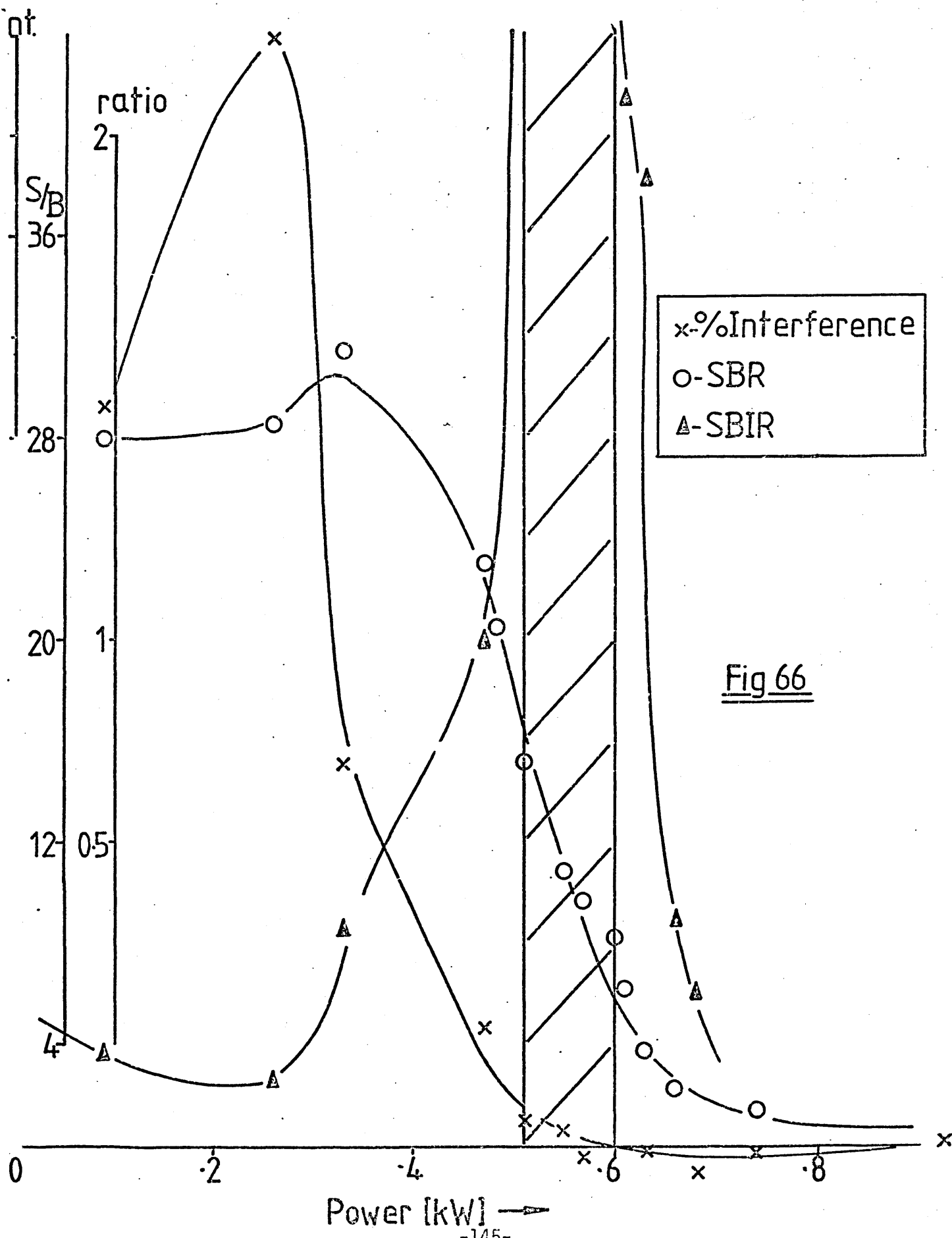


Fig 66

Conversely, however, in the nitrogen cooled plasma, increased coolant flow produces a 'tighter' smaller plasma which holds region 2 inside its central channel, and hence low interference is observed.

Finally figure 66 and 67 show a comparison of the effect of power on the Na interference in the two types of plasma.

It is interesting to note that as for viewing height and injector flow rate, the interference curves are very similar for variation of power. At low powers (0.2 - 0.4 KW) very small plasmas are produced with short and relatively large diameter central channels, such that an elongated region 2 is observed extending high into the tail flame. As the power is increased the volume of the plasma increases, the diameter of the central channel is reduced and the length of the yellow tongue becomes smaller until at c.a. 0.6 KW region 2 no longer extends into the viewing region and the large positive interferences disappear.

5.2.3 CONCLUSIONS

A number of discrete regions (Figure 57) apparently exist in the tail flame of the plasma when high concentrations of Na are being aspirated. The interference of Na on Mn has been shown to be critically dependent upon which of these regions is being observed during analysis.

Both enhancement and depression of the Mn ion line (257.6 nm) and Mn atom line (403.1 nm) have been observed in both types of plasma, which precludes an explanation of this phenomena by a similar mechanism of ionisation interference as occurs in flames or arc and spark sources.

The simplex minimisation of interference experiments have shown that all of the plasma operating parameters effect the relative size and position of the sodium interference regions, and hence

Univariate Search for Minimisation of Na Interference
 (Power, Ar/N₂ plasma)

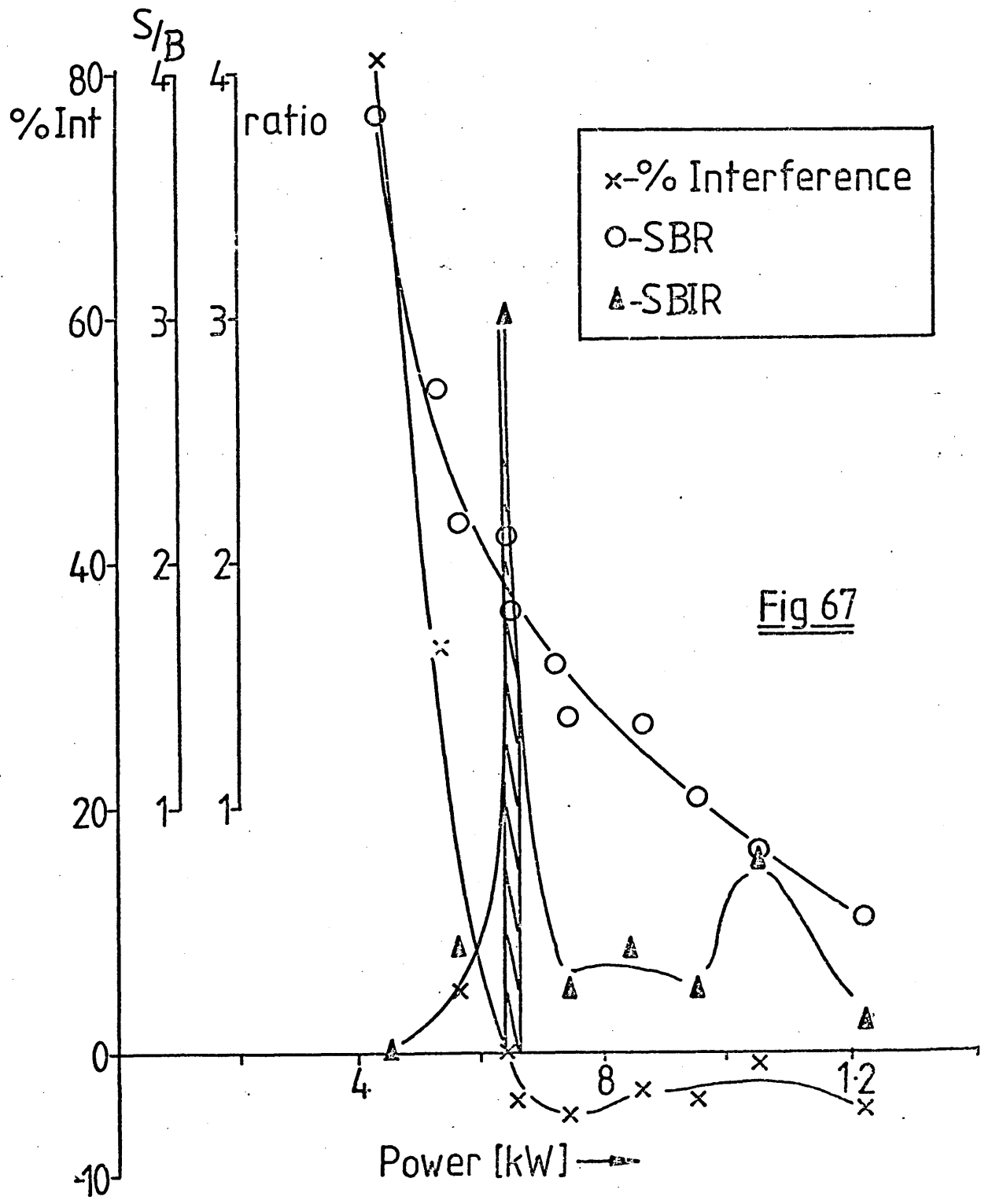


Fig 67

Effect of Minimisation of Na Interference on SBR

(MnI 403.1nm)

Coolant Gas	Gas Flows [l min ⁻¹]			Height /mm	Power / kW	SBR
	Coolant	Plasma	Injector			
1 Ar	8.7	14.0	0.58	26	0.5	12.0
2 Ar	4.0	11.0	0.36	25	0.55	1.9
1 N ₂	7.0	3.1	0.49	26	0.26	16.7
2 N ₂	6.0	9.0	0.50	17	0.65	2.1

1 Optimised for SBR

2 " " SBIR

Table 10

the magnitude of the interference. Viewing height and injector flow rate have, however, been identified as being most critical in the control of the Na interference.

The simplex experiments have also shown that the interferences can be 'tuned' out of the system by appropriate choice of operating conditions. For the Mn 403.1 nm atom line, however, this involves a loss in SBR since the Mn I optimum SBR conditions also give rise to large interferences from Na in both types of plasma. This is illustrated in table 10 where the optimum SBR values of the operating parameters are compared to the optimum SBIR values of the operating parameters along with the SBR for both sets of conditions.

For the argon cooled plasma there is a 'trade off' factor of 6 and in the nitrogen cooled plasma a factor of 8.

The practical applications of these results will be further discussed in chapter 7.

6. ANALYSIS OF METALLURGICAL SAMPLES

In recent years the ICP has found wide and varied applications (see chapter 1 section 1.3.1), amongst the reports in the literature have been the analysis of steels and various other metallurgical samples (e.g. 69 -79). There is, however, a lack of fundamental knowledge on the methodology and principles of applying ICP emission spectroscopy to the analysis of metallurgical samples as compared for example to the well documented flame and arc/spark sources.

The aim of this work has been to evaluate ICP atomic emission as a method of analysing a number of different metallurgical samples, and to identify those aspects of the technique where problems might be encountered.

6.1 METALLURGICAL SAMPLES ANALYSED IN THIS STUDY

The sponsoring company for this project have supplied seven different alloys to be analysed. These are listed below along with their approximate composition.

Alloy

TiAl - Ti 6 - 10%, Al 90 - 94%, + minor elements
AlTiB - Ti 5%, Al 94%, B 1%, + minor elements
BATS - Ti 15 - 20%, Al 10 - 20%, Mn 3 - 10%, B - 3%, Si 5%, Zr 4%
Cr metal - Cr + minor elements
Tungsten Carbide - WC 100%
CrAl - Cr 10 - 20%, Al 80 - 90%, + minor elements
SiAl - 50% Si, 50% Al, + minor elements

The above alloys were not standard materials, and since no similar reference materials to the samples supplied were available a set of six BCS steel samples were analysed to check the accuracy of the ICP analysis. The steel samples analysed are as follows:-

- i) BCS No. 215/3 0.9% Carbon steel;
- ii) BCS No. 224/1 Chromium Vanadium steel;
- iii) BCS No. 306/1 0.4% Carbon free-cutting steel;
- iv) BCS No. 402 Low Alloy steel;
- v) BCS No. 329 Mild Steel;
- vi) BCS No. 219/4 Nickel Chromium Molybdenum steel.

There are a number of points to be considered which arise directly from the type of samples being presented here for analysis.

Firstly each alloy must be presented to the ICP system in an amenable form for analysis, i.e. a solution. Since a multi-element analysis was to be performed it was necessary to ensure that the dissolution procedure produced a quantitative solution of all the elements to be determined. Previously the non-ferrous alloys had been analysed by a number of techniques (see chapter 1 section 1.4) particularly those alloys containing large amounts of silica (e.g. Si Al) where the silica was determined gravimetrically and hence not dissolved at all. Thus some modification of conventional solution methods was often required.

Secondly, there would be large quantities of aluminium present in the matrix of most of the alloy solutions as well as high concentrations of sodium for those alloys requiring a fusion step prior to dissolution (e.g. BATS). The presence of easily ionisable elements has been shown to cause interference effects (see chapter 5), thus care had to be taken to keep these effects to a minimum for samples analysed here.

Finally there are a number of elements present at high concentrations

in these alloys (e.g Ti, W, and Fe) which possess a large number of lines in their emission spectra, so that spectral interference effects would be an important factor to consider during analysis.

6.2 EXPERIMENTAL PROCEDURE FOR THE ANALYSIS OF METALLURGICAL SAMPLES

6.2.1 SAMPLE DISSOLUTION AND PREPARATION OF STANDARDS

For all preparations of both samples and standards Analar grade reagents, and 'specpure' metals were used.

For all alloys, apart from Si Al, the whole analysis of the sample has been carried out on the sample as dissolved without further dilutions as will subsequently be described in sample preparation. For Si Al alloy the Si content was determined on a one tenth dilution of the initial sample solution, the other elements being determined at original dilution of the sample.

a) Ti Al Alloy

Sample (2.5g) was dissolved in concentrated HCl (50 cm³), the solution was boiled to complete the reaction, cooled and diluted to 250 cm³ with distilled water.

The standards were made up from single element solutions in a synthetic matrix solution containing Al (9.4g) and Ti (0.6g) per 1l of solution.

b) Al Ti B Alloy

Sample (2.5g) was dissolved in 50 cm³ of concentrated HCl, the boron was then brought into solution by oxidation with concentrated HNO₃ (3 cm³). The resulting solution was then warmed producing a clear yellow liquid which was then cooled and diluted to 250 cm³ with distilled water.

The standards were made up from a multi-element solution containing Cr, Fe, Mn, Mg, Ni, V, Zn (1000 µg ml⁻¹), apart from

B, Si, and Ti which were made up from single element solutions. All the standards were matched to the matrix by being made up in a solution containing Ti (0.5g) and Al (9.5g) per 1l of solution, apart from the Ti standard which was matched with Al (9.5g l^{-1}) only.

c) BATS Alloy

Sample (0.5g) was fused in a zirconium crucible with sodium carbonate (1.5g) and sodium peroxide (4g). On cooling, the fusion was dissolved in concentrated HCl (35 cm^3) plus distilled water (100 cm^3). The dissolution was completed by warming, and on cooling was made up to 500 cm^3 with distilled water. Each standard was made up in 15g l^{-1} Na Cl solution to match the sodium content of the sample due to the fusion step.

d) Cr Metal

Sample (1.0g) was dissolved in concentrated HCl (15 cm^3), the solution was boiled to complete the reaction, cooled, and diluted to 100 cm^3 with distilled water. Single element standards were used and were made up in 10g l^{-1} Cr to match the matrix.

e) Tungsten Carbide

Sample (1.0g) was dissolved in concentrated H_3PO_4 (2.0 cm^3) + concentrated HNO_3 (10 cm^3) + distilled water (45 cm^3), the solution was then boiled to complete the reaction, cooled, and diluted to 100 cm^3 with distilled water. Single element standards were used, with sodium tungstate as the synthetic matrix (16.9 g l^{-1}) and hence sodium nitrate was added to the sample solutions (8.7g l^{-1}).

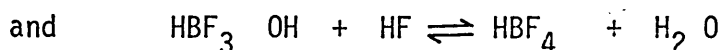
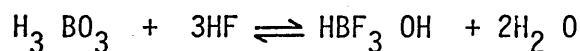
f) Cr Al Alloy

Sample (1g) was dissolved in concentrated HCl (15 cm^3), the

solution was then boiled to complete the reaction, cooled, and diluted to 100 cm³ with distilled water. Single element standard solutions were used and matrix matched with Al (8g) and Cr (2g) per 1l of solution.

g) Si Al Alloy

To a 1g sample distilled water, (40 cm³), concentrated HNO₃ (10 cm³) and concentrated HCl (15 cm³) were added. After the initial vigorous reaction had subsided 40% HF (10 cm³) was added and the solution was gently warmed and stirred. On completion of dissolution H₃ BO₃ (2g) was added to neutralise the excess HF by the following two step reaction (178).



The sample was then made up to 100 cm³ with distilled water.

Single element standards were used matrix matched with 5g l⁻¹ A .

h) B.C.S. Steels

Sample (0.5g) was dissolved in concentrated HCl (15 cm³), after the initial reaction had subsided a few drops of concentrated HNO₃ were added. The solution was then boiled, cooled and made up to 50 cm³ with distilled water.

The standards were made from a multi-element solution containing Ni, Cu, Cr, Mn, V (1000 µg ml⁻¹), apart from Si which was made up from a single element solution. Each standard was matrix matched with 10g l⁻¹ Fe.

For the Ti Al, Tungsten carbide, Cr Al and Si Al alloys two sets of calibration standards were prepared, one matched to the matrix elements and the other in distilled water.

6.2.2 PLASMA OPERATING CONDITIONS

The analysis of the Ti Al alloy was carried out prior to the simplex optimisation experiments with a nitrogen cooled plasma operated at the following conditions:

Injector Ar flow	-	0.5	l min ⁻¹
Plasma Ar flow	-	1.7	l min ⁻¹
Coolant N ₂ flow	-	5.4	l min ⁻¹
Power	-	0.5	kW
Viewing height	-	30	mm.

A slit height of 16 mm was used and the nebuliser operated at its natural uptake rate (0.9 ml min⁻¹).

For all other analyses an all argon plasma was used. The simplex optimisation of the all argon plasma had shown that similar operating conditions were optimal for the range of elements studied. The Mn 257.6 nm ion line optimal conditions were therefore chosen as a reasonable set of compromise operating conditions, which had also shown low interference effects from sodium (chapter 5).

Thus the compromise all argon plasma operating conditions were:-

Injector Ar flow	-	0.37	l min ⁻¹
Plasma Ar flow	-	14.0	l min ⁻¹
Coolant Ar flow	-	5.0	l min ⁻¹
Power	-	0.54	kW
Viewing height	-	18	mm

A slit height of 4 mm was used, and the nebuliser was pumped at

1.65 ml min⁻¹ sample uptake rate to prevent apparent interferences at the plasma due to the nebuliser system (see chapter 5, section 5.1.1).

6.2.3 SELECTION OF SPECTRAL LINES

For a given element the most sensitive line was chosen, as predicted by literature tables of ICP spectral lines (179,180). A solution of the element was then aspirated into the plasma and the selected line was scanned using the monochromator. A synthetic matrix solution, containing the major elements of the alloy to be analysed, was then aspirated and scanned over the spectral region where the analyte line was located. The two scans were then compared to check for spectral interference from the matrix. When the analyte line could not be resolved from the matrix line less sensitive lines were chosen until a line with no spectral interference was found.

In all analysis changes in background were corrected for by spraying a blank solution of the synthetic matrix at the analyte line wavelength and subtracting this value from the analyte signal when a sample solution was sprayed.

6.3 RESULTS AND DISCUSSION

6.3.1 Ti Al ALLOY

The results of the analysis, as obtained from the matrix matched calibration curves, are shown in Table 11 along with the results from the sponsoring company's (LSM) analysis of the alloys. The LSM analysis was carried out on 'button' samples on a direct-reading emission spectrometer, these samples were removed from the melt, and cast, whereas the samples used in this work were of drillings from the ingots produced from the melt. The results show reasonable agreement, although there are some discrepancies.

TiAl Analysis

Element	Wave-length /nm	Alloy No. 00188J		Alloy No. 13794J		Alloy No. 16529J		Matrix Difference %
		ICP Result % w/w	LSM Result % w/w	ICP Result % w/w	LSM Result % w/w	ICP Result % w/w	LSM Result % w/w	
Cr I	425.4	0.004	0.010	0.006	0.005	0.003	0.010	34.0
Fe II	259.9	0.19	0.18	0.25	0.15	0.21	0.24	-55.2
Mn I	403.1	0.005	<0.02	0.010	<0.02	0.006	<0.02	183
Mg II	279.5	<0.002	0.001	<0.002	<0.001	<0.002	0.001	-58.1
Ni I	352.4	0.016	<0.02	0.020	<0.02	0.016	<0.01	50.0
Si I	251.4	0.050	0.06	0.090	0.10	0.050	0.11	33.3
V II	292.4	0.29	0.18	0.14	0.11	0.14	0.11	-40.0
Ti II	252.5	6.0	5.36	9.4	10.72	6.7	6.01	—

Table 11

These could be due to differences in the two types of samples analysed.

Table 11 also shows the percentage difference in the result when standards dissolved in distilled water were compared to standards buffered with the appropriate amount of the major matrix metals. The effects of the matrix are probably due to one of two effects. Firstly, for this analysis, the nebuliser was operated at its natural uptake rate and not pumped, which could have produced differences in uptake rates between the matrix matched and the distilled water standards (see chapter 5, section 5.1.1). This would tend to lead to negative errors. Secondly, the presence of large quantities of aluminium in the matrix matched standards could have been responsible for similar interference effects as observed for sodium (see chapter 5, section 5.2), particularly since a low power (0.5 KW) and high injector flow rate (0.5 l min^{-1}) were used; conditions shown to produce large interference with sodium in chapter 5. This would tend to cause positive errors. It must be noted that the conditions used for the analysis of the Ti Al alloys were chosen before any simplex experiments had been performed on the plasma system.

It was perhaps unfortunate that the conditions chosen for this analysis were also those likely to cause interferences, nevertheless the size of the interferences shown in table 11 make clear the necessity for buffering standards with the major matrix elements of the sample. Accordingly for all of the following analyses the results have been calculated from the calibration curves obtained from buffered standards.

It is interesting to note from table 11 that the atom lines are enhanced and the ion lines depressed with respect to the non-buffered standards, although this effect seems to suggest an ionisation suppression, the results from the experiments reported in chapter 5 would suggest the mechanism to be more complex.

AlTiB Analysis

Element	ICP Results			AA Results			LSM Results
	Wave-length/ _{nm}	Result % w/w	RSD %	Wave-length/ _{nm}	Result % w/w	RSD %	
Mn I	403.1	0.006	25.3	279.5 I	0.003	5.0	0.003
Cr I	425.4	0.002	68.4	357.9 I	0.004	23.0	0.017
Mg II	279.5	<0.001	-	285.2 I	<0.0003	-	0.05
Ni I	352.4	0.011	15.0	232.0 I	0.003	4.3	0.051
Fe II	259.9	0.175	1.65	248.3 I	0.175	0.4	0.14
Zn I	213.9	0.025	4.9	213.9 I	0.018	< 0.01	-
V II	292.4	0.100	3.0	-	-	-	-
Si I	251.4	0.120	1.6	-	-	-	0.12
B I	249.8	1.03	1.1	-	-	-	1.0
Ti II	252.5	5.53	1.3	-	-	-	5.58

Table 12

6.3.2 Al Ti B ALLOY

The results for the Al Ti B alloy are shown in table 12. Some of the ICP results were also checked by AAS using a nitrous oxide/acetylene flame and the same set of standards as used for the ICP analysis.

The LSM results are based on the analysis of exactly the same sample as used in this work; Ti was determined colorimetrically (181), B by a neutron capture method (182) and the other elements by AAS.

The % RSD for the ICP and AAS results were calculated over six separate sample dissolutions of the same alloy.

As spectral interference, from the matrix elements, was observed on the most sensitive lines of Mn, Cr and Ni it was necessary to use less sensitive lines, and hence the % RSD values are poor. The sensitivity for Mg was limited by the Mg content of the blank matrix solution.

For the other elements RSD of 5% was observed as well as good agreement (particularly for Si, B and Ti) with the LSM results.

The AAS results, as carried out in this work also show reasonable agreement, with the ICP results particularly Fe, there are, however, more discrepancies with the LSM values.

6.3.3 BATS ALLOY

Two BATS alloys were supplied (BATS 79, and BATS Standard) fusions and dissolutions of five samples of each alloy were used for analysis. The composition of the two alloys as determined by ICP in this work, and LSM are shown in tables 13 and 14. Again LSM determined Ti colorimetrically, B by neutron capture and Si, Al and Mn by AAS.

BATS 79 Analysis

Element	Wave-length /nm	ICP Results		LSM Result % w/w
		Result % w/w	RSD %	
BI	249.8	1.37	0.40	1.12
Si I	251.4	8.01	0.87	5.4
Al I	396.2	23.4	0.51	23.3
Mn I	403.1	3.04	0.98	3.17
Ti II	334.9	16.6	0.73	17.3

Table 13

Standard BATS Analysis

Element	Wave-length /nm	ICP Results		LSM Result % w/w
		Result % w/w	RSD %	
BI	249.8	1.15	2.6	-
Si I	251.4	4.4	0.94	4.33
Al I	396.2	11.5	1.09	11.3
Mn I	403.1	9.0	0.53	-
Ti II	334.9	21.2	1.4	-

Table 14

Cr Metal Analysis

Element	Wave-length /nm	ICP Results		LSM Result % w/w
		Result % w/w	RSD %	
Cu I	327.4	0.003	5.1	0.0035
Mn II	257.6	<0.01	—	0.001
Al I	396.1	0.19	2.8	0.15
Fe II	259.9	0.15	1.7	0.22
As	228.8	<0.02	—	1.0×10^{-4}

Table 15

Apart from Si in the BATS 79 sample there is very good agreement between the ICP results and those obtained by LSM at RSD <3%. The spurious result for the Si was probably due to a poor silicon standard. A new Si standard was used for the Standard BATS sample producing close agreement with the LSM result, particularly with the major Al component of the alloy which is also determined at high precision (c.a. 1% RSD).

6.3.4 Cr METAL

One Cr metal sample was analysed in triplicate. The results are shown in table 15. The LSM results were determined on the same sample using flame AAS for Cu, Mn, Al, and Fe and carbon tube furnace AAS for the As. The level of Mn detected was limited by the amount of Mn in the blank synthetic matrix solution. For As the ICP did not offer sufficient sensitivity to determine the very low levels in the sample. For the other elements precision was good and the ICP results agreed well with those of LSM.

6.3.5 TUNGSTEN CARBIDE

One tungsten carbide sample was analysed (LSM sample number 41/4) in triplicate. The results are shown in table 16. The LSM results are not specific for this particular alloy, but give an indication of the approximate spread of values for each element that are routinely found in their tungsten carbide samples. The method of analysis used by LSM is direct reading emission spectrometry on the sample after it has been roasted in an oven to produce tungsten trioxide (WO_3).

The standards used in this work were matrix matched with sodium tungstate, as pure tungsten carbide was not available. Sodium could, therefore, not be determined using these standards. Attempts were made to determine sodium using standard additions, this was, however, unsuccessful due to the low amounts of sodium present

Tungsten Carbide Analysis

Element	Wave-length /nm	ICP Results			LSM
		Result % w/w	RSD %	Matrix % Difference	Result % w/w
Ca II	393.4	<0.001	—	-12.5	<0.01-0.02
Co I	345.4	0.004	28.7	18.1	<0.01-0.05
Cr I	425.4	0.007	14.0	-34.5	<0.01-0.05
Fe II	240.5	<0.04	—	—	<0.01-0.02
Mg II	279.5	<0.001	—	-26.7	<0.01-0.02
Mo I	379.8	<0.001	—	0.0	<0.01-0.02
Nb I	309.4	<0.03	—	—	<0.01-0.05
Ni I	352.4	0.003	47.3	0.0	<0.01-0.02
Si I	250.7	<0.06	—	—	<0.01
Ta I	269.4	<0.03	—	—	<0.01-0.05
Ti II	368.5	0.004	19.0	0.0	<0.01-0.05

Table 16

(<0.1 ppm in solution) and difficulties of accurately determining the background signal. For the remaining elements the quantities found in the sample are at, or approaching the detection limit of the system. It would be expected that an improved readout system, particularly a spectrometer with better resolution than that used in this work, could bring these levels of analyte present into a measurable range.

For the tungsten carbide, Cr Al, and Si Al alloys, the calibration curves from matrix matched standards were compared with calibration curves obtained from standards made up in distilled water. The % difference due to the matrix was then calculated and shown in tables 16, 17 and 18.

The origin of these interferences is probably due to easily ionisable elements (see chapter 5) in the alloy matrix solution (sodium in the tungsten carbide, and Al in the Cr Al, Si Al). Comparing the magnitude of these interferences with those shown in table 11, it can be seen that in general the interferences are smaller and in some cases no interference is observed when using the Mn 257.6 nm optimum conditions in an all argon plasma. The interference is, however, sufficiently large on some elements for matrix matched standards still to be necessary for accurate analysis.

6.3.6 Cr Al

Two Cr Al alloys were analysed (LSM sample numbers A8260(1188L) and A8294(1179L), using three sample solutions of each alloy. The results are shown in table 17, the LSM analysis was carried out on the same sample by AAS. Spectral interferences from Cr precluded the use of the more sensitive Si line (251.4 nm), the less sensitive 250.6 nm line giving poorer % RSD than the other very acceptable values for the other elements.

As the Cr Al alloys have only been analysed by one laboratory (LSM)

CrAl Analysis

Element	Wave-length /nm	ICP Results			LSM Results %w/w
		Result %w/w	RSD %	Matrix % Difference	
Cr I	429.0	(a) 18.6	1.57	—	19.8
		(b) 8.4	0.55		10.75
Cu I	324.7	< 0.001	—	14.8	< 0.02
		0.0065	1.0		< 0.01
Fe II	259.9	0.42	1.0	-40.6	0.37
		3.44	0.3		3.95
Mn I	403.1	0.0025	6.0	0.0	—
		0.0165	1.7		—
Si I	250.7	0.12	12.2	-29.4	—
		0.61	3.4		0.15
V II	292.4	0.023	2.8	-7.0	—
		4.88	1.5		

(a) Alloy No. A8260(1188L)

(b) Alloy No. A8294(1179L)

Table 17

and by one method, it is not possible to estimate whether the differences shown between the LSM and the ICP results are statistically significant. For these results where an LSM comparison was available the agreement is, however, reasonable.

6.3.7 Si Al

Two Si Al alloys were analysed (LSM sample numbers A8228(432L) and A8220(376L), using three sample solutions of alloy number A8220(376L) and one sample solution of alloy number A8228(432L). Initial attempts were made to fuse the sample in sodium carbonate so that the silicon would be brought into solution as sodium silicate. This was, however, unsuccessful and the aqua-regia / hydrofluoric acid attack was found to be the method of choice. The results are shown in table 18, the LSM analysis was carried out on the same sample using AAS. The Si results show very good agreement. The results for Cu and Mn showing greater sensitivity by the ICP analysis in this highly refractory sample matrix.

6.3.8 BCS STEELS

The comparison of the ICP results obtained in this work with the LSM results for the metallurgical samples provided, can give information as to the precision, and feasibility of the ICP technique for analysing the samples. As already discussed the comparison cannot give a rigorous indication of the absolute accuracy of the ICP analysis. A series of British Chemical Standard Steels was therefore used as suitable metallurgical standards to check the accuracy of the ICP system used in this work.

Six BCS steels were analysed in triplicate. The results are shown in table 19. Spectral interference from the iron matrix made necessary the use of a relatively insensitive spectral line for silicon producing poor precision. For the other five elements analysed, sufficiently sensitive lines could be chosen and have

SiAl Analysis

Element	Wave-length /nm	ICP Results			LSM Results % w/w
		Results % w/w	RSD %	Matrix % Difference	
Cu I	324.7	(a)0.003	—	9.2	0.02
		(b)0.0048	5.7		0.02
Fe II	259.9	0.370	—	-29.5	—
		0.333	0.53		—
Mn I	403.1	0.0048	—	35.4	0.02
		0.0045	3.7		0.02
Si I	251.4	49.5	1.2	—	48.8
		50.7	0.9		51.6

(a) Alloy No. A8228(432L)

(b) Alloy No. A8220(376L)

Table 18

produced excellent agreement with the standard certified composition of the steels. Thus showing that, provided the standards are buffered with the major elements in the sample and that spectral interference does not preclude the use of the more sensitive lines, ICP emission spectroscopy can be an accurate and precise (in general giving RSD values of 1 - 5%) analytical technique for metallurgical samples.

CONCLUSIONS

The analysis of the preceding set of metallurgical samples has highlighted a number of problems associated with ICP emission spectrometry.

For the more intractable samples used here (e.g. tungsten carbide and Si Al) the dissolution of the sample has proved to be the most difficult part of the analysis. Since ICP analysis is predominantly a solution sample method, the preparation of a quantitative multi-element solution of the sample is an important and primary consideration when using this method of analytical emission spectroscopy.

Comparisons of calibration curves between standards made up in distilled water and standards containing the major component elements of the alloy to be analysed; has shown that choice of operating conditions can be used to keep interference effects to a minimum (compare the interferences due to the matrix between the Ti Al analysis and the tungsten carbide, Cr Al, Si Al alloy analysis). Significant differences between the two types of calibration curve do, however, exist, thus, for the system used here, accurate analysis can only be performed when standards are buffered with the major matrix elements.

The limiting instrumental constraint on the success of the ICP in analysing the metallurgical samples provided has been the spectro-

BCS Steel Analysis

Element	Wave-length (nm)	BCS No.215/3			BCS No.224/1			BCS No. 306/1		
		Found %w/w	BCS %w/w	RSD %	Found %w/w	BCS %w/w	RSD %	Found %w/w	BCS %w/w	RSD %
Si I	288.2	0.12	0.23	7.2	0.38	0.30	3.2	0.07	0.16	25.1
V II	290.9	-	-	-	0.19	0.19	2.6	-	-	-
Cu I	324.7	0.048	0.052	1.9	0.08	0.09	1.9	0.34	0.34	1.6
Ni I	341.5	0.034	0.038	2.6	0.15	0.14	2.1	0.11	0.13	4.6
Cr I	359.4	0.04	0.04	10.0	1.06	1.06	0.7	0.07	0.07	4.4
Mn I	403.1	0.67	0.68	2.0	0.65	0.66	1.8	1.17	1.15	2.9

Element	Wave-length (nm)	BCS No. 402			BCS No.329			BCS No.219/4		
		Found %w/w	BCS %w/w	RSD %	Found %w/w	BCS %w/w	RSD %	Found %w/w	BCS %w/w	RSD %
Si I	288.2	0.34	0.27	3.0	0.09	0.15	14.0	0.06	0.079	17.4
V II	290.9	0.23	0.22	3.1	0.08	0.083	6.1	-	-	-
Cu I	324.7	0.23	0.23	2.3	0.07	0.072	4.2	0.08	0.088	2.7
Ni I	341.5	0.70	0.73	0.6	-	-	-	2.53	2.55	0.5
Cr I	359.4	0.55	0.55	1.3	-	-	-	0.66	0.66	1.1
Mn I	403.1	0.15	0.19	2.1	0.09	0.12	1.1	0.81	0.81	1.7

Table 19

meter used in this work.

The incidences of spectral interference as observed in this work could be greatly reduced by the use of higher resolving power than is available from the 0.5 m Ebert monochromator used. Further to this, a spectrometer with a band pass approaching the natural width of the spectral lines would increase the SBR and hence the detectability of the system.

Despite problems encountered, for those samples where sufficient sensitivity was available, ICP analysis of metallurgical samples has fulfilled the specifications required by the sponsoring company. These being the ability to provide an accurate and precise multi-element analysis of refractory alloys which have previously required two or three different methods for complete analysis. Additionally the long linear calibration range of the ICP allows both trace and major elements to be analysed from one sample dilution, which, combined with the use of multi-element standards, can produce a significant reduction in time spent on sample preparation.

7. CONCLUSIONS AND SUGGESTIONS FOR FURTHER WORK

7.1 COMPARISON OF ALL ARGON AND NITROGEN COOLED PLASMAS AT OPTIMUM CONDITIONS

The work performed here has allowed optimum operating conditions to be found for both nitrogen cooled and all argon plasmas, and thus the relative merits of the two types of plasma considered can then be fairly assessed.

In comparing the optimum SBR values as obtained with the system used here, for the same set of spectral lines with a distilled water matrix there appears to be very little to choose between the two types of plasma. It is interesting to note that the nitrogen cooled plasma usually produces the larger signal of the two types of plasma at optimum conditions, with, however, a proportionally higher background. This effect is illustrated in Table 20 where the ratio of the signals and the ratios of the backgrounds found in the two types of plasma for the Mn 403.1 nm atom line and the Mn 257.6 nm ion line operated at optimum conditions are shown. For both atom and ion lines the nitrogen cooled plasma gives the larger signal and also a higher background level, which is particularly noticeable for the lower wavelength line (the ratio of background being approximately three times that at the higher wavelength). This may be explained by studying the background spectra of the two types of plasma (Figures 68 and 69). The two background spectra were obtained at the following conditions:-

All Ar plasma

Injector Ar . - 0.5 lmin⁻¹

Plasma Ar	-	6.0 lmin ⁻¹
Coolant Ar	-	5.0 lmin ⁻¹
Viewing Height	-	30 mm
Power	-	0.5 kW

Nebuliser natural uptake rate 0.9 ml min⁻¹ aspirating water.

Nitrogen cooled plasma

Injector Ar	-	0.5 lmin ⁻¹
Plasma Ar	-	1.7 lmin ⁻¹
Coolant N ₂	-	5.4 lmin ⁻¹
Viewing Height	-	30 mm
Power	-	0.5 kW

Nebuliser natural uptake rate 0.9 mls min⁻¹ aspirating water.

The above conditions do not rigorously reproduce the relative intensities of the features of the two background spectra at optimised conditions, nevertheless they can be used to qualitatively show the differences in background structure in each type of plasma.

The background spectra shown in Figure 68 shows that at the ion line wavelength (257.6 nm) the background is higher than for the atom line (403.1 nm), whereas in Figure 69 the background in the all argon plasma is the same for both atom and ion line regions. Further to this the background spectra shown also illustrate that there are far more molecular bands in the nitrogen cooled plasma (due to molecular N₂ species) than in the all argon plasma where there is only one major band (due to OH) in the spectral region studied. The more highly structured background of the nitrogen cooled plasma can thus lead to enhanced spectral interference, and background correction problems during analysis.

Although studies of optimal SBR has yielded a certain amount of information, it is, however, the comparison of the values of the optimal conditions, and how they change from element to element that shows the interesting features and differences between each plasma type.

It is perhaps, the difference between optimal power settings that forms the most striking contrast between the plasmas studied. The all argon plasma appears to need only one relatively low power setting as optimal for a wide range of elements, whereas the optimal power in the nitrogen cooled plasma is proportional to the difficulty of excitation of the particular line being studied. This effect which is most probably due to differences in excitation mechanism in the plasmas, has practical implications. Firstly, because the optimum conditions (particularly the power) for the all argon plasma do not change greatly from element to element as compared to the nitrogen cooled plasma, the all argon plasma would seem to be more suited to simultaneous multi-element analysis where one set of compromise conditions must be used for all elements studied. This has been tentatively confirmed by the experiment reported in chapter 4 section 4.4.4, the results of which are shown in table 9. Secondly an all argon plasma would only require a low power R.F. generator (1-2 KW forward power) whereas a nitrogen cooled plasma might need at least 4 KW forward power for optimum performance. This would be an important factor in instrument design where low power generators would presumably lead to cheaper and less bulky instrumentation.

The results reported here can also give some insight into which spectral lines will be most suited by the different types of plasma. It has already been shown that a relatively low power argon plasma is able to produce optimal SBR for elements with a wide range of difficulties of excitation, for the nitrogen cooled plasma, however, lines with higher difficulties of excitation would require higher powers which may not be available in the instrumentation. The

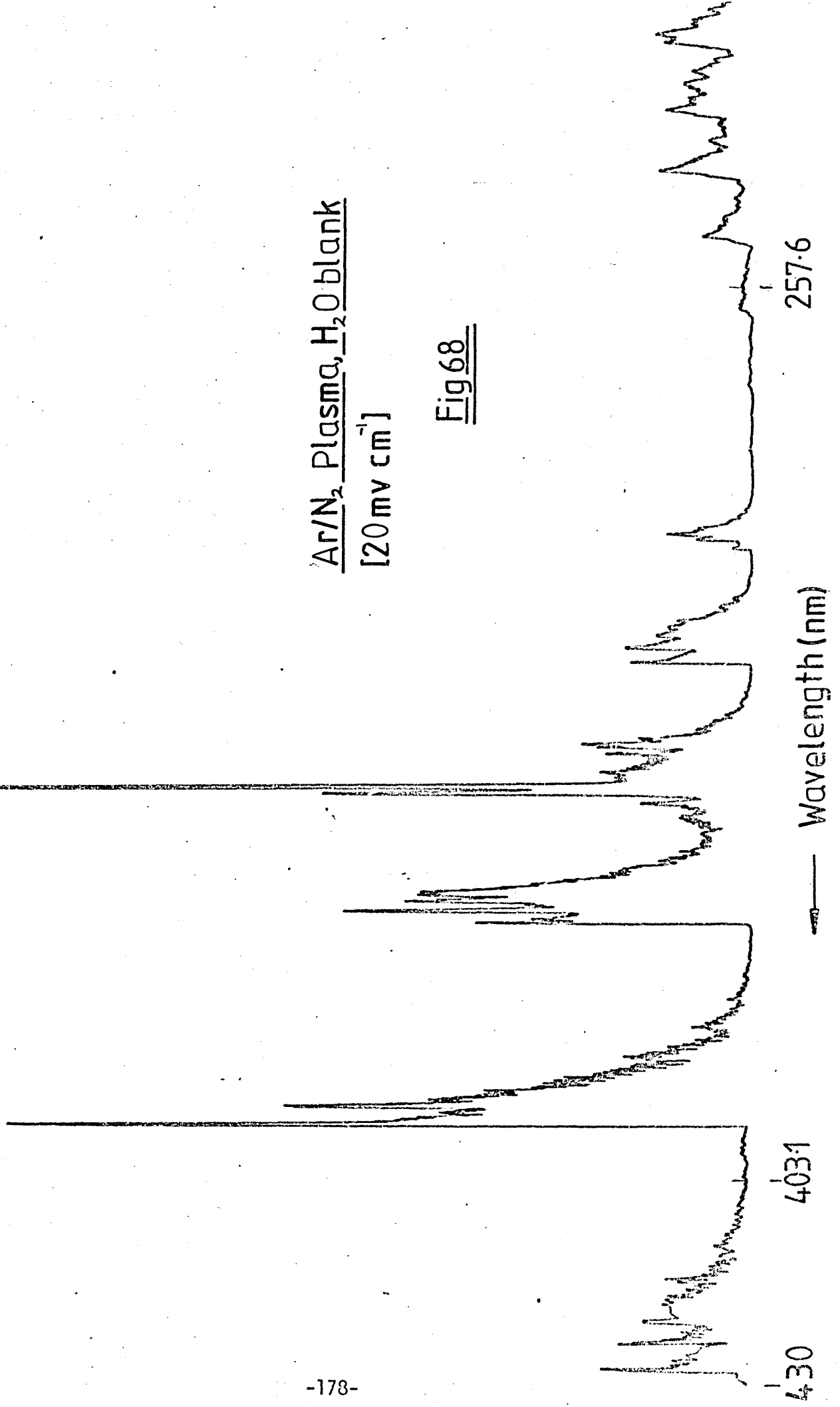
Comparison of Signal & Noise Levels for Mn Atom & Ion Lines in all Ar & N₂ Cooled Plasmas

Wavelength/nm	Ratio of Signals (All Ar/N ₂ cooled)	Ratio of Backgrounds (All Ar / N ₂ cooled)	Optimum SBR (All Ar plasma)	Optimum SBR N ₂ cooled plasma
403.1	0.52	0.73	11.9	16.7
257.6	0.70	0.39	4.2	2.3

Table 20

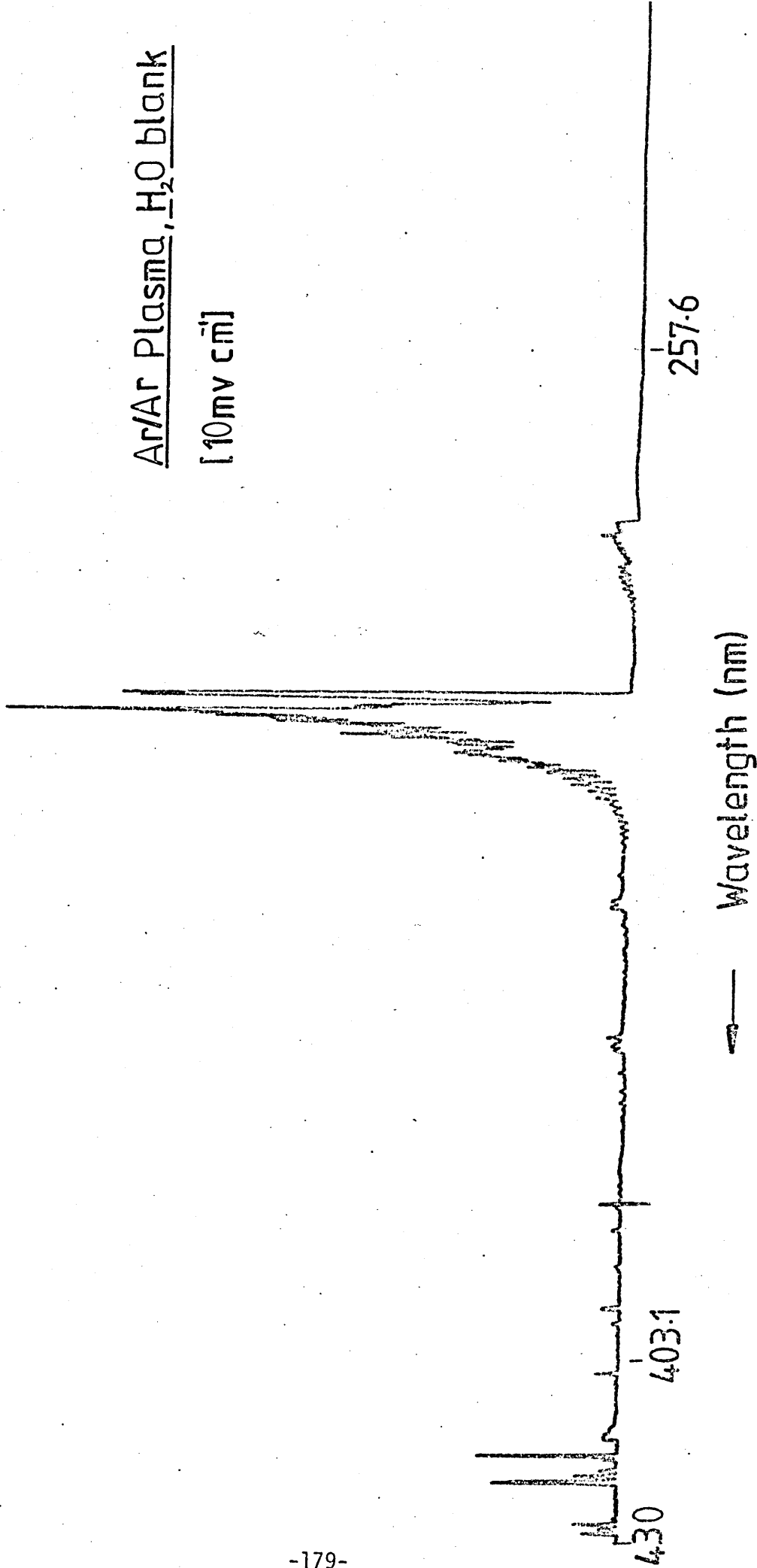
Ar/N₂ Plasma, H₂O blank
[20 mV cm⁻¹]

Fig 68



Ar/Ar Plasma, H₂O blank

[10mV cm⁻¹]



430

403.1

257.6

Wavelength (nm)

Fig69

nitrogen cooled plasma is further limited at the higher energy end of the spectrum (low wavelengths) by the higher background in this region (see Figure 68).

The conclusions shown, so far, have been based on optimal conditions obtained for solutions containing low levels of one element (in the $\mu\text{g ml}^{-1}$ range) made up in distilled water. In real analysis, however, (particularly metallurgical samples) the sample solution often contains many concomitant elements, some at high concentrations, as well as the analyte species. In section 4.4.5 of chapter 4 the effect of high concentrations of chrome in the sample matrix was shown to alter the As 228.8 nm atom line optimal conditions for the all argon plasma, whereas, for the nitrogen cooled plasma the optimal conditions remained approximately the same. The reason for this is, in all probability, due to the nature of the excitation mechanisms occurring within each plasma. There has been considerable evidence to show that the all argon plasma is not in LTE (e.g. 108,109,110,114,115,116,126), and its ability to excite high energy lines ($\sim 11\text{eV}$) is due to the postulated Penning ionisation mechanism (see chapter 1 section 1.3.1) which involves Ar metastable species. The nitrogen cooled plasma has been suggested to be closer to LTE than its argon cooled counterpart (157) and hence its excitation mechanism is dominated by electron collisions. Recently workers have suggested that the non LTE conditions of the all Ar plasma can be 'disturbed' by the presence of various materials passing through it.

Alder et al. (126) have shown that when a distilled water aerosol is passed through an all argon plasma the electron density is substantially increased, bring the system closer to LTE where an electron collision mechanism is more important. Whilst Broekaert et al. (171) have tentatively suggested that an interference due to borate anion in the sample aerosol was caused by quenching of the Ar metastables by the interfering species.

The changes in the optimal operating conditions for the all Ar

plasma in this work would therefore be due to a combination of the above effects, the Cr matrix being responsible for 'thermalising' the system and quenching the Ar metastable species producing conditions where LTE prevails. For the nitrogen cooled plasma it is postulated that the LTE already exists so that the Cr matrix has little effect on the optimum conditions. The shift to higher optimal powers for the all argon plasma can then be explained by observing that higher power was optimal for the nitrogen system (i.e. the LTE system) and hence as the Cr matrix thermalised the all argon system higher powers were then necessary for optimal performance. If this mechanism is correct and the observed effects were to occur in the general case the advantages of the all argon plasma as previously discussed would be seriously reduced when concentrated matrix elements were present. Clearly the effect of matrix elements on optimal analyte conditions requires further study for different elements and concomitant species before more rigorous conclusions can be made. Of particular interest would be a repeat study of the optimal powers in the all Ar plasma for spectral lines of varying difficulty of excitation, with high concentrations of matrix element present, to see if the graph of optimal power against difficulty of excitation moved from a horizontal straight line to a straight line with a slope similar to that found for the nitrogen cooled plasma (see Figure 42).

The studies of sodium interference have shown both plasma types to exhibit a number of separate viewing zones in the tail flame when high concentrations of sodium are aspirated, and that the emission from both Mn atom and ion lines undergoes different types of effects according to which of the observed zones is viewed (chapter 5 section 5.2.2). For both types of plasma the sodium interference has been shown to be virtually identical when either the atom or ion line was being observed. Similar zones have also been observed by Koirtjohann (183). It is also interesting to note that when the data shown in Figure 49 is replotted in the form of a spatial profile (Figure 70) very similar effects are shown as to those published by Kawaguchi et. al. (154) (see Figure 48) and Horlick and

Blades (153), showing that the similar effects are occurring in each plasma system studied, (both these latter workers were using crystal controlled generators) in which the presence of easily ionisable element concomitants produces a shift in the spatial profile. The shift in profile apparently caused the signal from the viewing region to change thus producing an interference effect. This cannot be the whole explanation, since the conditions used in this work were optimal for the given spectral line and when sodium was added the signal was enhanced (particularly for the Mn 403.1 nm atom line) and since the background was virtually unaltered the SBR was increased to a value higher than the optimal SBR when no sodium was present, so that some form of physical enhancement of the emission from the analyte species must be occurring. Robin (127) suggests that this is due to the sodium producing an increase in volatility of the analyte species, which would explain the similar effects observed on both atom and ion lines.

The formation of the observed zones due to the sodium (see Figure 57) can be explained in terms of a temperature gradient set up in the plasma tail flame. As the sodium aerosol passes through the plasma fireball primary heating occurs causing intense yellow emission from the 'D' lines doublet thus producing the 'yellow tongue' region (region 2 Figure 57). Further into the tail flame the temperature rises, depopulating the sodium ground state energy level, with the majority of atoms occupying higher energy levels and hence the yellow emission disappears forming the colourless (or bleached) region (region 3 Figure 57). Higher still in the tail flame the temperature begins to fall as the analyte species moves away from the influence of the hot fireball and the lower Na energy levels are repopulated and again the yellow emission is observed (region 4 Figure 57). The mechanism and reason for enhancements in these 'cooler' zones is still not easily explained.

The size of these interferences, as observed in this work under particular operating conditions have been shown to be alarmingly

Effect of Na on the Mn 257.6nm Ion Line Emission
Profile (Ar/Ar plasma)

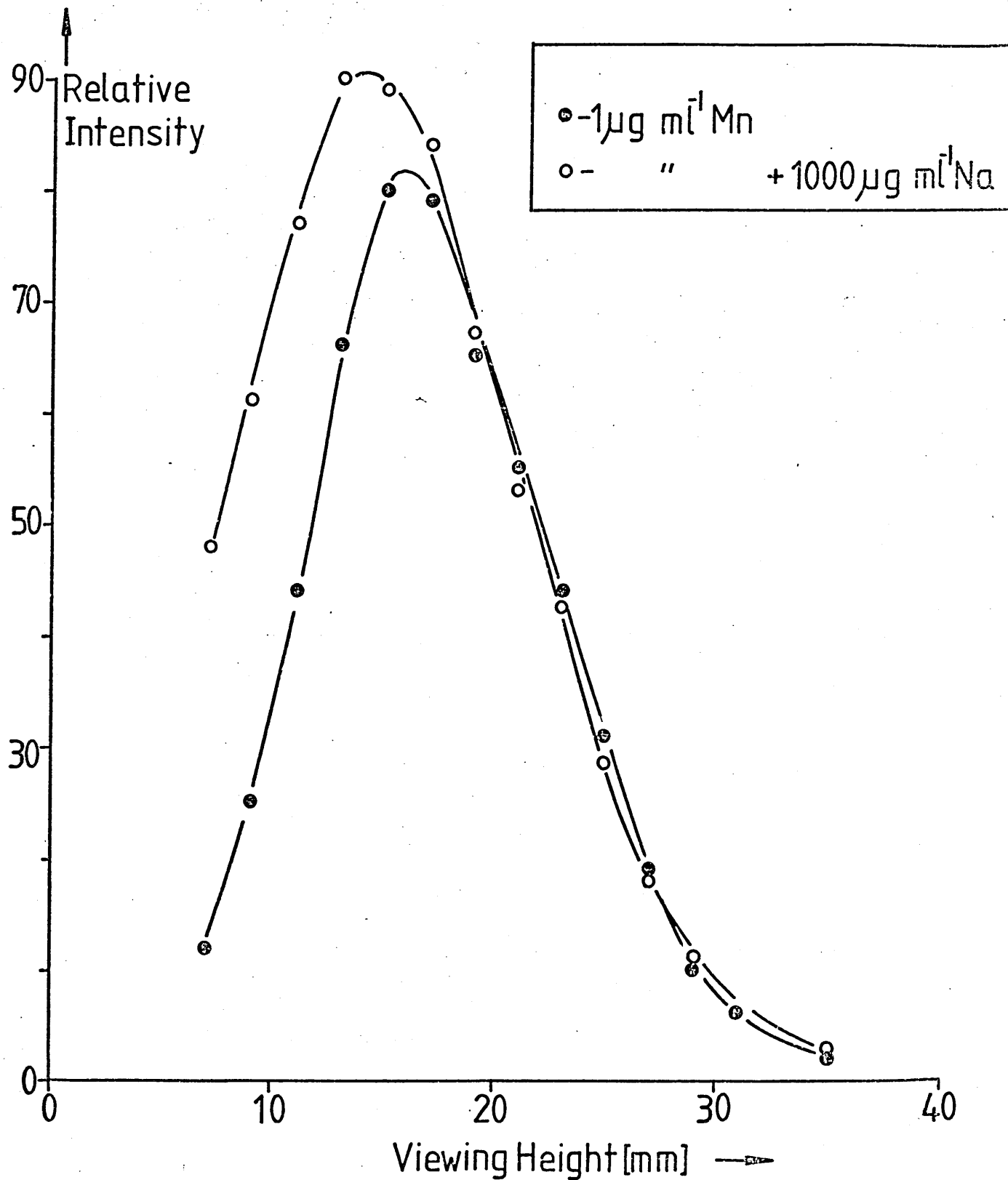


Fig 70

high (i.e. as much as 400%), but it is reassuring to note that sensitive operating conditions could be found where the interferences were reduced to negligible values. Again this is an area open to further study. The effect of other easily ionisable elements on other analyte species would be worth further investigation to see if similar behaviour occurs with other analyte/interferent systems. The differences between the buffered and distilled water standard calibration curves as seen for the various aluminium alloy analyses (chapter 6) suggest that this could be so.

7.2 SIMPLEX OPTIMISATION AS APPLIED TO THE ICP

Simplex optimisation has been shown to be an efficient and flexible method for studying different aspects of ICP emission spectrometry.

In this work simplex has been used to compare the performance of different modifications to the plasma system (i.e. torch designs and different coolant gases). Optimum operating conditions for a number of different elements have been found for plasmas with Ar and N₂ coolant gas flows. Further studies of trends within these optimal conditions have allowed fundamental differences between plasma types to be elucidated. Further to this, simplex optimisation has also been shown capable of studying the effect of concomitant elements on analyte optimum conditions, and also as a method for minimising interference effects from easily ionisable elements.

There is obviously much scope for expanding the simplex optimisation work already carried out here, not only in continuing similar optimisation experiments on a wider range of elements and spectral lines, but also to look at new systems (e.g. an all nitrogen plasma has recently been reported(184)).

Recent developments in ICP instrumentation appear to be moving away from direct reader simultaneous detection systems to more flexible computer controlled scanning sequential spectrometers (185,186). Since sequential systems no longer require one set of compromise

operating conditions, as operating parameters can be changed to suit each element in turn, it is logical to extend the computer control to the operation of the controlling parameters of the ICP as well (i.e. gas flows, viewing height and power). Such a system would be ideally suited to simplex optimisation studies, not only to give information about the fundamental mechanisms of plasma systems, but also for every day analytical work where optimisation of operating parameters for varying elements in differing matrices could be quickly and efficiently achieved.

7.3 METALLURGICAL ANALYSIS USING THE ICP

The analysis of alloys reported in chapter 6 has shown ICP emission spectrometry to offer many advantages over other analytical techniques (see chapter 6 section 6.4). It must be stressed, however, that great care must be taken over preparing solution samples, for no matter how good the instrumentation the result can only be considered accurate if the solution sample used contains representative concentrations of the elements to be determined in the original solid alloy sample. The increased range of elements which can be determined on a single solution (e.g. Si and major as well as minor metals) places increased demands on sample dissolution procedures as compared to other techniques such as AAS.

Although the ICP proves to be a sensitive technique for many of the more refractory elements which other techniques cannot match (e.g. Si, Ti, W, B), the so called 'tramp' elements (e.g. As and Se) cannot be determined at the very low levels sometimes required in metallurgical analysis, without some form of sample preconcentration method (e.g. hydride generation). Further research into reliable methods of presenting solid samples to the plasma may alleviate some of the problems encountered with such elements and also remove the troublesome dissolution step in sample preparation.

The results of the optimisation studies carried out here suggest

that an all argon plasma would be most suited to metallurgical analysis. A low powered (and hence less expensive) generator being required but allowing a large range of sensitive spectral lines from which to choose with a minimum of background correction and spectral interference problems from the argon background spectrum. If a direct reading spectrometer is chosen to analyse the emission signal, the highest possible resolution must be used to prevent background interference on the fixed set of lines. If a more flexible sequential scanning spectrometer is the instrument of choice the resolution must be of high quality, but spectral interferences can be more easily overcome by the selection of a different spectral line.

It is hoped that some of the fundamental insights into plasma operation and optimisation gained in this work will be of value in metallurgical analysis and enable the full promise of the ICP as an analytical tool to be achieved in a demanding field of application.

REFERENCES

1. Mandelshtam, S. L., Spectrochim Acta, 33B, 1978, 577.
2. Sharp, B. L., Selected Annual Reviews of the Analytical Sciences, 4, 1976, 37.
3. Kirchhoff, G., and Bunsen, R., Pogg. Ann., 110, 1860, 161.
4. Fassel, V.A., Myers, R. B., and Kniseley, R. N., Spectrochim Acta, 19B, 1963, 1187.
5. Slavin, M., and Manning, D. C., Anal. Chem., 35, 1963, 253.
6. Boumans, P. W. J. M., and De Boer, F. J., Spectrochimica Acta, 27B, 1972, 391.
7. Schrenk, W. G., "Analytical Atomic Spectroscopy", Plenum Press, 1975.
8. Barnes, R. M., "Emission Spectroscopy", Dowden Hutchinson and Ross, 1976.
9. Slavin, M., "Emission Spectrochemical Analysis", Wiley, 1971.
10. Petit, R., 19th Congress of GAMS, Paris, 1956, 111.
11. Grimm, W. Spectrochim Acta, 23B, 1968, 443.
12. Ferreira, N. P. Analyst, 103, (1978), 607.
13. Pille, P., Lowe, P. R., Gillespie, A. M., and Butler, L. R. P. Anal. Chim. Acta, 104, 1979, 11.
14. Bubert, H., Haggengah, W. D., Laqua, K., Spectrochim Acta, 34B, 1979, 19.
15. Harrison, W. W., and Prakash, N. J. Anal. Chim. Acta, 49, 1970, 151.
16. Gatehouse, B. A., and Walsh, A., Spectrochim Acta, 16, 1960, 602.
17. Ottaway, J. M., Shaw, F., Anal. Chim. Acta, 99, 1978, 217.
18. Epstein, M. S., Rains, T. C., Brady, T. J., Moody, J. R., Barnes, J. L., Anal. Chem., 50, 1978, 874.
19. Thorne, A. P. "Spectrophysics", Chapman and Hall, London, 1974.
20. Keirs, C. D. and Vickers, T. J., Appl. Spectrosc. 31, 1977, 273.
21. Greenfield, S. McGeachin, H. Mc D., and Smith, P. B., Talanta 22, 1975, 553.
22. Reednick, J., Am. Lab. 11(3), 1979, 53.
23. Lichte, F. E., and Skogerboe, R. K., Anal. Chem. 45, 1973, 399.

24. Dagnall, R. M., Pratt, S. J., West, T. S., and Deans, D. R. *Talanta*, 17, 1970, 1009.
25. Beenakker, C. I. M., *Spectrochim Acta*, 32B, 1977, 173.
26. Babat, G. I., *Vestn. Elektroprom.* 1942, No. 2, 1 : No. 32.
27. Idem., *J. Inst. Elec. Engrs. (London)*, 94, 1947, 27.
28. Reed, T. B. *J. Appl. Phys.*, 32, 1961, 821.
29. Idem., *Ibid.*, 32, 1961, 2534.
30. U.K. Pat., 1, 109, 602, 1968.
31. U.S. Pat., 3, 467, 471, 1969.
32. Greenfield, S., McGeachin, H. McD., and Smith, P. B., *Talanta*, 23, 1976, 1.
33. Greenfield, S., Jones, I. Ll., and Berry, C. T., *Analyst*, 89, 1964, 713.
34. Wendt, R. H., and Fassel, V. A., *Anal. Chem.*, 37, 1965, 920.
35. Veillon, C., and Margoshes, M., *Spectrochim Acta*, 23B, 1968, 503.
36. Greenfield, S., Jones, I. Ll., Berry, C. T., and Bunch L. G., *Proc. Soc. Anal. Chem.*, 2, 1965, 111.
37. Greenfield, S., Berry, C. T., and Bunch, L. G., 'Spectroscopy with a High Frequency Plasma Torch', *Radyne Publication* 196.
38. Hoare, H. C., and Mostyn, R. A., *Anal. Chem.*, 39, 1967, 1153.
39. Mermet, J. M., and Robin, J., *Proc. Colloq. Spectrosc. Int.* 14th, 2, 1967, 715.
40. Dickinson, G. W. and Fassel, V. A., *Anal. Chem.*, 41, 1969, 1021.
41. Greenfield, S., and Smith, P. B., *Anal. Chim. Acta.*, 59, 1972, 341.
42. Kirkbright, G. F., Ward, A. F., West, T. S., *Anal. Chim. Acta*, 62, 1972, 241.
43. Idem. *Ibid.*, 64, 1973, 353.
44. Pforr, G. and Aribot, O., *Z. Chem.*, 10, 1970, 78.
45. Dagnall, R. M., Smith, D. J., West, T. S., Greenfield, S., *Anal. Chim. Acta*, 54, 1971, 397.
46. Boummans, P. W. J. M., and de Boer, F. J., *Spectrochim Acta*, 27B, 1972, 391.

47. Fassel, V. A., XVI Coll. Spect. Intern. Heidelberg 1971, Plenary Lecture Reprint, p63, Hilger, London, 1972.
48. Kirkbright, G. F., and Ward A. F., *Talanta*, 21, 1974, 1145.
49. Fassel, V. A., and Kniseley, R. N., *Anal. Chem.*, 46, 1974, 1110A, 1155A.
50. Greenfield, S., Jones, I. L., McGeachin, H. McD., and Smith, P. B., *Anal. Chim. Acta*, 74, 1975, 225.
51. Greenfield, S., McGeachin, H. McD., and Smith, P. B., *Talanta*, 22, 1975, 1.
52. Barnes, R. M., C.R.C., *Crit. Rev. Anal. Chem.*, 7, 1978, 203.
53. Fassel, V. A., *Science*, 202, 1978, 183.
54. Fassel, V. A. *Anal. Chem.*, 51, 1979, 1290A.
55. de Galan, L., *Chem. Weekbl. Mag.*, July, 1978, 447.
56. de Galan, L., *Proc. Anal. Div. Chem. Soc.*, 16, 1979, 179.
57. Barnes, R. M. in "Applications of I.C.P. to Emission Spectroscopy", Barnes, R. M., Ed.; Franklin Inst. Press Philadelphia Pa., 1978.
58. Barnes, R. M., *Toxicol, Environ. Chem. Rev.*, 2, 1978, 187.
59. Robin, J., *I.C.P. Inf. Newsl.*, 4, 1979, 495.
60. Winge, R. K., Fassel, V. A., Kniseley, R. N., De Kalb, E., and Haas, W. J., *Spectrochim. Acta.*, 32B, 1977, 327.
61. Ronan, R., *I.C.P. Inf. Newsl.*, 1, 1976, 164.
62. Kerfoot, W. B., and Crawford, R. L., *I.C.P. Inf. Newsl.*, 2, 1977, 289.
63. Varnes, A. W., 1979 Federation of Anal. Chem. and Spectroscopy Soc., Abs No. 117.
64. Scott, R. H. Strasheim, A., and Kotot, M. L., *Anal. Chim. Acta.*, 82, 1976, 67.
65. Walsh, J. N., *Spectrochim. Acta.*, 35B, (1980), 107
66. Watson, A. E., Russell, G. M., and Balaes, G., *I.C.P. Inf. Newsl.*, 2, 1976, 205.
67. Uchida, H., Uchida, T., Iida, C., *Anal. Chim. Acta.*, 116, (1980), 433.
68. Alder, J. F., Gunn, A. M., and Kirkbright, G. F., *Anal. Chim. Acta.*, 92, 1977, 43.
69. Ohls, K., Koch, K. H., and Grote, H. Z., *Anal. Chem.*, 284, 1977, 177.

70. Butler, C. C., Kniseley, R. N., and Fassel, V. A., *Anal. Chem.*, 47, 1975, 825.
71. Newland, B. T. N., *I.C.P. Inf. Newsl.*, 3, 1977, 263.
72. Scott, R., *I.C.P. Inf. Newsl.*, 2, 1976, 117.
73. Watson, A. E., and Russell, G. M., *I.C.P. Inf. Newsl.*, 3, 1977, 273.
- 74a. Butler, C. C., Kniseley, R. N., and Fassel, V. A., *Anal. Chem.* 47, 1975, 825.
- 74b. Wunsch, G., *Talanta*, 26, 1979, 291.
75. Diemiaszonek, R., *Analisis*, 7(2), 1979, 96.
76. Locke, J., *Anal. Chim. Acta*, 113, 1980, 3.
77. Ward, A. F., and Marciello, L. F., *Anal. Chem.* 51(13), 1979, 2264.
78. Zamechek, W., Lewandowski, R. J., Parkhurst, R. G., and Ellgren, A. J., *Applications of I.C.P. to Emission Spectroscopy, 1977 Eastern Analytical Symposium*, Franklin Inst. Press, 169.
79. Hammer, R. M., De'Aeth, L. A., *Talanta* 27, 1980, 535.
80. Gunn, A. M. Kirkbright, G. F., and Opheim, L. N., *Anal. Chem.*, 49, 1977, 1492.
81. Boyer, K. W., Tanner, J. T., and Gojan, R. J., *I.C.P. Inf. Newsl.*, 2, 1977, 302.
82. Warren, J., *I.C.P. Inf. Newsl.*, 2, 1977, 262.
83. Charalambous, G., and Bruckner, K. J., *I.C.P. Inf. Newsl.*, 3, 1977, 239.
84. McHard, J. A., Foulk, S. J., Nikdel, S., Ulman, A. H., Pollard, B. D., and Winefordner, J. D., *Anal. Chem.*, 51(11), 1979, 1613.
85. Jones, J. W., *Applications of I.C.P.s to Emission Spectroscopy, 1977 Eastern Analytical Symposium*, Franklin Inst. Press, 83.
86. Greenfield, S. and Smith, P. B., *Anal. Chim. Acta.*, 59, 1972, 341.
87. Dahlquist, R. L., and Knoll, J. W., *Appl. Spectrosc.* 32, 1978, 1.
88. Irons, R. D., Schenk, E. A., Giauque, R. D., *Clin. Chem.* 22, 1976, 2018.
89. Scott, R. H., and Strasheim, A., *Anal. Chim. Acta.*, 76, 1975, 71.
90. Allain, P., and Mauras, Y., *Anal. Chem.*, 51, (13), 1979, 2089.
91. Mauras, Y., Allain, P., *Anal. Chim. Acta.*, 110, 1979, 271.
92. Wendt, R. H., Fassel, V. A., *Anal. Chem.*, 39, 1967.

93. Greenfield, S., Smith, P. B., Breeze, A. E. and Chilton, N. M. D., Anal. Chim. Acta., 41, 1968, 385.
94. Barnett, W. B., Fassel, V. A., and Kniseley, R. N., Spectrochim Acta., 23B, 1968, 643.
95. Idem., Ibid., 25B, 1970, 139.
96. Bordonali, C., Biancifiori, M. A., Donata, A., and Morello, B., Metall. Ital., 61, 1969, 360.
97. Bordonali, C., and Biancifiori, M. A., U.S. Patent 3,684,884, 1972.
98. Veillon, C., Margoshes, M., Spectrochim. Acta., 23B, 1968, 503.
99. Magyar, B., Aeschbach F., G.I.T. Fachz. Lab., 22, 1978, 756.
100. Abdallah, M. H., Diemiszzonek, R., Jarosz, J., Mermet, J. M., Robin, J., Trassy, C., Anal. Chim. Acta., 84, 1976, 271.
101. Montaser, A., and Fassel, V. A., Anal. Chem. 48(11), 1976, 1490.
102. Epstein, M. S., Nikdel, S., Bradshaw, J. D., Kosinski, M. A., Bower, J. N., and Winefordner, J. D., Anal. Chim. Acta., 113, 1980, 221.
103. Epstein, M. S., Nikdel, S., Omenetto, N., Reeves, R., Bradshaw, J., and Winefordner, J. D., Anal. Chem. 51(13), 1979, 2071.
104. Omenetto, N., Nikdel, S., Epstein, M. S., Reeves, R. D., Winefordner, J. D., Anal. Chem. 51(9), 1979, 1521.
105. Windsor, D. L., and Bonner Denton, M., Anal. Chem. 51(8), 1979, 1116.
106. Sommer, D., and Ohls, K., Fresenius Z, Anal. Chem., 295, 1979, 337.
107. Morita, M., Uehiro, T., Keiichiro, F., Anal. Chem., 52, 1980, 351.
108. Mermet, J. M., Spectrochim. Acta., 30B, 1975, 383.
109. Jarosz, J., and Mermet, J. M., J. Quant. Spectrosc. Radiat. Transfer, 17, 1977, 237.
110. Mermet, J. M., and Robin, J., Anal. Chim. Acta., 75, 1975, 271.
111. Abdallah, M. H., Mermet, J. M., and Trassy C., Anal. Chim. Acta., 87, 1976, 329.
112. Alder, J. F., and Mermet, J. M., Spectrochim. Acta., 28B, 1973, 421.
113. Abdallah, M. H., and Mermet, J. M., J. Quant, Spectrosc. Radiat. Transfer, 19, 1978, 83.
114. Kalnicky, D. J., Fassel, V. A., and Kniseley, R. N., Appl. Spectrosc., 31, 1977, 137.
115. Idem., Spectrochim. Acta., 30B, 1975, 511.

116. Kornblum, G. R., and de Galan, L., Spectrochim. Acta., 29B, 1974, 71.
117. Idem., Ibid., 32B, 1977, 71.
118. Idem., Ibid., 32B, 1977, 455.
119. Larson, G. F., Fassel, V. A., Scott, R. H., and Kniseley, R. N., Anal. Chem., 47, 1975, 238.
120. Larson, G. F. and Fassel, V. A., Anal. Chem., 48, 1976, 1161.
121. Boumans, P. W. J. M., and De Boer, F. J., Spectrochim. Acta., 31B, 1976, 355.
122. Idem., Ibid., 30B, 1975, 309.
123. Idem., Ibid., 32B, 1977, 365.
124. Idem., Ibid., 30B, 1975, 449.
125. Jarosz, J., Mermet, J. M., and Robin, J. P., Spectrochim. Acta., 33B, 1978, 55.
126. Alder, J. F. Bombelka, R. M., and Kirkbright, G. F., Spectrochim. Acta, 35B, 1980, 163.
127. Robin, J. I.C.P. Inf. Newsl., 4, 1979, 495.
128. Greenfield, S., The Spex Speaker, 22(3), 1977, 1.
129. Scott, R. H. I.C.P. Inf. Newsl., 3, 1978, 425.
130. Miller, C., and Ayen, J., J. Appl. Phys., 40, 1969, 5260.
131. Barnes, R. M., and Schleicher R. G., Spectrochim. Acta. 30B, 1975, 109.
132. Allemann, C. D., and Barnes, R. M., Appl. Spectrosc., 31, 1977, 434.
133. Savage, R. N., and Hiefje, G. M., Anal. Chem., 51(3), 1979, 408.
134. Allemann, C. D., and Barnes, R. M., Anal. Chem., 51(14), 1979, 2392.
135. Kornblum, G. R., Wouter Van der Waa, and de Galan L., Anal. Chem., 51(14), 1979, 2378.
136. Mermet, J. M., and Trassy, C., Appl. Spectrosc. 31(3), 1977, 237.
137. Ohls, K., and Krefta, K., I.C.P. Inf. Newsl., 1, 1976, 168.
138. Lichte, F. E., and Koirtyohann, S. R., I.C.P. Inf. Newsl., 1, 1976, 200.
139. Windsor, D. L. Heine, D. R. and Denton, M. B., Appl. Spectrosc., 33(1), 1979, 56.
140. Genna, J. L., and Barnes, R. M., Allemann, C. D., Anal. Chem., 49(9), 1977, 1450.

141. Meinhard, J. E., I.C.P. Inf. Newsl., 2, 1976, 163.
142. Kniseley, R. N. Amenson, H., Butler, C. C., and Fassel, V. A., Appl. Spectrosc., 28(3), 1974. 285.
143. Meddings, B., Kaiser, H., and Anderson, H., International Winter Conference on Developments in Atomic Plasma Spectrochemical Analyses, (San Juan, Puerto Rico, 1980).
144. Novak, J. W., Lillie, D. E., Boorn, A. W., and Browner, R. F., Anal. Chem., 52, 1980, 576.
145. Suddendorf, R. F., and Boyer, K. W., Anal. Chem. 50(13), 1978, 1796.
146. Wolcott, J. F., and Sobel, C. B., Appl. Spectrosc., 32(6), 1978, 591.
147. Apel, C. T., Bieniewski, T. M., Cox, L. E., and Steinhaus, D. W., I.C.P. Inf. Newsl., 3(1), 1977, 1.
148. Scott, R. H., Fassel, V. A., and Kniseley, R. N., Anal. Chem., 46(1), 1974, 75.
149. Greenfield, S., McGeachin, H. McD., and Smith, P.B., Anal. Chim. Acta., 84, 1976, 67.
- 150a. British Standard Specification B.S. 1799: 1952.
- 150b. Greenfield, S., and McGeachin, H. McD., Anal. Chim. Acta., 100, 1978, 101.
151. Greenfield, S., Proc. Anal. Div. Chem. Soc., 19, 1976, 279.
152. Horlick, G., Appl. Spectrosc., 30(2), 1976, 113.
153. Horlick, G., and Blades, M. W., Appl. Spectrosc., 34(2), 1980, 229.
154. Kawaguchi, H., Ito, T., Ota, K., and Mizuike, A., Spectrochim. Acta, 35B, 1980, 199.
155. Savage, R. N., and Hieftje, G. M., Anal. Chem., 52, 1980, 1267.
156. Greenfield, S., and Thorburn Burns, D., Spectrochim. Acta., 34B, 1979, 423.
157. Idem., Anal. Chim. Acta., 113, 1980, 205.
158. Nelder, J. A., and Mead, R., Comput. J., 7, 1965, 308.
159. Spendley, W., Hext, G. R., and Himsforth, F. R., Technometrics, 4, 1962, 441.
160. Long, D. E., Anal. Chim. Acta, 46, 1969, 193.
161. Routh, M. W., Swartz, P. A., and Denton, M. B., Anal. Chem., 49(9), 1977, 1422.
162. Brissey, G. F., Spencer, R. B., and Wilkins, C. L., Anal. Chem. 51(13), 1979, 2295.

163. Ryan, P. B., Barr, R. L., and Todd, H. D., *Anal. Chem.*, 52(9), 1980, 1460.
164. Deming, S. N., and Parker, L. R., *C.R.C. Crit. Rev. Anal. Chem.*, 7, 1978, 187.
165. Yarbrow, L. A., Deming, S. N., *Anal. Chim. Acta.*, 73, 1974, 391.
166. Michel, R. G., Coleman, J., and Winefordner, J. D., *Spectrochim. Acta.*, 33B, 1978, 195.
167. Scott, R. H. Rept. FIS 51, National Physical Laboratory, C.S.I.R., Pretoria S. Africa, 1974.
168. Reeves, R. D., Nikdel, S., and Winefordner, J. D., *Appl. Spectrosc.*, 4, 1980, 477.
169. Merryfield, R. N., and Loyd, R. C., *Anal. Chem.*, 51, 1979, 1965.
170. Mermet, J. M., and Robin, J., *Anal. Chim. Acta.*, 87, 1976, 329.
171. Broekaert, J. A. C., Leis, F., Laqua, K., *Spectrochim. Acta.*, 34B, 1979, 167.
172. Ediger, R. D., and Hoult, D. W., *Atomic Spectrosc.* 1, 1980, 41.
173. Larson, G. F. Fassel, V. A., Winge, R. K., Kniseley, R. N., *Appl. Spectrosc.*, 30, 1976, 384.
174. Fassel, V. A., Katzenberger, J. M., Winge, R. K., *Appl. Spectrosc.*, 33, 1979, 1.
175. Larson, G. F., and Fassel, V. A., *Appl. Spectrosc.*, 33, 1979, 592.
176. Ediger, R. D. and Fernandez, F. J. *Atomic Spectrosc.*, 1, 1980, 1.
177. Cresser, M. S., and Browner, R. F., *Spectrochim. Acta.*, 35B, 1980, 73.
178. Bernas, B., *Anal. Chem.*, 40, 1968, 1682.
179. Boumans, P. W. J. M., and Bosveld, M., *Spectrochim. Acta.*, 34B, 1979, 59.
180. Winge, R. K. Peterson, V. J. and Fassel, V. A. *Appl. Spectrosc.*, 33, 1979, 206.
181. Pribil, R., and Scheider, P., *Chem. Listy*, 45, 1951, 7.
182. Pierce, T. B., Boswell, C. R., and Peck, P. F., '*Analyst*', 99, 1974, 774.
183. Koirtiyohann, S. R., International Winter Conference on Developments in Atomic Plasma Spectrochemical Analyses, (San Juan, Puerto Rico, 1980).
184. Barnes, R. M., and Meyer, G. A., *Anal. Chem.*, 52, 1980, 1523.
185. Carr, C. D., Borst, J. E., Sixth Annual Meeting of the Federation of Analytical Chemistry and Spectroscopy Societies, Philadelphia, Pa., 1979, Paper 90.
186. Schleicher, R. G., and Smith, S. B., Sixth Annual Meeting of the Federation of Analytical Chemistry and Spectroscopy Societies, Philadelphia, Pa., 1979, Paper 91.

POSTGRADUATE STUDIES

The following lecture courses and meetings were attended.

1. Lecture Course

Selected lectures from the CNAA M.Sc. course in 'Instrumental Chemical Analysis' on Atomic Spectroscopy and Metal Analysis.

2. Meetings

- i) Analytical Division of the Chemical Society.
- ii) Modern Methods of Analysis Group of the Sheffield Metallurgical and Engineering Association.
- iii) Departmental research colloquia and research colloquia in the joint Polytechnic/University, Analytical Chemistry Discussion Group.

Publications

1. 'A Versatile New Torch for Inductively Coupled Plasma Spectrometry', L. Ebdon, D. J. Mowthorpe and M. R. Cave, Anal. Chim. Acta, 115, 1980, 171.
2. 'Simplex Optimisation of Inductively Coupled Plasmas', L. Ebdon, M. R. Cave and D. J. Mowthorpe, Anal. Chim. Acta, 115, 1980, 179.
3. 'Fundamental Studies of the Application of the Inductively Coupled Plasma to Metallurgical Analysis', M. R. Cave, D. Kaminaris, L. C. Ebdon and D. J. Mowthorpe, Proc. Anal. Div. Chem. Soc. (in Press).

ACKNOWLEDGEMENTS

This project has been jointly sponsored by the Science Research Council and the London Scandinavian Metallurgical Company Limited.

I should like to thank the Science Research Council for providing financial assistance to myself in the form of a Research Assistantship.

I wish to express my sincerest gratitude to my supervisors Dr. L. C. Ebdon and Dr. D. J. Mowthorpe for their invaluable encouragement, help and guidance throughout my research and during the writing up of this thesis.

I am also indebted to Mr. G. Holmes of London Scandinavian Metallurgical Company Limited for acting as my external supervisor, and to Dr. S. Greenfield and Albright and Wilsons Limited for the loan of the dummy load and silica condenser used in this work for plasma power measurements.

SIMPLEX OPTIMISATION OF INDUCTIVELY COUPLED PLASMAS

L. EBDON*, M. R. CAVE and D. J. MOWTHORPE

Department of Chemistry, Sheffield City Polytechnic, Pond Street, Sheffield, S1 1WB (Gt. Britain)

(Received 4th October 1979)

SUMMARY

Meaningful comparisons of the analytical performances of different inductively coupled plasmas necessitate preliminary optimisation. The variable step-size simplex procedure is applied to optimise signal-to-background ratios for the five continuously variable operating parameters of a plasma, i.e. the power in the plasma, the observation height, and the injector, plasma and coolant gas flow rates. A series of univariate searches confirmed the results and also illustrated the importance of the various parameters. Results are presented for the manganese 257.6-nm ion line in both argon- and nitrogen-cooled plasmas and for the arsenic 228.8-nm atom line with argon coolant. Optimal power levels in these three cases were identified as 0.59, > 1.2 and 0.57 kW, respectively.

The inductively coupled plasma (ICP) source offers a number of attractive advantages in analytical optical emission spectrometry, e.g. low detection limits, long linear calibration ranges, relative freedom from interference effects and multi-element capability. Two groups of workers are most closely identified with the development of the ICP as a practical analytical tool. These groups, one led by Greenfield [1] and the other by Fassel [2], at an early stage took divergent routes: the former used higher power with nitrogen as coolant and the latter used lower power with argon as coolant. More recently, there has been considerable discussion in the literature [3–5] of the effect of power on analytical sensitivity, and the advocates of high power and low power have tended to polarise. Similarly the use of argon or nitrogen as coolant gas has been the subject of controversy.

It would at first appear to be a simple matter to resolve such arguments by experimentation, at least as regards the effect of power and coolant gas on obtainable limits of detection. This is, however, deceptive as the role of the spectrometer and measurement system must be considered and any true comparison must compare systems working at optimal conditions. Thus, for example, the results of Boumans and de Boer [5] showing the effect of power on the signal-to-background ratio cannot be taken as conclusive because, for example, a fixed observation height was used and the optimum viewing region may vary with the power in the plasma. Clearly, a rigorous optimisation technique is required which will enable a true optimum involving

all the plasma variables to be established, and an acceptable comparison of intrinsic merit independent of the associated spectrometric system to be achieved.

In this paper, the use of the simplex technique [6–8] is described for optimisation of different plasmas based on signal-to-background ratio criteria. The simplex method allows numerous interrelated continuously variable parameters to be optimised with relative ease and speed. The intrinsic merit of two or more plasmas may be compared on a given spectrometer by using the net signal-to-background ratio criterion [9]. The order of merit of the plasmas should remain unchanged even though the spectrometer is altered. Thus it should be possible to make a true comparison of the relative advantages of high or low power generators, differing torch designs and plasma gases.

A large number of parameters may affect the analytical performance of the plasma. These include the five parameters directly associated with the operation of the plasma (i.e., the power, the height of observation, and the flow rates of the coolant, plasma and injector gases) and the parameters associated with the spectrometer system (e.g., monochromator slit width, photomultiplier voltage and amplifier gain). When the signal-to-background criterion is used, these latter parameters may be ignored in order to arrive at a comparison of the intrinsic merit of different plasmas. One parameter of importance in the operation of the plasma has, however, not always been defined unambiguously. Some workers report 'the power' as the forward power from the generator, while others report the difference between the forward and the reflected power. Greenfield and McGeachin [10] have recently demonstrated that the power coupled into the plasma may be measured by a simple calorimetric method by using a dummy load consisting of a bundle of copper and iron rods. Since the power coupled into the plasma may vary with different gas flows, it seems sensible to use the term 'power' as meaning power coupled into the plasma. Accordingly, in the work reported here power measurements were made by the method of Greenfield and McGeachin, and throughout this paper the term 'power' refers to the power coupled into the plasma.

Simplex optimisation

The five continuously variable parameters mentioned above which affect the analytical performance of an ICP are clearly interrelated (e.g., the height of observation and the injector gas flow rate, and the power in the plasma and the plasma and coolant gas flow rates). Thus a true optimum cannot be achieved by varying one factor while keeping the others constant. Traditionally, a factorial optimisation experiment is used to solve such a problem but these experiments may be very time-consuming and tedious, unless some factors are given priority, with attendant risks of not obtaining a true optimum. Greenfield and Burns [11] have successfully used an alternating variable search method for optimising the plasma. An alternative approach is a modi-

fication of the simplex procedure of Nelder and Mead [7] which offers an elegant and speedy solution to the problem.

The use of simplex optimisation in analytical chemistry has recently been reviewed by Deming and Parker [8]. Nelder and Mead's modification [7] of the original sequential simplex procedure of Spendley et al. [6] has been most widely applied. In the present case, a five-dimensional simplex was constructed, defined by six points in factor space, and each of these factors was varied according to the rules of the simplex algorithm [12]. The variable step-size simplex [7] was chosen as this speeds the optimisation, prevents the attainment of a false optimum and permits closer definition of the optimum. The choice of the initial step size is a critical feature of this optimisation procedure. Yarbrow and Deming [12] have demonstrated that it is desirable to begin with a large step size to ensure that most of the factor space is explored before the simplex collapses onto the optimum. These authors described a matrix and accompanying equations which can be used to design the initial simplex. The simplex was terminated when no significant difference was observed in the signal-to-background ratio of successive new vertices. A univariate search [13], in which four of the parameters were held constant and the fifth varied as the signal-to-background ratio was measured, was used to confirm the success of the simplex optimisation. This search also yielded valuable information on the influence of each parameter on the performance of the plasma.

EXPERIMENTAL

Instrumentation

The instrumental system and the free-running r.f. generator as well as the versatile modified torch used in this comparison have already been described [14].

The dummy load used for power measurements and the method of measurement were the same as described by Greenfield and McGeachin [10]. Additional measurements were made with the brass support of the demountable torch [14] in position.

Operation of the simplex

An initial simplex was drawn up where the step size for each variable (S_n) was calculated by subtracting the smallest value experimentally achievable from the largest possible value of that parameter. The experimental constraints were whether or not a stable plasma could be formed on the equipment used and the physical limits of this equipment. The p and q values described by Yarbrow and Deming [12] were then evaluated and the initial vertices were calculated according to their method. The rules of the Nelder—Mead algorithm [7] were used to move the simplex to search for the largest signal-to-background ratio.

RESULTS AND DISCUSSION

The power dissipated in the dummy load was measured calorimetrically for various power settings on the generator; a series of graphs was drawn for different grid current values. Above a grid current value of 7.5 mA, it was possible to fit an empirical equation to the data by the least-squares technique. At low grid currents, the power in the plasma decreased rapidly and the equation did not apply; in such cases the power in the plasma had to be interpolated from the experimental graphs. The empirical equation was:

$$\text{Power in the plasma (kW)} = 0.351 \text{ plate power (kVA)} + 0.047 \text{ grid current (mA)} - 1.29$$

This enabled the power in the plasma to be calculated from the plate power and grid current readings. Figure 1 shows the close agreement between this empirical equation and the experimental values obtained with the dummy load, with and without the brass support of the demountable torch in position. This confirms that within experimental error there were no power losses to the brass support of the plasma torch.

Progress towards the optimum by the simplex procedure was fairly rapid. Plasma parameters were optimised successfully by using both signal-to-noise ratio and signal-to-background ratio criteria. The latter criterion is more universally applicable and is easier to measure. Thus an optimum was normally achieved in approximately 25 steps. That an optimum had in fact been achieved was then confirmed by using univariate search.

Figure 2 demonstrates the successful confirmation of the simplex optimisation for the five essential parameters; these results were obtained for the manganese 257.6-nm ion line with a $1\text{-}\mu\text{g Mn ml}^{-1}$ solution and the modified torch (argon coolant) [14]. The shaded area on each graph corresponds to the region identified as optimal by the simplex procedure. Figure 2A shows the flow rate of injector gas to be a critical parameter and confirms the success of the optimisation experiment. The plasma gas flow rate was not very critical (Fig. 2B); above about 10 l min^{-1} little change was observed in the signal-to-background ratio despite large variations in the plasma gas flow rate. Figure 2C illustrates the success of the simplex procedure in identifying the optimum coolant argon flow rate. Similarly, the optimum observation height was clearly identified by the simplex (Fig. 2D) as approximately 20 mm above the top-turn of the three-turn load coil.

It is perhaps the identification of the optimum power to be used in plasma spectrometry which has generated the greatest controversy. Figure 2E illustrates how well the simplex procedure enables optimum power to be defined; in this case, with an argon-cooled plasma, a relatively low optimum power was indicated. This finding for an argon-cooled plasma is in agreement with the findings of Greenfield and Burns [11].

Other lines for manganese, and for other elements, were also optimised by using the simplex procedure. The use of this procedure to evaluate the

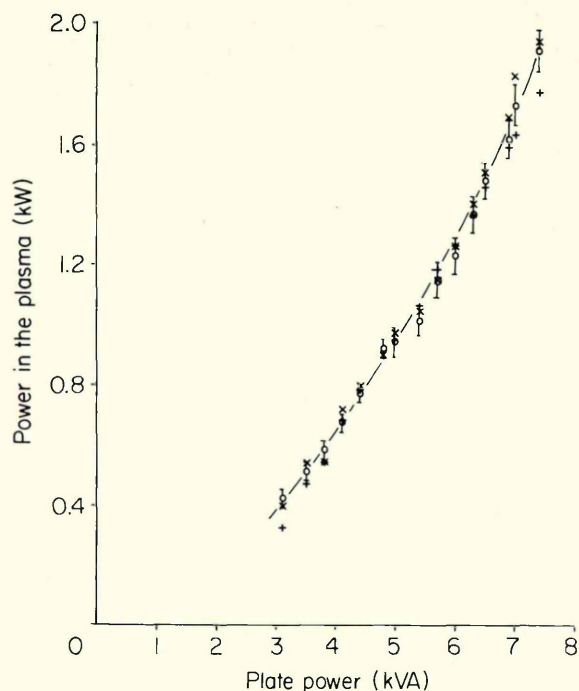


Fig. 1. Variation of power coupled into the plasma. (o) Measured with dummy load without brass support in position; (x) measured with dummy load with brass support in position; (+) calculated from empirical equation.

analytical performance of plasma torches has been described elsewhere [14]. In all cases the only problems encountered in optimisation were when optimal settings beyond the physical limits of the equipment were indicated. An instructive illustration of the utility of the technique and of the univariate searches is given in Fig. 3. These show the optimal settings for a nitrogen-cooled and an argon-cooled plasma with manganese(II) solution aspirated ($1 \mu\text{g ml}^{-1}$; measurements at 257.6 nm) and for an argon-cooled plasma with arsenic(III) solution aspirated ($100 \mu\text{g ml}^{-1}$; measurements at 228.8 nm). While plasma spectrometry is traditionally regarded as being particularly suited to the determination of manganese, arsenic is often regarded as a difficult element. All results were obtained with the new modified torch [14] and the argon- and nitrogen-cooled plasmas can be compared on the basis of their performance for manganese.

The injector gas flow rate is a critical parameter with the new design of torch, as can be seen from the sharp peaks shown in Fig. 3A. In all cases the optimum is at about 0.4 l min^{-1} , which suggests that a universal setting for this parameter is possible. The plasma gas flow rate is less critical (Fig. 3B), and again a compromise plasma gas flow rate for these two elements can be used without much loss in sensitivity. The shallow nature of the manganese

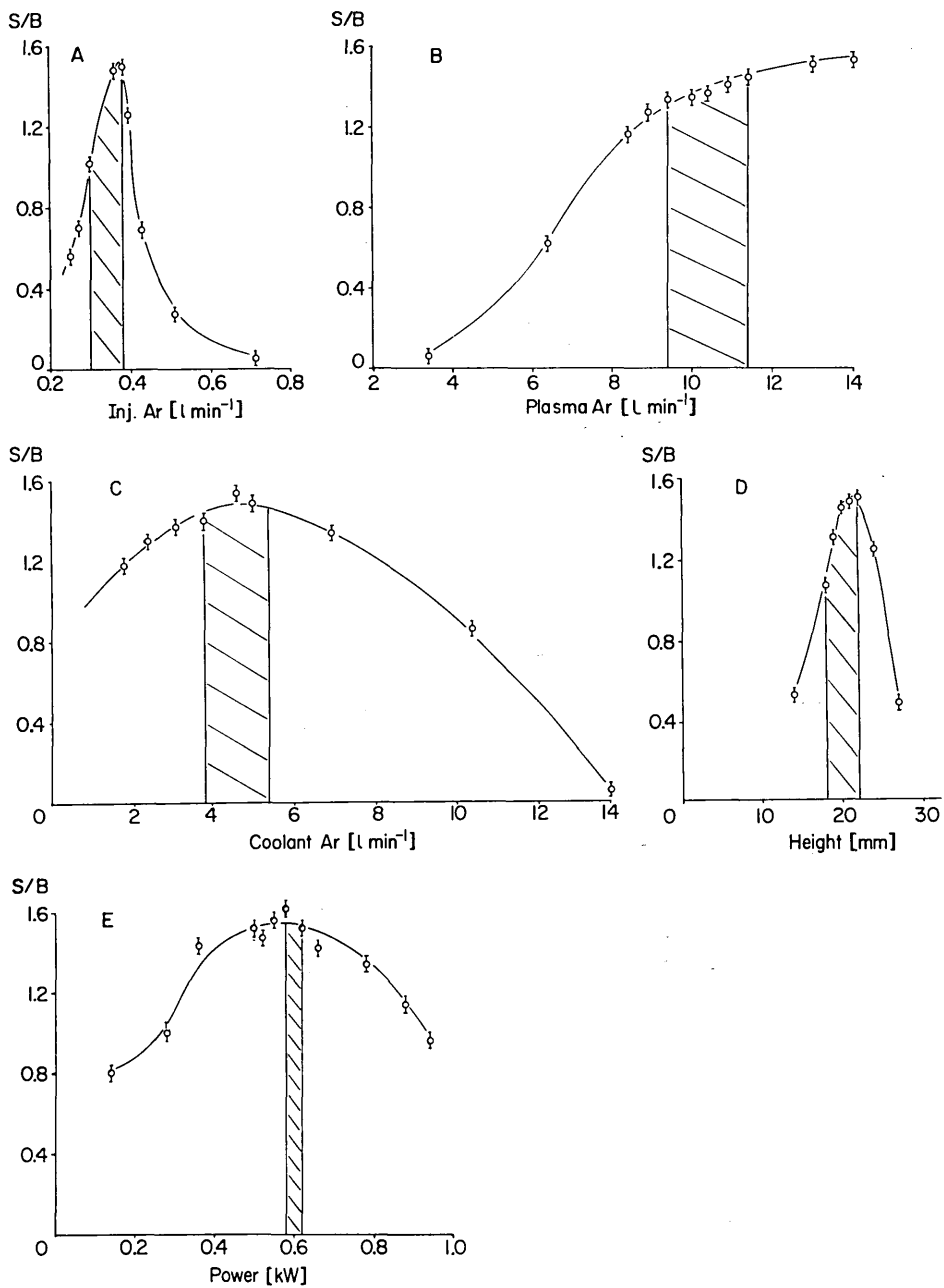


Fig. 2. Confirmation of the simplex optimisation for the five variables studied. The shaded areas indicate the regions identified as optimal by the simplex method. Argon-cooled plasma; manganese 257.6-nm ion line. (A) Injector gas flow rate; (B) plasma gas flow rate; (C) coolant argon gas flow rate; (D) observation height (mm above the load coil); (E) power coupled into the plasma.

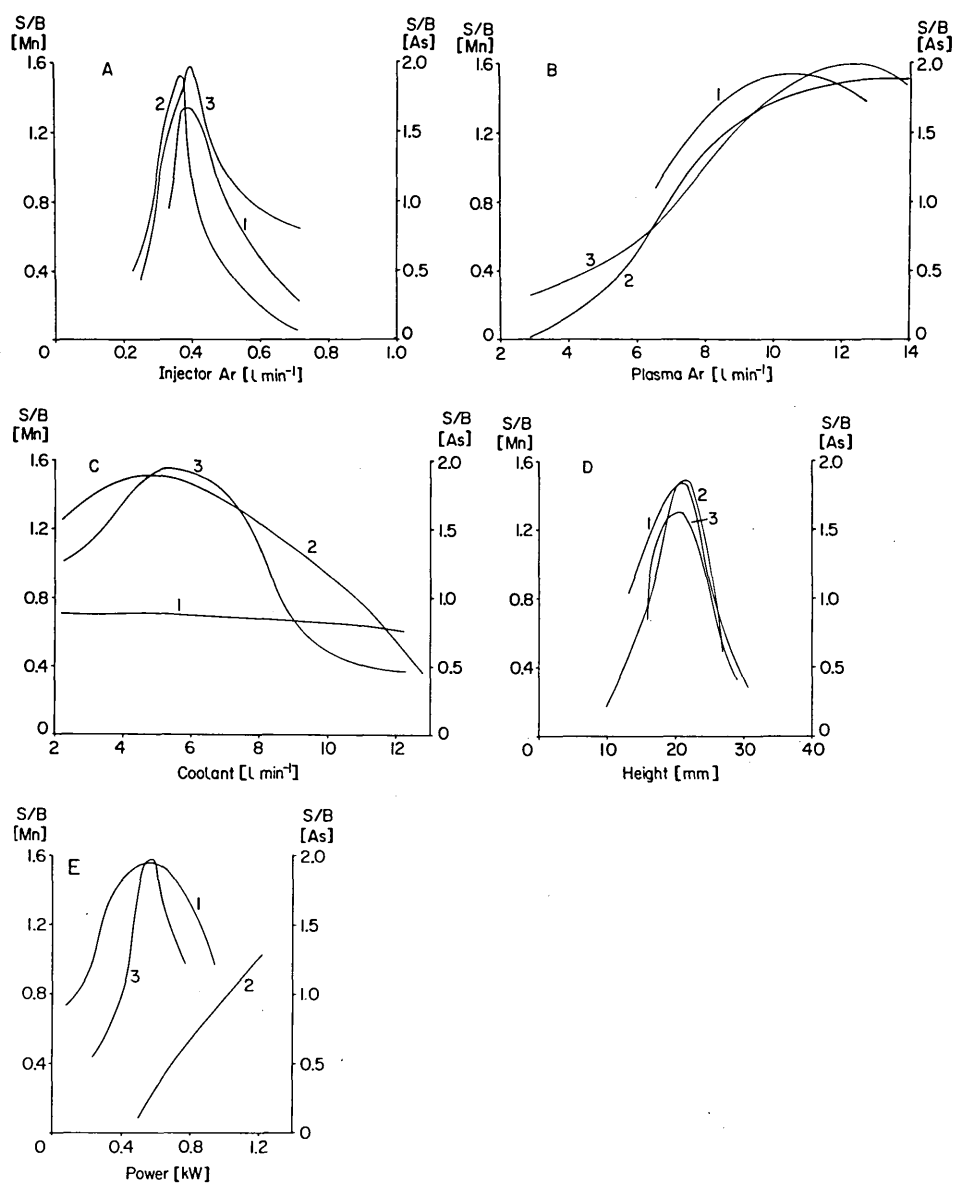


Fig. 3. Effects of gas flow rates, observation height and power on signal-to-background ratios for manganese and arsenic lines in different plasmas. Curves (1) nitrogen-cooled plasma, manganese 257.6-nm ion line; (2) argon-cooled plasma, manganese 257.6-nm ion line; (3) argon-cooled plasma, arsenic 228.8-nm atom line. (A) Injektor gas flow; (B) plasma gas flow; (C) coolant gas flow; (D) observation height; (E) power coupled into the plasma.

curve when a nitrogen-cooled plasma is used creates problems in identifying rapidly the optimum but such a situation is advantageous as regards day-to-day analytical reproducibility.

In general, with nitrogen as the coolant the outer gas flow rate has little effect on the signal-to-background ratio but with argon as coolant this flow rate is more critical (Fig. 3C). This behaviour presumably derives from the fact that argon may play a role in the propagation of the plasma whereas nitrogen does not.

The optimal viewing height in all three experiments was essentially similar (Fig. 3D) being approximately 20 mm above the load coil. This somewhat unexpected conclusion, and the similar optimal injector gas flow rates, could arise from the relatively large section of the plasma tail flame viewed (16 mm). Such a large section was used in order to minimise ionisation interferences in multi-element work, but it may disguise subtle differences in optimal viewing heights and injector gas flow rates. Accordingly, further experiments with a smaller monochromator entrance slit are required:

With regard to the controversy referred to above, Fig. 3E may serve to justify claims that low power is optimal in an all-argon plasma whereas higher power is needed to optimise a nitrogen-cooled plasma. Apparently the nitrogen-cooled plasma required more power to reach an optimum for manganese than could be coupled into the plasma with the generator available here at the gas flow rates indicated by the simplex, i.e. ca. 1.2 kW. In an argon-cooled plasma, however, an optimum for this manganese 257.6-nm ion line was reached at 0.59 kW even though more power was available. The arsenic 228.8-nm atom line could be optimised at only 0.57 kW. Although there is quite a large difference in the energies required to excite these two lines, the difference in the optimum power in an argon-cooled plasma is small (0.02 kW). For the manganese ion line, the sum of the ionisation energy and the excitation energy is 12.2 eV, whereas for the arsenic atom line the excitation energy is 6.7 eV. Preliminary optimisation experiments on these and other lines in a nitrogen-cooled plasma tend to confirm the relationship between optimum power in this plasma and the difficulty of exciting a line, as reported by Greenfield and Burns [11]. In practical terms it appears that compromise multi-element operating conditions will be less detrimental to individual element sensitivities with the argon-cooled plasma, or that the greatest improvements in analytical sensitivity for a given element may be achieved by judicious line and power selection with the nitrogen-cooled plasma.

The authors thank the Science Research Council and the London Scandinavian Metallurgical Co., Rotherham, for help in purchasing the equipment, and the Science Research Council for financial support for one of us (M.R.C.). We are grateful to Dr. S. Greenfield for helpful discussions and for the loan of the dummy load used.

REFERENCES

- 1 S. Greenfield, I. Ll. Jones and C. T. Berry, *Analyst*, 89 (1964) 713.
- 2 R. H. Wendt and V. A. Fassel, *Anal. Chem.*, 37 (1965) 920.
- 3 S. Greenfield, I. Ll. Jones, H. McD. McGeachin and P. B. Smith, *Anal. Chim. Acta*, 74 (1975) 225.
- 4 S. Greenfield, *Proc. Anal. Div. Chem. Soc.*, 19 (1976) 279.
- 5 P. W. J. M. Boumans and F. J. de Boer, *Spectrochim. Acta, Part B*, 32 (1977) 365.
- 6 W. Spendley, G. R. Hext and F. R. Himsforth, *Technometrics*, 4 (1962) 441.
- 7 J. A. Nelder and R. Mead, *Comput. J.*, 7 (1965) 308.
- 8 S. N. Deming and L. R. Parker, *CRC Crit. Rev. Anal. Chem.*, (1978) 187.
- 9 S. Greenfield and D. Thorburn Burns, *Spectrochim. Acta, Part B*, in press.
- 10 S. Greenfield and H. McD. McGeachin, *Anal. Chim. Acta*, 100 (1978) 101.
- 11 S. Greenfield and D. Thorburn Burns, *Anal. Chim. Acta*, 113 (1980) 205.
- 12 L. A. Yarbrow and S. N. Deming, *Anal. Chim. Acta*, 73 (1974) 391.
- 13 R. G. Michel, J. Coleman and J. D. Winefordner, *Spectrochim. Acta, Part B*, 33 (1978) 195.
- 14 L. Ebdon, D. J. Mowthorpe and M. R. Cave, *Anal. Chim. Acta*, 115 (1980) 171.

A VERSATILE NEW TORCH FOR INDUCTIVELY COUPLED PLASMA SPECTROMETRY

L. EBDON,* D. J. MOWTHORPE and M. R. CAVE

Department of Chemistry, Sheffield City Polytechnic, Pond Street, Sheffield S1 1WB (Gt. Britain)

(Received 4th October 1979)

SUMMARY

A modified torch for optical emission spectrometry with an inductively coupled plasma source is described. The demountable torch incorporates a flared intermediate tube, a capillary injector tube and interchangeable jets at the gas inlets. The optimised performance of the torch is compared with that of a conventional torch. The new torch can be operated over a wide range of gas flows and shows considerable promise in work with an argon-cooled plasma. The ability to operate at high or low gas flow rates, and the possibility of interchanging tubes and jets easily illustrate the versatility of the new design.

The design of the plasma torch is obviously an important consideration in optical emission spectrometry with an inductively coupled plasma (ICP) source. The basic requirement of a torch is the production of a stable plasma with low background emission and analyte signal noise, and with high emission intensity. The major design problems centre about the geometry of the torch which influences the production and characteristics of the plasma. The achievement of a narrow central channel called the toroid, first described by Greenfield et al. [1], is largely responsible for linear calibration curves which often cover five orders of magnitude. The gas flow characteristics are directly related to torch geometry; the gas flows should provide for a rapid increase in the ion population, and thus plasmas which are easily ignited and stable, whilst maintaining the necessary thermal isolation of the silica tubes comprising the torch. In turn, these tubes must prevent the discharge from jumping to the induction coil, while allowing an unrestricted view of the analytical region of the plasma.

In routine analytical applications, a versatile and economical torch is desirable. Incautious operation may require replacement of the silica; samples in both aqueous and non-aqueous solvents may be presented for analysis; some laboratories, particularly those with free-running r.f. generators, use both argon and nitrogen as the outer coolant gas. The high gas consumption of some torches indicates that further improvements in the efficiency of gas utilisation should be possible in such cases. Where possible, torches should be designed for maximum ease of adjustment of parameters and replacement of silica tubes.

The purpose of this study was to design and evaluate a torch which incorporated many of the advances in torch design made by other workers, but with maximum interchangeability of components. In this paper, the design and versatile operational characteristics of the resulting torch are reported.

Different plasma torch designs

The three concentric tube design with tangential gas introduction, first used by Reed [2] in his pioneering plasma work, has not yet been superseded although the shapes of the tubes and the nature of the gas flows have been modified by several workers. The two designs of torch which have been most widely used in analytical work are those of Greenfield et al. [3] and Fassel and Kniseley [4]. Both these designs are of fixed geometry but have different diameters (25 mm and 18 mm i.d., respectively) in keeping with the different diameters of the induction coils used by these two groups of workers. The torch of Fassel and Kniseley also incorporates a flared inner plasma tube, often referred to as the 'tulip configuration'. By modifying computer models of the ICPs devised by Miller and Ayen [5] and Barnes and Schleicher [6], Allemand and Barnes [7] were able to design a streamlined torch configuration. Their torch was machined from boron nitride; the inner tube was also flared, which markedly reduced the consumption of coolant argon.

Early torch designs were of fixed geometry, with one- or two-piece pre-aligned silica tubes. A more versatile arrangement can be obtained by using a holder into which the tubes can be inserted or removed at will. This allows replacement of single tubes for given experiments or after accidents. Such demountable torches have been used by various workers [8–10].

Reed [2] recognised that plasma stability is achieved when the gases, particularly the coolant gas, are introduced tangentially into the torch, producing a vortex flow. Although plasmas can be operated with laminar flows, tangential flow is still the preferred method of gas introduction. Genna et al. [11] described a modification of the gas flow introduction which both promoted easy ignition and reduced coolant gas consumption. This was achieved by producing a high swirl velocity with an essentially constant axial velocity by means of an injection nozzle.

The two types of injector tube commonly employed are a capillary injector [3, 12] and a jet injector [4, 7]. The orifice diameter of the injector must produce sufficient linear velocity to enable the aerosol to penetrate the base of the discharge without transporting the sample through the plasma too rapidly. Some workers have reported coalescence of the aerosol on the injector orifice; the capillary injector is said to overcome this [12].

Considerations in torch construction

Given the dimensions of the induction coil of the generator available here, it was decided to construct a torch of similar diameter to the Greenfield

torch but to incorporate and evaluate as many as possible of the reported successful modifications of the Fassel torch. Conventionally the Greenfield torch is operated with a nitrogen coolant; when an all-argon plasma is operated on such a torch, experience suggests that very high argon coolant gas flows (20–40 l min⁻¹) are required. A torch equally adaptable for the use of nitrogen or argon as coolant gas was sought.

A demountable construction obviously offered maximum versatility and ease of exchange of tubes, as well as enabling the effects of injector and inner tube shapes to be investigated. A brass support also permitted ready exchange of jets at the plasma and coolant gas entry ports. The use of gas entry port jets and a flared inner tube seemed advisable in order to promote ease of ignition and reduce gas consumption. The design reported here evolved from these initial considerations.

EXPERIMENTAL

Instrumentation

The equipment was as follows: a Radyne R50P 27-MHz free-running r.f. generator with integral gas box (Radyne Ltd., Wokingham, Surrey); an all-glass concentric nebulizer built as recommended by Scott [13], with a double-pass cloud chamber; a 0.5-m Ebert scanning grating monochromator (Model 82-529-SP, Jarrell-Ash); entrance optics comprising a 2.5-cm focal length quartz lens, 1:1 image, slit width 25 μ m, slit height 16 mm; an R106 photomultiplier (Hamamatsu T.V. Co. Ltd., Japan); a linear picoammeter amplifier (LM10; Chelsea Instruments Ltd., London); and a three-pen potentiometric recorder (Type MC641-3Z, Watnabe Inst. Corp., Tokyo, Japan).

Torch construction

The design of the torch is shown in Fig. 1. Two silica tubes (1.5 mm thick) were mounted into a support machined from brass. Given the need to align the tubes precisely with a 0.5-mm annulus between the outer and intermediate tube, the tubes were cemented into the support with an epoxy resin and held in position with a former while the glue hardened. It was not practicable to maintain the critical alignment with O-ring seals. The tubes could be released simply by heating the brass support in an oven. The injector tube was made from borosilicate glass, the top being held 6 mm below the top of the intermediate tube. Injector tubes with a capillary tip or a jet at the tip (Fig. 2) were tested.

The gas inlets (removable threaded brass jets) were fitted tangentially, as shown in Fig. 1. A series of jets of differing sizes (1, 2, 3 and 4 mm i.d.) were prepared, enabling different gas velocities to be achieved.

The torch assembly was mounted on a nylon base plate which bolted onto the moveable staging supplied with the generator to align the torch within the induction coil.

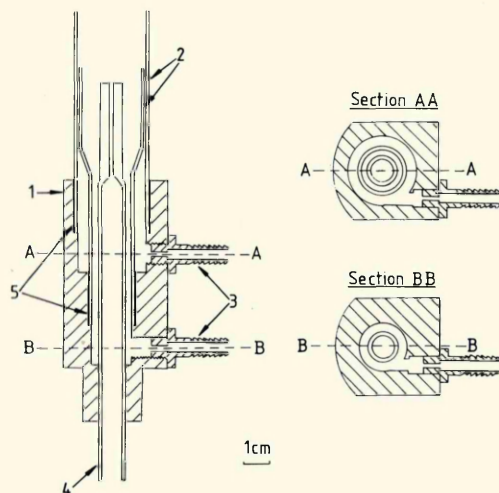


Fig. 1. Scale diagram of torch construction: (1) brass support; (2) silica tubes; (3) threaded-brass gas-inlet jets; (4) borosilicate glass injector tube; (5) epoxy resin bonds.

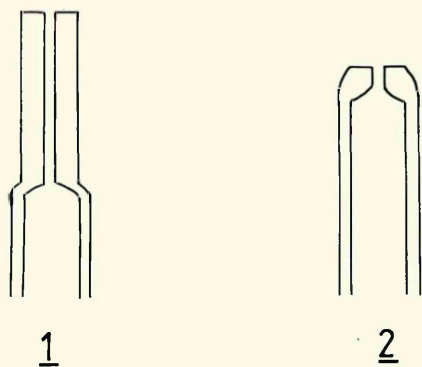


Fig. 2. Types of injector tube tips: (1) capillary tip (2 mm i.d.); (2) jet tip (2 mm orifice).

Evaluation of the torch

The torch was evaluated by comparing the signal-to-background ratio obtained with this new design of torch operated under optimised conditions with the ratio obtained when a two-piece Greenfield torch [3] was operated under optimal conditions. It must be stressed that the operating parameters (power, viewing height, coolant, plasma and injector gas flows) were optimised for both types of torch. The systems were optimised by using the simplex procedure described subsequently [14]. In the studies reported here the manganese 257.6-nm ion line was used. The Greenfield torch was optimised for the nitrogen-cooled argon plasma for which it was designed;

problems were encountered with softening of the silica tubes of this torch when argon was used as coolant. The operation of the new design torch was optimised with both argon and nitrogen as coolant gas.

After completion of the simplex a univariate search was used to verify the simplex [14]. Four parameters were held constant whilst the signal-to-background ratio was measured as the fifth parameter was varied.

RESULTS AND DISCUSSION

Early results showed that the jet injector (2 in Fig. 2) was tolerant to a wider range of aerosol drop sizes without condensation occurring at the tip. The misting observed when a glass plate was held above the injector without switching on the plasma showed that the aerosol from the jet injector 'fanned out', possibly indicating that some of the analyte would pass around and not through the central plasma channel. The capillary injector was observed to produce a narrow filament of aerosol. Under identical operating conditions the jet injector was found to give rise to noisier signals than the capillary injector and also to give a poorer absolute signal. Although condensation of the aerosol on the walls of the capillary caused some initial problems, these were overcome by adjustment of the nebulization chamber to reduce the droplet size of the emergent aerosol. Thus, on account of the superior signal-to-noise ratio, the capillary injector was used for all later work.

With four jet sizes available for each of the two gas inlets, it was necessary to make some initial investigations of different sizes of jets in order to select the most promising combination for the later simplex studies. This study resulted in the use of the 2 mm i.d. jet at the coolant gas inlet and the 3 mm i.d. jet at the plasma gas inlet.

The univariate searches confirmed that the simplex had, where possible, identified true optima; the exceptions occurred where instrumental constraints precluded achievement of the indicated value. The univariate searches (Fig. 3) were also instructive in indicating the different characteristics of the torches. Throughout this paper, power is taken to mean the power coupled into the plasma (measured as described elsewhere [14, 15] and the terms injector, plasma and coolant gas refer to the central, intermediate and outer gas flows, respectively.

Figure 3A shows that similar nitrogen coolant gas flows were optimal for either torch. Only when argon was used did the coolant gas flow rate appear to be critical; presumably argon exercises a greater control over the signal-to-background ratio by participating in the propagation of the plasma. Figure 3B shows clearly that lower flows of argon as plasma gas were optimal in the operation of the Greenfield torch. The flared nature of the intermediate tube in the modified torch probably explains this phenomenon. In contrast, the lower optimal injector gas consumption for the modified torch compared to the Greenfield torch (Fig. 3C) was probably the result of a more complex interrelationship between gas flows and plasma characteristics. Figure 3D

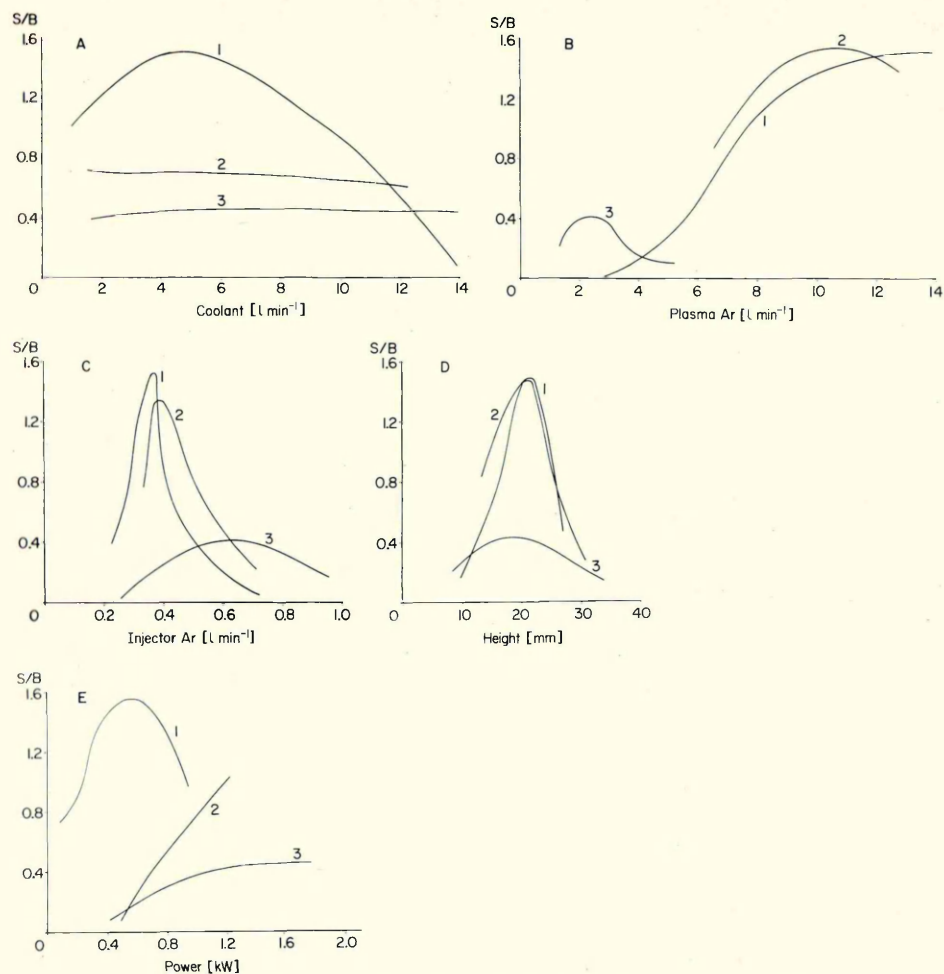


Fig. 3. Effects of gas flow rates, observation height and power. Curves (1) argon-cooled plasma, new design torch; (2) nitrogen-cooled plasma, new design torch; (3) nitrogen-cooled plasma, Greenfield torch. (A) Coolant gas flow; (B) plasma gas flow; (C) injector gas flow; (D) height of observation; (E) power coupled into plasma.

shows the optimal viewing height to be essentially similar for each combination; however, it should be recalled that a slit height of 16 mm and a 1:1 image were used and this may have disguised more subtle differences. As is shown elsewhere [14, 16], lower power is optimal in the all-argon plasma compared to the nitrogen-cooled plasma (Fig. 3E). Unfortunately, under the optimal gas flows it was not possible to couple more than ca. 1.2 kW power into the plasma when the present design of torch was used with nitrogen coolant.

Table 1 summarises the optimised plasma conditions for both the torches

TABLE 1

Comparison of optimised operating conditions

Torch	Coolant gas	Gas flow rates (l min ⁻¹)			Height (mm)	Power (kW)	Signal-to-background ratio
		Coolant	Plasma	Injector			
Greenfield design	N ₂	4.0	2.5	0.6	19	1.3	0.4
New design	N ₂	4.6	10.0	0.4	21	1.2	1.2
New design	Ar	4.6	13.0	0.38	20	0.6	1.5

investigated and also shows the signal-to-background ratio obtained on aspiration of a 1 $\mu\text{g ml}^{-1}$ solution of manganese at optimum conditions. Clearly there is a significant improvement of a factor of three in the signal-to-background ratio with the new design of torch. Further work is in progress to confirm whether this is a general gain in sensitivity. Noise levels observed with both torches are equivalent and therefore there should also be a gain in detectability.

The new design of torch can be used over a wide range of gas flows without fear of softening the silica tubes. Thus it would appear to be preferable for use with an all-argon plasma, which for this particular line gave the best signal-to-background ratio. Coolant gas flow as low as 1.5 l min⁻¹ can be used without difficulty with an all-argon plasma, and thus the total gas consumption can be as low as 3 l min⁻¹ of argon, although these flows do not, as can be seen, produce the best analytical performance.

Once the performance of an argon-cooled plasma on the new design of torch with the 3-mm plasma inlet jet and the 2-mm coolant gas jet had been optimised, the effect of varying the jet sizes on the univariate searches was investigated. Although not a rigorous optimisation, and therefore not a true comparison, such experiments can produce useful information. Figure 4A shows the effect of altering the plasma gas inlet jet on the signal-to-background ratio as the plasma gas flow rate is varied. Larger jet sizes increase gas consumption but improve sensitivity. The effect of changing jet sizes for the coolant gas inlet is more interesting (Fig. 4B). A high tangential velocity seems required here and above a certain jet size analytical performance deteriorates.

No evidence can be offered on the relative ease of the ignition of the torches as no problems have been encountered in igniting plasmas on any of the torches described.

The new torch described offers considerable promise in optical emission spectrometry with an inductively coupled plasma source. It would appear to offer considerable advantages when argon-cooled plasmas are used and in situations requiring either operation over a wide range of gas flows or in other non-routine situations where versatility is required.

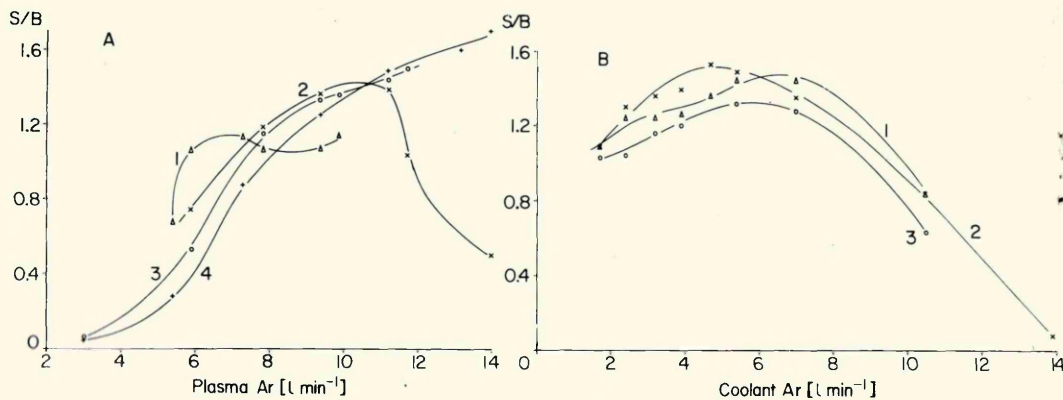


Fig. 4. Influence of inlet jet size for (A) the plasma gas and (B) the coolant gas on signal-to-background ratio at varying argon gas flow rates: (1) 1 mm jet; (2) 2 mm jet; (3) 3 mm jet; (4) 4 mm jet. For (A) the coolant flow rate was constant at 4.6 l min^{-1} , and for (B) the plasma gas flow rate was 13 l min^{-1} .

The authors thank the Science Research Council and the London Scandinavian Metallurgical Co., Rotherham, for the provision of equipment used in this study and the Science Research Council for financial support for one of us (M.R.C.).

REFERENCES

- 1 S. Greenfield, I. Ll. Jones and C. T. Berry, *Analyst*, 89 (1964) 713.
- 2 T. B. Reed, *J. Appl. Phys.*, 32 (1961) 2534.
- 3 S. Greenfield, I. Ll. Jones, H. McD. McGeachin and P. B. Smith, *Anal. Chim. Acta*, 74 (1975) 225.
- 4 V. A. Fassel and R. N. Kniseley, *Anal. Chem.*, 46 (1974) 1155A.
- 5 C. Miller and J. Ayen, *J. Appl. Phys.*, 40 (1969) 5260.
- 6 R. M. Barnes and R. G. Schleicher, *Spectrochim. Acta, Part B*, 30 (1975) 109.
- 7 C. D. Allemand and R. M. Barnes, *Appl. Spectrosc.*, 31 (1977) 434.
- 8 R. M. Dagnall, D. J. Smith, T. S. West and S. Greenfield, *Anal. Chim. Acta*, 54 (1971) 397.
- 9 J. F. Alder and J. M. Mermet, *Spectrochim. Acta, Part B*, 28 (1973) 421.
- 10 D. L. Windsor, D. R. Heine and M. B. Denton, *Appl. Spectrosc.*, 33 (1979) 56.
- 11 J. L. Genna, R. M. Barnes and C. D. Allemand, *Anal. Chem.*, 49 (1977) 1450.
- 12 R. H. Scott and M. L. Kokot, *Anal. Chim. Acta*, 75 (1975) 257.
- 13 R. H. Scott, *I.C.P. Inf. Newsl.*, 3 (1978) 425.
- 14 L. Ebdon, M. R. Cave and D. J. Mowthorpe, *Anal. Chim. Acta*, 115 (1980) 179.
- 15 S. Greenfield and H. McD. McGeachin, *Anal. Chim. Acta*, 100 (1978) 101.
- 16 S. Greenfield and D. Thorburn Burns, *Anal. Chim. Acta*, 113 (1980) 205.